NUREG/CR-2331
BNL-NUREG-51454
VOL. 2, NO. 1

SAFETY RESEARCH PROGRAMS SPONSORED BY OFFICE OF NUCLEAR REGULATORY RESEARCH

QUARTERLY PROGRESS REPORT
JANUARY 1 — MARCH 31, 1982

Date Published — July 1982

DEPARTMENT OF NUCLEAR ENERGY, BROOKHAVEN NATIONAL LABORATORY
UPTON, NEW YORK 11973

Prepared for the U.S. Nuclear Regulatory Commission
Office of Nuclear Regulatory Research
Contract No. DE-AC02-76CH00016

NUREG/CR-2331
BNL-NUREG-51454
VOL. 2, NO. 1
AN, R-1,4,5,7,8

SAFETY RESEARCH PROGRAMS SPONSORED BY OFFICE OF NUCLEAR REGULATORY RESEARCH

QUARTERLY PROGRESS REPORT
JANUARY 1 — MARCH 31, 1982

Herbert J.C. Kouts, Department Chairman
Walter Y. Kato, Deputy Chairman

Principal Investigators:

R.A. Bari
R.J. Cerbone
T. Ginsberg
G.A. Greene
J.G. Guppy
R.E. Hall
W.J. Luckas, Jr.
M. Reich
P. Saha
C. Sastre
J.R. Weeks
W. Wulff
D. van Rooyen

Compiled by: Allen J. Weiss
Manuscript Completed June 1982

DEPARTMENT OF NUCLEAR ENERGY
BROOKHAVEN NATIONAL LABORATORY, ASSOCIATED UNIVERSITIES, INC.
UPTON, NEW YORK 11973

Prepared for the
OFFICE OF NUCLEAR REGULATORY RESEARCH
U.S. NUCLEAR REGULATORY COMMISSION
CONTRACT NO. DE-AC02-76CH00016
FIN NOS. A-3017,-3014,-3015,-3016,-3024,-3041,-3208,-3215,-3216,-3219,-3225,-3226,-3227,-3254

FOREWORD

The Advanced and Water Reactor Safety Research Programs Quarterly Progress Reports have been combined and are included in this report entitled, "Safety Research Programs Sponsored by the Office of Nuclear Regulatory Research Quarterly Progress Report." This progress report will describe current activities and technical progress in the programs at Brookhaven National Laboratory sponsored by the Division of Accident Evaluation, Division of Engineering Technology, and Division of Facility Operations of the U. S. Nuclear Regulatory Commission, Office of Nuclear Regulatory Research.

The projects reported are the following: HTGR Safety Evaluation, SSC Development, Validation and Application, Generic Balance of Plant Modeling, Thermal Hydraulic LWR and LMFBR Safety Experiments, RAMONA-3B Code Modification and Evaluation, LWR Plant Analyzer Development, LWR Code Assessment and Application, Stress Corrosion Cracking of PWR Steam Generator Tubing, Standards for Materials Integrity in LWRs, Probability Based Load Combinations for Structural Design, Mechanical Piping Benchwork Problems, Soil Structure Interaction, Human Error Rate Data Analysis, and Criteria on Human Engineering Regulatory Guides. The previous reports have covered the period October 1, 1976 through December 31, 1981.

CONTENTS

Page

FOREWORD iii

I. DIVISION OF ACCIDENT EVALUATION. 1

SUMMARY. 1

1. HTGR Safety Evaluation 5
   1.1 Graphite and Ceramics 5
   1.2 Materials 31
   1.3 Fuel and Fission Products 58
   1.4 Analytical. 67
   References 78

2. SSC Development, Validation and Application. 79
   2.1 SSC-L Code. 79
   2.2 SSC-P Code. 81
   2.3 SSC-S Code. 82
   2.4 SSC Validation. 82
   References and Publications. 83

3. Generic Balance of Plant Modeling. 85
   3.1 MINET (Momentum Integral Network) 85
   3.2 MINET Improvement 85
   3.3 MINET Improvements in Process 86
   3.4 Balance of Plant Models 87
   3.5 MINET Input Deck C-1. 87
   3.6 CRBRP Part Load Study 87
   3.7 MINET Applications to CRBRP Station Blackout. 89
   References and Publications. 89

4. Thermal-Hydraulic LWR and LMFBR Safety Experiments 91
   4.1 Core-Concrete Heat Transfer Studies 91
   4.2 LWR Steam Spike Phenomenology 93
   References 97

5. RAMONA-3B Code Modification and Evaluation 99
   5.1 Partial-ATWS Calculation. 99
   5.2 Programming Consideration 101
   5.3 Code Improvements 101
   5.4 Code Documentation. 102
   References 102

6. LWR Plant Analyzer Development 105
   6.1 Introduction. 105
   6.2 Assessment of Existing Simulators 106
   6.3 Acquisition of Special-Purpose Peripheral Processor 106
   6.4 Software Implementation on AD10 Processor 107
   References 109

Page

7. LWR Code Assessment and Application. 111
7.1 TRAC-PD2/MOD1 Assessment. 111
7.2 TRAC-PF1 (Version 7.0) Assessment 117
7.3 RELAP/MOD1 (Cycle 14) Assessment. 130
References 134

II. DIVISION OF ENGINEERING TECHNOLOGY 135

SUMMARY. 135

1. Stress Corrosion Cracking of PWR Steam Generator Tubing 137

2. Standards for Materials Integrity in LWRs. 143

3. Probability Based Load Combinations for Structural Design 145
3.1 Structural Analysis and Limit State Identification. 145
3.2 Reliability Analysis Methods. 145
3.3 Load Combination Methodology. 145
3.4 Consensus Estimation of Loads 148

4. Mechanical Piping Benchmark Problems 153
4.1 Elastic Benchmark Development 153
4.2 PSAFE1/PSAFE2 Code Modifications. 153
4.3 HDR URL Loop Piping Evaluations 154
4.4 Physical Benchmark Development. 156
4.5 Multiple-Supported Piping Systems 157

5. Soil Structure Interaction 187
5.1 Mark III Type Containment Ultimate Capacity Calculations. 187

III. DIVISION OF FACILITY OPERATIONS. 189

SUMMARY. 189

1. Human Error Rate Data Analysis 191

2. Criteria on Human Engineering Regulatory Guides. 193

References 193

I. DIVISION OF ACCIDENT EVALUATION

SUMMARY

HTGR Safety Evaluation

Initial planning of a long term exposure loop for large (127 mmϕ x 254 mm length) graphite samples has begun. Helium density profiling of such samples is under investigation. A final "cocoon" specimen was oxidized and the profiling technique revamped. The study of oxidizing atmosphere on strength and reactivity was continued; some data are shown. Oxidation in the uniform flow apparatus continued, with addition of "large" grade Stackpole 20-20 planned. Results of elemental impurities analysis for PGX graphite are given.

Analysis of U-Th mixture run at very high temperatures in H451 graphite continues. The migration rates of uranium and thorium are much greater than predicted by SORS. The data infer that the migration of uranium is inhibited by the addition of thorium to the mixture and vice versa.

Testing of Incoloy 800H to evaluate the effect of loss-of-cooling accidents on high-cycle fatigue strength has been completed. It is shown that 24h thermal excursions to 760°C and 871°C (1400° and 1600°F) reduce the fatigue strength measured at 538°C (1000°F). Detailed scanning electron microscopy shows no significant bulk differences in the tractographs for uninterrupted tests at 538°C, and those for which thermal transients were imposed. It is concluded that the loss in fatigue strength results from recrystallization of the machined surface layers on the specimens during the thermal transient. Optical and scanning electron microscopy were carried out on fractured high cycle fatigue specimens to investigate the surface recrystallization effects and oxidation characteristics in the test helium.

Long term creep tests and thermal cycling tests are continuing on Incoloy 800H and Hastelloy X specimens in air and helium environments. One of the Incoloy 800H specimens which ruptured during this reporting period in the helium shows about a 20% increase in rupture life compared to a same test in the air.

The extent of Sr aerosol formation from a heated graphite release source is shown to be independent of initial loading in the concentration range of approximately 1 to 10 mg Sr per g graphite. The lower concentration corresponds to about one monolayer coverage of Sr in graphite. Electron micrographic examinations of simulated Ag aerosols indicate that the primary particles, 0.06 to 0.08 μm in diameter, are of the condensational type.

Experiments have been performed on the interaction of SrO with H-451 graphite. The reaction occurs rapidly at temperatures below 1300°C. The experimental results are complicated by the fact that release of strontium may occur during the decomposition of $Sr(NO_3)_2$, as well as during the interaction of SrO with graphite.

Work is continuing on simulation of primary loop thermohydraulics during various transients connected with unrestricted core heatup accidents, using the GA code RATSAM6. During Feburary this effort was redirected in support of the upcoming siting study for the 2240 MWt reactor. Conversion of the RATSAM code input data from the case of a 3000 MW reactor to those for a 2240 MW reactor is almost complete. Long term UCHA runs considering pressure history to blowdown and MTRC are scheduled for the coming quarter. As part of this study, a review of the thermal liner cooling system performance has been initiated.

SSC Development, Validation and Application

The Super System Code (SSC) Development, Validation and Application Program encompasses a series of three computer codes: (1) SSC-L for system transients in loop-type LMFBRs; (2) SSC-P for system transients in pool-type LMFBRs, and (3) SSC-S for long term shutdown transients. In addition to these code development and application efforts, validation of these codes is an ongoing task.

During this quarter, the primary attention continued to be on providing direct support for the recently renewed CRBRP licensing activities within NRC. The calculational capability using SSC-L was directed toward analysis of various CRBR plant transient events, including: (1) loss of heat sink, (2) station blackout, and (3) pipe break. Data decks were prepared/modified and test cases run. The low heat flux sodium boiling modeling and implementation into SSC were completed. These add a powerful extension to the code capabilities.

Due to the recent refocusing of this program to support the CRBRP licensing effort, work on the SSC-P code has been slowed.

Under SSC-S activities, the DRACS model has been revised and tested to simulate the CRBRP Direct Heat Removal Service (DHRS) design. Further calculations are being deferred pending receipt of certain design specific information requested from the CRBRP Project Office.

SSC validation work remains centered on the FFTF natural circulation tests. Additionally, extensive testing was accomplished prior to release of the new official export version of SSC-L.

Generic Balance of Plant Modeling

The Generic Balance of Plant (BOP) Modeling Program deals with the development of safety analysis tools for system simulation of nuclear power plants. It provides for the development and validation of models to represent and link together BOP components (e.g., steam generator components, feedwater heaters, turbine/generator, condensers) that are generic to all types of nuclear power plants. This system transient and analysis package is designated MINET to reflect the generality of the models and methods, which are based on a momentum integral network method.

The initial version of MINET is operational and is interfaced to the steam generator and forms the BOP representation for the SSC code. As such, it can presently represent pumps, pipes, heat exchangers, valves and accumulators. A stand-alone version is being developed. Modifications to MINET currently being made include: improvements to present models; improvements to certain computational techniques; standardization of an input deck and modeling of new components such as an air-cooled condenser and three region non-equilibrium steam drum. MINET applications include an assessment of the heat removal capability of major CRBR components and analysis of the CRBR steam generator system for a station blackout event.

Thermal-Hydraulic LWR and LMFBR Safety Experiments

An analytical model was developed to characterize the liquid entrainment regime of heat transfer between horizontal immiscible liquid layers agitated by a vertical gas flux. The model combines the Szekeley surface renewal model with a model for entrainment which is represented as a product of mass rate of entrainment and the excess enthalpy of the entrained phase. The model contains an empirical coefficient which is evaluated from available BNL and KFK data.

Superheated particle bed quenching experiments continued as part of the steam spike phenomenology effort. Experiments were carried out with hot and cold test vessel walls. The results indicate that the cold wall allows liquid to bypass the bed and flow to the bottom of the test vessel. The quench process in this case proceeded in an upward cooling pattern. With the hot wall, the quench process proceeds in a two-stage frontal pattern.

RAMONA-3B Code Modification and Evaluation

The partial-ATWS calculation reported in the previous quarterly progress report was recomputed from 300 seconds with a high boron injection rate to demonstrate the effect of boron in RAMONA-3B prediction. It has been found that as the boron concentration in the core reaches a level of approximately 300 ppm, the core power is reduced significantly. This demonstrates that the effect of boron is being correctly taken into account in RAMONA-3B.

Work has also begun in improving the code in the areas of low and reverse flows, level tracking, and the carryunder from steam separator. The block diagrams and control equations for the feedwater and recirculation flow controls have also been formulated.

LWR Plant Analyzer Development

The LWR Plant Analyzer Program is being conducted to develop an engineering plant analyzer capable of performing accurate, real-time and faster than real-time simulations of plant transients and small break loss of coolant

accidents (SBLOCA) in LWR power plants. The current program phase is being carried out to establish the feasibility of achieving faster than real-time simulations and faster than main-frame general-purpose computer (CDC-7600) simulations through the use of modern, interactive high-speed special-purpose minicomputers, which are specifically designed for interactive time-critical systems simulations. The results of this program are important for reactor safety analyses and also for on-line plant monitoring and accident diagnosis, for accident mitigation, further for developing operator training programs and for assessing existing and future training simulators.

Existing simulator capabilities and limitations regarding their representation of the Nuclear Steam Supply System have been assessed previously. Current simulators have been found to be limited to steady-state simulations and to restricted quasi-steady transients within the range of normal operating conditions.

A special-purpose, high-speed peripheral processor has been selected earlier, which is specifically designed for efficient systems simulations at real-time or faster computing speeds. The processor is the AD10 from Applied Dynamics International (ADI) in Ann Arbor, Michigan. A PDP-11 minicomputer serves as the host computer to program and control the AD10 peripheral processor. Both the host computer and the peripheral processor are now operating at BNL.

An existing model for nonequilibrium, nonhomogeneous two-phase flow in a specific BWR system is being implemented on the AD10 processor for the purpose of comparing the computing speed and accuracy of the AD10 with those of the CDC-7600 main-frame computer. The program under development is called HIPA-PB2 for High-Speed Interactive Plant Analysis of the Peach Bottom-2 BWR power plant. The implementation of HIPA-PB2 is being carried out in the high-level language MPS10 of the AD10.

LWR Code Assessment and Application

The independent assessment of TRAC-PD2/MOD1 code with the BCL 2/15-scale downcomer tests has been completed. The results are consistent with earlier calculations presented in the previous quarterly progress reports.

Independent assessment of TRAC-PF1 (Version 7.0) and RELAP5/MOD1 (Cycle 14) codes has begun with various separate effects tests. These include: Marviken critical flow test, B&W steam generator (OTSG and IEOTSG) tests, FLECHT-SEASET steam generator tests, GE large vessel blowdown test, and University of Houston flooding tests. Comparisons between the data and the code predictions are presented and several areas for further code improvements have been identified.

1. HTGR SAFETY EVALUATION

1.1 Graphite and Ceramics (J. H. Heiser III, J. J. Barry, J. Colman, M. S. Davis, C. C. Finfrock, F. B. Growcock, D. G. Schweitzer and D. R. Wales)

Characterization of HTGR graphites and the study of strength loss mechanisms continues to be the main emphasis of this program. In order to gain much needed information on large specimens, initial planning of a long term exposure loop for large samples (127mm ϕ x 254mm length) has begun. Since such samples will show minimal burnoff (0.01 - 0.1% per yr.), conventional testing methods for density profiles, fracture strength loss, etc. are not sensitive enough. Therefore, the technique of profiling, using helium density measurements, is currently being investigated.

Testing of the Helium Impurities Loop is continuing. Start-up of long term exposure experiments using mid-size (76mm ϕ x 152 mm length) ''large'' grade Stackpole 20-20 graphite will follow.

1.1.1 Characterization of HTGR Graphites

A final H-451 graphite ''cocoon'' specimen was oxidized to 7.0% burnoff in 4% O_2/He at 550°C. Density profiling using a new holding jig is in progress. The machining process involves placing the outer shell of the ''cocoon'' on an aluminum jig (Figure 1.1.7). The sample may now be held by the aluminum, thereby eliminating weight loss due to wear on the graphite. The machining process for the inside of the shell differs from previous techniques only in that a protective layer of tape is wrapped around the outside of the shell. The shell is now handled only by the taped portion. The remainder of the machining process is as reported earlier (Growcock, et al, Dec. 1981).

The study of the effects of oxidizing atmosphere on strength and reactivity was continued. Data for ASR-1RG and Stackpole 20-20 oxidized in 2% O_2/He or 2% CO_2/He are presented in Tables 1.1.1 - 1.1.5. Curves of rate vs. time are currently being tabulated; the results will follow.

Specimen location for the six reactor grade graphites used in this study are outlined in Figures 1.1.1 - 1.1.6. An attempt will be made to correlate rate and impurities levels to sample location.

Short term accelerated oxidation of ''large'' grade Stackpole 20-20 specimens (36mm ϕ x 72mm length) will begin in a uniform flow apparatus (U.F.A.). The oxidizing atmosphere will be 0.165% H_2O/1.7% H_2/He and the temperature will be varied from ~700° C to ~900°C.

Oxidation of PGX log EL-3 in a U.F.A. with 0.165% H_2O/1.7% H_2/He at 700°C and 800°C is near completion. Oxidation versus strength loss and density profile curves will be generated. Oxidation of PGX log 4 will follow. This log sample is a pie wedge consisting of ~1/8 a full log. Previous samples were cross-sectional slices (~6 in. thick) of either the log end or middle. The study of rate to sample location for log 4 will encompass axial distance from center as well as radial distance. Such a study may allow for better insight in characterizing the whole log.

Table 1.1.1 ASR-1RG Specimens Oxidized at 500°C, 2% O_2/He, 746 hrs.

SAMPLE #		PERCENT BURNOFF	AVERAGE RATE G/MIN	DENSITY BEFORE OXIDATION G/CC	DENS.AFTER OXID. G/CC
5	COMP	9.172674709	1.14796E-05	1.74229912	1.582483690
15	COMP	3.958215697	4.69682E-06	1.720458902	1.652359427
26	COMP	4.109490753	5.11669E-06	1.737898748	1.666475165
36	COMP	19.95845687	2.51078E-05	1.75117283	1.401665757
5	TENS	3.047300025	1.12965E-05	1.725564076	1.672980961
35	TENS	7.363450207	2.75466E-05	1.748250545	1.619518987
38	TENS	8.895030573	3.34964E-05	1.750195205	1.594514806
44	TENS	5.259360409	1.96985E-05	1.737211674	1.64584545

Table 1.1.2 ASR-1RG Compressive Specimens Oxidized at 450°C, 2% O_2/He,881 hrs.

SAMPLE #	PERCENT BURNOFF	AVERAGE RATE G/MIN	DENSITY BEFORE OXIDATION G/CC	DENS.AFTER OXID. G/CC
1	4.776649103	4.99054E-06	1.743727814	1.660436055
10	2.545844888	2.69202E-06	1.730610175	1.694347857
23	3.53272066	3.73061E-06	1.737351446	1.675975673
25	1.205338698	1.26939E-06	1.735398405	1.714480976
30	1.3983112	1.46614E-06	1.726551028	1.702408471
35	5.130256957	5.45781E-06	1.75269018	1.66277267
40	1.329293148	1.39425E-06	1.724723701	1.701797067
50	1.44850082	1.48695E-06	1.689875926	1.665398059

Table 1.1.3 2020 (Regular) Specimens Oxidized at 500°C, 2% O_2/He, 336 hrs.

SAMPLE #		PERCENT BURNOFF	AVERAGE RATE G/MIN	DENSITY BEFORE OXIDATION G/CC	DENS.AFTER OXID. G/CC
1	COMP	2.281329393	6.54762E-06	1.800843626	1.75976045
10	COMP	5.587823653	1.58433E-05	1.795373104	1.695050821
20	COMP	5.329767336	1.51240E-05	1.798826737	1.702953457
30	COMP	7.536424304	2.13998E-05	1.797607447	1.662132122
5	TENS	3.464328307	2.98264E-05	1.795842524	1.733628643
11	TENS	4.285491573	3.68155E-05	1.788929674	1.712265244
35	TENS	6.447477087	5.53770E-05	1.798482689	1.682525929
45	TENS	6.112290335	5.25645E-05	1.796017323	1.686239530

Table 1.1.4 2020 (Regular) Tensile Specimens Oxidized at 850°C, 2% CO_2/He, 138.8 hrs.

SAMPLE #	PERCENT BURNOFF	AVERAGE RATE G/MIN	DENSITY BEFORE OXIDATION G/CC	DENS.AFTER OXID. G/CC
3	5.765723125	1.19916E-04	1.801571581	1.697697952
7	7.581867482	1.57095E-04	1.794143662	1.658114067
12	4.872944172	1.00624E-04	1.791396339	1.704102596
17	5.682913517	1.17491E-04	1.797521855	1.695370242
23	5.473937366	1.13121E-04	1.790330189	1.692328636
27	5.467370111	1.14454E-04	1.791858127	1.693890612
32	5.828896481	1.21044E-04	1.797135467	1.692382301
38	5.266489065	1.09830E-04	1.800840301	1.705999244

Table 1.1.5 ASR-1RG Tensile Specimen Oxidized at 850°C, 2% CO_2/He, 61.4 hrs.

SAMPLE #	PERCENT BURNOFF	AVERAGE RATE G/MIN	DENSITY BEFORE OXIDATION G/CC	DENS.AFTER OXID. G/CC
3	7.365766586	3.18245E-04	1.739945528	1.611785201
7	5.11477357	2.22078E-04	1.743496159	1.654320279
12	3.281750427	1.41874E-04	1.73429284	1.677377678
17	6.871334615	2.99586E-04	1.741962225	1.622366172
32	2.764423077	1.16667E-04	1.[illegible]4363	1.646620672
36	7.627389477	3.33540E-04	1.749190978	1.615773370
42	5.185553247	2.24172E-04	1.7364451	1.646400815
47	2.766620975	1.19617E-04	1.727089864	1.679307833

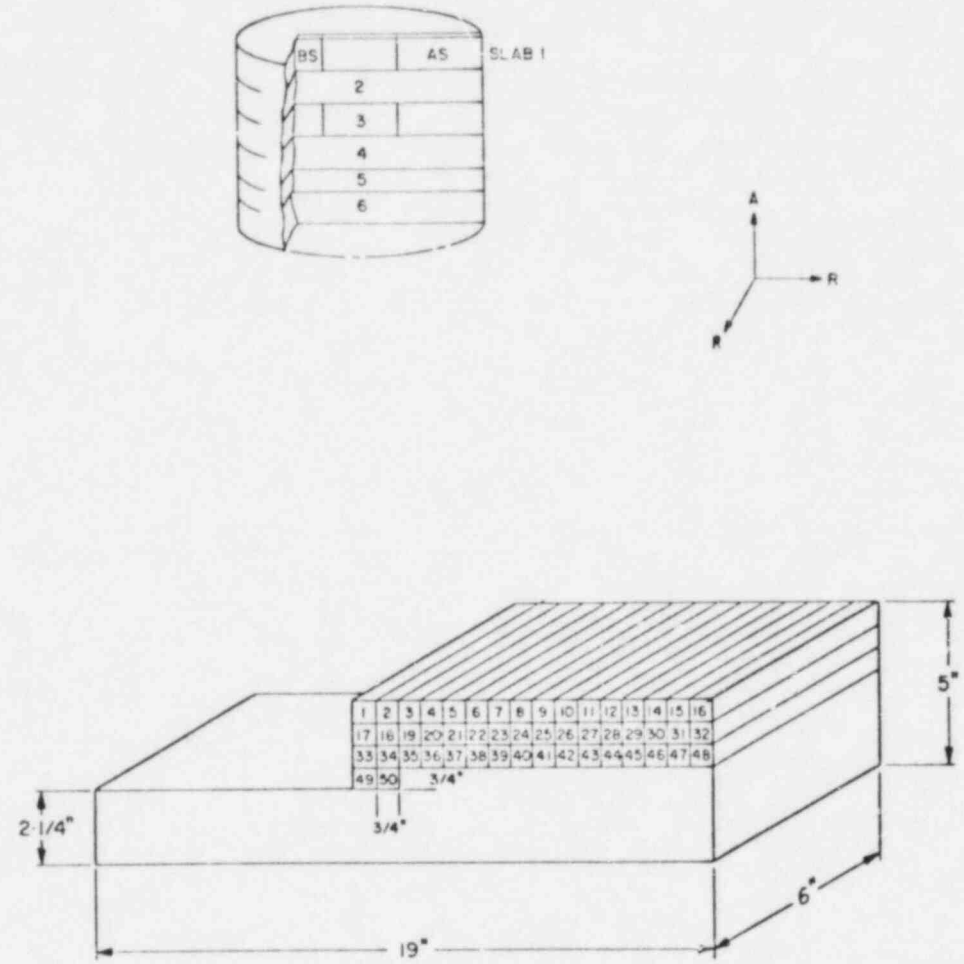

Figure 1.1.1 ASR-1RG #7637-55 (Sigri- German).

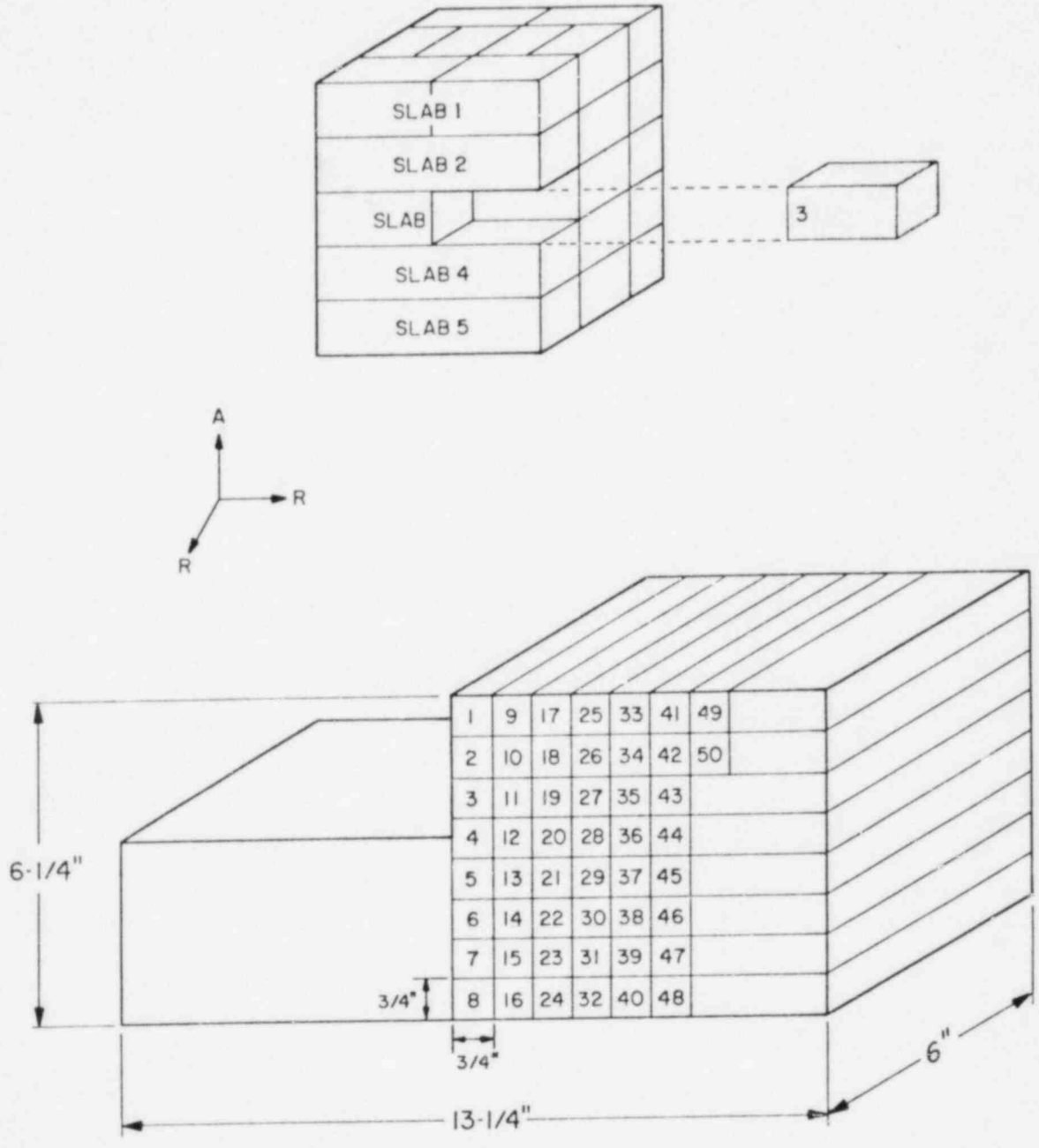

Figure 1.1.2 Large 20-20 #7637-53 (Stackpole).

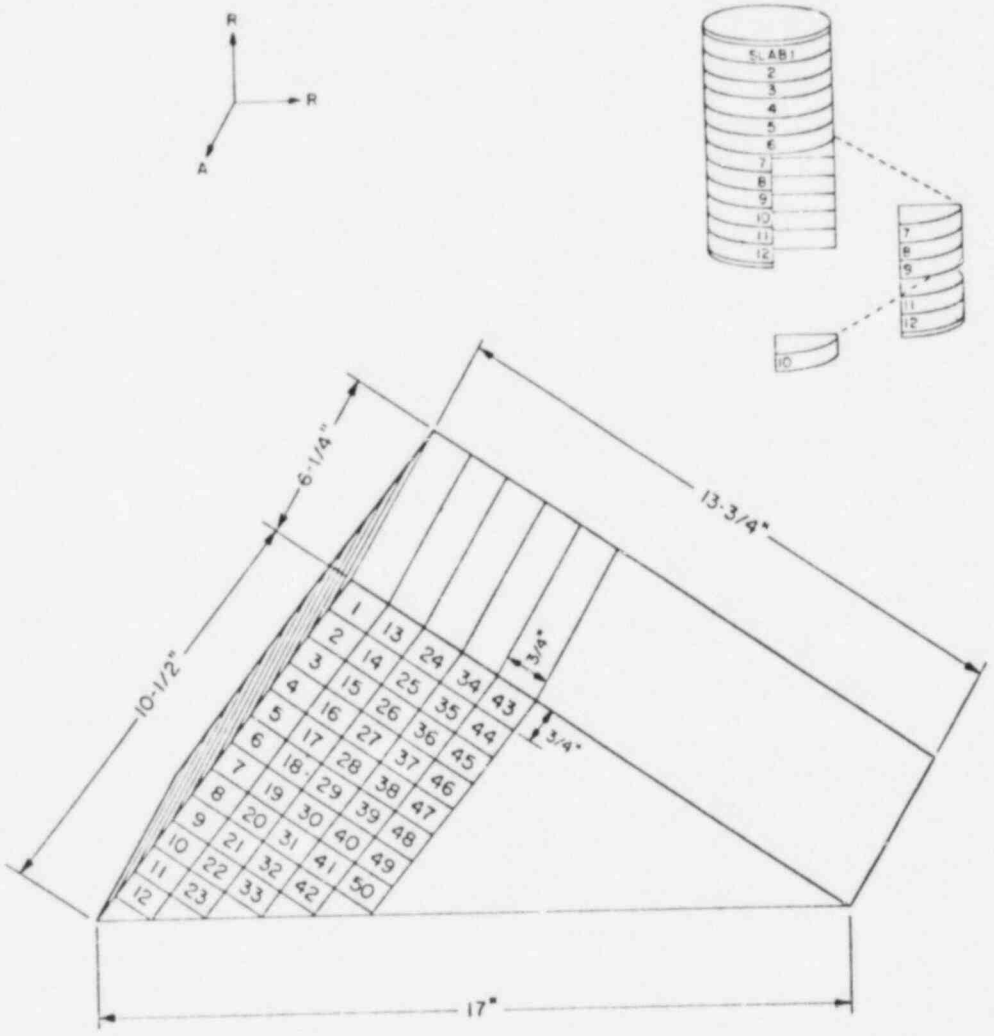

Figure 1.1.3 PGX #6484-112 (Union Carbide).

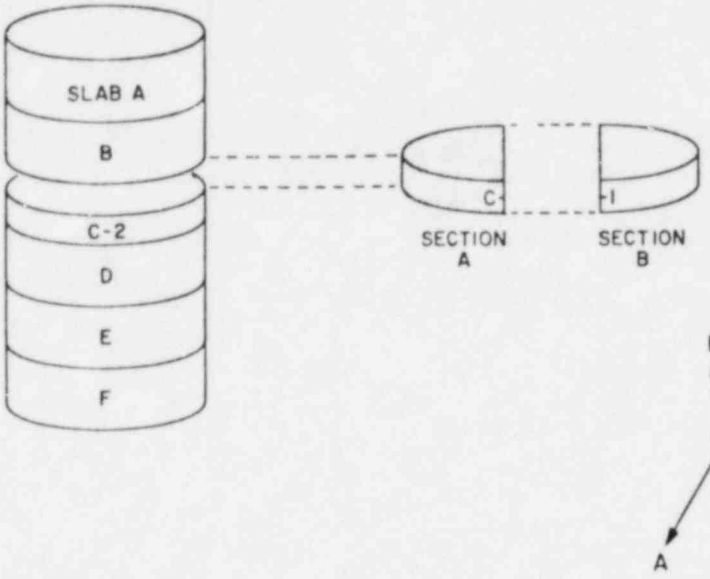

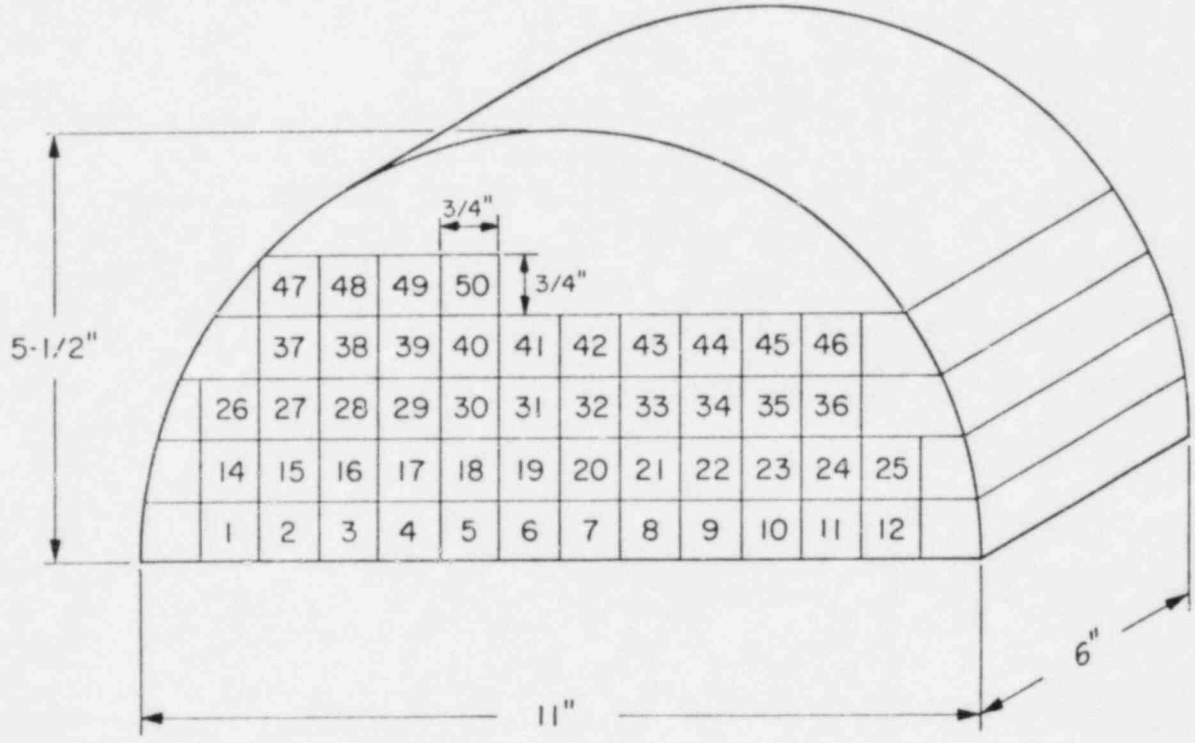

Figure 1.1.4 Regular 20-20 #7637-9A (Stackpole).

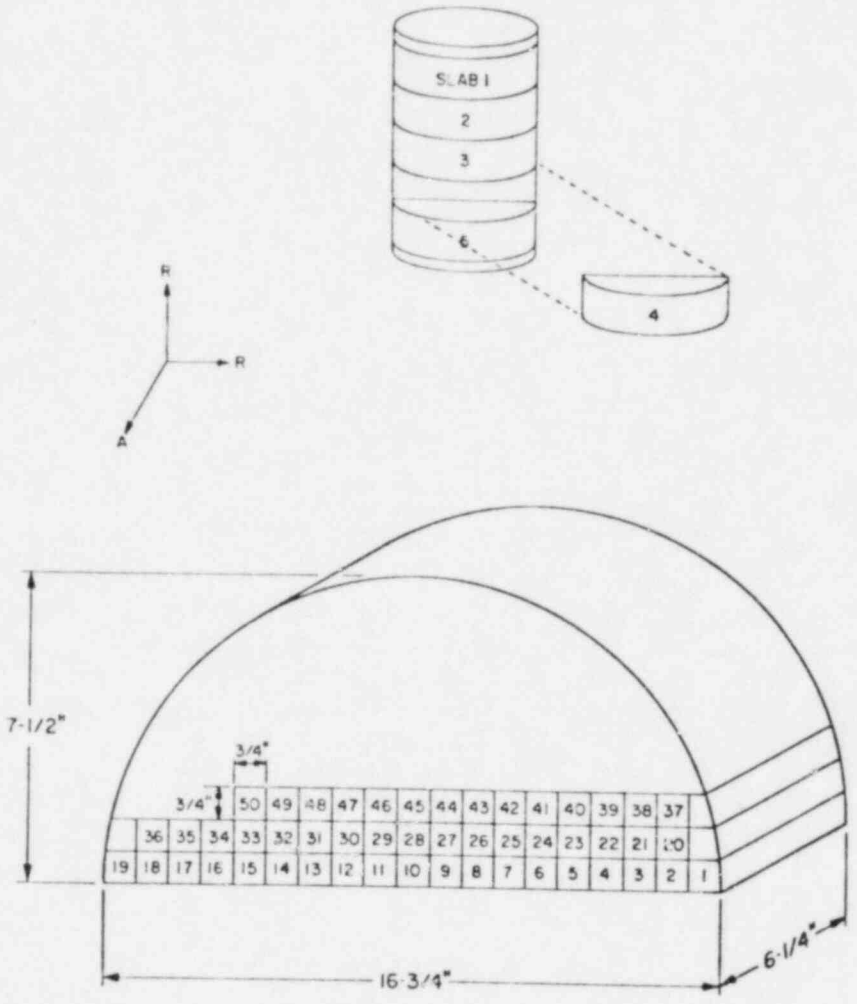

Figure 1.1.5 H-451 #7194-87 (Great Lakes Carbon Corp.).

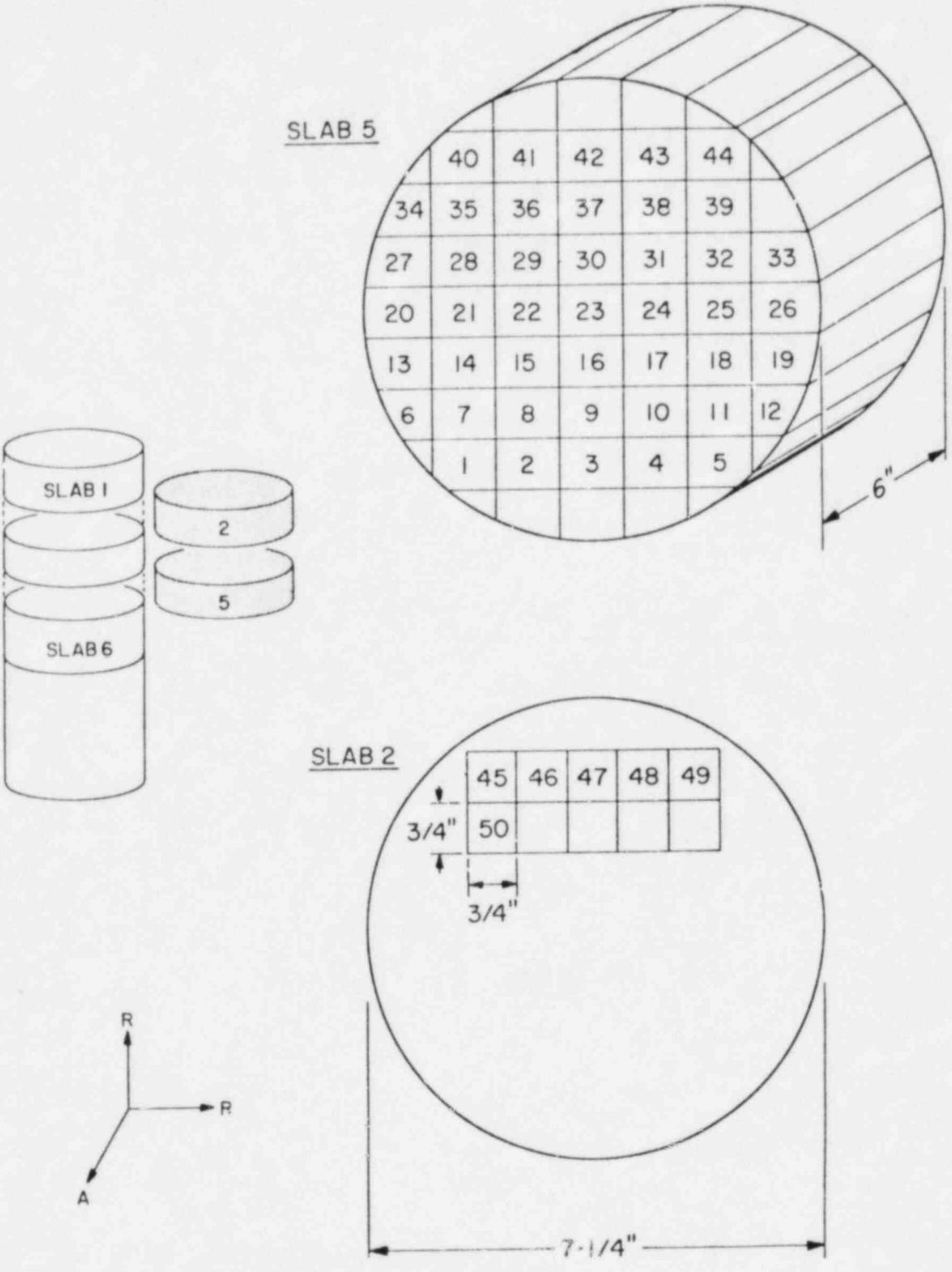

Figure 1.1.6 V-483-T #7637-3 (Sigri-German)

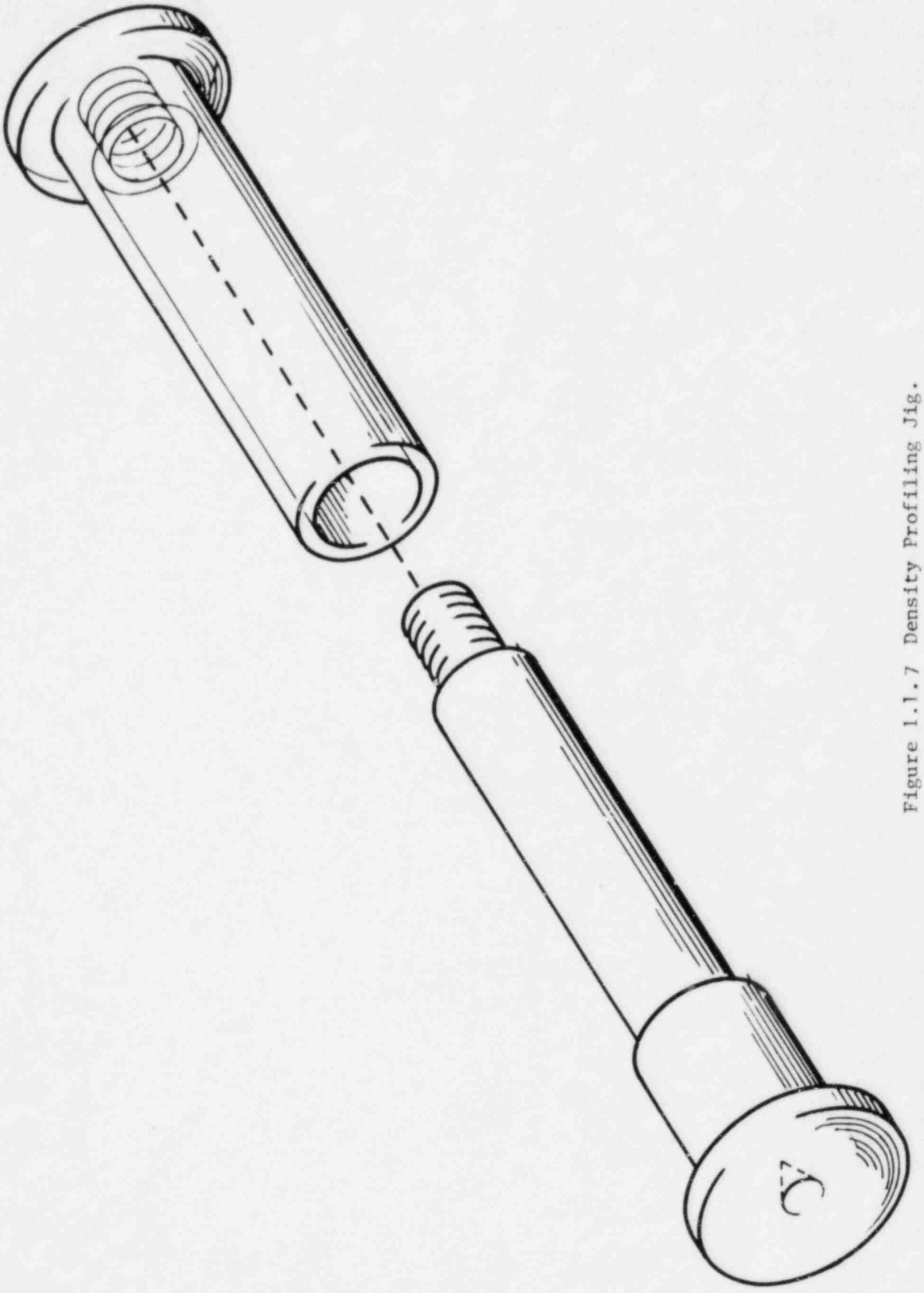

Figure 1.1.7 Density Profiling Jig.

1.1.2 Elemental Analysis of PGX Graphite

Analysis of rate versus impurities concentration for PGX graphite was completed. Plots of individual impurities versus rate are shown in Figures 1.1.8 - 1.1.20. A plot of total impurities versus rate is given in Figure 1.1.21. A similar study on ''large'' grade Stackpole 20-20 will be performed on samples oxidized in the uniform flow apparatus.

IRON VS. RATE, PGX GRAPHITE

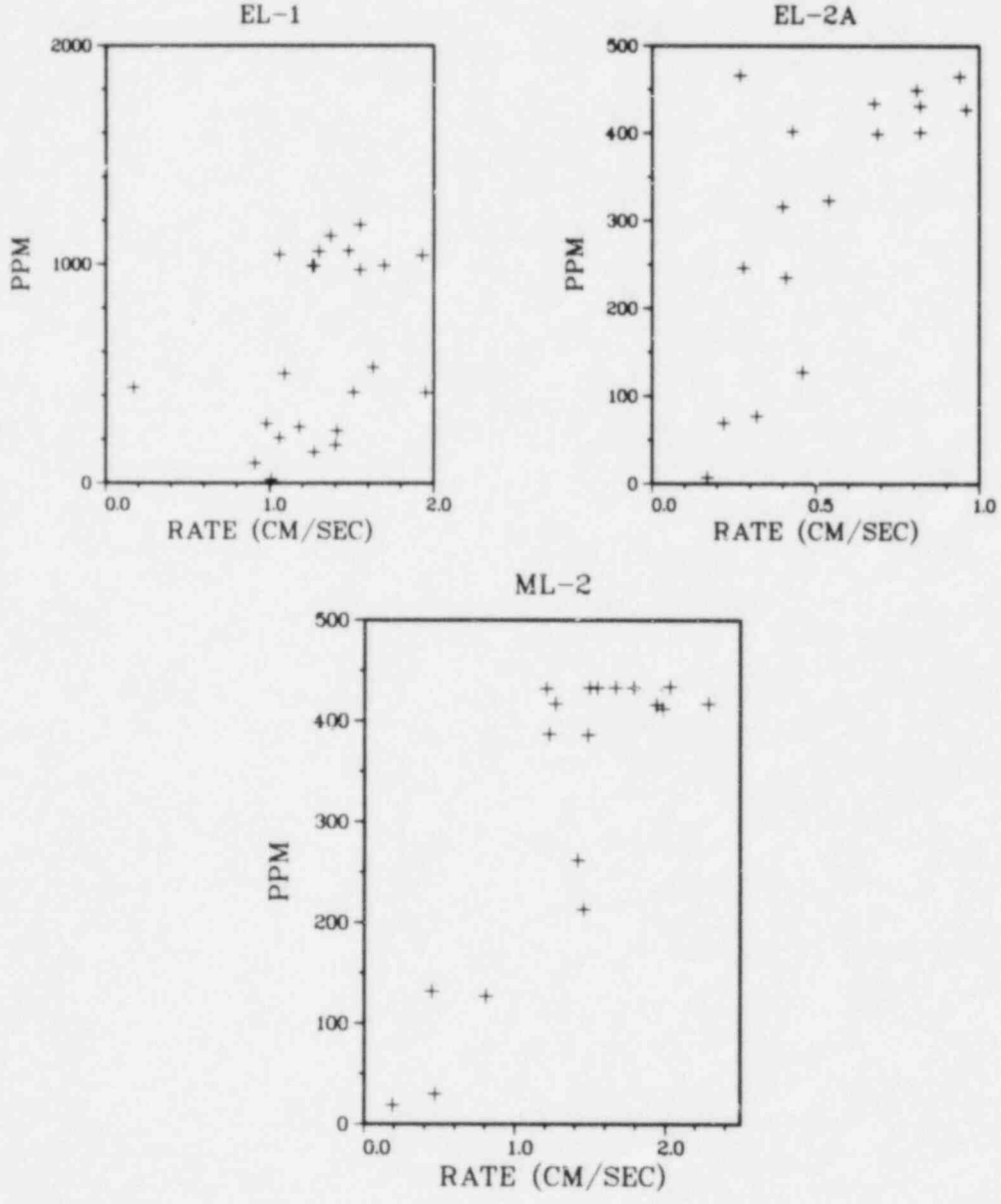

Figure 1.1.8

VANADIUM VS. RATE, PGX GRAPHITE

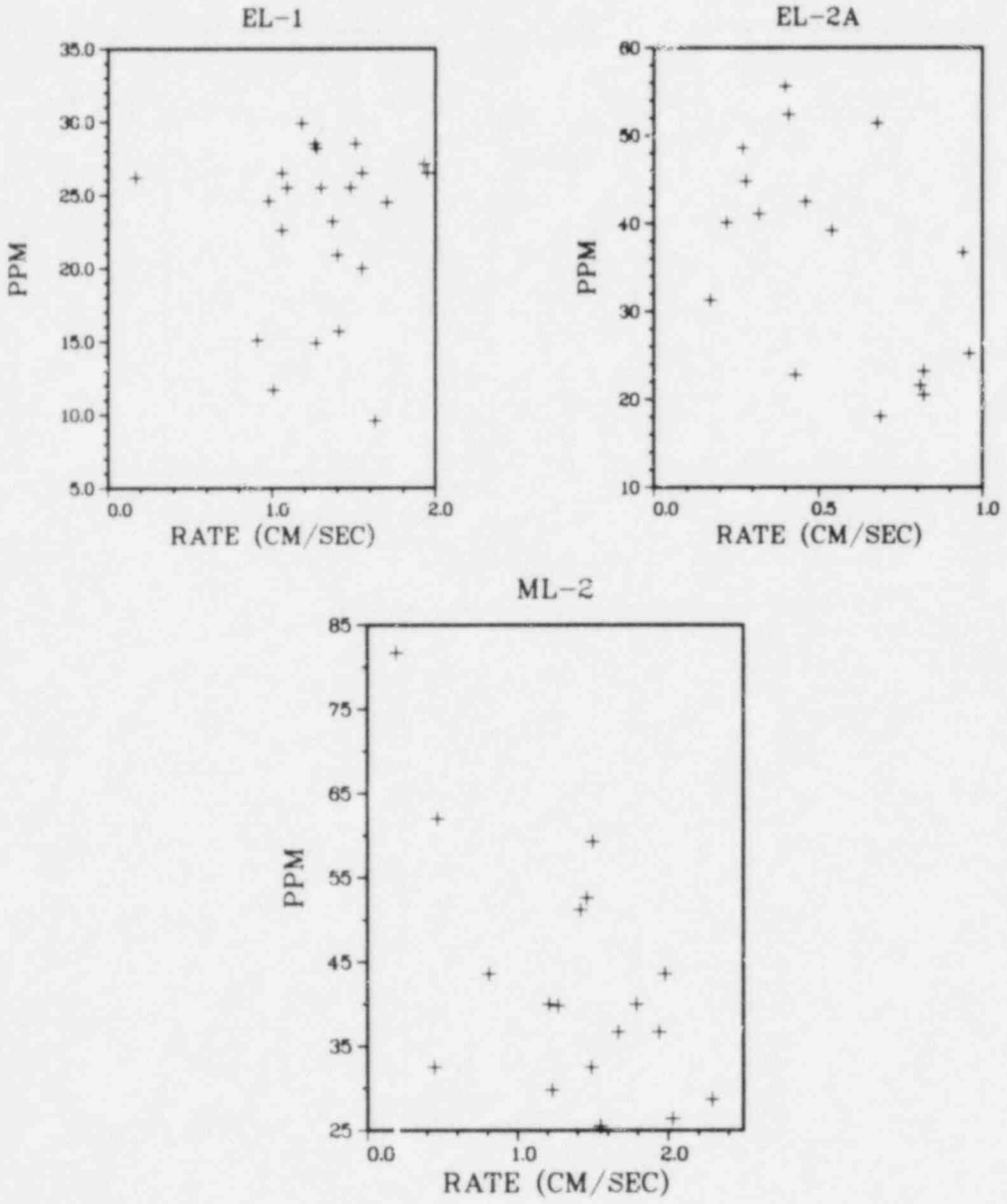

Figure 1.1.9

MANGANESE VS. RATE, PGX GRAPHITE

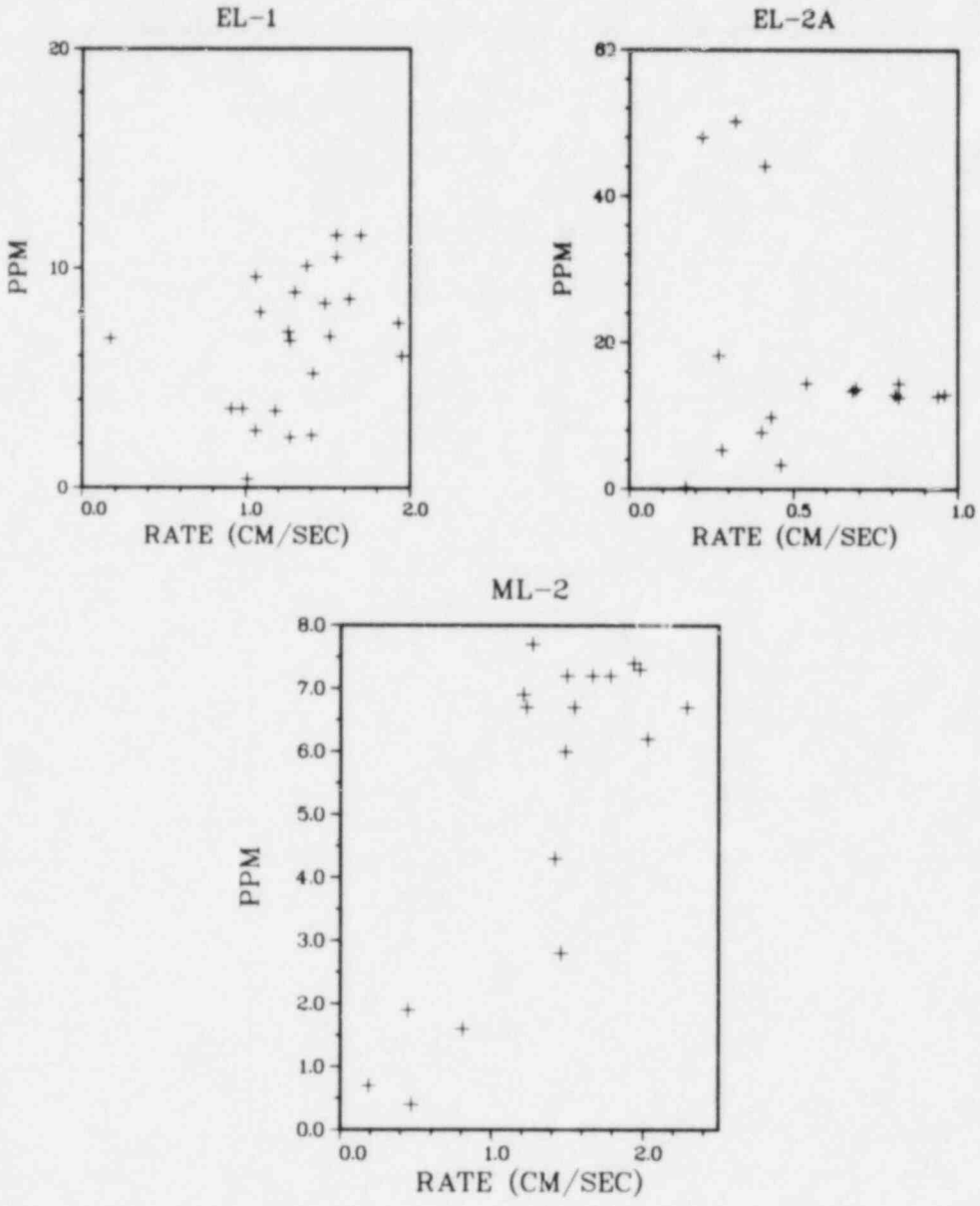

Figure 1.1.10

MAGNESIUM VS. RATE, PGX GRAPHITE

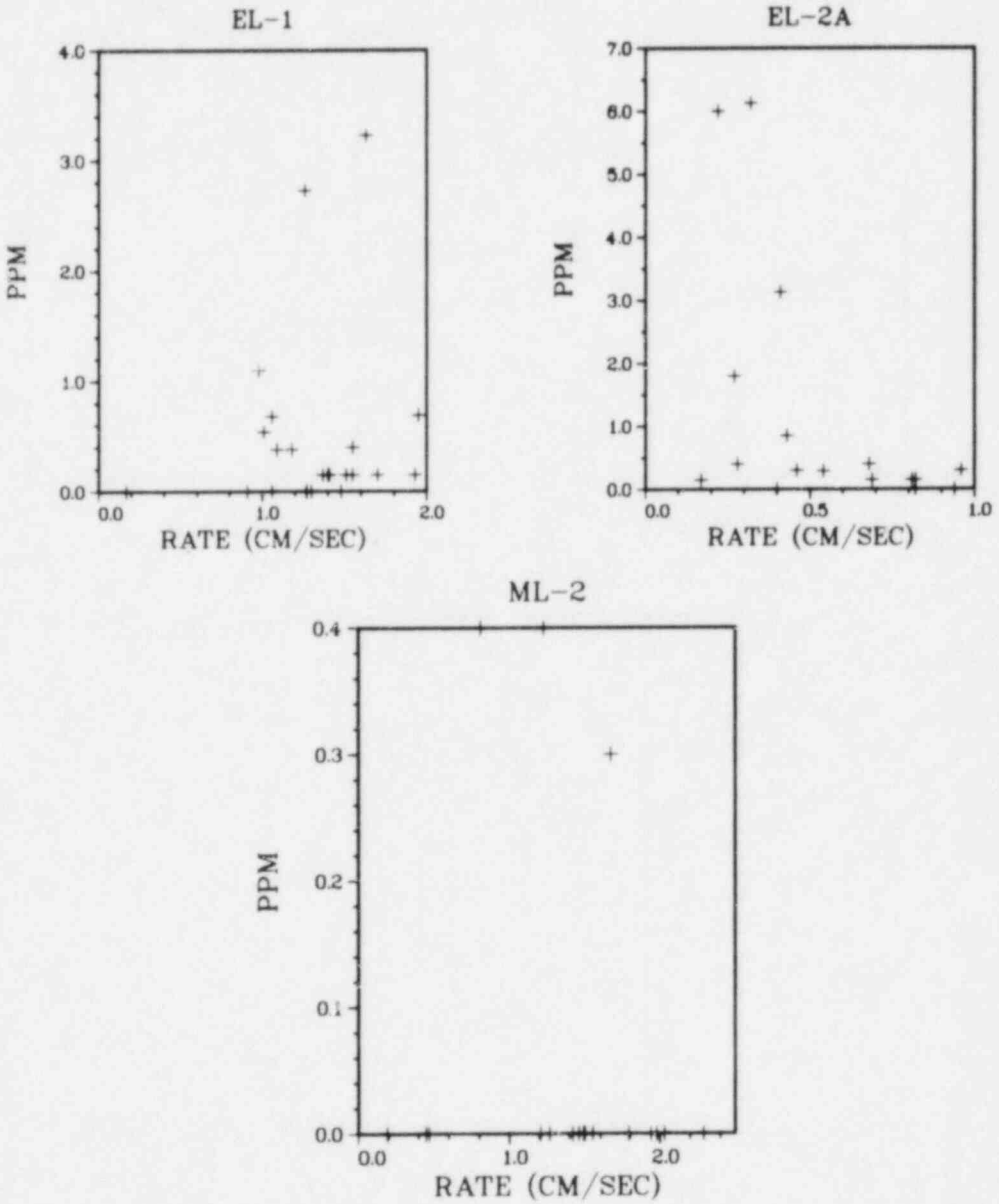

Figure 1.1.11

STRONTIUM VS. RATE, PGX GRAPHITE

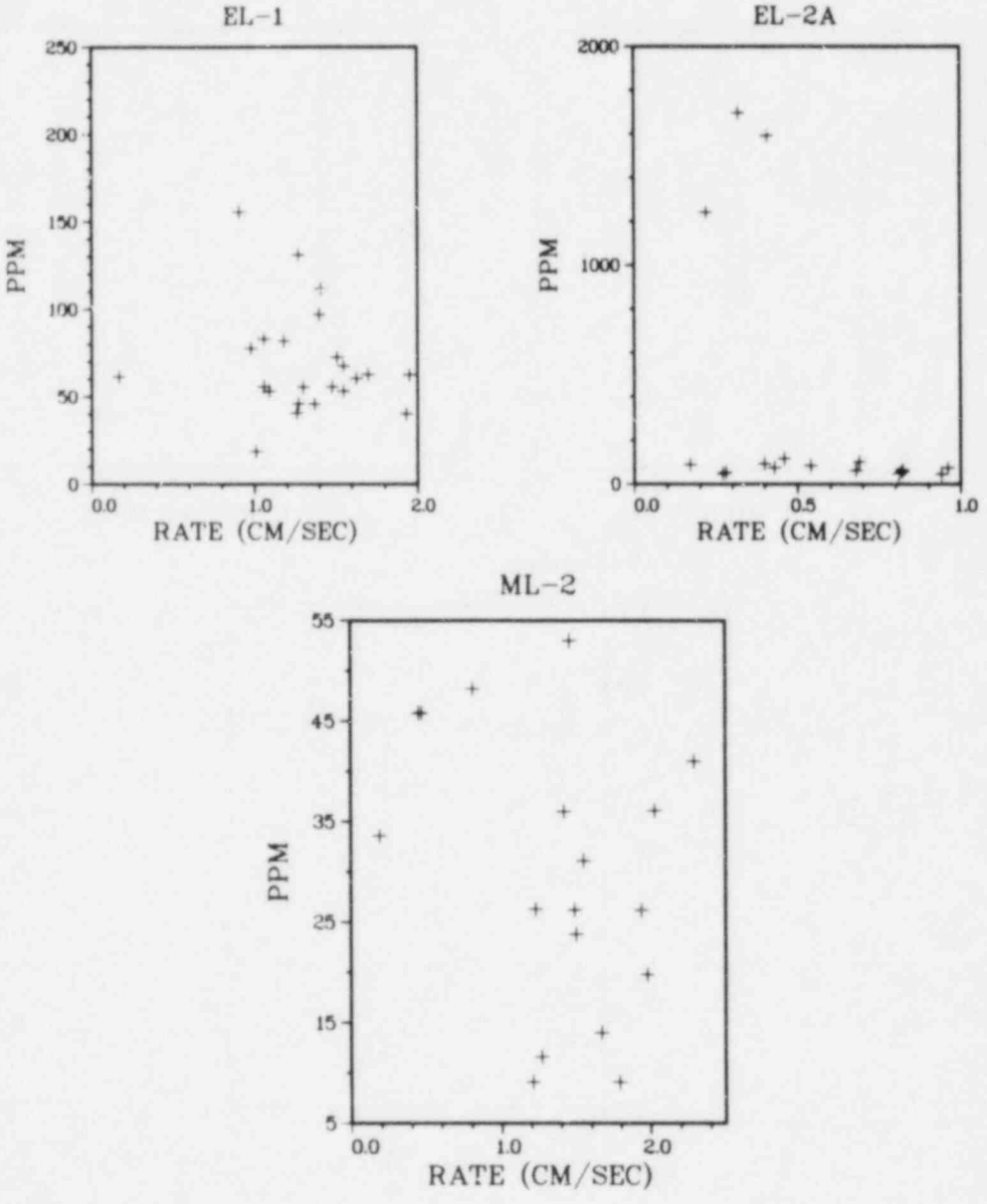

Figure 1.1.12

BARIUM VS. RATE, PGX GRAPHITE

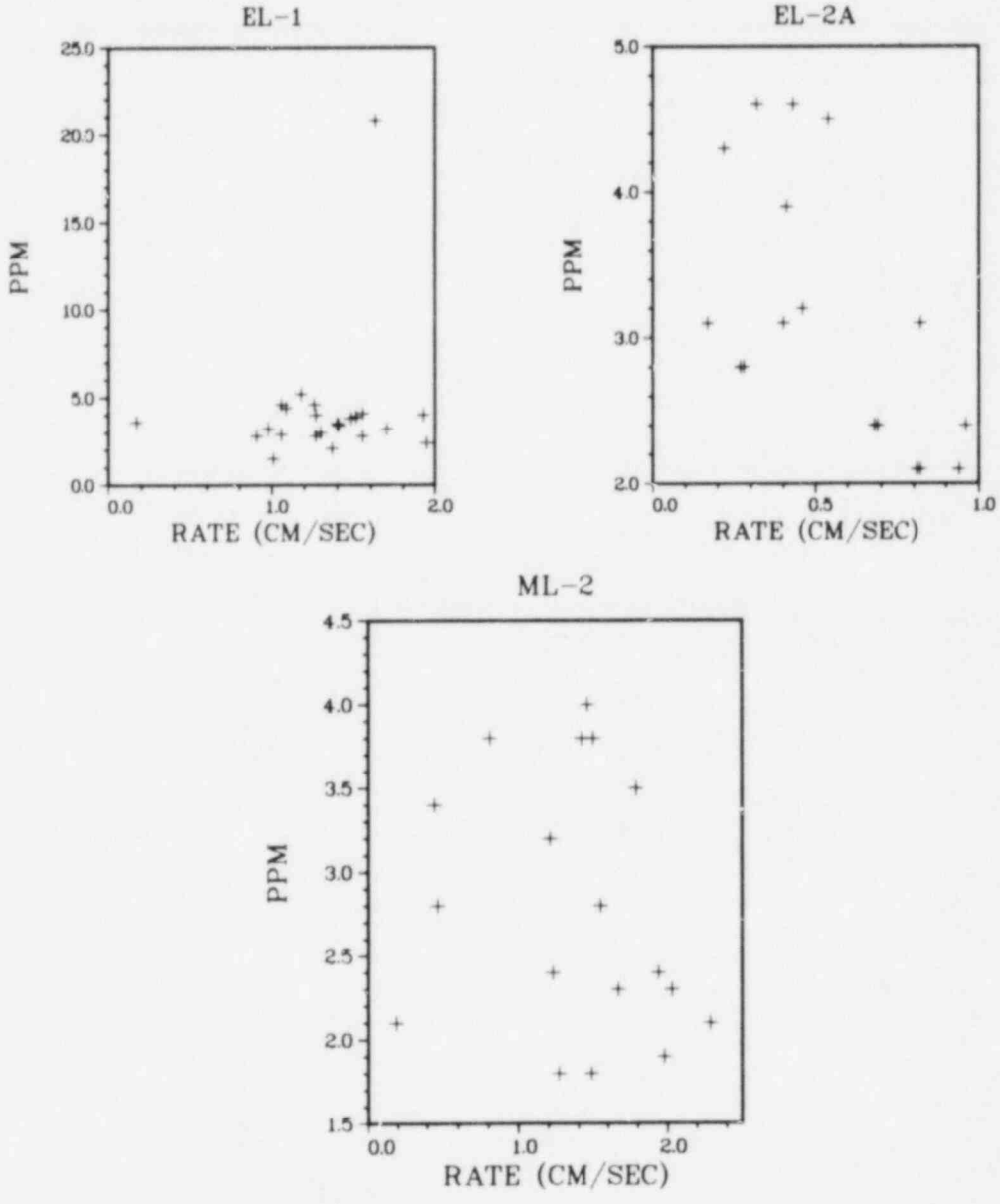

Figure 1.1.13

CALCIUM VS. RATE, PGX GRAPHITE

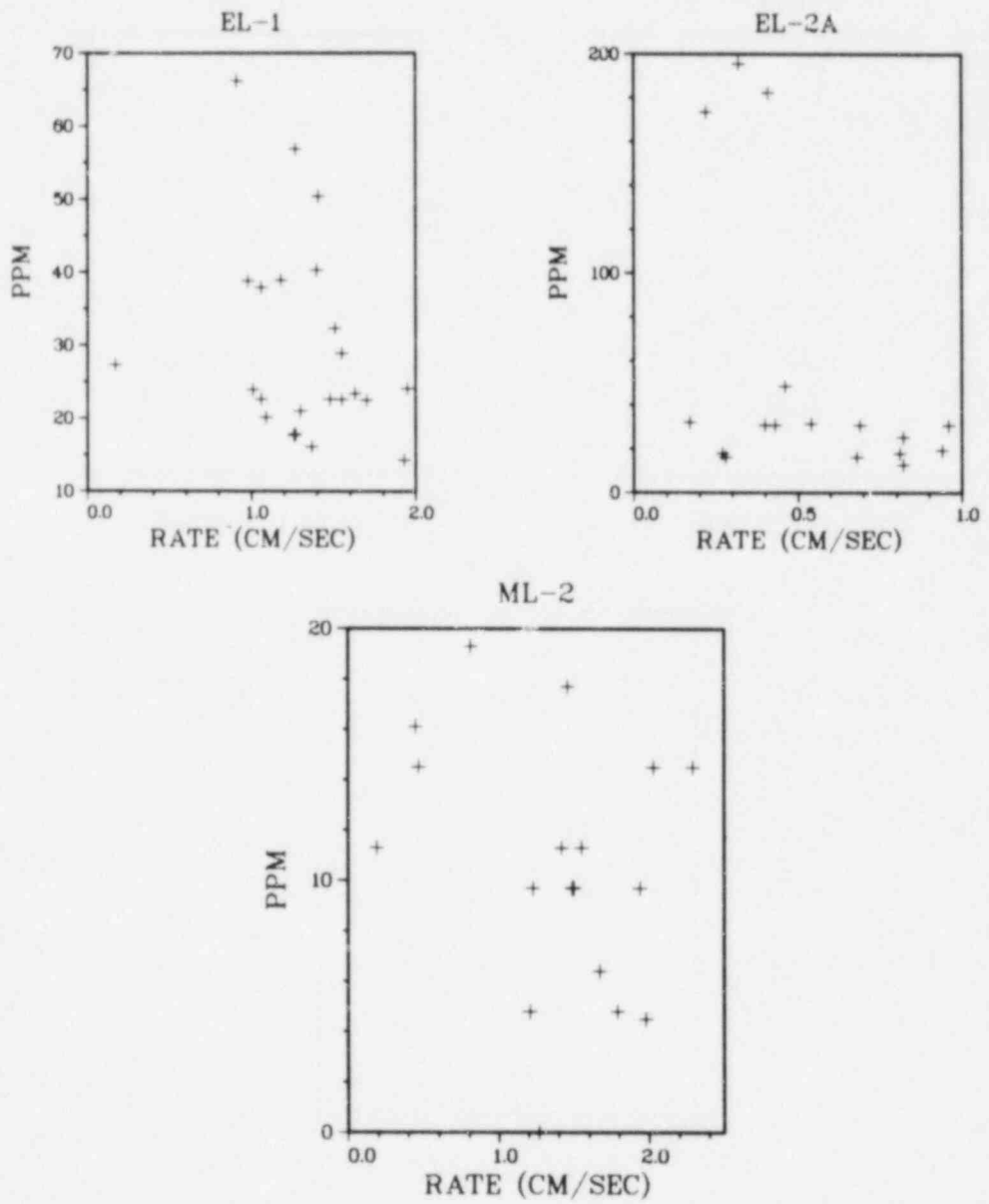

Figure 1.1.14

TITANIUM VS. RATE, PGX GRAPHITE

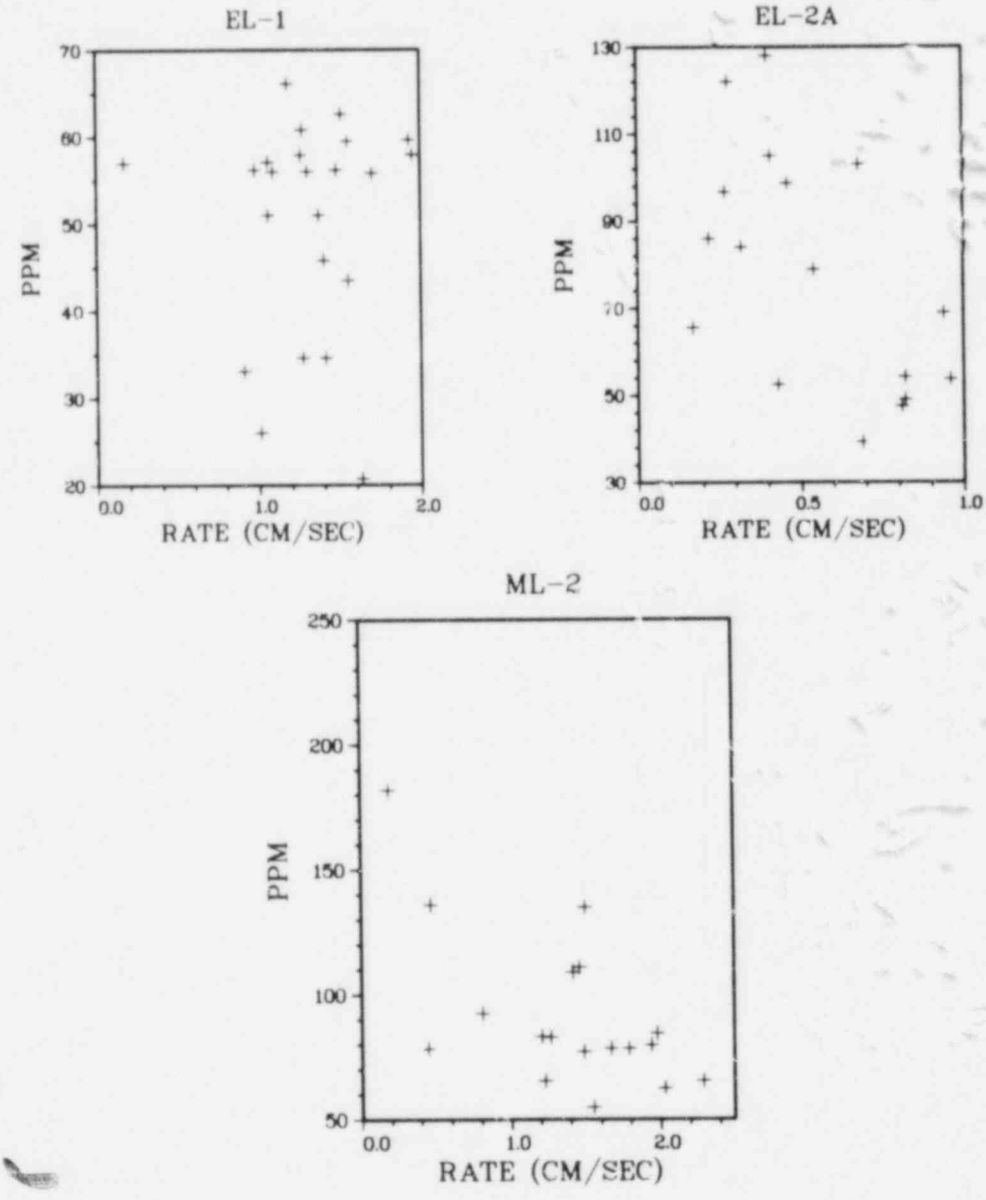

Figure 1.1.15

NICKEL VS. RATE, PGX GRAPHITE

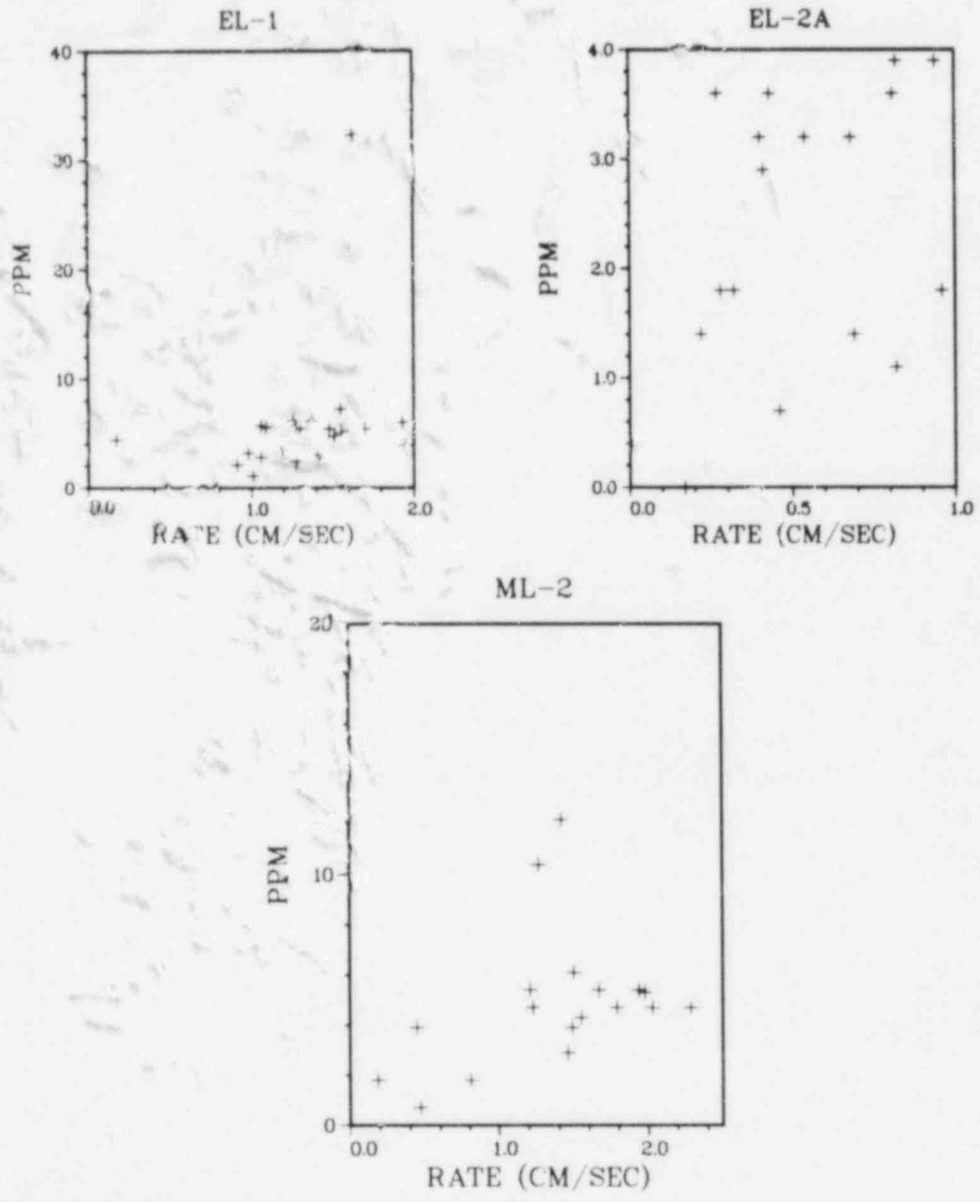

Figure 1.1.16

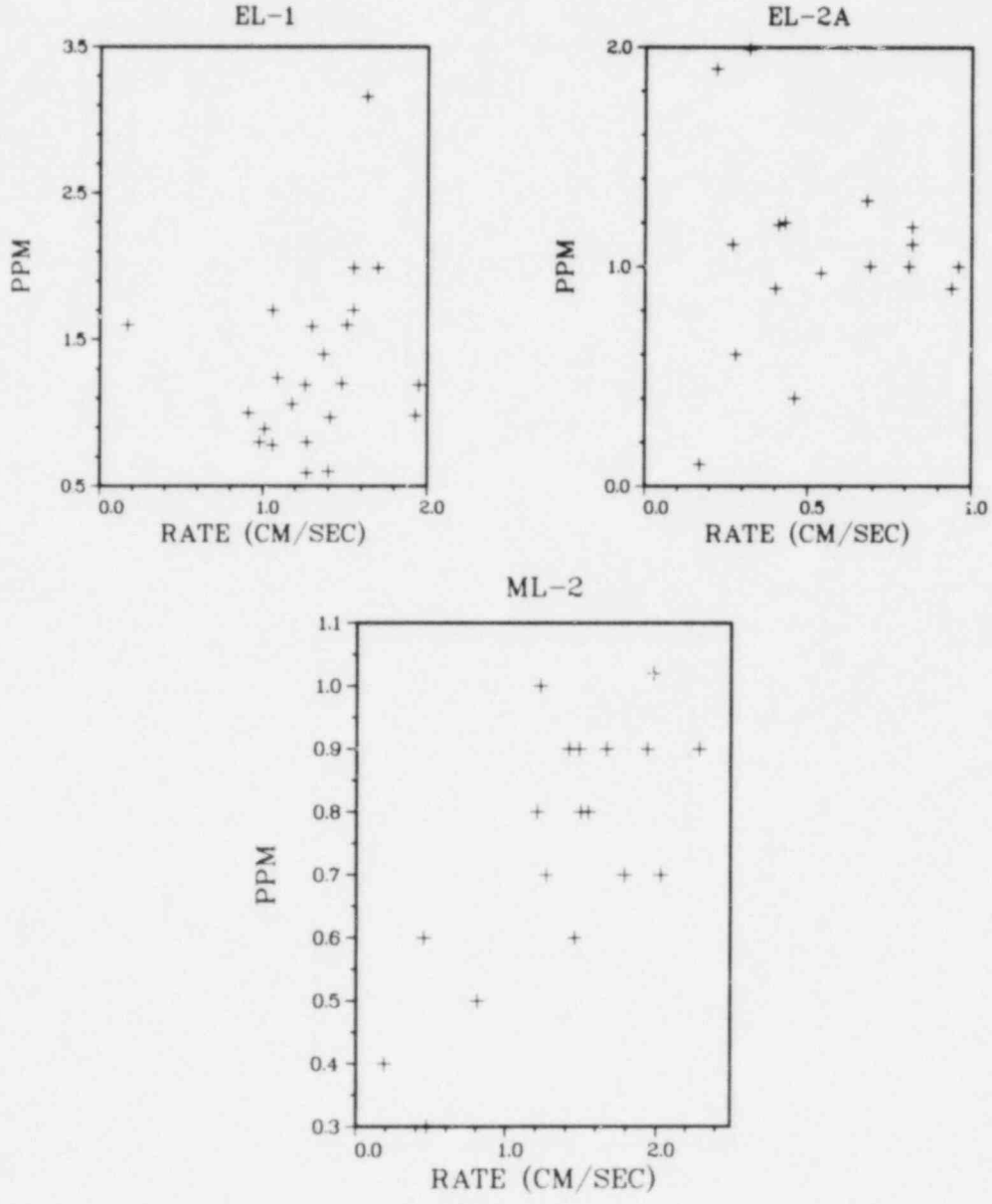
COPPER VS. RATE, PGX GRAPHITE
EL-1
PPM
3.5
2.5
1.5
0.5
0.0
1.0
2.0
RATE (CM/SEC)
EL-2A
PPM
2.0
1.0
0.0
0.0
0.5
1.0
RATE (CM/SEC)
ML-2
PPM
1.1
1.0
0.9
0.8
0.7
0.6
0.5
0.4
0.3
0.0
1.0
2.0
RATE (CM/SEC)

Figure 1.1.17

SULFUR VS. RATE, PGX GRAPHITE

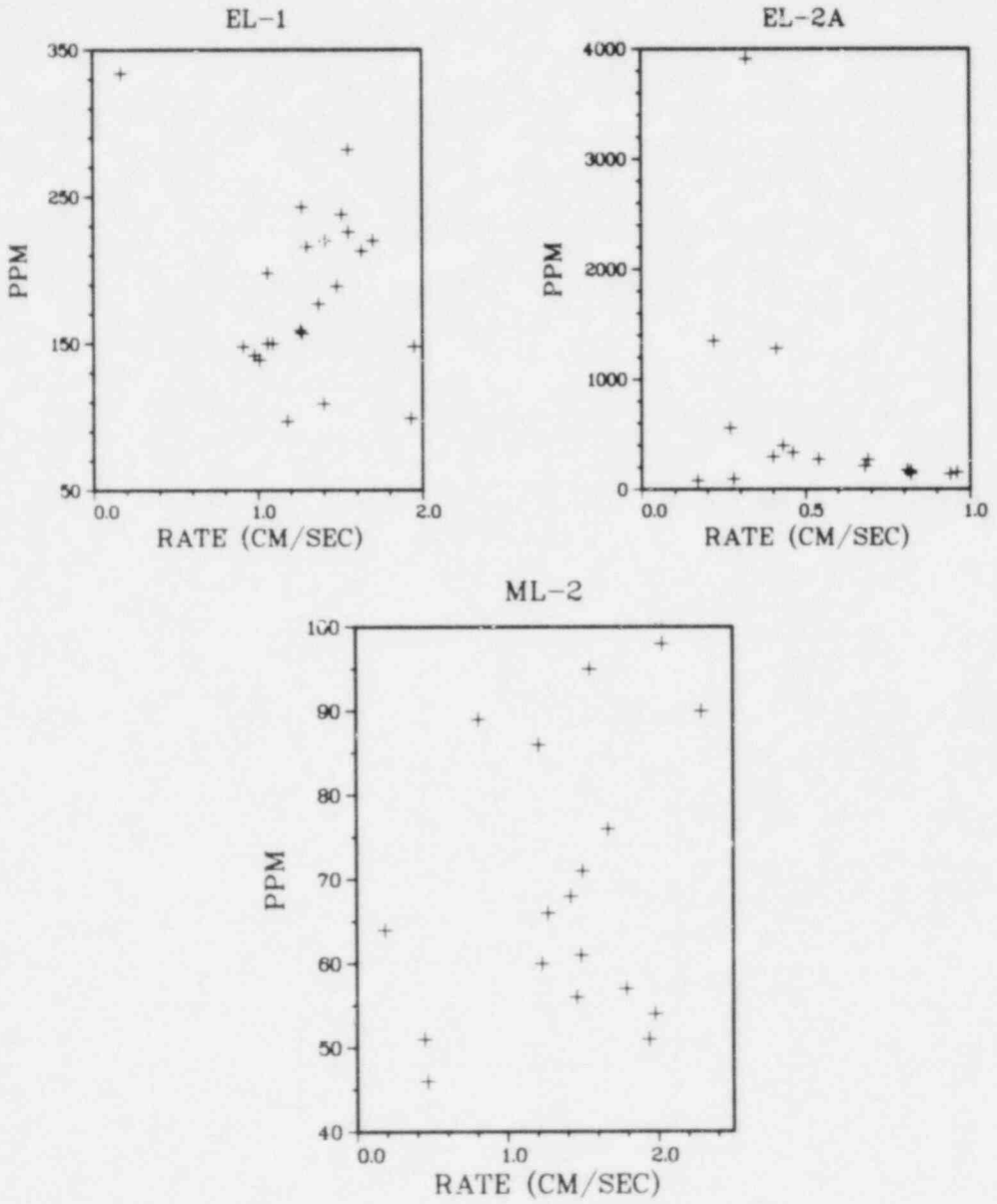

Figure 1.1.18

SILICON VS. RATE, PGX GRAPHITE

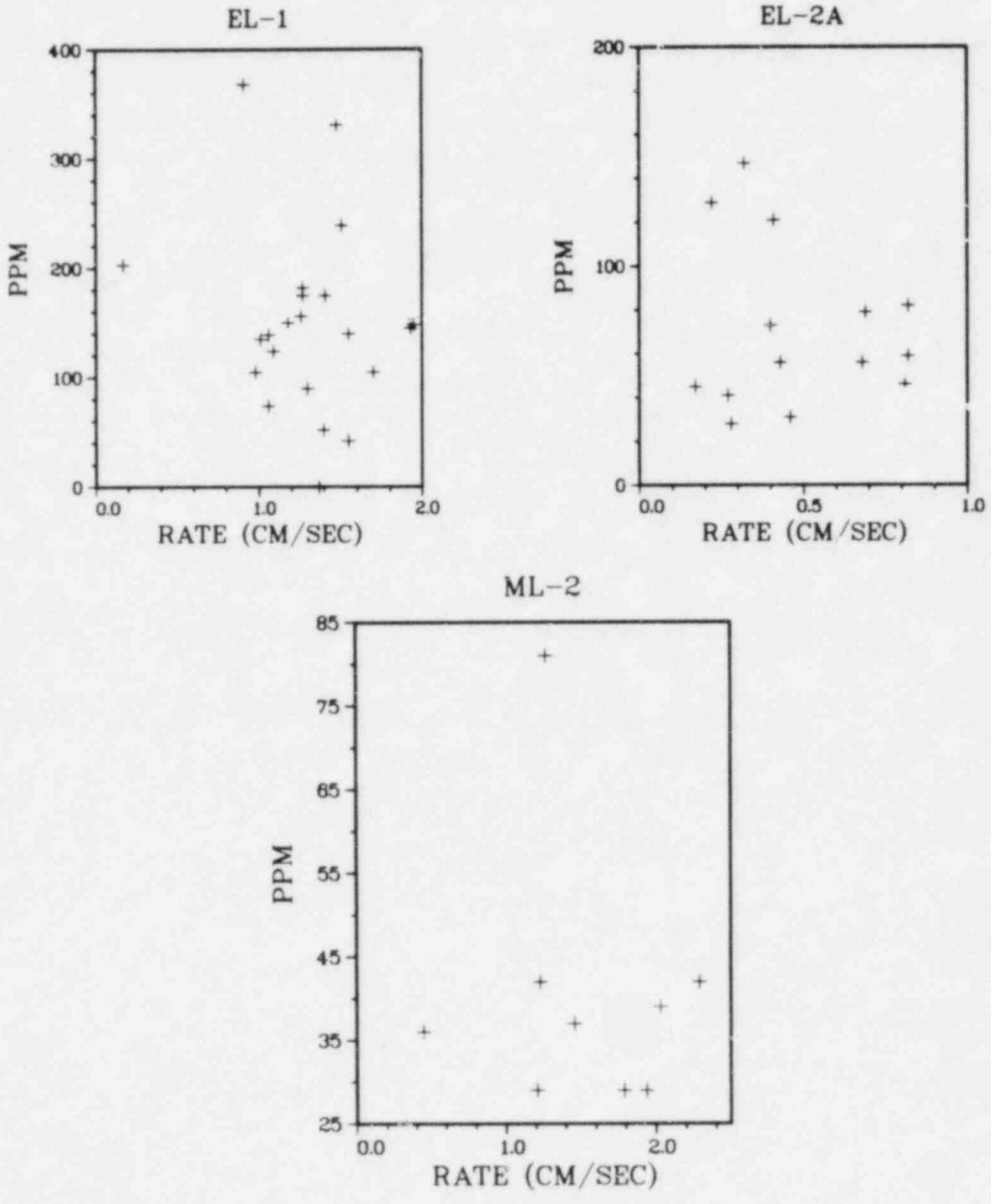

Figure 1.1.19

ALUMINIUM VS. RATE, PGX GRAPHITE

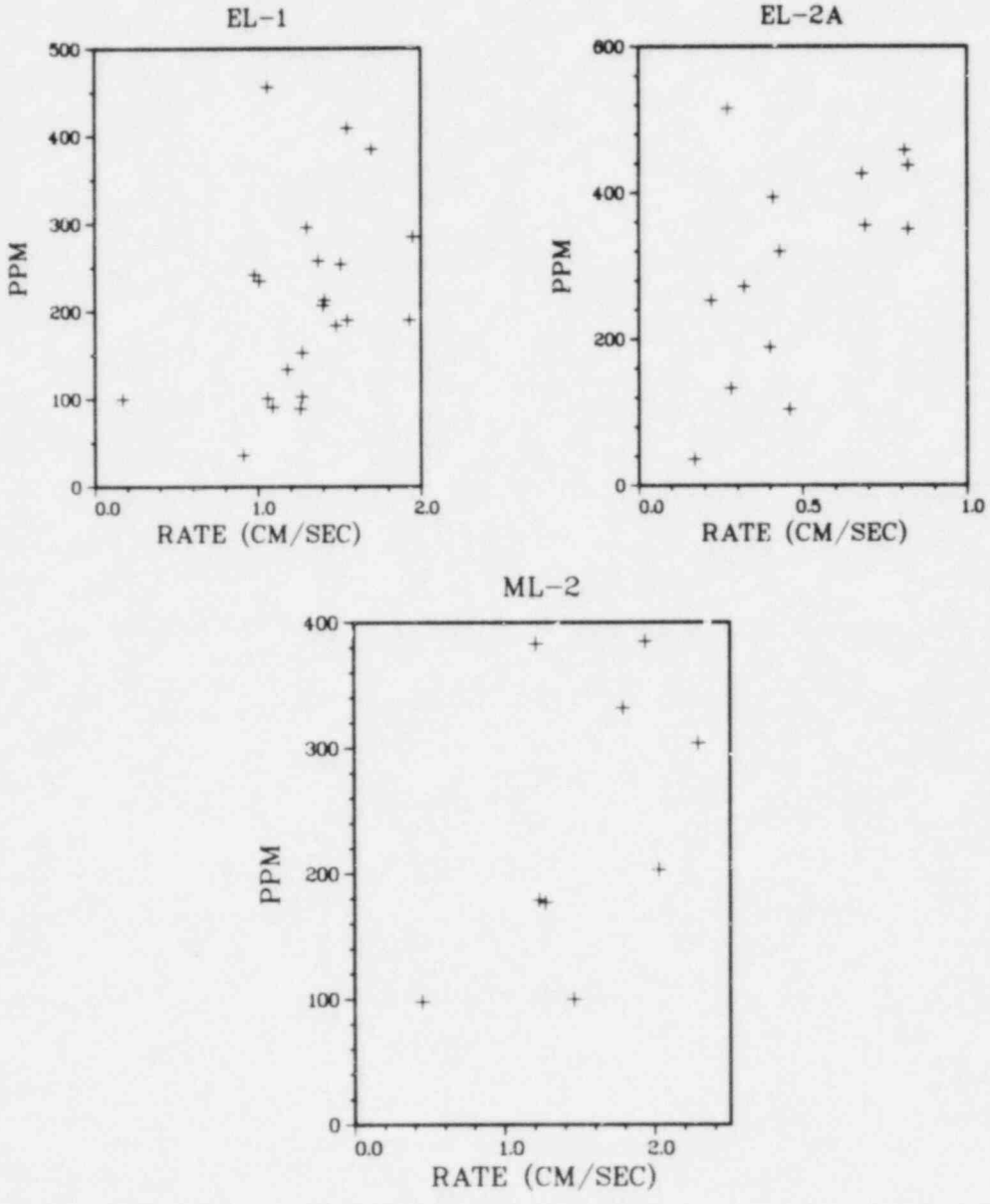

Figure 1.1.20

TOTAL IMPURITIES VS. RATE, PGX GRAPHITE

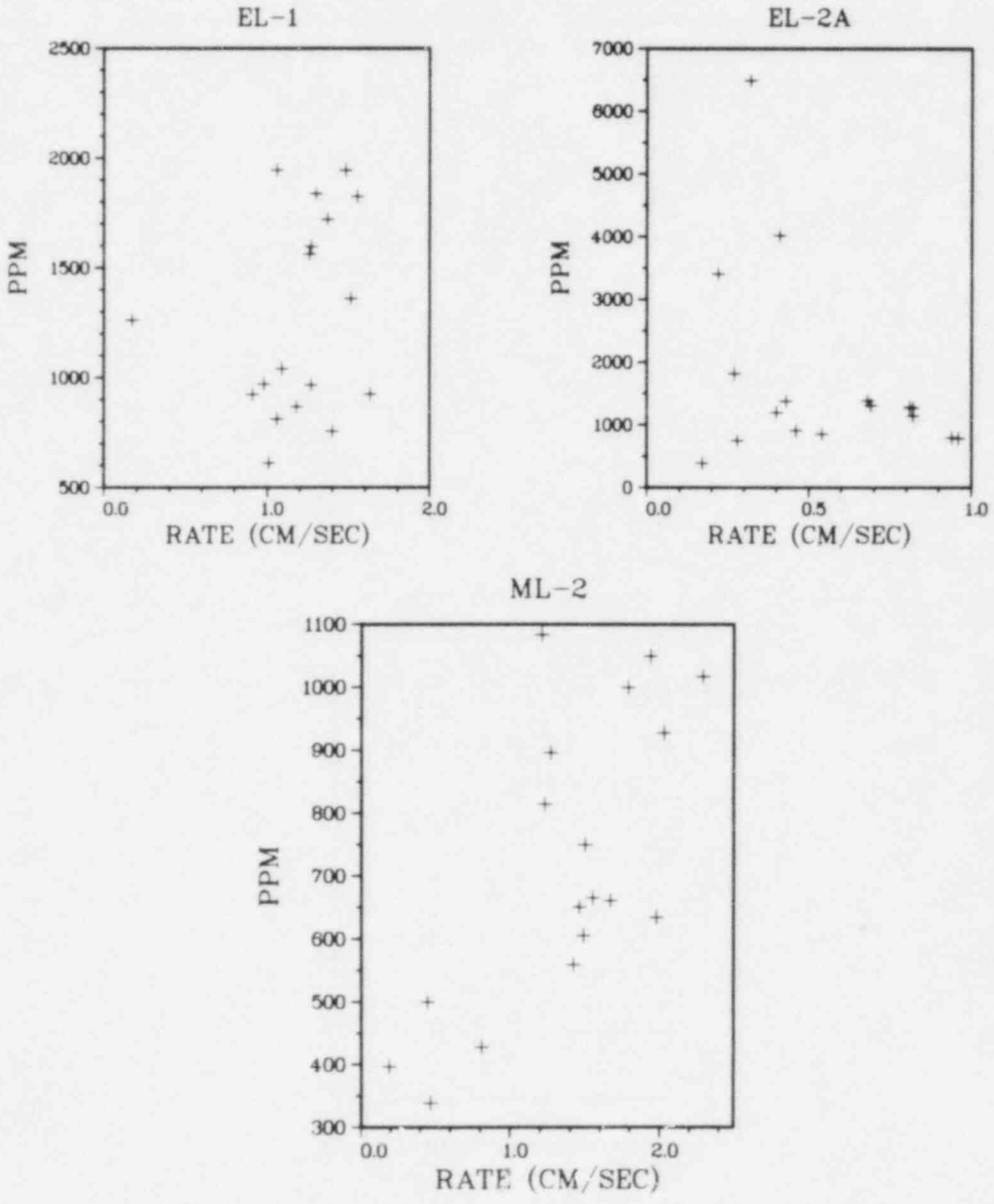

Figure 1.1.21

1.2 Materials

This program covers the evaluation of the mechanical properties of metallic materials. The objectives of the work are to critically review available materials data pertinent to steam cycle HTGR safety, identify areas where information is sparse or unavailable, and to design and initiate experiments to yield data which will permit accurate assessments to be made of materials related safety problems.

1.2.1 Fatigue of Structural Materials (P. Soo, R. Sabatini, L. Gerlach)

The current program on high cycle fatigue is designed to evaluate potential safety problems connected with mechanical failure in rapidly vibrating HTGR components such as those to be found in steam generators, thermal barriers and helium circulators, etc. At the present time the effect of large accumulations of fatigue cycles is largely unknown so that the lifetimes of many components in an HTGR system cannot be accurately quantified. In addition, the high temperatures that are frequently present may cause surface oxidation of metals as well as internal structural changes which must be understood if the integrity of a component is to be assured over the life of the reactor.

Chemical analyses for test alloys are given in Table 1.2.1. At the present time the main alloy being evaluated in this work is Incoloy 800H, used in steam generator tubing.

Table 1.2.1

Chemical Analyses of Test Materials

	C	P	S	Mn	Si	Cr	Ni	Mo	Fe	Others
Incoloy 800H (Ht. HH7427A)	0.05	NA	0.003	0.67	0.46	19.83	32.17	NA	Bal.	0.65 Cu 0.43 Ti 0.39 Al
Hastelloy-X (Ht. 4-2809)	0.11	0.02	0.008	0.50	0.41	20.67	Bal.	8.86	18.66	2.10 Co 0.55 W

Note: NA = Not analyzed. All concentrations in wt. percent.

All current in-helium testing is carried out using gas obtained from the Materials Test Loop (MTL) operating at a pressure of 1.3 atmospheres. The flow rate through each test capsule is 2 liter/min. (4 cu.ft./hr.). The test helium contains 5-10 μatm. H_2O, 200 μatm. H_2, 40 μatm. CO, 20 μatm. CH_4, and 10 μatm. CO_2. Fatigue tests are being performed with MTS machines under load control at a frequency of 40 Hz. A sinusoidal load waveform is used.

1.2.1.1 Incoloy 800H Loss-of-Cooling Tests

During this quarter, the loss-of-cooling tests on Incoloy 800H were completed. This series of tests was initiated to determine whether high temperature thermal transients could adversely affect high-cycle fatigue strength during subsequent reactor operations. The baseline test temperature for

fatigue cycling was chosen to be 538°C (1000°F) with all tests being carried out in the HTGR helium specified in Section 1.2.1. The thermal transient tests were carried out using the following standardized procedure:

(a) Fatigue specimens at 538°C to 10^5 cycles at a frequency of 40 Hz and stop the test.

(b) Ramp the temperature from 538°C (1000°F) to 871°C (1600°F) in a time of about 30 minutes and hold at 871°C for 24 h. Cool to 538°C in about 15 minutes. Maintain a stress of approximately zero during the transient by applying a very small 'ripple' stress to the specimen. In a second series of tests the same procedure was used but the transient adopted was 24h/760°C (1400°F).

(c) Cycle the sample to failure at 538°C (1000°F) at the original stress level.

(d) Compare the total cycles to failure (including the initial 10^5 cycles) to the N_f values for uninterrupted tests.

Table 1.2.2 and Figure 1.2.1 show results obtained. For the 871°C (1600°F) transient there is a large loss in fatigue strength compared to the uninterrupted tests in helium. This strength loss begins after about 2 x 10^5 cycles. For the 871°C (1600°F) transient tests a new fatigue limit of 190 MPa (28 ksi) becomes established after approximately 10^8 cycles. In the case of the 760°C (1400°F) transient there is a much smaller loss in strength and the fatigue limit is decreased by about 5 percent.

An interesting point to note is the much lower fatigue strength observed in the uninterrupted air tests. The strength in air at 10^6 cycles is approximately 20 percent lower than that for helium. The fatigue limit for air is similar to that for the 871°C (1600°F) transient tests.

In the last quarterly report (Soo, 1982) a fractographic analysis was performed to determine if there were noticeable differences in the fracture behavior of specimens tested continuously in helium and those subjected to the two thermal transients. Specimens which failed after about 10^6 cycles were selected for evaluation. A comparison of fracture characteristics observed under the scanning electron microscope revealed no significant differences for the 3 conditions. In this reporting period, 3 similar but long term test specimens were evaluated which had accumulated between 5-9 x 10^6 cycles in order to determine whether the significant differences in fatigue strength shown in Figure 1.2.1 could be explained in terms of a change in fracture characteristics. Figures 1.2.2 through 1.2.6 show the data obtained. In common with the 10^6 cycle specimens examined previously, there were no significant fractographic differences. Ductile behavior was always noticed. Any changes brought about by the high temperature transient are apparently not distinguishable by standard fractographic analysis using the scanning electron microscope.

Table 1.2.2
Effect of High-Temperature Thermal Excursions on the High-Cycle Fatigue Life of Incoloy 800H at 538°C (1000°F) in Dry Helium

Specimen	Test Temp (°C)	Test Temp (°F)	Test Env.	Thermal Excursion	Cyclic Stress (MPa)	Cyclic Stress (ksi)	Cycles to Failure (N_f)
MNF-328	538	1000	Air	None	276.0	40.0	1.4×10^4
MNF-330	538	1000	Air	None	262.0	38.0	5.0×10^4
MNF-340	538	1000	Air	None	262.0	38.0	2.0×10^4
MNF-327	538	1000	Air	None	248.0	36.0	1.3×10^5
MNF-331	538	1000	Air	None	241.0	35.0	1.3×10^5
MNF-332	538	1000	Air	None	228.0	33.0	2.2×10^5
MNF-336	538	1000	Air	None	214.0	31.0	1.3×10^5
MNF-334	538	1000	Air	None	207.0	30.0	2.1×10^5
MNF-337	538	1000	Air	None	207.0	30.0	1.1×10^5
MNF-341	538	1000	Air	None	200.0	29.0	3.0×10^5
MNF-334	538	1000	Air	None	200.0	29.0	$>1.1 \times 10^5$
MNF-333	538	1000	Air	None	193.0	28.0	$>1.0 \times 10^5$
MNF-301	538	1000	He	None	290.0	42.0	1.5×10^4
MNF-300	538	1000	He	None	276.0	40.0	4.0×10^4
MNF-303	538	1000	He	None	269.0	39.0	2.3×10^5
MNF-304	538	1000	He	None	262.0	38.0	9.8×10^4
MNF-298	538	1000	He	None	255.0	37.0	8.7×10^4
MNF-302	538	1000	He	None	248.0	36.0	$>1.9 \times 10^7$ (1)
MNF-299	538	1000	He	None	241.0	35.0	6.3×10^4
MNF-311	538	1000	He	None	234.0	34.0	$>1.9 \times 10^7$ (1)
MNF-312	538	1000	He	None	234.0	34.0	$>2.5 \times 10^5$
MNF-318	538	1000	He	24h/760°C	269.0	39.0	1.4×10^5
MNF-338	538	1000	He	24h/760°C	269.0	39.0	4.4×10^5
MNF-315	538	1000	He	24h/760°C	255.0	37.0	4.8×10^5
MNF-323	538	1000	He	24h/760°C	248.0	36.0	4.1×10^5
MNF-314	538	1000	He	24h/760°C	241.0	35.0	2.1×10^5
MNF-324	538	1000	He	24h/760°C	234.0	34.0	5.1×10^5
MNF-335	538	1000	He	24h/760°C	234.0	34.0	5.4×10^5
MNF-316	538	1000	He	24h/760°C	228.0	33.0	9.3×10^5
MNF-321	538	1000	He	24h/760°C	228.0	33.0	$>2.3 \times 10^5$
MNF-325	538	1000	He	24h/760°C	228.0	33.0	5.7×10^7
MNF-322	538	1000	He	24h/760°C	221.0	32.0	$>7.7 \times 10^7$
MNF-317	538	1000	He	24h/760°C	207.0	30.0	$>2.0 \times 10^5$
MNF-309	538	1000	He	24h/871°C	276.0	40.0	1.0×10^5 (2)
MNF-306	538	1000	He	24h/871°C	269.0	39.0	2.4×10^5
MNF-305	538	1000	He	24h/871°C	255.0	37.0	1.7×10^5
MNF-308	538	1000	He	24h/871°C	248.0	36.0	1.3×10^5
MNF-307	538	1000	He	24h/871°C	241.0	35.0	1.9×10^5
MNF-310	538	1000	He	24h/871°C	228.0	33.0	6.3×10^5
MNF-313	538	1000	He	24h/871°C	207.0	30.0	2.2×10^5
MNF-320	538	1000	He	24h/871°C	193.0	28.0	$>3.3 \times 10^5$

Notes:
(1) Test terminated owing to failure in threaded shank region
(2) Failed after an additional 5300 cycles, i.e. total cycles to failure were 105,300.

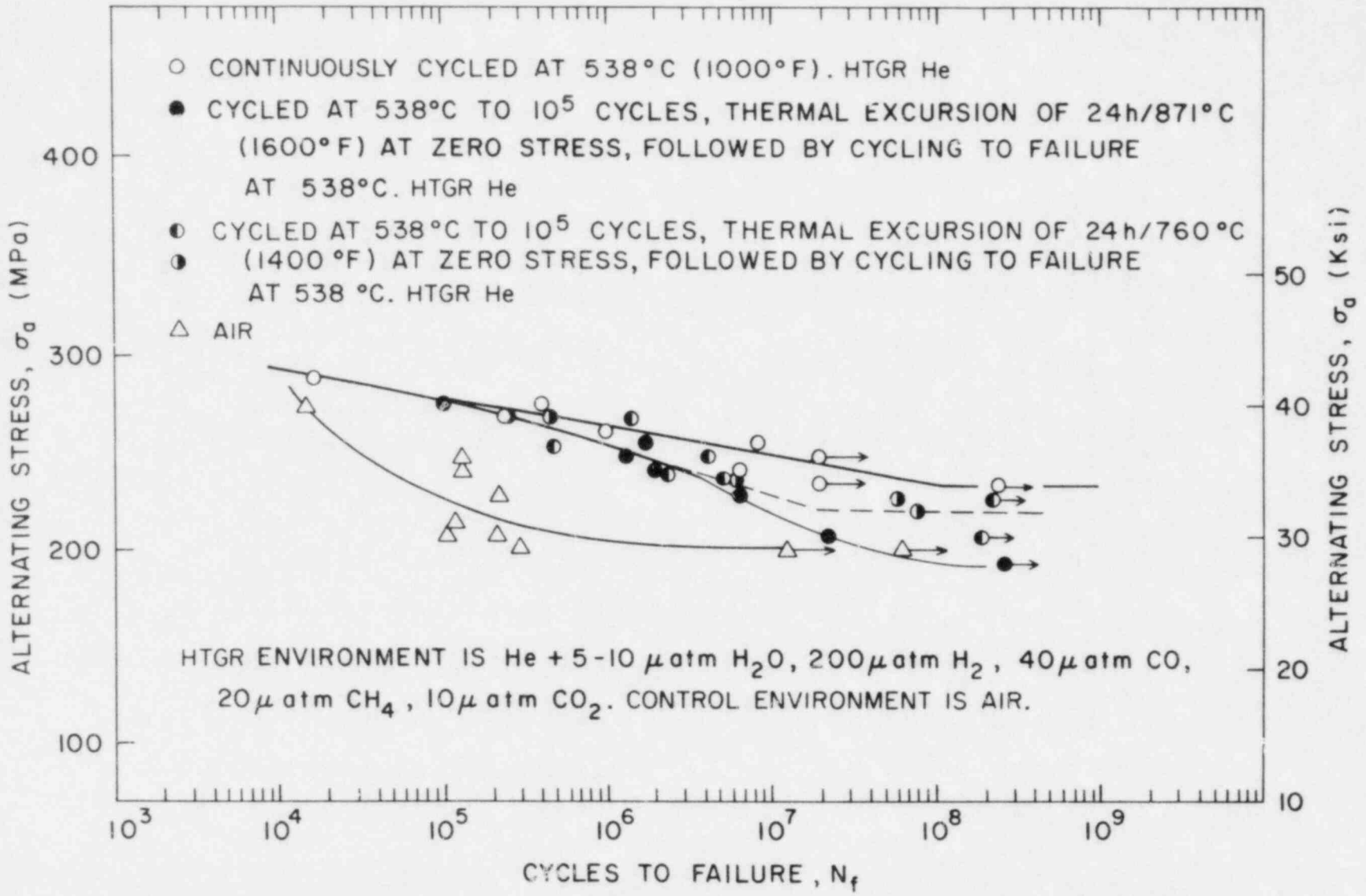

EFFECT OF HIGH TEMPERATURE THERMAL EXCURSIONS ON THE HIGH CYCLE FATIGUE OF INCOLOY 800H AT 538°C (1000°F) IN DRY HTGR HELIUM.

Figure 1.2.1

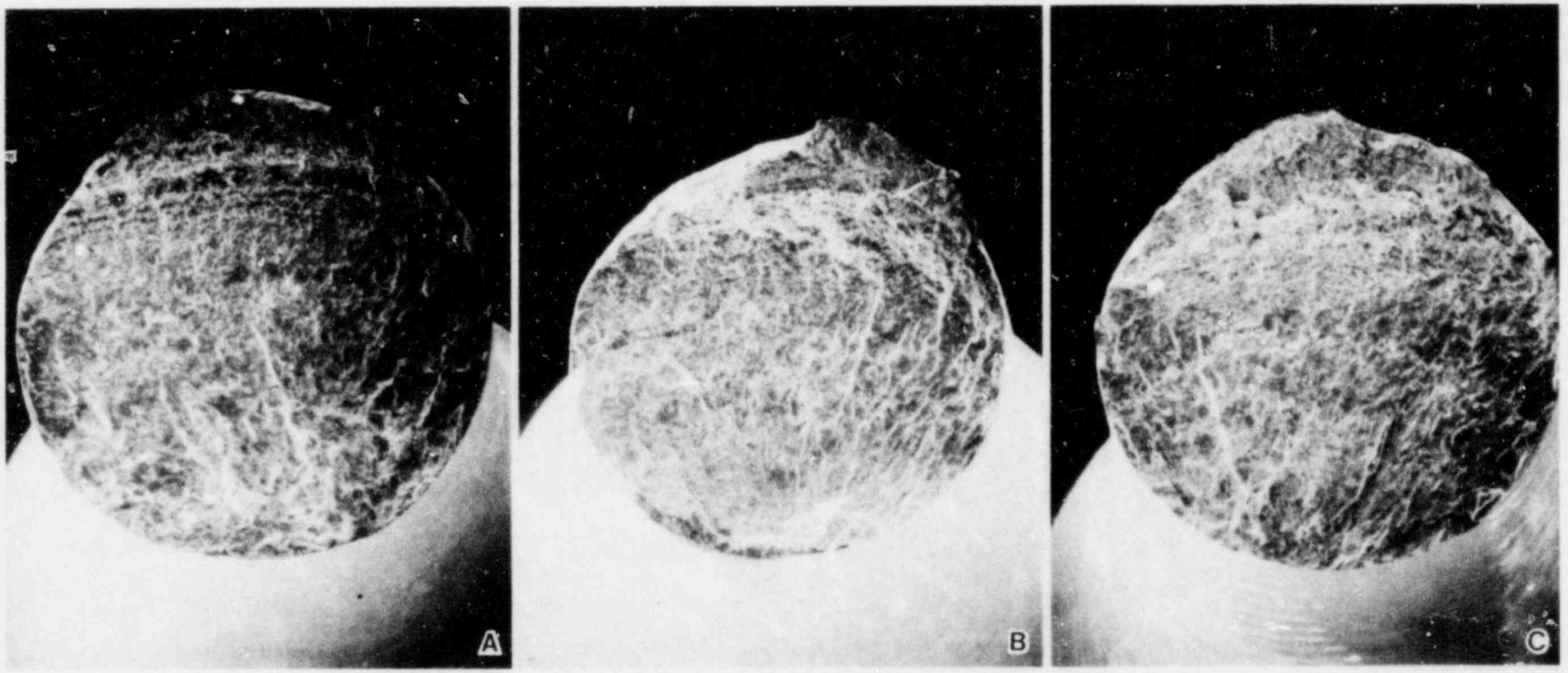

Fractographs of Incoloy-800H high cycle fatigue specimens tested at 538°C (1000°F) in HTGR He containing 5-10 μatm H_2O; (A) uninterrupted test; (B) thermal excursion after 10^5 cycles of 24 h/760°C (1400°F) at zero stress; (C) as for (B) but for 24 h/871°C (1600°F). Magnifications 9X.

Figure 1.2.2

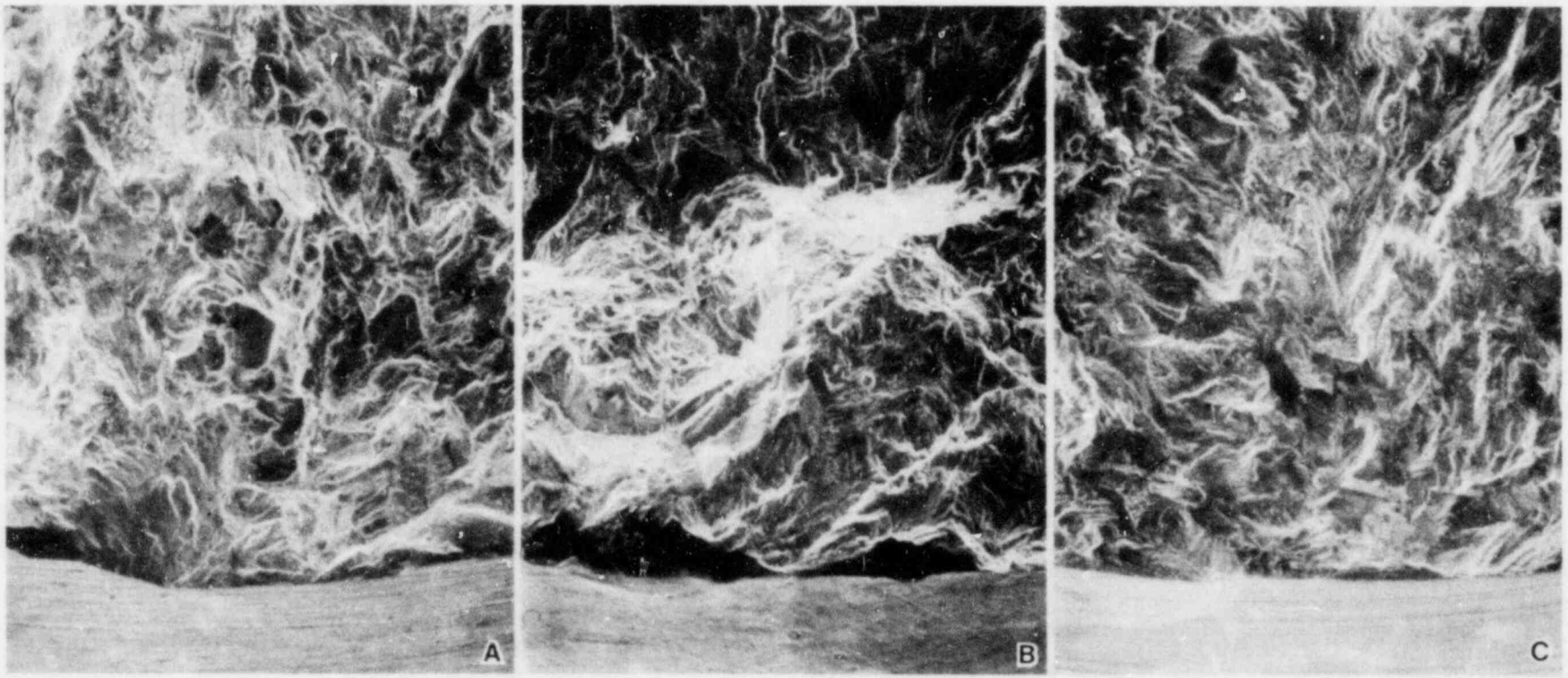

Crack initiation points in Incoloy-800H high cycle fatigue specimens tested at 538°C (1000°F) in HTGR He containing 5-10 μatm H_2O; (A) uninterrupted test; (B) thermal excursion after 10^5 cycles of 24 h/760°C (1400°F) at zero stress; (C) as for (B) but for 24 h/871°C (1600°F). Magnifications 90X.

Figure 1.2.3

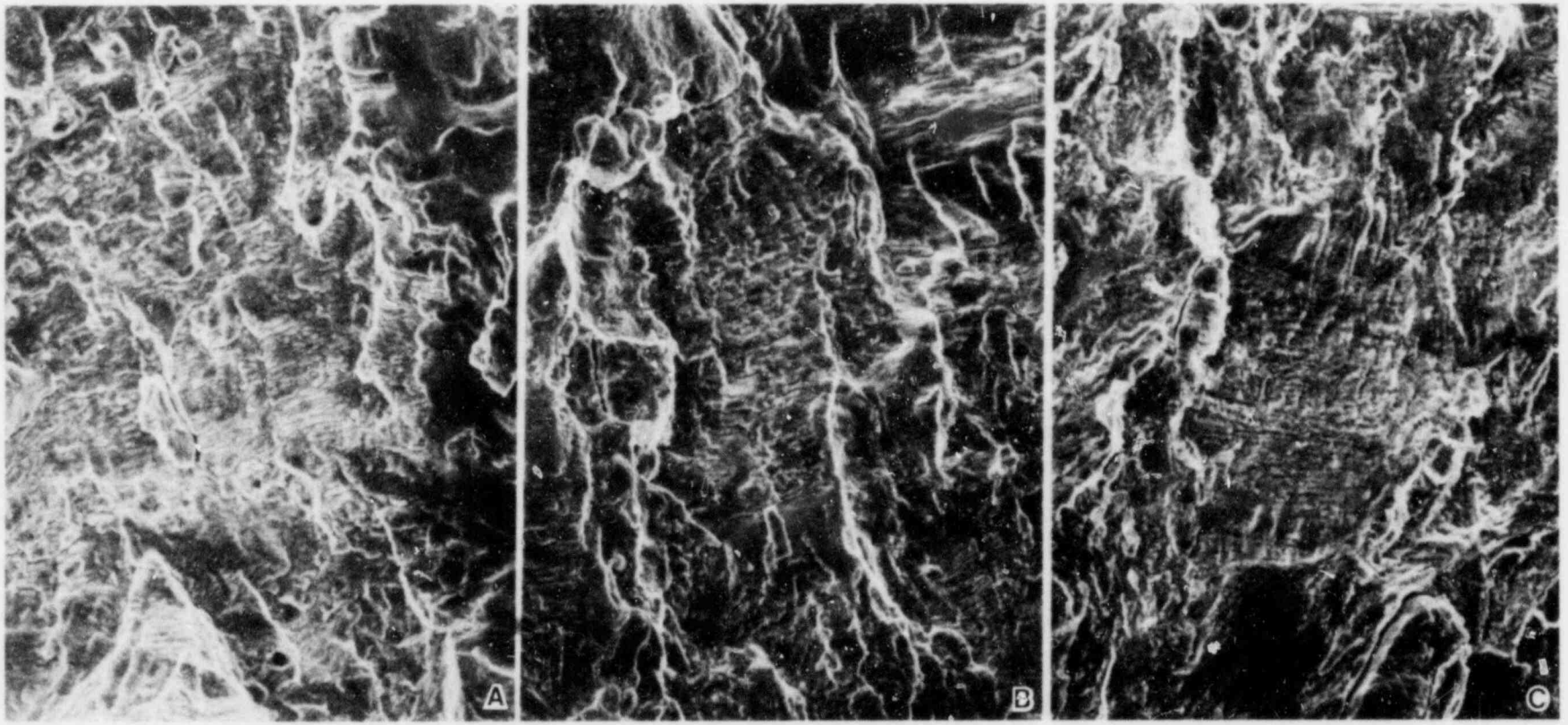

Striations in Incoloy-800H high cycle fatigue specimens tested at 538°C (1000°F) in HTGR He containing 5-10 μatm H_2O; (A) uninterrupted test; (B) thermal excursion after 10^5 cycles of 24 h/760°C (1400°F) at zero stress; (C) as for (B) but for 24 h/871°C (1600°F). Magnifications 200X.

Figure 1.2.4

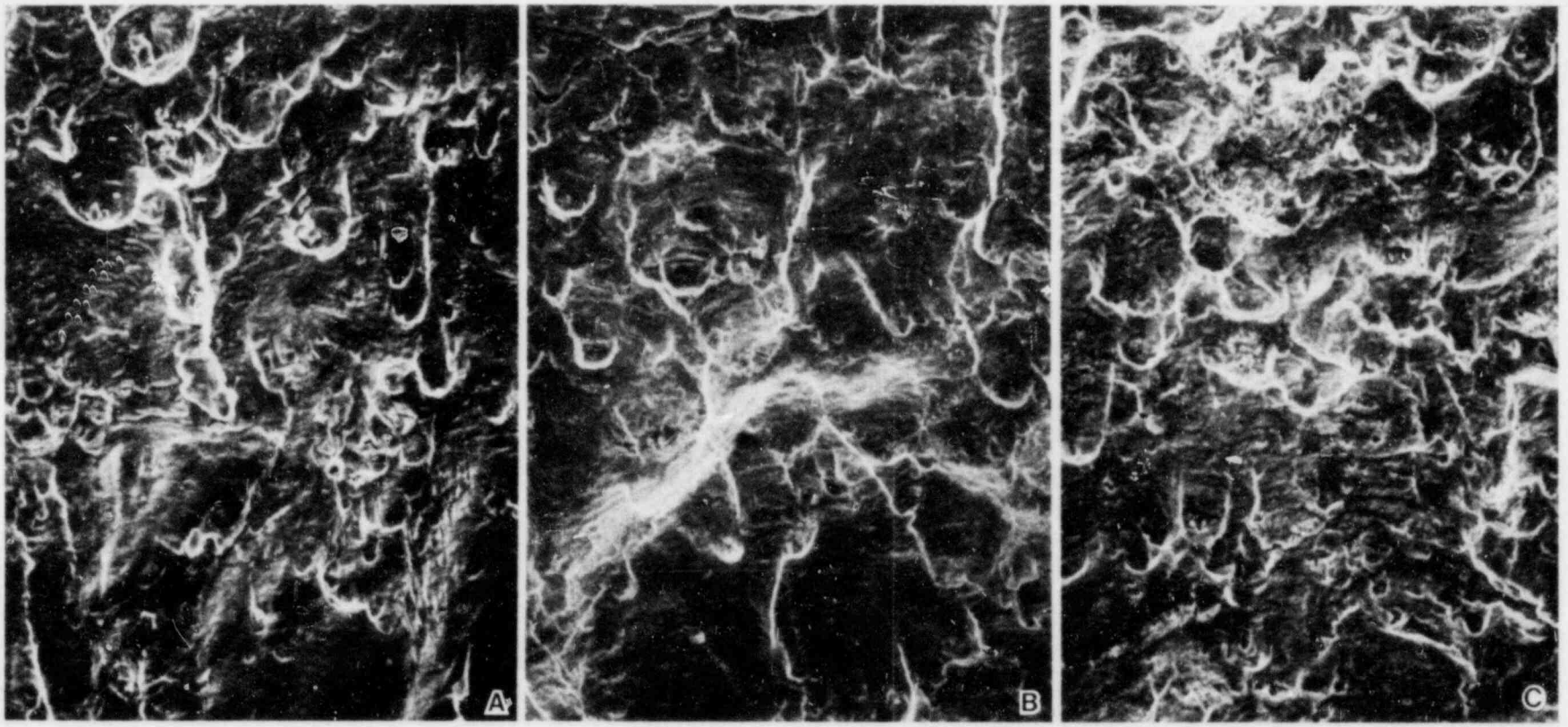

Ductile Dimples in Incoloy-800H high cycle fatigue specimens tested at 538°C (1000°F) in HTGR He containing 5-10 μatm H_2O; (A) uninterrupted test; (B) thermal excursion after 10^5 cycles of 24 h/760°C (1400°F) at zero stress; (C) as for (B) but for 24 h/871°C (1600°F). Magnifications 200X.

Figure 1.2.5

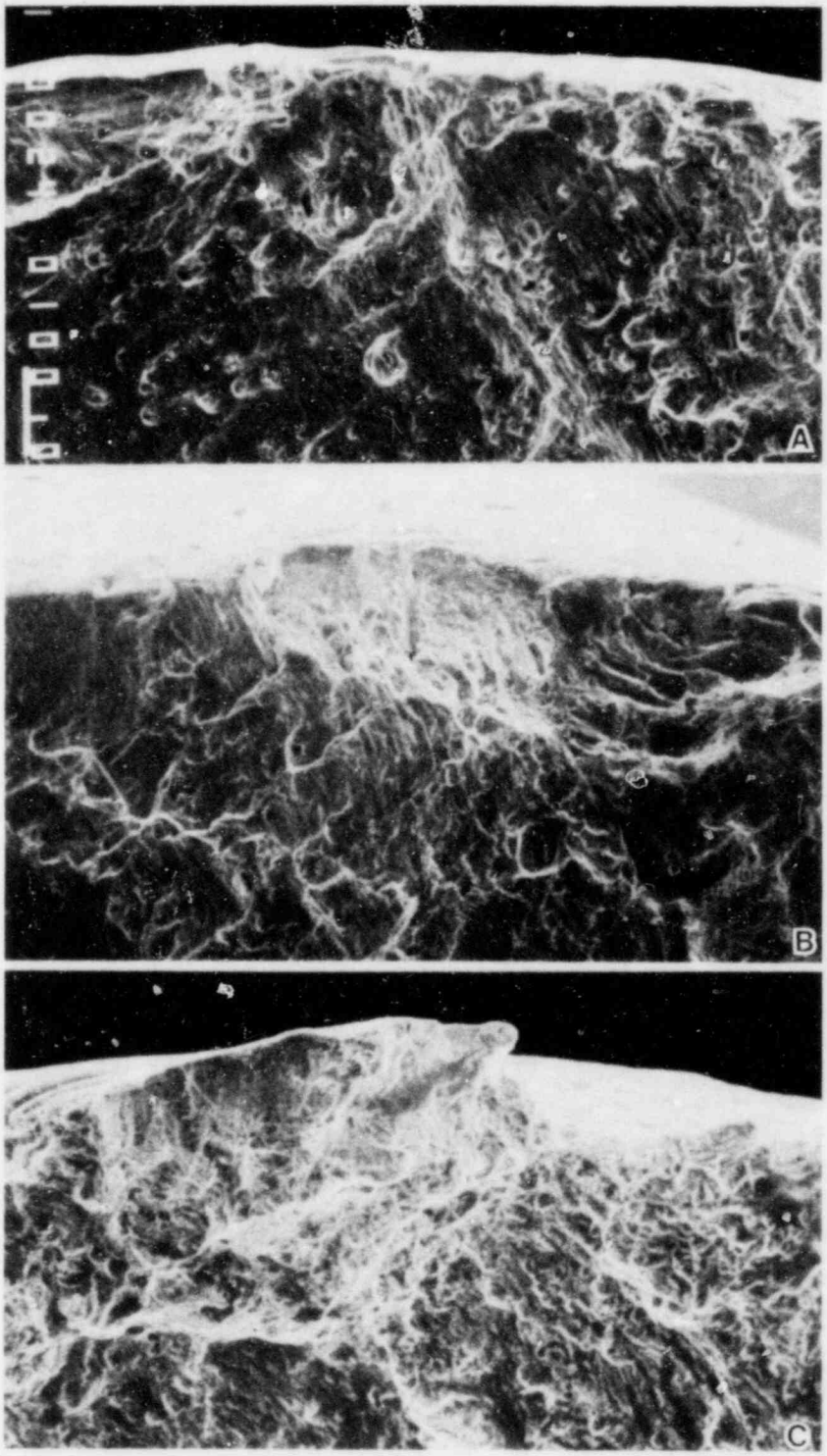

Appearance of edges of fracture surfaces in Incoloy-800H high cycle fatigue specimens tested at 538°C (1000°F) in HTGR He containing 5-10 μatm H_2O; (A) uninterrupted test; (B) thermal excursion after 10^5 cycles of 24 h/760°C (1400°F) at zero stress; (C) as for (B) but for 24 h/871°C (1600°F). Magnifications 120X.

Figure 1.2.6

As stated in the previous quarterly report (Soo, 1982) there are several mechanisms which could explain strength losses after a thermal transient. The most likely, however, is concerned with recrystallization of the cold worked surfaces of the specimens which were introduced by surface grinding during fabrication. These layers generally give rise to beneficial compressive stresses which give enhanced resistance to crack initiation. If they are removed by annealing processes, there would be an attendant loss in fatigue life.

Figure 1.2.7 shows data taken from earlier work by Soo (1980) for tests carried out in air and wet HTGR helium. They show microhardness measurements taken across the polished sections of failed fatigue samples. The locations of the individual curves give the approximate failure times. Note that for the helium tests at 760°C (1400°F) failed specimens such as MNF-145 show a very high surface hardness, indicating that the cold worked layer is still present. On the other hand, for specimens tested to about 10^7 cycles (100 h), surface recrystallization occurs. In the case of specimen MNF-142 it is complete, but specimen MNF-143 retains some surface deformation. These data give an explanation for the observed strength losses in the current loss-of-cooling tests. For example, some relaxation of the beneficial surface stresses will occur during the 24h/760°C (1400°F) thermal transient. This will probably not give complete recrystallization at the surface, so only a small loss in strength would result. However, for the 24h/871°C (1600°F) transient, complete surface recrystallization will occur, possibly with some recovery of the bulk work hardening introduced by the 10^5 fatigue cycles. At this temperature, then, a major loss in fatigue life would be expected upon refatiguing at 538°C (1000°F).

1.2.1.2 Metallography of Fatigued Incoloy-800H Specimens

Failed fatigue specimens of Incoloy 800H were sectioned, polished and examined under the optical and scanning electron microscopes to determine surface recrystallization and oxidation characteristics. Specimens evaluated were continuously cycled to failure at 760° and 871°C (1400 and 1600°F) in the reference helium test gas. Figure 1.2.8 shows micrographs of regions adjacent to the failure zones. With the exception of specimen MNF-276 all samples showed surface recrystallization. For the 760°C (1400°F) tests, however, there are small second phase particles in the surface layer, indicating that recrystallization may not be complete. Specimen MNF-269 shows two secondary transcrystalline fatigue cracks. Their etching characteristics show a broad crack 'width' consisting of an oxidized region adjacent to the crack itself. Earlier work (Soo,1980) showed that such cracks are indicative of a corrosion-fatigue process in which enhanced oxidation at the crack tip causes a reduction in fatigue strength when compared to an air environment.

A study was conducted on the nature of the oxide scale formed on fatigue specimens during cycling. Figure 1.2.9 shows scanning electron microscope/microprobe line scans across the sectioned polished surfaces of 2 Incoloy 800H specimens. One was tested at 760°C (1400°F) and the other at 871°C (1600°F). The oxide scale is very thin and, for the 760°C (1400°F) test, is fragmented. Beneath the scale the recrystallized surface region is well defined by the metallographic etching process. Compared to earlier tests carried out in air and wet (2500 μatm H_2O) helium the oxide scales observed show significantly different characteristics. For example, in the current

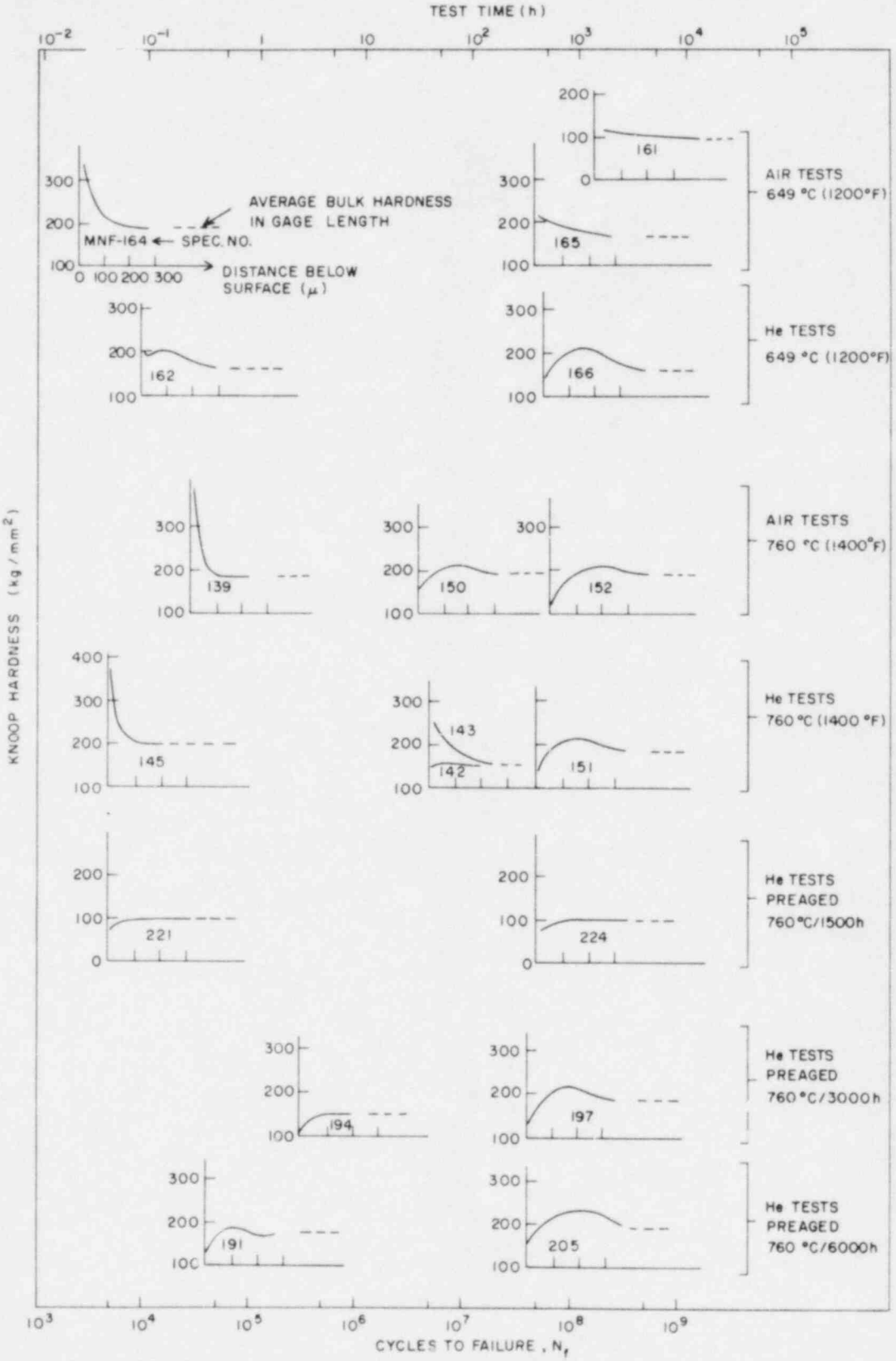

SCHEMATIC OF SURFACE HARDNESS PROFILES FOR INCOLOY 800H FATIGUE SPECIMENS AS A FUNCTION OF TEST TEMPERATURE, TEST ENVIRONMENT AND THERMAL PREAGING CONDITION.

Figure 1.2.7

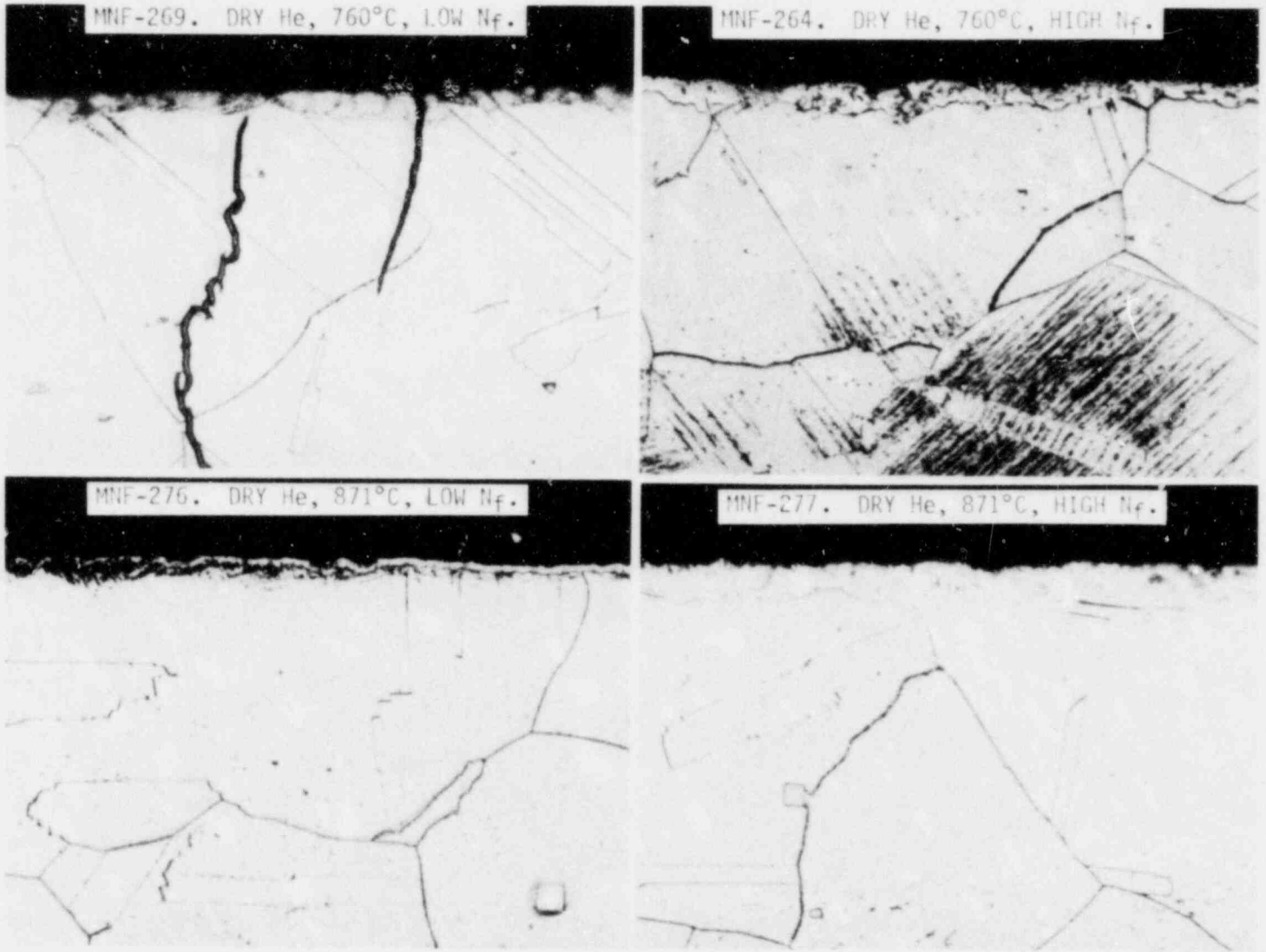

Figure 1.2.8. Effect of test time and test temperature on the surface microstructure of Incoloy-800H high cycle fatigue specimens tested in HTGR helium containing 5-10 μatm H_2O. Magnifications 450X.

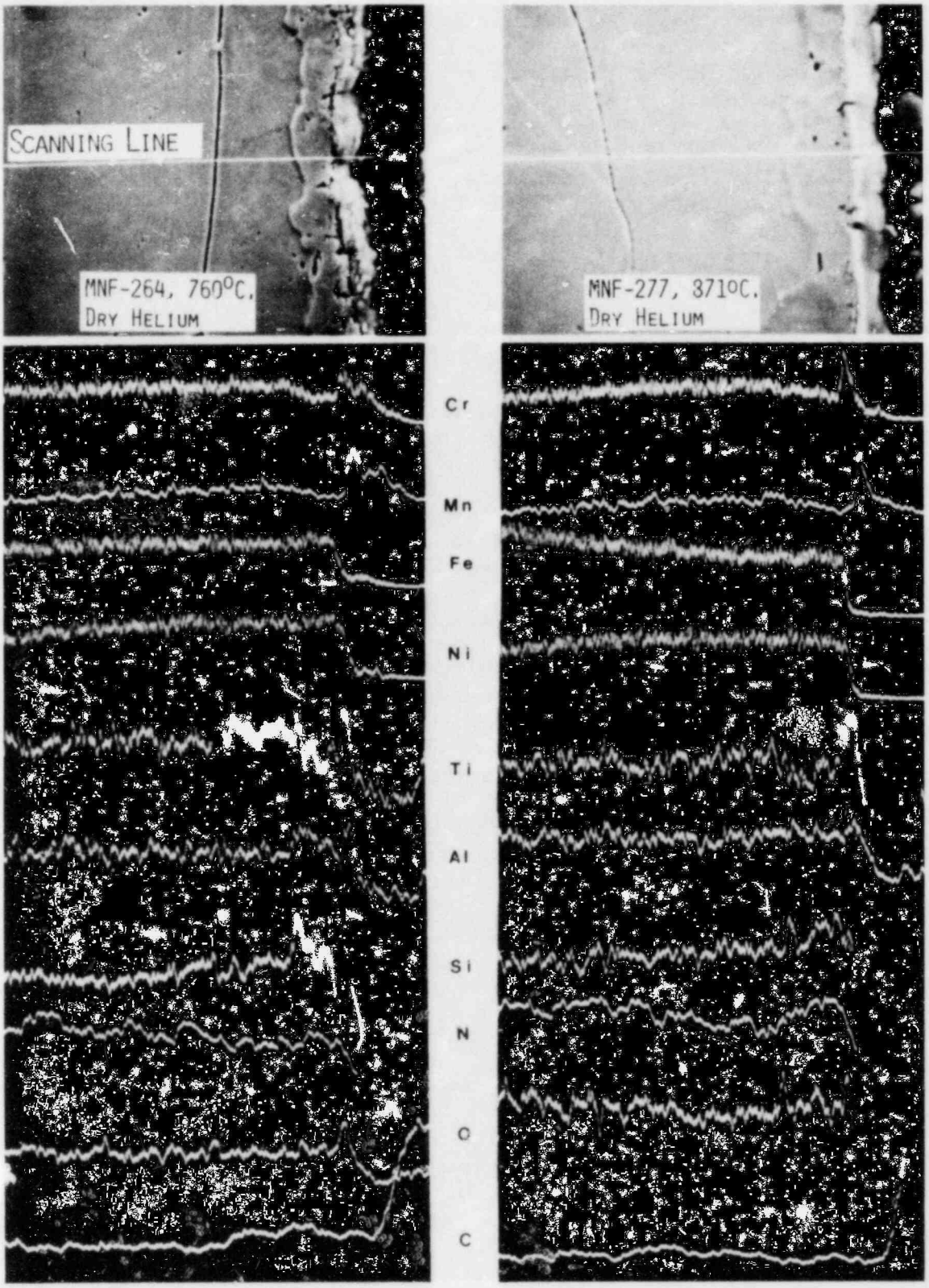

Figure 1.2.9. Scanning electron microscope/microprobe line scans through the surfaces of Incoloy-800H high cycle fatigue specimens tested at 760°C (1400°F) and 871°C (1600°F) in HTGR helium containing 5-10 μatm H_2O. Magnifications 500X.

dry helium there are only very small amounts of Fe and Ni in the scale region compared to specimens in the wet helium tests (Soo, 1980). Apparently, helium with low water concentrations, Fe and Ni oxides are unstable and the main oxides are those of Cr, Mn, Ti and Al, with Cr and Mn being dominant. For air the oxide is predominantly a Mn/Cr type (Soo, 1980). In the test at 760°C (Figure 1.2.8) there appears to be a slight enrichment in carbon in the surface region, indicative of carburization. However, such behavior is not seen in the test at 871°C (1600°F). If carburization occurs it is probably a minor effect for the test conditions employed here.

1.2.1.3 Metallography of Fatigued Hastelloy X Specimens

In Figure 1.2.10 are shown micrographs of fractured Hastelloy X samples tested in the reference helium gas. Specimen MHF-95 tested at high stress (low N_f) at 760°C (1400°F) shows much deformation at the surface as well as the presence of planar slip bands in the specimen interior. The slip bands are revealed by decoration from precipitated (presumably) carbide phases. A denuded zone exists in the region immediately beneath the surface. For the same test temperature, the low stress (high N_f) test shows a similar denuded zone. Because of the lower stress level, the slip bands are not as pronounced as those in Specimen MHF-95 and precipitation is much more random, although there is still evidence of preferential alignment along slip planes.

At a test temperature of 871°C (1600°F), Figure 1.2.10, precipitation on the slip panes is far more prevalent, especially for the higher stress levels (Specimen MHF-8[illegible]). Note that this specimen also shows a denuded zone near the surface. For longer test times, however, precipitation is less concentrated on the slip planes and precipitation occurs in previously denuded zones (see specimen MHF-88).

Figure 1.2.11 shows scanning electron microscope/microprobe line scans for longer term tests at 760 and 871°C (1400 and 1600°F). At the lower temperature the oxide scale is rich in Mn, W, and Si. It is, however, a relatively thin scale since Hastelloy-X is very resistant to oxidation at this temperature. For the 871°C (1600°F) test (Figure 1.2.11) the scale is more well defined, and rich in Mn, Cr and Si. Examination of the C trace gives a firm indication of carburization in the surface zones. This may be explained in terms of the thinner oxide scale in the dry helium which permits more easy migration of carbon from the test gas to the specimen interior. The presence of strong carbide forms such as Mo, W, Cr and Si in Hastelloy-X would also encourage carbon pickup from the test gas.

1.2.2 Creep Rupture Properties of Primary Circuit Structural Materials (K. S. Lee and L. Gerlach)

The safety of an HTGR relies greatly on the structural integrity of materials throughout the design life of the reactor. In an HTGR, the primary circuit materials are exposed to helium with impurities and interaction between the materials and the impurities in helium coolant may cause degradation of mechanical properties and result in premature structural failure of these materials. The objectives of the current program are to evaluate the effects of impurities in the helium coolant on the long term creep properties of primary circuit structural metals at high temperatures and to assess the changes in properties compared to standard air testing.

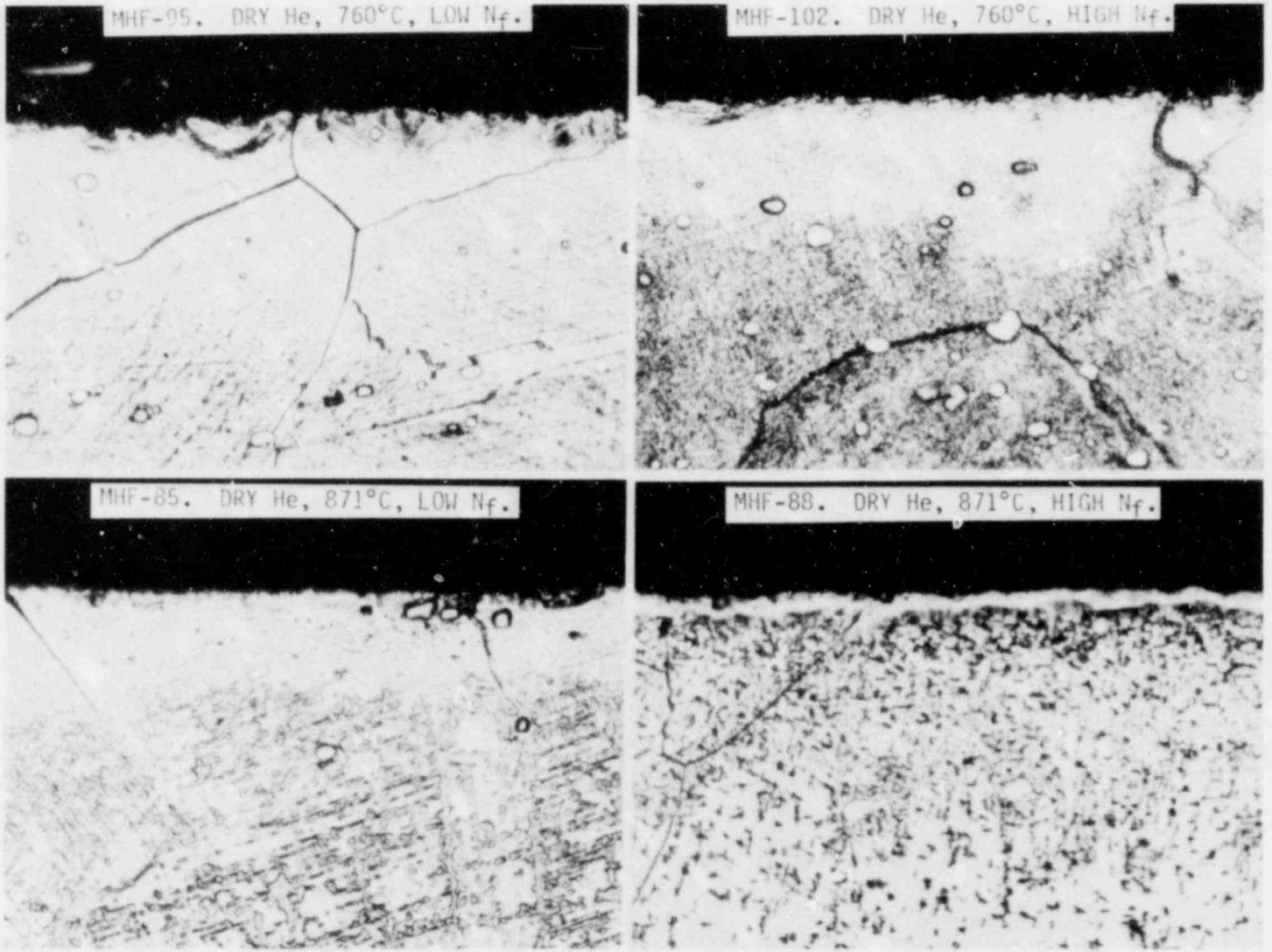

Figure 1.2.10. Effect of test time and test temperature on the surface microstructure of Hastelloy-X high cycle fatigue specimens tested in HTGR helium containing 5-10 μatm H_2O. Magnifications 450X.

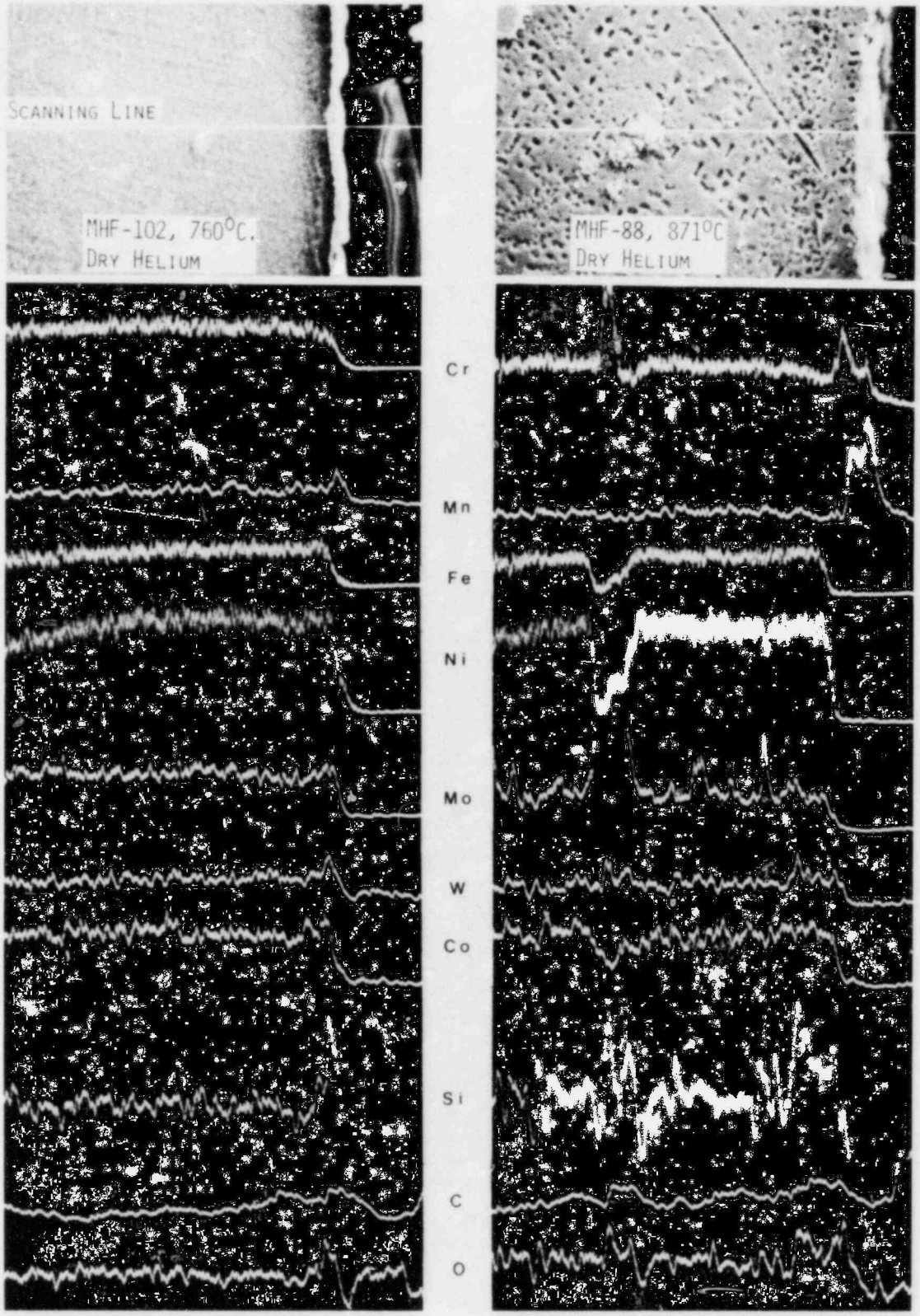

Figure 1.2.11. Scanning electron microscope/microprobe line scans through the surfaces of Hastelloy-X high cycle fatigue specimens tested at 760°C (1400°F) and 871°C (1600°F) in HTGR helium containing 5-10 μatm H_2O. Magnifications 500X.

The composition of impurities in helium gas supplied from the Materials Test Loop (MTL) and the chemistries of test alloys are given in Section 1.2.1. The creep tests have been concentrated on Incoloy 800H and Hastelloy X which are used in the steam generator and the thermal barrier cover plates, respectively.

The creep testing facilities consist of 20 lever arm testing units; 14 of them are equipped with environmental retorts for in-helium testing. At the present time all 20 units are in operation.

1.2.2.1 Creep of Incoloy 800H

The status of creep tests in progress at 649°C (1200°F) and 760°C (1400°F) in air and in helium environment are summarized in Table 1.2.3.

Table 1.2.3

Status of Creep Tests on Incoloy 800H

Specimen No.	Environment	Test Temp. (°C)	Test Temp. (°F)	Stress Level (MPa)	Stress Level (ksi)	Time (hours)	Total Creep Strain (%)
MNT-229	Air	649	1200	103.3	15.0	25,533	12.2
MNT-172	Air	649	1200	82.7	12.0	30,751	2.6
MNT-173	Air	649	1200	82.7	12.0	29,784	4.4
MNT-182	Air	760	1400	34.4	5.0	31,233	7.4
MNT-243 *	He	649	1200	124.0	18.0	15,750	43.8
MNT-246	He	649	1200	103.3	15.0	9,643	1.9
MNT-245	He	760	1400	41.3	6.0	13,463	8.6
MNT-247	He	760	1400	34.4	5.0	9,308	0.3

* Specimen ruptured.

Specimen MNT-229 is in the tertiary creep range, while the rest of the specimens are still in the steady state creep region.

During this reporting period, specimen MNT-243 which was loaded to 124.0 MPa (18.0 ksi) at 649°C (1200°F) in the dry helium has ruptured after 15,752 hours. Compared to the air test at the same load, there is about 20% increase in rupture life. This improvement in rupture life may be due to the reduction in the minimum creep rate from 1.36×10^{-6} in/in/hr in air to 7.5×10^{-7} in/in/1hr in the dry helium environment. The rupture ductility was slightly lower (~15%) in the dry helium.

Figure 1.2.12 shows the rupture life data obtained to date from the air, wet and dry helium tests. The tests in progress and the tests terminated before rupture are also included with their total elongations in parentheses. The solid line represents the air data. It is clear from this figure that the helium environment increases the rupture life of Incoloy 800H at 649°C (1200°F) and 760°C (1400°F) compared to the air tests.

The results from the long term tests in progress will be quite important to determine whether extrapolation of rupture life from the shorter term tests can be done conservatively and to assess the BNL data in a comparison with the Code minimums.

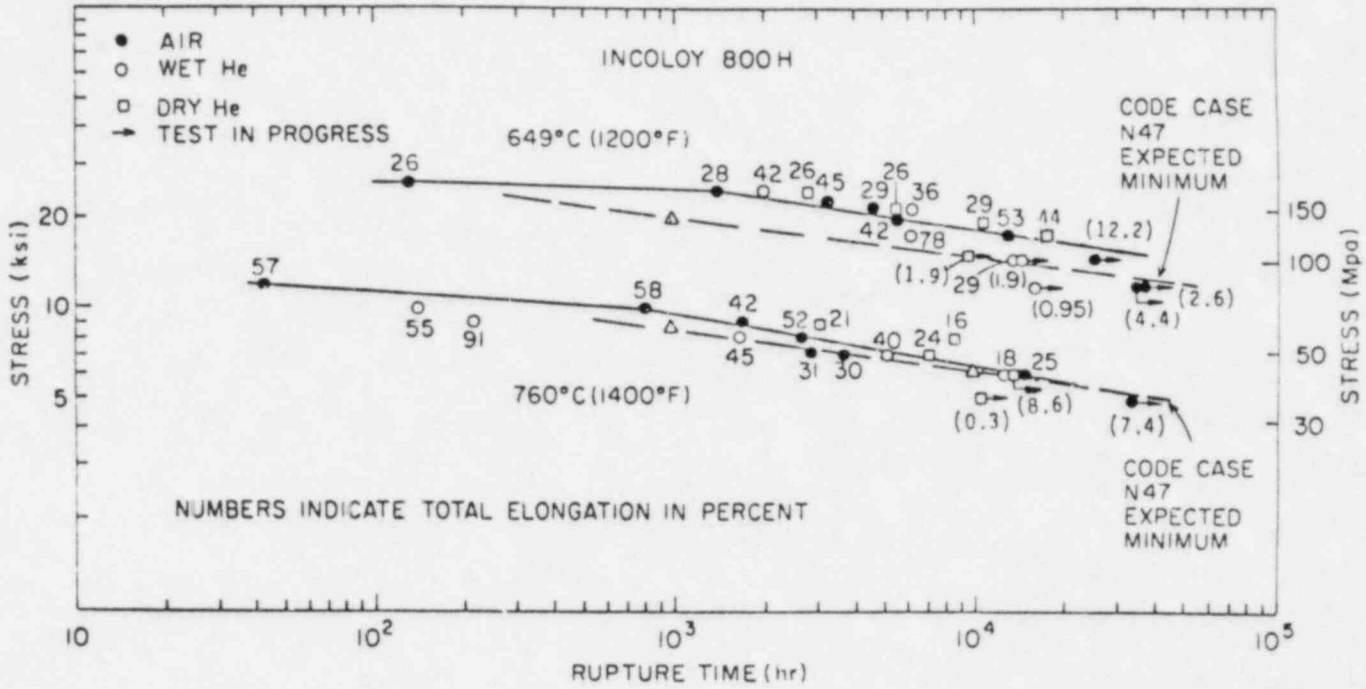

STRESS RUPTURE LIFE OF INCOLOY 800 H TESTED AT 649°C AND 760°C IN AIR AND IN HTGR HELIUM

Figure 1.2.12

1.2.2.2 Creep of Hastelloy X

There has been no specimen failure since the last reporting period. The status of creep tests on Hastelloy X at 760°C (1400°F) and 871°C (1600°F) in air and in the dry helium environment are shown in Table 1.2.4.

Table 1.2.4

Status of Creep Tests on Hastelloy X

Specimen No.	Environment	Test Temp. (°C)	(°F)	Stress Level (MPa)	(ksi)	Time (hours)	Total Creep Strain (%)
MHT-08	Air	760	1400	68.9	10.0	37,278	25.6
MHT-14	Air	760	1400	55.1	8.0	35,668	1.4
MHT-52	He	760	1400	82.7	12.0	16,998	21.0
MHT-55	He	760	1400	68.9	10.0	16,124	11.3
MHT-57	He	760	1400	55.1	8.0	13,774	9.6
MHT-53	He	871	1600	34.4	5.0	16,915	21.5
MHT-65	He	871	1600	27.6	4.0	4,313	0.8

Specimens MHT-08, MHT-52 and MHT-53 are in the tertiary creep range and rupture is imminent.

Figure 1.2.13 summarizes the rupture life data obtained to date from air, wet and dry helium tests. The tests currently in progress are included. The solid lines are drawn through the air data. These data show that the dry helium environment increases the rupture life compared to the air tests. This improvement is more pronounced at 871°C (1600°F). It has been reported previously that one of the long term tests at 871°C failed far below the expected rupture life because of thermal aging effects. Information on thermal aging effect on long term rupture life at the lower temperature (649°C) will be obtained when the tests in progress are completed.

1.2.2.3 Effects of Thermal Transients on Creep

Figure 1.2.14 shows the results of thermal cycling tests on Hastelloy X specimens initially loaded to 34.5 MPa (5.0 ksi) at 815°C (1500°F) in air. This loading condition will rupture the specimens at 250,000 hours according to linear extrapolation. A one hour transient to 1093°C (2000°F) gave 16% elongation and to 1065°C (1950°F) a 6% elongation. Both strains far exceed the design failure limit. A one hour transient to 1038°C (1900°F) yielded a 2.7% elongation and during the second cycle showed about the same amount of strain. A temperature cycle to 982°C (1800°F) for one hour gave an increase in strain of about 0.3% and this damage is cumulative in each cycle.

There is an increase in creep rate after the cycles to 1093°C and 1065°C, but no significant changes after each cycle to 1038°C and 982°C.

Similar tests will be performed for a 20.7 MPa (3.0 ksi) stress at 1500°F loading condition which will give 1% strain in 250,000 hours. Also the effect of the thermal transient on the rupture properties will be investigated.

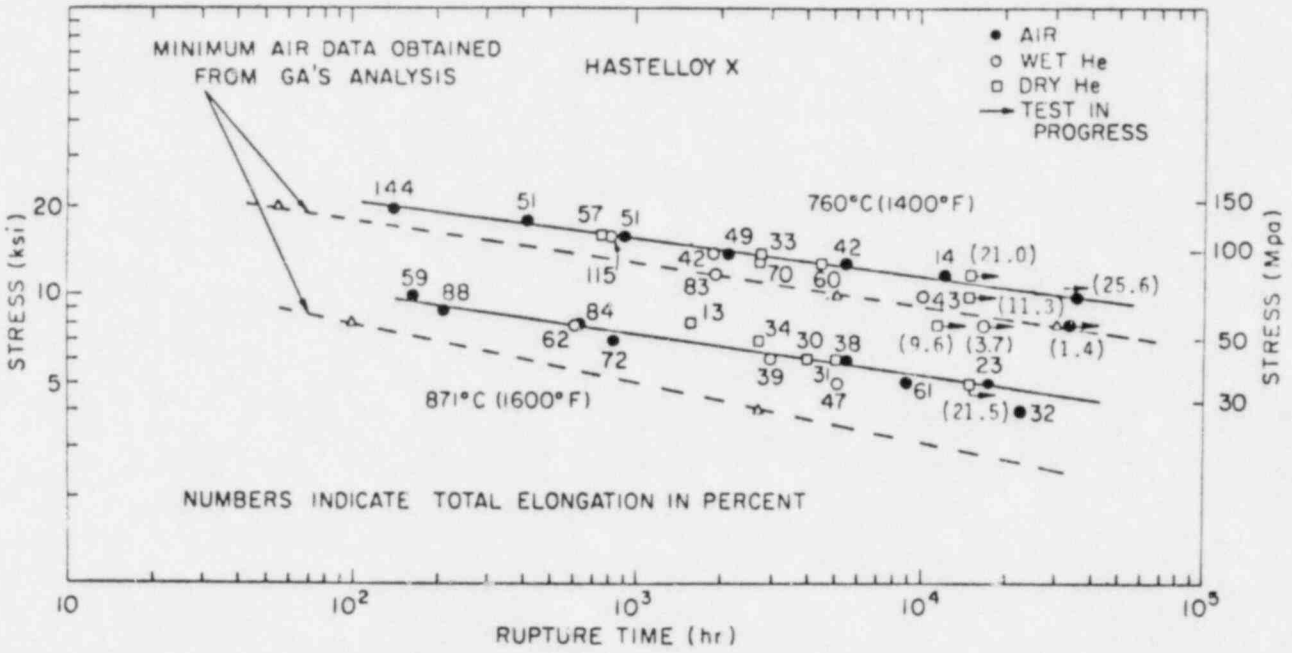

STRESS RUPTURE LIFE OF HASTELLOY X TESTED AT 760°C AND 871°C IN AIR AND IN HTGR HELIUM

Figure 1.2.13

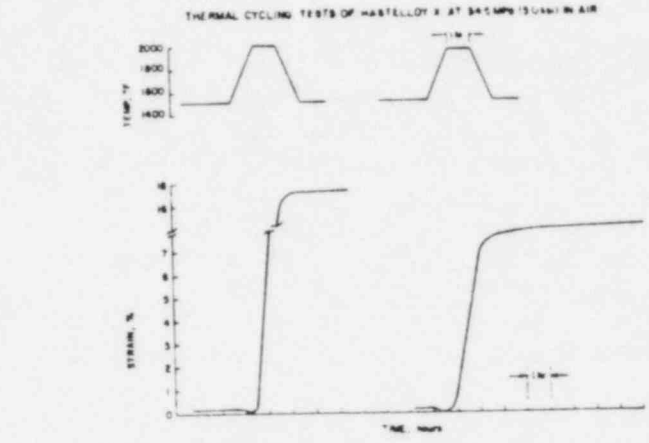
THERMAL CYCLING TESTS OF HASTELLOY X AT 345 MPa (50 ksi) IN AIR
TEMP, °F
2000
1800
1600
1400
STRAIN, %
TIME, hours

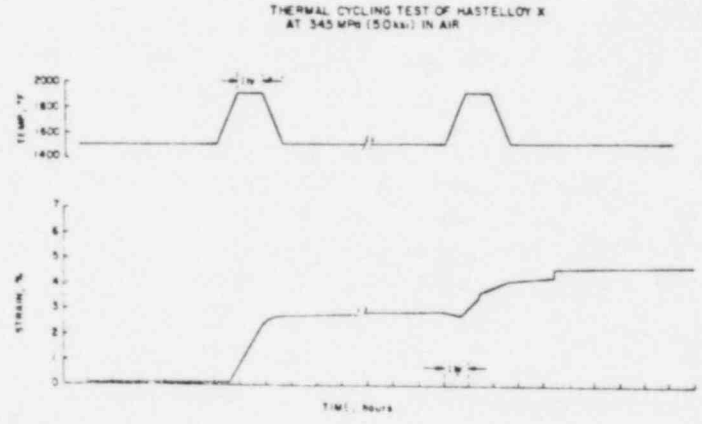
THERMAL CYCLING TEST OF HASTELLOY X
AT 345 MPa (50 ksi) IN AIR
TEMP, °F
2000
1800
1600
1400
STRAIN, %
TIME, hours

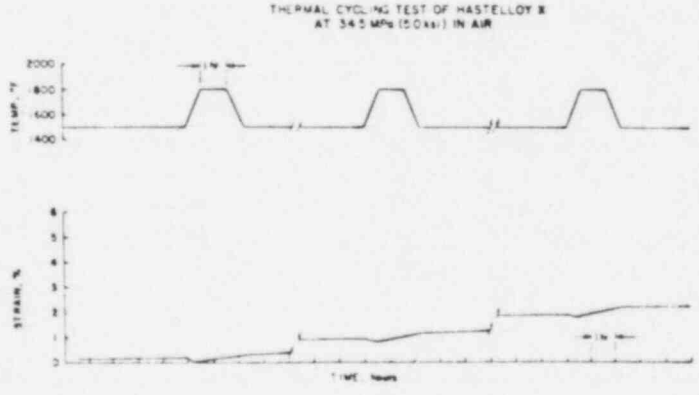
THERMAL CYCLING TEST OF HASTELLOY X
AT 345 MPa (50 ksi) IN AIR
TEMP, °F
2000
1800
1600
1400
STRAIN, %
TIME, hours

Figure 1.2.14

Figure 1.2.15 shows the results of thermal cycling tests on Incoloy 800H initially loaded to a 20.7 MPa (3.0 ksi) at 760°C (1400°F). A one hour transient to 1093°C (2000°F) gave a 4.7% strain during the transient, and a 3.7% strain on returning to 760° (1400°F). This may be due to the thermal expansion and contraction of the specimen.

A one hour transient to 1038°C (1900°F) showed an increase of strain of 0.25% after the first cycle and 0.33% strain after the second cycle. Again, the strains that occurred during each cycle are cumulative. There is an increase in creep rate after a one hour transient to 1098°C.

Similar tests will be continued on Incoloy 800H for different initial loading conditions and the effects of thermal transient on the long term rupture properties will be examined.

1.2.3 The Effect of Carburization on Oxidation Resistance (D. Gan)

Carburization of metal components is a problem in HTGR. Carbon in the graphite core can be carried out as methane, carbon monoxide and carbon dioxide. The carbon is deposited on the surface of metal components and diffuses into them to cause carburization. This research was recently initiated to investigate the possible deterioration of oxidation resistance by carburization.

Hatelloy X is used in this investigation. The composition of this Ni-base alloy is (in weight percent) 20.63% Cr, 9.13% Mo, 18.41% Fe, 2.10%Co, 0.62% Mn and 0.07% C. The thickness is 3.2 mm. Specimens were precarburized at 1000°C in helium with 1% methane at a flow rate of 10ℓ/min. The depth of carburization was about 0.8 mm after 72 hours of exposure. Another group of control specimens were annealed under the same condition but without methane. These specimens were polished and then oxidized in air and HTGR helium at 1000°C.

Figure 1.2.16 is a scanning electron microscope photograph of an annealed specimen oxidized in air for 145 hours. The surface is covered by a 9 μm thick Cr_2O_3 scale which provides protection against oxidation by the very slow growth rate. A very small amount of internal oxidation is observed below the oxide scale. Figure 1.2.17 is a photograph of a precarburized specimen which was oxidized in air for the same 145 hours. Since the specimen was unetched the contrast of the precipitates is the atomic number contrast. Elements with smaller atomic number appear darker because of the reduced backscattered electrons. Two kinds of carbides are identified in the photograph. The dark precipitates are the Cr-rich $M_{23}C_6$ type carbides which precipitate as a result of carburization. As chromium combines with carbon to form this type of carbide it is depleted from the matrix. The other precipitates are the Mo-rich M_6C type carbides which appear lighter in the picture. This type of carbide is present even without carburization. The thickness of the oxide scale in carburized specimen is about the same as that of the annealed specimen. A zone of approximately 30 μm below the oxide scale is devoid of the $M_{23}C_6$ type carbides. Apparently the Cr-rich carbides have dissolved and released Cr to form the Cr_2O_3 scale on surface. However, the M_6C type carbides are not affected and remain in the $M_{23}C_6$-dissolved zone.

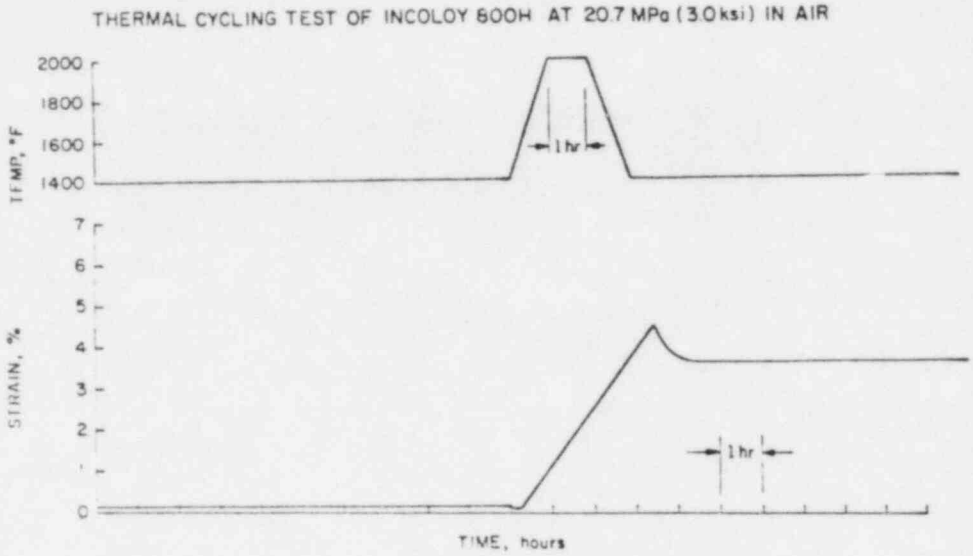
THERMAL CYCLING TEST OF INCOLOY 800H AT 20.7 MPa (3.0 ksi) IN AIR
TEMP, °F
2000
1800
1600
1400
1 hr
STRAIN, %
7
6
5
4
3
2
1
0
1 hr
TIME, hours

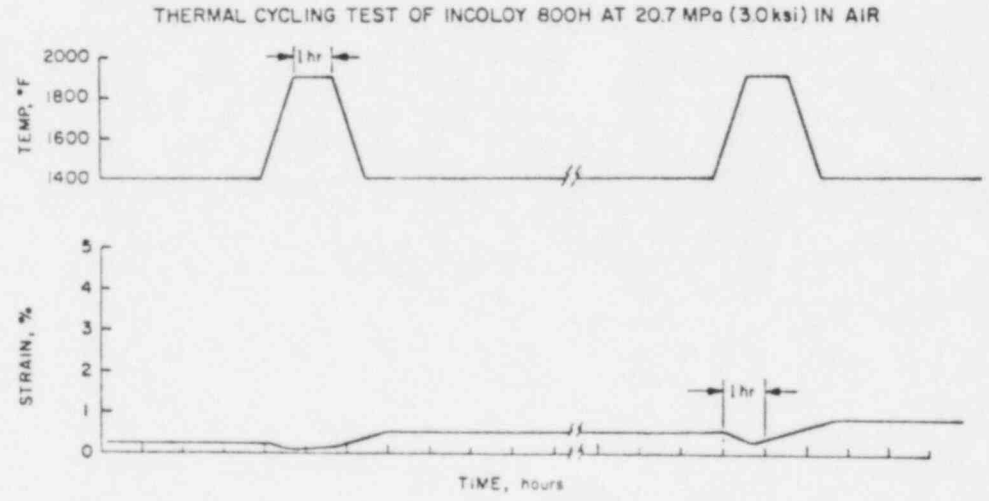
THERMAL CYCLING TEST OF INCOLOY 800H AT 20.7 MPa (3.0 ksi) IN AIR
TEMP, °F
2000
1800
1600
1400
1 hr
STRAIN, %
5
4
3
2
1
0
1 hr
TIME, hours

Figure 1.2.15

Figure 1.2.16 Specimen Oxidized in Air for 145 hours at 1000°C.

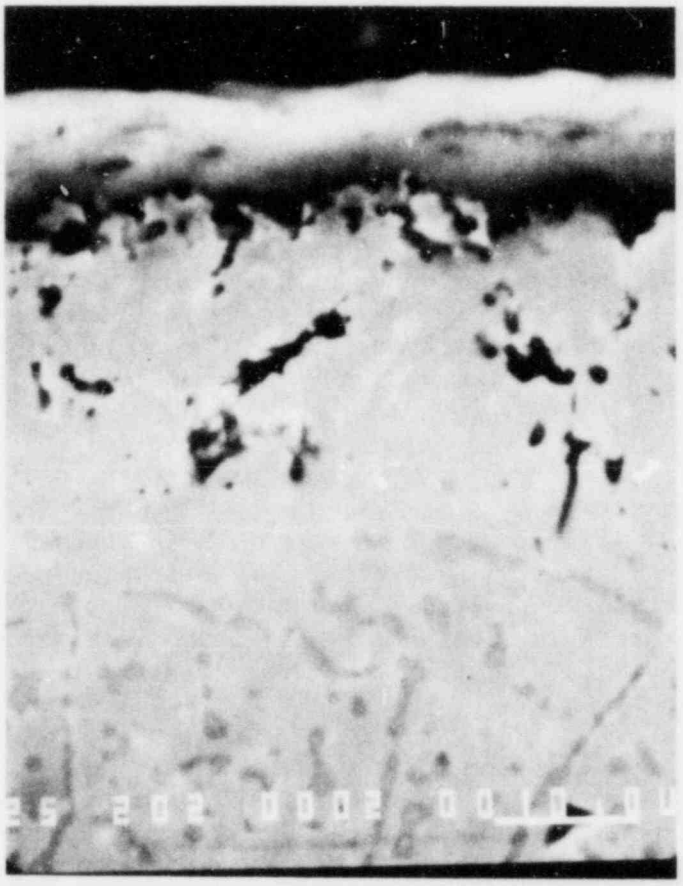

Figure 1.2.17 Specimen Precarburized and Oxidized in Air for 145 hours at 1000°C. The Internal Oxidation and Cavitation are very serious.

A striking difference in the oxidation of carburized specimens is the extent of internal oxidation and cavitation. In the uncarburized specimen there is little internal oxidation but in the carburized specimen the internal attack is very severe. The average depth of internal attack is 20 μm, and the maximum depth can reach the undissolved $M_{23}C_6$ type carbide at a depth of 30 μm. Another example of oxidation is shown in Figure 1.2.18. The specimen was precarburized and then oxidized in air for 24 hours at 1000°C. The oxide scale is 4 μm thick, the $M_{23}C_6$-depleted zone is 12 μm, and the average depth of internal attack is 7 μm. The internal oxidation and cavitation are clearly not restricted to the grain boundary. They are distributed rather uniformly, though the deep ones are generally along the grain boundary. The internal oxidation and cavitation are especially dense at the metal-oxide interface where they become almost continuous.

The extensive cavitation at the metal-oxide interface also reduces the adherence of the protective oxide scale. In fact, the amount of spalled oxide left in specimen holder after oxidation shows that the spallation is much more severe in the carburized specimen than in the uncarburized one. The loss in the adherence of oxide scale can certainly reduce the oxidation resistance significantly.

From these results it is clear that carburization is very detrimental to the oxidation resistance of Hastelloy X. The Cr-rich $M_{23}C_6$ type carbides precipitate as a result of carburization. Though these carbides can dissolve and release Cr to form Cr_2O_3 scale, the internal oxidation and cavitation proceed rapidly into the metal. The reduced adherence of oxide scale by internal attack further undermines the oxidation resistance of this alloy. It is possible that cracks can be initiated by internal cavitation and reduce the fatigue and creep lives.

Systematic investigation is now under way to measure the oxidation and internal oxidation rates of carburized specimen in both air and HTGR helium. Analyses of the behavior of carbides, the corrosion products, and the causes for internal cavitation are now being performed with scanning and transmission electron microscopes and x-ray diffraction. Another important property of oxidation resistance is the healing ability in case of scale rupture. The oxide scale in carburized specimen can be ruptured by temperature cycling and the healing ability will be studied in subsequent oxidation test.

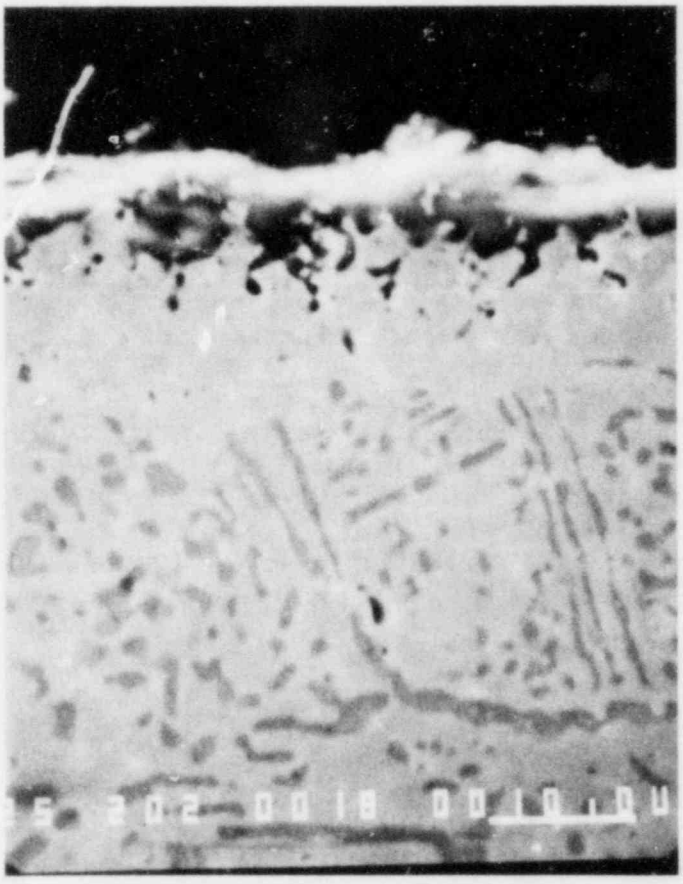

Figure 1.2.18 Specimen Precarburized and Oxidized in Air for 24 hours at 1000°C.

1.3 Fuel and Fission Products

1.3.1 Fission Product Migration in H451 Graphite. (G. Uneberg and C. Sastre)

In this quarter we have continued the analysis of the experiments which were finished last quarter. We now have experimental data for Uranium-Thorium mixtures at temperatures of 2900°C and 3000°C. Uranium-Thorium mixtures run at temperatures of 2700°C and 2800°C have not yet been assayed. We also have data for single component runs for Uranium and Thorium at a temperature of 2900°C. It should be noted that the multi-component mixtures (U-Th) have been twice run at 2900°C and 3000°C and assayed on at least two different occasions and the results are in agreement.

1.3.1.1 Experimental

The experiments are performed by loading a thin layer of U, Th, and Carbon into a flat bottomed cavity in a H451 graphite (Great Lakes Carbon Corp.) cylinder used as the susceptor of a 30 kw induction furnace. The mixture is stoichiometric for formation of a 50/50 mole ratio of UC_2 to ThC_2.

After heating the sample to temperatures spanning the melting points of the carbides (>2700°C), the graphite is machined to separate the cylindrical portion lying directly below the plane of the melt. This cylinder is then sliced along planes parallel to the plane of the melt and these slices are ashed and assayed. This results in values of concentration averaged over the volume of the slice for various distances from the source.

1.3.1.2 Results

It is noteworthy that the family of curves generated by this series of experiments seem to extrapolate back to a ''virtual source'' whose concentration is orders of magnitude less than the ''real'' source. This would seem to indicate that there is more than one phenomenon involved in the diffusion process. The determination of this ''virtual'' source is important in the determination of a diffusion coefficient because it is necessary to the normalization process. As of this time, we still have several experiments which are in the process of being assayed, and we should have a better handle on this problem when these data are ready. In any case, a comparison of the experimental data with SORS (Figure 1.3.4) indicates that the migration of Uranium and Thorium is much greater than expected, and we anticipate that the experimentally obtained diffusion coefficient shall be several orders of magnitude greater than that given in SORS.

Comparison of the multicomponent diffusion profile with the single component profile run at the same temperature (see Figure 1.3.1 and Figure 1.3.3) raises a very interesting question. Does the addition of another component to the diffusate have an inhibitive effect upon migration? It would appear to be so. One can see in Figure 1.3.1 that Uranium, when present in a U-Th mixture at 2900°C, has a smaller diffusion profile than when it is run at 2900°C by itself. The same holds true for Thorium (see Figure 1.3.3). If this result holds true for other fission products, then it would appear that the only realistic way to obtain representative diffusion coefficients under HTGR conditions is to use representative mixtures of the appropriate fission products which are normally present under operating conditions.

URANIUM ANALYSIS

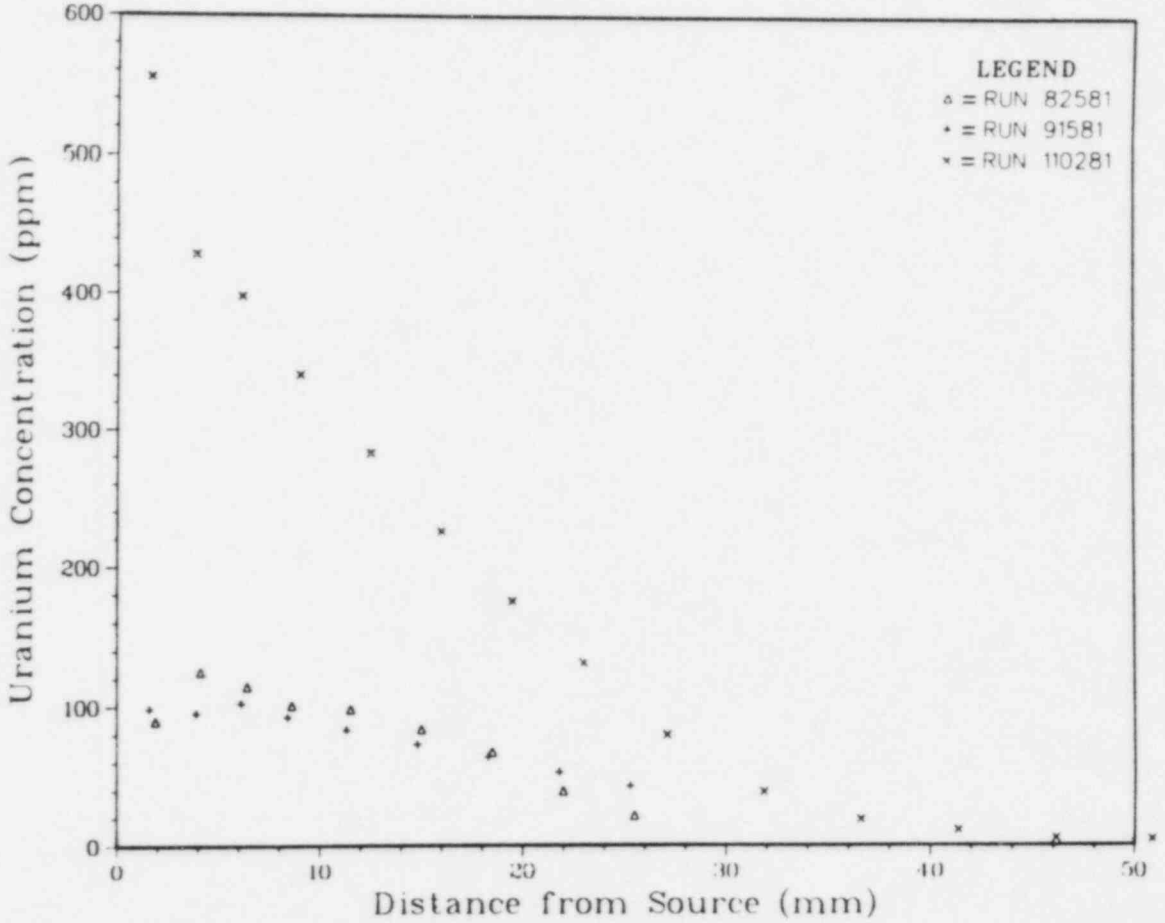

Figure 1.3.1

Δ = Run 82581 - UC_2 + ThC_2 @ 2900°C for 100 minutes.
+ = Run 91581 - UC_2 + ThC_2 @ 3000°C for 120 minutes.
X = Run 110281- UC_2 alone @ 2900°C for 105 minutes.

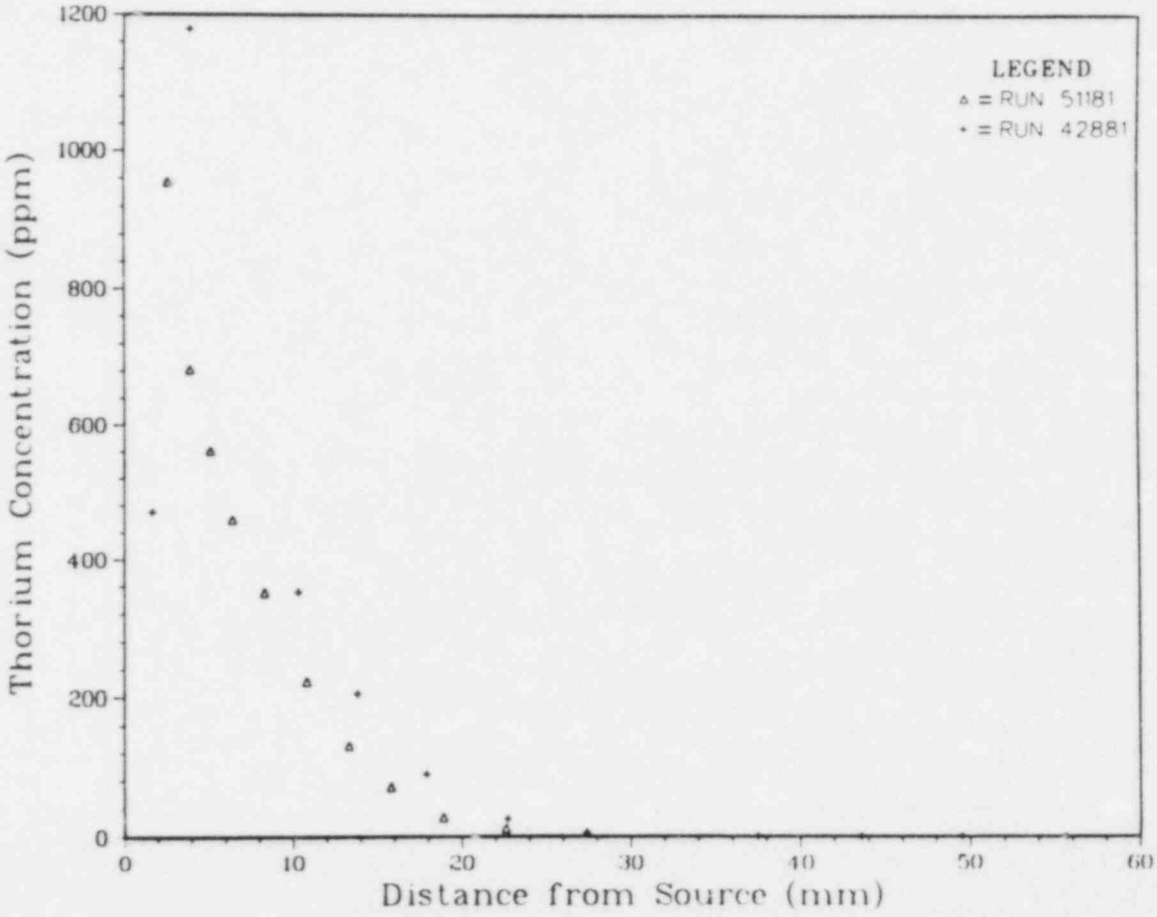

Figure 1.3.2

Δ = Run 51181 - UC_2 + ThC_2 @ 3000°C for 1.0 hour.
+ = Run 42881 - UC_2 + ThC_2 @ 2900°C for 2.0 hour.

THORIUM ANALYSIS

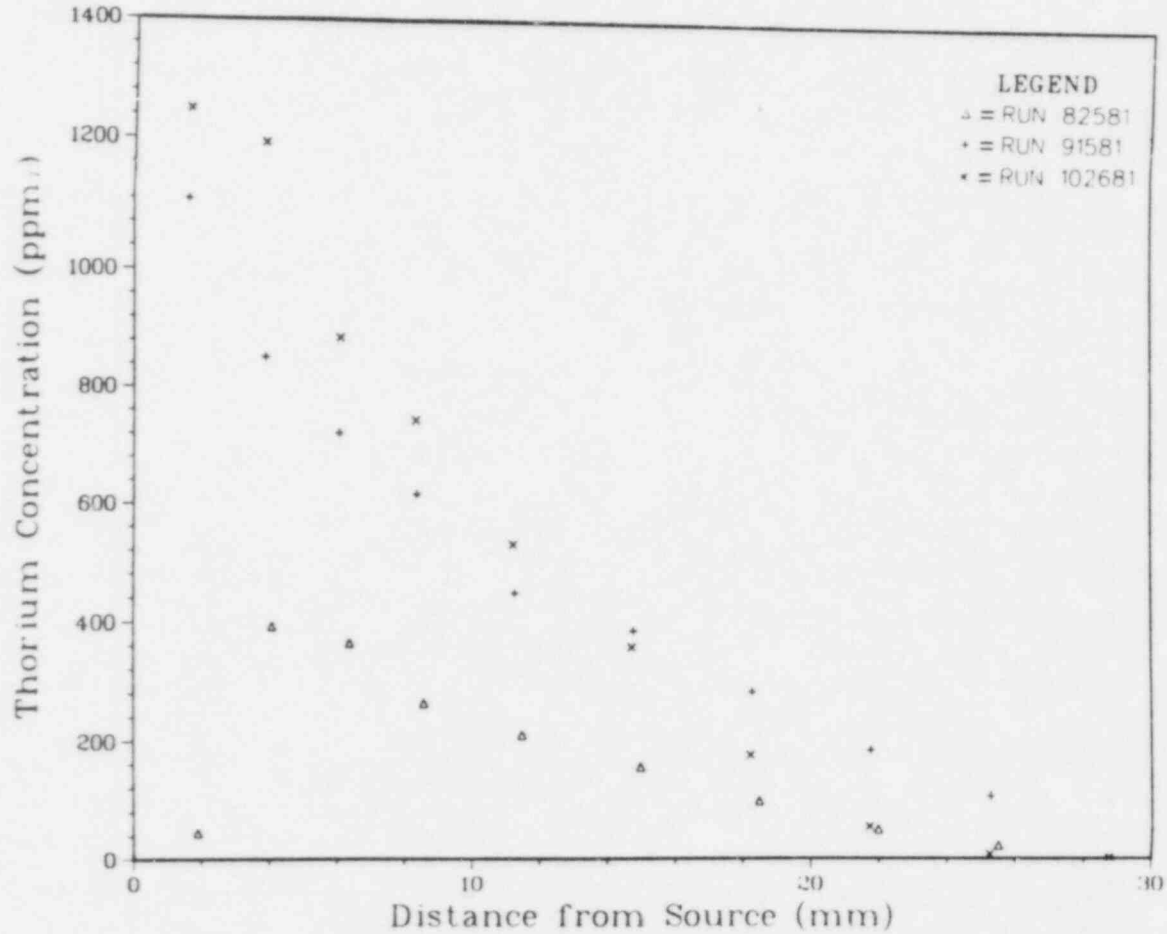

Figure 1.3.3
Δ = Run 82581 - UC_2 + ThC_2 @ 2900°C for 100 minutes.
+ = Run 91581 - UC_2 + ThC_2 @ 3000°C for 120 minutes.
X = Run 102681- ThC_2 alone @ 2900°C for 105 minutes.

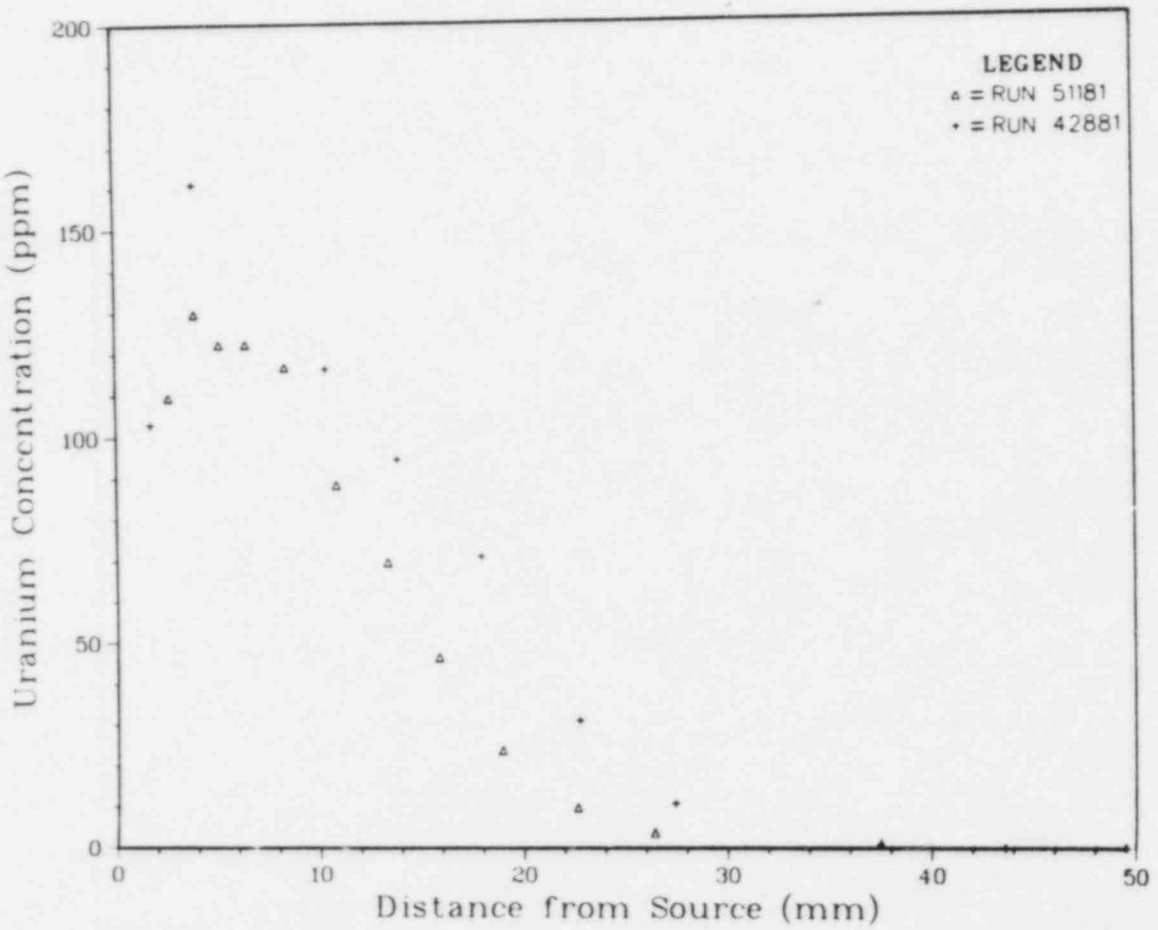

Figure 1.3.4

Δ = Run 51181 - UC_2 + ThC_2 @ 3000°C for 1.0 hour.
+ = Run 42881 - UC_2 _ ThC_2 @ 2900°C for 1.0 hour.

1.3.2 Gas-phase Transport of Refractory Fission Products (I. N. Tang and H. R. Munkelwitz)

The experimental results of our investigation to date have clearly demonstrated that the formation of nuclear aerosols under certain HTGR accident conditions could be an important mechanism by which vaporized fission products such as Sr, Ba and Ag are transported in the gas phase. In our experiments, however, only simulated fission products were used. They were impregnated in the graphite matrix with concentrations between approximately 1 mg of, say, Sr to 10 mg per g of graphite. A legitimate question then arises as to whether or not the extent of aerosol formation depends on the initial loading of fission product in the graphite matrix. To answer this question, we present the results from six experiments made under identical conditions in Figure 1.3.5, where the % Sr collected on filter is plotted vs. initial Sr loading in the heated graphite samples. In addition, the concentration corresponding to one monolayer coverage on graphite was calculated for Sr on the basis of an estimated graphite surface area of 1 m^2/g. As shown in Figure 1.3.5, the extent of aerosol formation in terms of percentage collected on filter as particulate matter is independent of the initial loading for concentrations down to approximately one monolayer coverage of F.P. in H451 graphite. Work is continuing to reduce the initial Sr concentration further down to below one monolayer coverage. It would be desirable for confirmatory purposes to carry out additional aerosol experiments with irradiated HTGR fuels.

Figure 1.3.6 shows a composite of electron micrographic pictures of Ag aerosols at 4 different magnifications. The aerosols, produced in the same manner as Sr and Ba aerosols, were collected on a nucleopore filter for better examination. Unlike Sr or Ba aerosols which are chemically reactive in ambient air, Ag aerosols are stable in air and, therefore, they provide a good means for studying the morphology of fission product aerosols. The information is needed to understand the aerosol formation mechanism. In this particular case, agglomerates consisting of primary particles almost uniform in sizes (0.06-0.08 μm in diamter) are clearly revealed, indicating the condensational nature of the particles as opposed to fission product adsorption on existing particles.

1.3.3 Interaction of Fission Product SrO and BaO with Graphite (S. Aronson and T. Yeh, Brooklyn College)

The experimental procedure which we are using to study the interaction of SrO and BaO with graphite involves first the absorption of the metal nitrate into the graphite pores, the subsequent decomposition of the nitrate to the oxide and finally, the reaction of the oxide with graphite. Two experiments were performed to obtain preliminary data on this complex process. The data are summarized in Table 1.3.1.

In the first experiment, the doped H-451 graphite samples (4 discs, 3/8'' diam by 3/16'' thick) were heated in vacuo to 950°C. The system was then closed off from the vacuum pump and the temperature was raised to 1290°C. The system reached a steady pressure of 2.1 torr in a few minutes. In the second experiment, the outgassing and the nitrate decomposition were executed at 890°C. The closed system was then heated to 1220°C. A steady pressure of 5.5

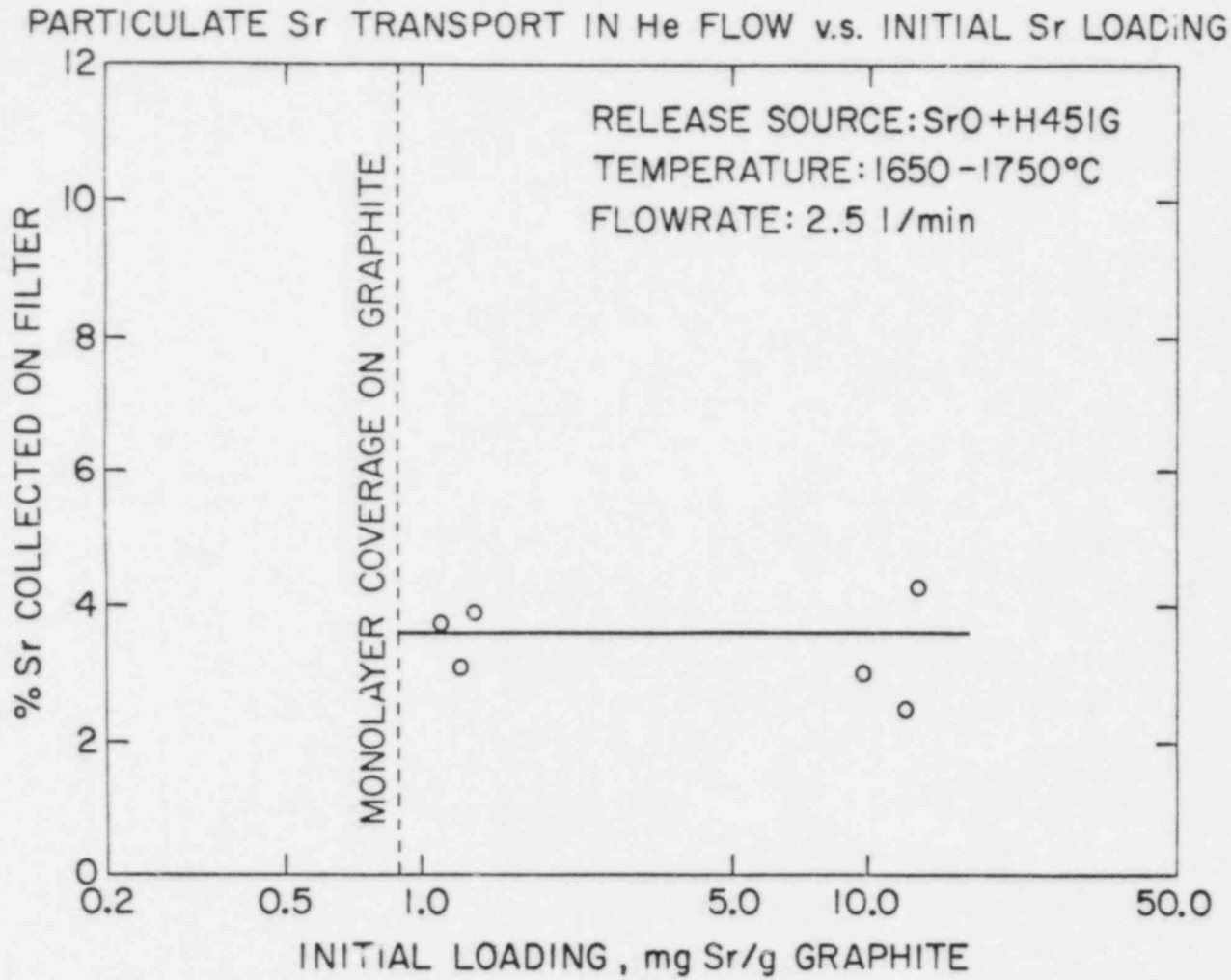
PARTICULATE Sr TRANSPORT IN He FLOW v.s. INITIAL Sr LOADING
RELEASE SOURCE: SrO+H451G
TEMPERATURE: 1650-1750°C
FLOWRATE: 2.5 l/min
MONOLAYER COVERAGE ON GRAPHITE
% Sr COLLECTED ON FILTER
0
2
4
6
8
10
12
0.2
0.5
1.0
5.0
10.0
50.0
INITIAL LOADING, mg Sr/g GRAPHITE

Figure 1.3.5

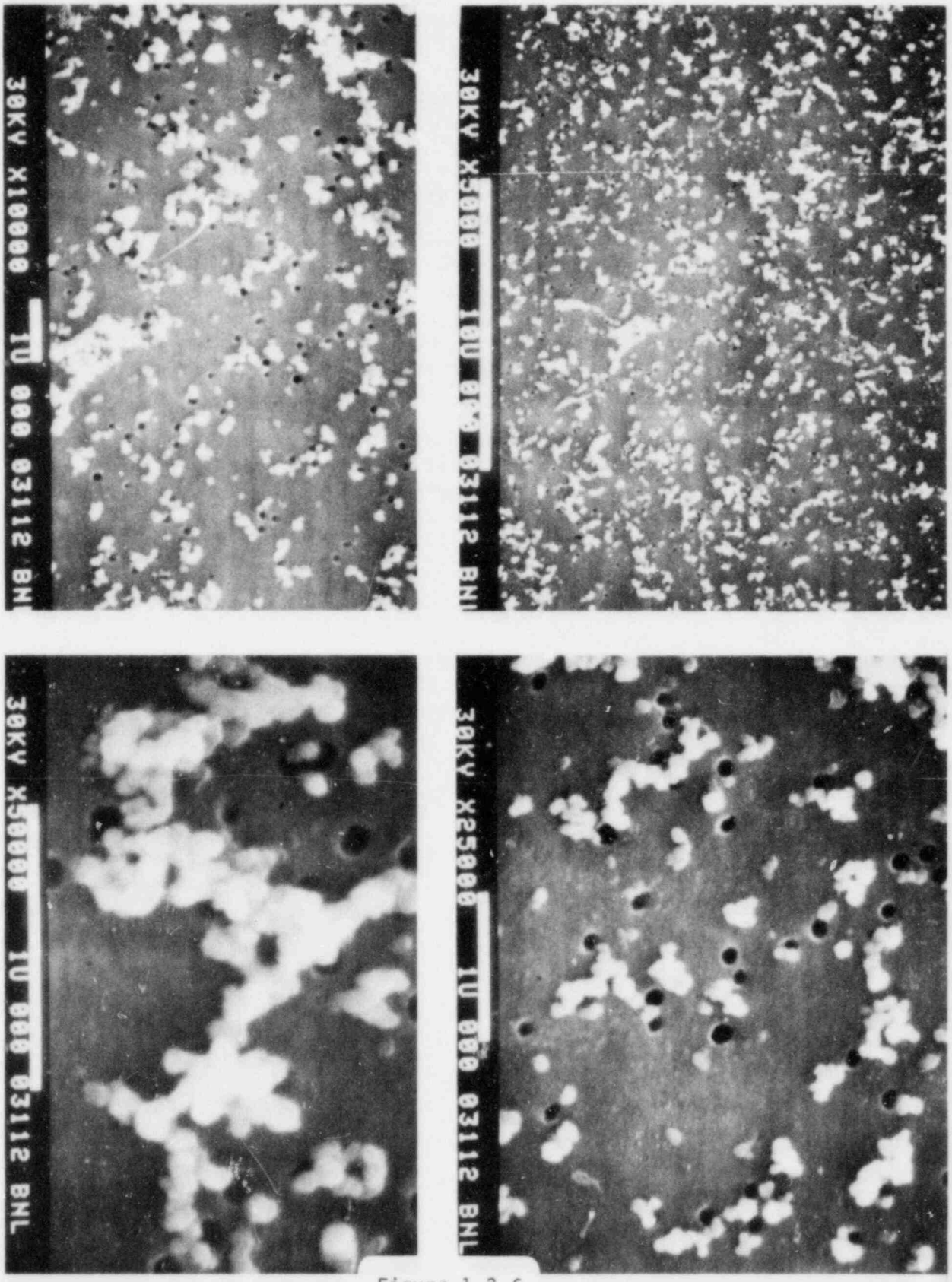
30KV X100000 1U 000 03112 BNL
30KV X50000 1U 000 03112 BNL
30KV X25000 1U 000 03112 BNL
30KV X50000 1U 000 03112 BNL

Figure 1.3.6

torr was attained in about 15 minutes. The system was evacuated for a moment and was then closed again. A buildup of pressure was not observed indicating that the reaction of SrO with graphite was complete.

The quantities of strontium present in the discs, in the crucible, the crucible cover and on the wall of the quartz heating tube were determined by atomic adsorption spectroscopy. It was found that 18% of the strontium originally present in the discs was released to the wall of the quartz tube in the first experiment and 32% in the second experiment. From the quantities of gas collected, presumed to be CO, 8% of the strontium, in the form of SrO, reacted with the graphite in the first experiment and 15% in the second experiment.

Consideration of all the data obtained in the two experiments indicates that the conversion of $Sr(NO_3)_2$ to SrO and the reaction of SrO with graphite may not be distinct processes. Some loss of strontium may have occurred during the decomposition of the nitrate. Only a small fraction of the strontium in the samples reacted with graphite at the reaction temperature to form CO.

The results indicate that it may be useful to experimentally separate the two parts of the process. The conversion of nitrate to oxide and the reaction of SrO with graphite should be studied separately. In future experiments, data on gas release and strontium distribution will be obtained on both parts of the process. Mass spectrometric analysis of the evolved gases will also be performed.

Table 1.3.1

Experimental Data on the Interaction of $Sr(NO_3)_2$ with Graphite.

Outgas Temp.	Reaction Temp.	Initial Wt. Sr	Pressure of CO	Wt. Sr from CO	Wt. Sr on Wall
950°C	1290°C	43.3 mg	2.1 torr	3.6 mg	7.7 mg
890°C	1220°C	52.7 mg	5.5 torr	7.8 mg	16.9 mg

1.4 Analytical

1.4.1 HTGR Code Library (J. Colman)

Table .4.1

HTGR Code Library - Alphabetic Code Order

Program	Origin/ Code Date	BNL Status	Function
BLAST	ORNL/ACC 8/76 (BNL 1/80)	OP	A dynamic simulation of the HTGR reheater-steam generator module.
BLOOST/ BLOOST-7	GA/SAI 1/70	OP	Performs zero-dimensional reactor kinetics calculations.
CHAP-1 (Jan. 1978)	LASL 2/77	OP	Simulates the overall HTGR plant with both steady state and transient solution capabilities.
CIRC (JETS)	BNL 4/78	OP	Calculates fluid dynamics in an HTGR containment vessel following a depressurization accident.
CNTB-7	GA 7/79	OP	Analysis of Partially mixed containment atmospheres during depressurization events.

ACC = Argonne Code Center.
BAW = Babcock and Wilcox.
BNL = Brookhaven Nat. Lab.
BPNW = Battelle Pacific N.W.
GA = General Atomic.
LASL = Los Alamos Scientific Lab.
NOP = Non-Operational.
OP = Operational
ORNL = Oak Ridge National Lab.
P = Proprietary.
SAI = Science Applications, Inc.

Table 1.4.1 (Cont'd.)

Program	Origin/ Code Date	BNL Status	Function
CONTEMP-G (CONTEMPT-G)	GA-BAW 2/74	OP (P)	Simulates temperature-pressure response of an HTGR containment atmosphere to postulated coolant circuit depressurization.
CORCON	GA 7/74	OP (P)	Computes the temperature history and fission product redistribution following a loss of all convective cooling of the core.
CORTAP	ORNL ACC 1/77 (BNL 1/80)	OP	A coupled neutron kinetics - heat transfer program for the dynamics simulation of the HTGR core.
DECAYREM	ORNL 5/74	OP	RSIC Data Library Collection.
DIFFTA	BNL 11/75	OP	Finite element method code for Steady State Heat Conduction, Fission Product Migration and Neutron Diffusion Calculations.
ENDFB and Satellite Codes	BNL	OP	Evaluated Nuclear Data File/B and file manipulation codes.
EVAP	BNL 5/78	OP	A model for the Migration of Fission Products along the coolant channels of an HTGR following a hypothetical accident of complete loss of cooling.
EXREM	ORNL 2/75	OP	Calculates external radiation doses.
FENG	LASL 2/77	OP	One of three codes which create or add to the reactions data library for QUIL and QUIC codes. Reactions added are of type Free Energy.
FEVER-7	GA	OP	Performs one-dimensional, diffusion theory, burnup and reload calculations.

Table 1.4.1 (Cont'd.)

Program	Origin/ Code Date	BNL Status	Function
FLAC	GA	OP	Calculates steady state flow distributions in arbitrary networks with heat addition.
FPPROD	BNL 3/78	OP	Performs simplified fission product production analysis.
FYSMOD	LASL 9/76	NOP	Calculates the two-dimensional solution of HTGR core blocks subjected to external motion.
GAKIT	GA 9/68	OP	Performs one-dimensional multigroup kinetics calculations with temperature feedback.
GAMBLE	GA	OP	A program for the solution of the multigroup neutron-diffusion equations in two dimensions, with arbitrary group scattering.
GGC4	GA/ACC	OP	Prepares broad thermal cross sections from the tape produced by WTFG and MAKE.
GOPTWO/ GOP-3	BPNW 6/75 BPNW 10/76	OP NOP	Graphite Oxidation Program. Analyzes the steady state graphite burnoff and the primary circuit levels of impurities.
HAZARD	BNL 3/77	OP	Analyzes gas layering and flammability in an HTGR containment vessel following a depressurization accident.
H-CON1	BNL 5/76	OP	Calculates one-dimensional heat conduction for an HTGR fuel pin by finite difference method.
HYDRA-1	BNL 5/76	OP	A program for calculating changes in enthalpy single phase liquid due to external heat source.
INREM	ORNL 2/75	OP	Calculates internal radiation doses.

Table 1.4.1 (Cont'd.)

Program	Origin/ Code Date	BNL Status	Function
INTERP	GA MICROX LIBRARY	OP	Prepares broad group cross sections from MICROX output data tapes.
JANAF	Dow Chemical Company 11/78	OP	JANAF Thermochemical Tables.
LARC-1	LASL 11/76	NOP	Calculates fission product release from BISO and TRISO fuel particles of an HTGR during the LOFC accident for single isotopes.
LARC-2	LASL	NOP	Similar to LARC-1; in addition, handles release from isotope chains.
LASAN-BNL LASAN-LASL	LASL/BNL 4/78	OP	A general systems analysis code consisting of a model independent systems analysis framework with steady state, transient and frequency response solution capabilities. There are two versions of the code available - the original LASL version and the converted BNL version.
LEAF	LASL 11/76	NOP	Calculates fission product release from a reactor containment building.
MAKE	SAI	OP	Prepares fine group fast cross section tape from GFE2 for spectrum codes.
NONSAP-C	LASL 10/78	NOP	Calculates static and dynamic response of three-dimensional reinforced concrete structures, in addition to creep behavior.
ORECA-1	ORNL-ACC 4/76	OP	Simulates the dynamics of HTGR cores for emergency cooling analyses. (Ft. St. Vrain)

Table 1.4.1 (Cont'd.)

Program	Origin/ Code Date	BNL Status	Function
ORIGEN	ORNL 4/75	OP	Solves the equation of radioactive growth and decay for large numbers of isotopes with arbitrary coupling.
ORTAP	ORNL-ACC 9/77	OP	A nuclear steam supply system simulation for the dynamic analysis of HTGR transients.
OXIDE-3	GA 1/74	OP (P)	Analyzes the transient response of the HTGR fuel and moderator to an oxidizing environment.
POKE	GA 7/70	OP (P)	Calculates steady state 1-D flow distributions and fuel and coolant temperatures in a gas cooled reactor.
PREPRO	GA	OP (P)	Prepares input data and source code revisions for RECA code.
PRINT	SAI	OP	Reads the fast cross section tape produced by MAKE.
QUIC	LASL 2/77	OP	Solves complex equilibrium distribution in chemical environments.
QUIL	LASL 2/77	OP	Solves complex equilibrium distribution in chemical environments.
RATE	LASL 7/78	OP	One of three codes which create or add to the reactions data library for QUIL and QUIC codes. Reactions added are of type Rate.
RATSAM-6	GA 5/77	OP	Analyses the transient behavior of the HTGR primary coolant system during accidents.
RECA	GA 8/70	NOP	Calculates time dependent flow distributions and fuel and coolant temperatures in the primary system.
RICE	LASL 3/75	OP	Solves transient Navier-Stokes equations in chemically reactive flows.

Table 1.4.1 (Cont'd.)

Program	Origin/ Code Date	BNL Status	Function
SODEMME	BNL 8/77	OP	Calculates transient thermal hydraulic aspects of circulating gas systems.
SOLGASMIX	ORNL 4/77	OP	Calculates equilibrium relationships in complex chemical systems.
SORS	GA 4/74		
SORSD	GA	OP (P)	Computes the release of volatile fission products from an HTGR core during thermal transients.
SORSG	GA	OP	Computes the release of non-volatile gaseous fission products from an HTGR core during thermal transients.
SPRINT	GA/SAI	OP	Reads the thermal cross section tape produced by WTFG.
SURF	LASL 2/77	OP	One of three codes which create or add to the reactions data library for QUIL and QUIC codes. Reactions added are of type Surface.
SUVIUS	LASL	NOP	Solves the behavior of fission gases in the primary coolant of a gas-cooled reactor.
TAC2D	GA 9/69	OP	Performs two-dimensional, transient conduction analyses.
TAP	GA	OP (P)	Calculates the transient behavior of the integrated HTGR power plant.
TEMCO/TEMCO7	GA	OP	Computes reactor temperature coefficients from input cross section data.

Table 1.4.1 (Cont'd.)

Program	Origin/ Code Date	BNL Status	Function
THGRAF	BNL 11/77	OP	Calculates position and velocity of the thermo-chromatograph as a function of time for various models.
WTFG	GA	OP	Prepares fine group thermal cross section tape from GAND2 or FLANGE for spectrum codes.
1-DX		OP	Performs one-dimensional, diffusion theory, steady state calculations.

1.4.2 Initial Reactor Trip During Unrestricted Core Heatup Accident (J. Colman, C. J. Hsu, P. G. Kroeger)

The GA code RATSAM6 simulates the primary loop thermohydraulics during various accident transients. Its original design was for design basis depressurization accidents (Deremer and Shih, 1977), but it has also been used extensively for unrestricted core heatup accidents, (UCHA), (GA staff report GA-A15000, 1978; and Deremer et al, 1977). In this latter application, different vendor analyses have indicated significantly varying pressure time histories to initial blowdown, the results apparently being very sensitive to side cavity flow resistances and heat transfer conditions. Our initial efforts were therefore geared at investigating this aspect for the 3000 MWt reactor.

Initial familiarization runs were made, beginning with a circulator trip, resulting in flow coast down and SCRAMM. Some typical results for the first 100 sec are shown in Figures 1.4.1 and 1.4.2, showing an initial cooldown and lowering of the system pressure subsequent to SCRAMM, as the flow decreases and reverses in the core and steam generators.

These runs were scrutinized very closely, investigating the specific reasons for many individual cases of flow and temperature reversals, and checking for conservation of mass, energy, and momentum. Virtually all system responses were found to be reasonable. Mass and energy conservation were found to be excellent under all conditions (within 5 to 6 significant digits). Momentum conservation was good, if the user forces a sufficiently small time step. The internal time step control did not reduce the time step sufficiently by itself. However, even if the user did not force a very small time step, momentum conservation errors occurred only during the very short time period of rapid flow transients as the circulators coast to zero speed, (0 to 5 sec), and these potential inaccuracies had no long term effect on the results after about 20 sec.

Efforts to increase the time step after about 20 sec, when all rapid transients have subsided, were disappointing in that no significant increase in time steps was found possible, as would be desired for the longer UCHA transients.

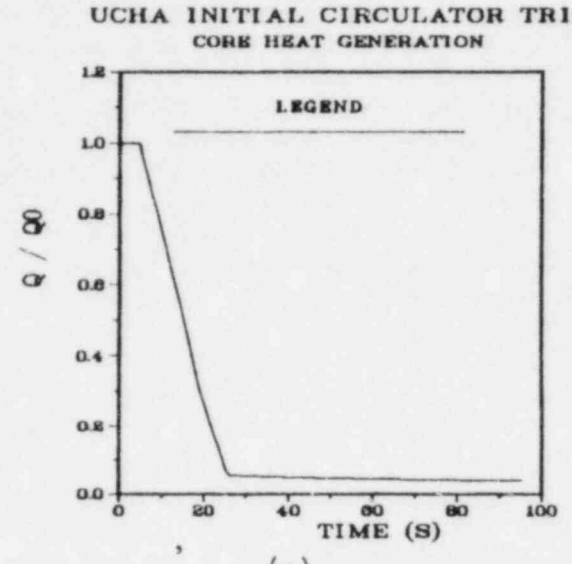

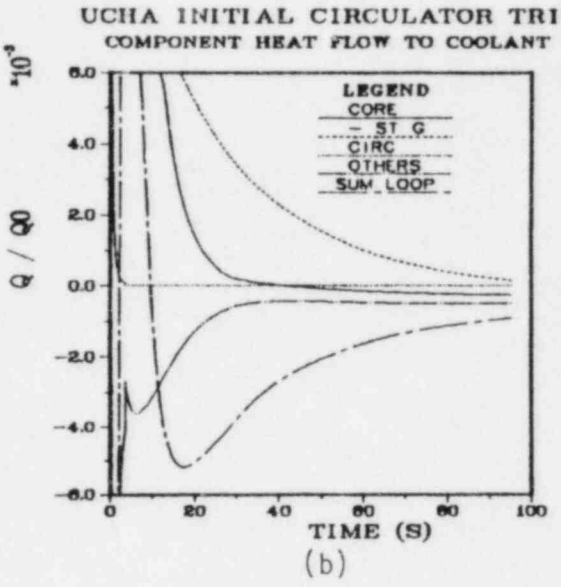

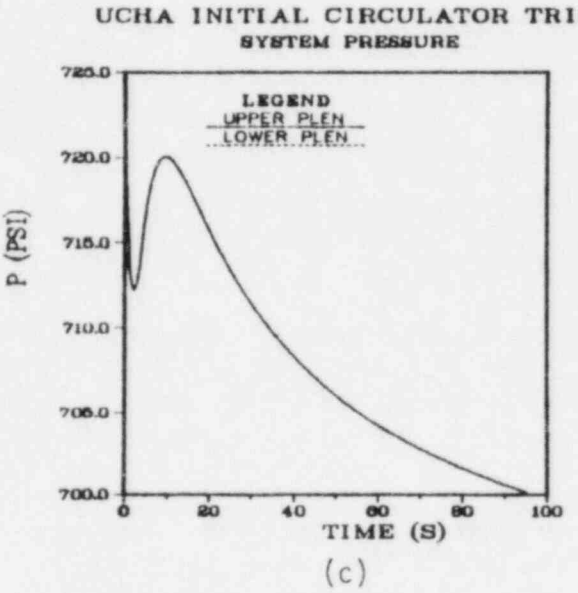

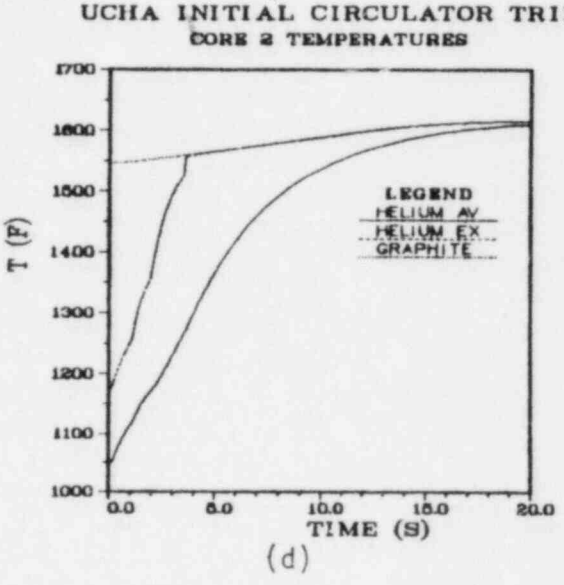

Figure 1.4.1 Typical Initial Primary Loop Response to Circulator Trip at Time Zero.

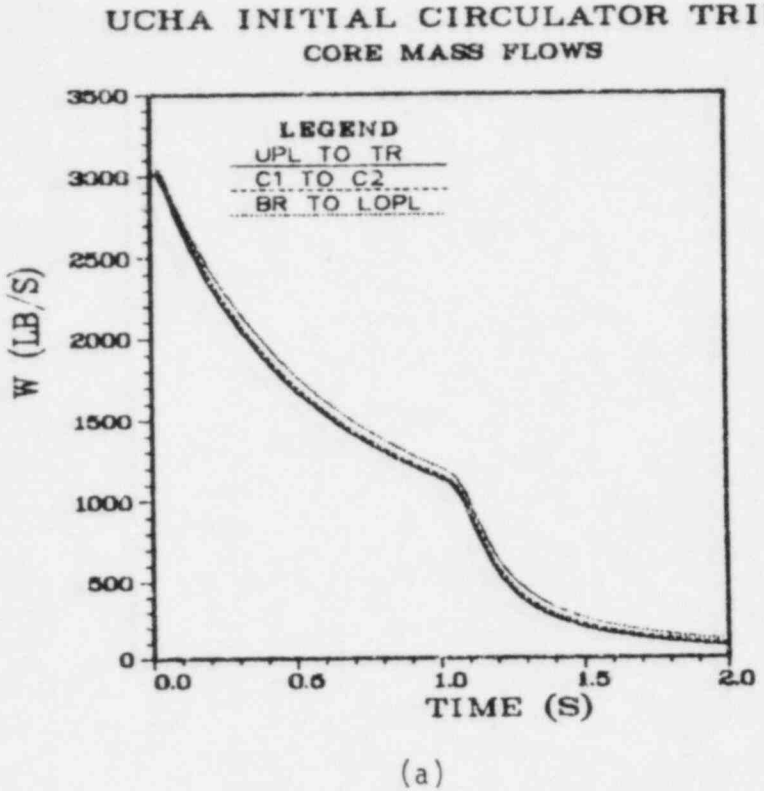

(a)

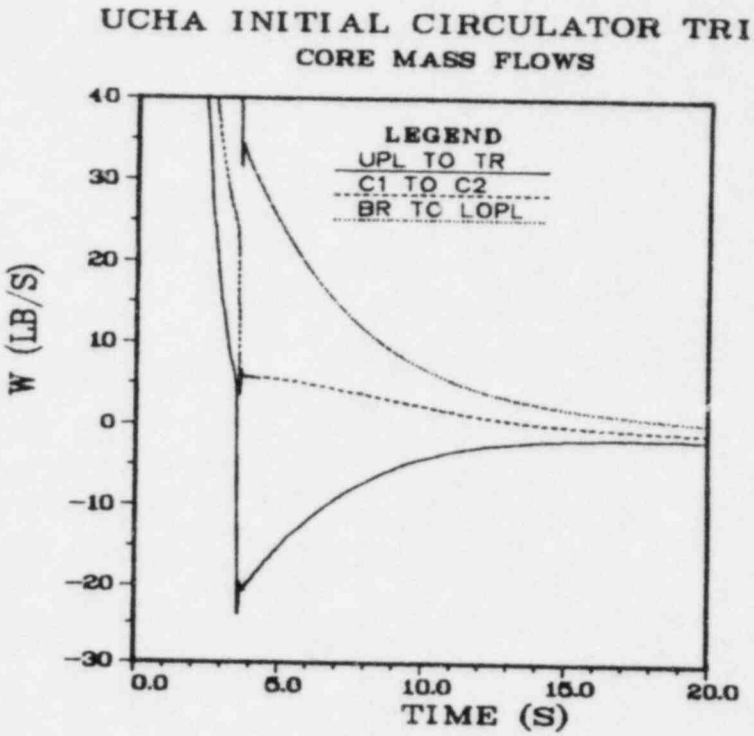

(b)

Figure 1.4.2 Typical Short Term Core Mass Flows Following Circulator Trip at Time Zero.

During February this effort was redirected in support of the upcoming siting study for the 2240 MWt reactor. Conversion of the RATSAM code input data from the case of a 3000 MW reactor to those for a 2240 MW reactor is almost complete. The new input data are currently being tested for proper steady-state conditions. Some of the relevant information such as fuel element data and PCRV geometry, core cavity inlet temperature, coolant flow rate, circulator power and helium pressure at circulator discharge etc. were obtained from design data reports supplied by General Atomic for this siting study. Distribution of the helium pressure and both the coolant and solid temperatures throughout the primary-side nodes has been calculated, and they are found to yield good steady-state conditions. Further attention is currently being given to some of the flow resistances, to substitution of a butterfly-type check valve instead of a motor operated shutoff valve in the steam generator flow paths, revision of the steam generator secondary side data and to the side cavity cooling subsequent to SCRAMM.

Initial circulator trip and SCRAMM runs are giving reasonable results for a single core channel model, as well as for a core model consisting of two parallel channels.

The possibility of going to a quasi-steady form of some of the coolant conservation equations for the longer UCHA transients is currently being considered. Long term UCHA runs considering pressure history to blowdown and MTRC are scheduled for the coming quarter.

1.4.3 Thermal Liner Cooling System Analysis (P. G. Kroeger)

The primary function of the thermal liner cooling system is to maintain low concrete temperatures during normal operation. During UCHA, i.e., in the absence of all forced circulation this system provides some remaining cooling capability. In the Fort St. Vrain reactor, the liner cooling system was designed to provide sufficient cooling for safe decay heat removal. In the 3000 MWt reactor the system was not designed to achieve this purpose, but the AIPA Phase II Study (GA-A15000) showed it to be capable of terminating UCHA accidents with about 90% probability.

For the 2240 MWt reactor, subject of the current siting study, an enhanced thermal liner cooling system was designed to provide sufficient cooling to prevent concrete degradation during UCHA, and thus ''turn around'' the hypothetically most serious accidents by avoiding ultimate containment failure.

As the functioning of this backup system can have a controlling effect on the ultimate progression of the most serious hypothetical accidents, it was decided to consider its various characteristics in more detail.

As part of BNL support for the 2240 MWt reactor siting study, design data for the thermal liner cooling have been requested from GA, and have been received. An initial review has been initiated.

The major potential failure mode of the liner cooling system would occur only 120 to 180 hrs into a UCHA sequence. Excessive radiation from the top reflectors can lead to the failure of some of the cover plates in the upper plenum, which can expose part of the liner to the high thermal load of direct

radiation from the top reflectors. If a sufficient length of any of the cooling system pipes were to be exposed leading to boiling in such pipe, this would result in increased pressure drop in that flow path, causing a flow reduction and further temperature increase, ultimately leading to potential burnout of the liner and tube at that point. It should be noted that this scenario will only occur with few selective cover plate failures. If a sufficiently large number of cover plates fails, the liner cooling capacity would be sufficient to cool the top reflector and thus reduce the radiative heat flux from the top reflectors to the liner, which could then again function to prevent excessive concrete temperatures.

Initial results show that subcooled boiling conditions can occur locally in the horizontal cooling tubes which are welded to the liner, but that as long as the bulk of the fluid within each pipe remains subcooled, the resulting increase in friction pressure drop will be less than 3% with a corresponding decrease in coolant flow of less than 2%, which would be inconsequential except under very extreme conditions. An initial quasi-steady thermal analysis of the liner indicates a potential for relatively high peak liner temperatures beyond 800F and very high temperature gradients across the liner to tube weld. However, none of the indicated liner temperatures present a danger to the integrity of the liner or the coolant tubes.

1.4.4 Estimation of Radiant Heat Interchange Between the Core and the Reflector Regions during an Unrestricted Core Heatup Accident. (C. J. Hsu)

During the later phase of an UCHA with no forced coolant circulation, the decay heat is transferred from the core region to the inlet plenum region mainly by conduction and radiation. Within a coolant channel, the channel wall temperatures in the core region are considerably higher than those in the top or bottom reflecter regions, and, hence, there may be appreciable radiation heat interchange among those wall surfaces of a coolant channel. To study the relative importance of this radiant interchange as compared to the conductive heat transfer, attempt was made to estimate the magnitude of such radiation heat transfer. For this purpose, however, it is necessary to have the knowledge of radiation shape factors between two arbitrary ring elements formed by the cylindrical coolant channel wall. During the reporting period, the shape factor equation was derived for the radiant interchange between two finite emitting and reflecting ring surfaces by integrating the expression for the shape factor for two infinitesimal ring elements given by Sparrow and Cess (1966) followed by applications of the angle-factor algebra.

Preliminary calculations using this equation indicated that radiant heat interchange between the core region and the reflector region is not small compared to the conduction heat transfer. However, since this item is not of critical impact on the current HTGR siting study, further efforts have been deferred at this time.

REFERENCES

DEREMER, R. K. and SHIH, T.:''RATSAM: A Computer Program to Analyze the Transient Behavior of the HTGR Primary Coolant System During Accidents,'' General Atomic Co., Report No. GA-A13705, May 1977.

DEREMER, R. K., et al: ''Primary Coolant System Response to an HTGR Core Heatup,'' Proceedings of the ANS Topical Meeting on Thermal Reactor Safety, July/August 1977, Sun Valley, Idaho.

GROWCOCK, F. B., BARRY, J. J., FINFROCK, C. C., HEISER, J. H. III, RIVERA, E., and WALES, D. R., ''Graphite and Ceramics,'' Reactor Safety Research Quarterly Progress Report , Oct. - Dec. 1981, Brookhaven National Laboratory, pending.

SOO, P., SABATINI, R and GERLACH, L., ''Fatigue of Structural Materials'' in Advanced Reactor Systems Quarterly Progress Report, Oct - Dec. 1981, to be published.

SOO, P., SABATINI, R. L., EPEL, L. A. and HARE, J. R.,Sr., ''High Cycle Fatigue Behavior of Incoloy 800H in a Simualted High-Temperature Gas-Cooled Reactor Helium Environment'', BNL-NUREG-51156, 1980.

SPARROW, E. M. and CESS, R. D., ''Radiation Heat Transfer,'' Brooks/Cole Publishing Co., p. 133 (1966)

STAFF: ''HTGR Accident Initiation and Progressijon Analysis Status Report; Phase II Risk Assessment,'' General Atomic Co., Report No. GA-A15000, April 1978.

2. SSC DEVELOPMENT, VALIDATION AND APPLICATION (J. G. Guppy)

The Super System Code (SSC) Development, Validation and Application Program deals with advanced thermohydraulic codes to simulate transients in LMFBRs. During this reporting period, work on three codes in the SSC series was performed. These codes are: (1) SSC-L for simulating short-term transients in loop-type LMFBRs; (2) SSC-P which is analogous to SSC-L except that it is applicable to pool-type designs and (3) SSC-S for long-term (shutdown) transients occurring in either loop- or pool-type LMFBRs. This program is currently focused to provide direct support to the on-going CRBRP licensing activities within NRC. In addition to these code development and application efforts, validation of these codes is an on-going task. Reference is made to the previous quarterly progress report (Guppy, 1981) for a summary of accomplishments prior to the start of the current period.

2.1 SSC-L Code (M. Khatib-Rahbar)

2.1.1 CRBRP Loss of Heat Sink Application (W. C. Horak, G. J. Van Tuyle, R. J. Kennett, J. G. Guppy)

Several CRBRP input decks for SSC-L are being refined and expanded to reflect the latest design parameters in order to provide analytical capabilities for various plant transients.

For one case (also being conducted in support of the Sandia accident delineation study), a two-loop simulation has been run. The scenario involves: 1) station blackout and plant trip; 2) total loss of heat sink past the IHXs; 3) pony motor flow in one loop only; 4) check valve closure in the two non-powered loops following onset of flow reversal in these loops and 5) unavailability of the direct heat removal service (DHRS). The simulation was terminated at 9200 seconds when the coolant temperature in the hot channel exceeded the sodium saturation temperature. A restart tape was stored for future use in the low heat flux boiling model validation. Analyses such as these provide one means of scoping the time available for the plant operators to act to mitigate the effects of the postulated transient.

2.1.2 CRBR Station Blackout Transient Simulation (W.C. Horak, R. J. Kennett, G. J. Van Tuyle)

Station blackout transients under investigation include: 1) station blackout with no pony motor flow and the steam generator auxiliary heat removal system operating per design; 2) station blackout with no pony motor flow and total loss of auxiliary feedwater and all protected air-cooled condensers and 3) transients starting from 40% power (the lower limit on CRBRP load-follow capabilities).

In the latter case (i.e., from 40% power), difficulties occurred in the steam generator system due to lack of sufficient design information, where, because the recirculation pump is running at full speed, the energy balances were inconsistent and calculations lead to unlikely results. This problem was resolved when it was found that a bleed-off flow from the steam drum to the topping heater is included in the CRBR design which accounts for some of the

discrepancy. A data deck for a more complete representation of the CRBR steam generator system has been developed.

A CRBR station blackout umbrella transient was simulated for a total of 1800(s). The simulation, which used the shorter pump coastdown time, showed that the hottest channel coolant exit temperature remained more than 100°K subcooled. Due to a steam table function with a narrow range of applicability, it was necessary to run this transient with the auxiliary feedwater temperature at 550°K, which is approximately 200°K above the PSAR value. Attempts are being made to run this transient at more realistic feedwater conditions, now that the steam table limitation has been corrected. Additionally, data are being requested from the Project Office to permit a more realistic simulation of the auxiliary feedwater flow for this transient.

An additional station blackout transient, involving unavailability of auxiliary feedwater, is being pursued. Emptying of the steam drum liquid inventory was indicated at approximately eight minutes. This run is being analyzed further.

2.1.3 CRBRP Pipe Break Application (B. C. Chan, E. G. Cazzoli)

The latest information from the PSAR has been used to modify the CRBRP pipe break data representations. This model was tested using a two-loop simulation, the break located at the reactor vessel inlet after the check valve in one of the two loops. Primary and intermediate pumps trip at 0.6 seconds after pipe break, with check valves and pony motors in operation. Double-ended pipe break and half-pipe area break events were performed; results are under study.

2.1.4 Assessment of CRBRP Heat Removal Capability (G. J. Van Tuyle)

The latest available information from the CRBRP PSAR was used to obtain the anticipated system temperatures and mass flow rates at operating conditions between 40% and 100% of full power. Using SSC, the plausibility of these projected conditions was assessed. The SSC results for the IHX and superheater tend to support their analysis. However, our analysis shows that a potential problem area exists in the evaporator. Further discussion of this assessment is contained in Section 3 of this report under CRBRP Part Load Study.

2.1.5 Sodium Boiling Model (M. Khatib-Rahbar, E. G. Cazzoli)

Work on the present boiling model was completed. A draft report describing the model, and the interface with the SSC code, along with initial applications is nearing completion. Work is underway toward validation of the present model using ORNL experimental data and some two-dimensional calculations.

The steady state model was used to generate boiling map characteristics for a CRBRP fuel assembly with maximum power for various inlet subcooling conditions. Results indicated that steady state single-phase natural convection exists up to 160 MW/m^3 to the point of flow excursion which occurs at about 200 MW/m^3 (approximately 15% assembly power); beyond this power density, flow excursion occurs leading to enthalpy burnout. The analysis also

indicated that any boiling occurring as a result of power and flow mismatches (which can occur during transition to natural circulation) can lead to unstable boiling and subsequent premature excursion and dryout for power densities greater than approximately 50 MW/m^3 (4% assembly power).

The transient model was used to verify the above observations. The results showed that boiling can occur during the initial transition period to natural convection heat removal and can indeed lead to cladding dryout. Furthermore, the boiling process, and existence of conditions conducive to flow excursion, is highly transient and path dependent.

2.1.6 Code Maintenance (T. C. Nepsee)

In order to accommodate the need for increased global container size, several measures have been taken in SSC to make more efficient use of small core memory (SCM). These include: (1) more efficient data packing within the module data abstraction; (2) revision of global pointer allocation tables and (3) improved segmentation. The above measures are now incorporated in SSC-L Cycle 40.

Other potential areas for SSC improvement have been identified. These include estimation of redundant code, modularity improvements, and global data cleanup. Major benefits to be achieved in the process are better SCM usage and improved maintainability.

An initial investigation into the use of the 1977 ANSI FORTRAN (FTN 5) suggests that it could be of considerable benefit in eliminating most of the current portability problems. Further flexibility studies are indicated before making any commitments.

2.1.7 User Support (G. J. Van Tuyle, T. Iwashita/PNC)

An update data set to represent a helical coil steam generator was made. A verification of steady state calculations in the steam generator module is being made by using PNC's experimental data.

Since the data obtained from the Instability Test Rig (ITR) in OEC (Oarai Engineering Center of PNC) include water/steam-side temperature behavior, temperature distributions along the tube can be compared with calculated values. Input data for a 70% load case (0.7 MWt) for the ITR were prepared. Feedwater flow, temperature and steam pressure obtained from the experimental data were used as transient boundary conditions. The initial temperature distribution was compared with experimental data. As expected, the Schrock-Grossman's equation underestimated of the heat transfer in the boiling region. After surveying several steady-state cases, transient comparisons will be done.

2.2 SSC-P Code (E. G. Cazzoli)

2.2.1 Code Maintenance (E. G. Cazzoli)

Due to the focusing of this program to provide direct support for the CRBRP licensing activities, work on the SSC-P code has been slowed. However, modification of SSC-P to maintain its compatibility with the latest cycle of the SSC program library is continuing, but on a reduced level.

2.3 SSC-S Code (B. C. Chan)

2.3.1 Direct Reactor Auxiliary Cooling System (DRACS) for LMFBRs (B. C. Chan)

A preliminary report describing the DRACS modeling used for the LMFBR Conceptual Design Study design is being written.

2.3.2 Direct Heat Removal Service (DHRS) for CRBRP (B. C. Chan)

Work has been completed on the existing DRACS model to represent the DHRS to provide reactor vessel decay heat removal capability for CRBRP simulations. This includes modifications to the sodium and NaK hydraulic models, overflow (Na-to-NaK) heat exchanger and air blast (NaK-to-air) heat exchanger models.

Several test cases have been performed. Preliminary results show that the DHRS model for the thermal and hydraulics calculations is correctly coupled with the primary loop(s) in SSC. The calculations of the decay heat removal for CRBRP loss of normal heat sink event simulations cannot be carried further at this time because some specific design information (requested from the applicant) for the DHRS is still unknown.

2.4 SSC Validation (W. C. Horak)

2.4.1 Testing of New Export Version (W. C. Horak, R. J. Kennett)

The new export cycle of SSC was tested for several one and two loop transients. The code performed satisfactorily although some discrepancies with earlier versions of SSC were noted.

A change was made in the fuel-gap conductance calculation so that the maximum value of the gap conductance would not exceed the value of the user specified contact conductance for a closed gap. Additionally, an error in the calculation of the in-pin radial power distribution was identified and corrected.

Null transients were run to validate the new export cycle of SSC. Several minor bugs involving the master clock timestep calculation were detected and fixed.

2.4.2 FFTF Natural Circulation Calculations (W. C. Horak, J. G. Guppy)

Minor code modifications are continuing to allow FFTF cases to be run with the latest cycle of the SSC-L code. Since the DHX representation will no longer be utilized during the transient, changes are required such that the coolant gravitational head on the sodium side will be properly calculated and interfaced with the code. The DHX sodium outlet temperature will be a boundary condition with the input supplied directly from test data.

It has been decided that the pressure drop across the DHX modules will be initially simulated with two components only: 1) the gravity head using a density based on the average of the inlet and outlet temperatures to the DHX and 2) a form loss proportional to the square of the velocity. Since natural circulation is the driving force, it may become necessary to model the pressure drop with a Reynolds number dependent frictional pressure drop explicitly.

The 19 channel core case has been modified and tested for a total of 30(s) transient simulation time on a 100% power natural circulation transient. Some minor modifications are being made to the input channel power and flow fractions in order to match them better with the actual test conditions.

REFERENCES

GUPPY, J. G., et al., (1981), "SSC Code Development", in Reactor Safety Research Programs Quarterly Progress Report, October 1 - December 31, 1981, Brookhaven National Laboratory, (to be published), 1982.

PUBLICATIONS

CHAN, B. C., et al., "Direct Reactor Auxiliary Cooling System Modeling in SSC", to be published (1982).

HORAK, W. C., et al., "A Numerical Procedure for Calculating Temperature Profiles in LMFBR Coolant Channels", Trans. Am. Nuc. Soc., 39, 495, (1981).

HORAK, W. C., "A Nodal Coarse-Mesh Method for the Efficient Numerical Solution of Laminar Flow Problems", Trans. Am. Nuc. Soc., 39, 1031, (1981).

HORAK, W. C., et al., "Validation of the In-Vessel Energy Balance Module in SSC for Natural Circulation Transients, (to be published), 1982.

JAMALI, K. M. and KERR, W., "Probabilistic Methods for Accident Progression Analysis", Proceedings of ANS/ENS International Topical Meeting on Probabilistic Risk Assessment, 649, (1982).

KHATIB-RAHBAR, M. and CAZZOLI, E. C., "Flow Excursion Induced Dryout at Low Heat Flux Natural Convection Boiling, (to be published), (1982).

KHATIB-RAHBAR, M., et al., "LMFBR System-Wide Transient Analysis: The State of the Art and U.S. Validation Needs (to be published), (1982).

VAN TUYLE, G. J., "Analysis of CRBRP Loss of Electric Power Using the New SSC Steam Generator", (to be published), (1982).

3. GENERIC BALANCE OF PLANT MODELING (J. G. Guppy)

The Generic Balance of Plant (BOP) Modeling Program deals with the development of safety analysis tools for system simulation of nuclear power plants. It provides for the development and validation of models to represent and link together BOP components (e.g., steam generator components, feedwater heaters, turbine/generator, condensers) that are generic to all types of nuclear power plants. This system transient analysis package is designated MINET to reflect the generality of the models and methods, which are based on a momentum integral network method. Reference is made to the previous quarterly progress report (Guppy, 1981) for a summary of accomplishments prior to the start of the current period.

3.1 MINET (Momentum Integral Network) (G. J. Van Tuyle)

The former steam generator system transient analysis package within SSC (Agrawal, 1978), until this time referred to as the steam generator network, has been renamed MINET. This name more accurately reflects the generality of the models and methods, which are based on a momentum integral network method.

Export Cycle 2 of SSC contains the current version of MINET, which can represent pumps, pipes, heat exchangers, valves and accumulators (voluminous components, such as the CRBRP steam drum). This version of MINET forms the basis for our balance-of-plant (BOP) modeling effort.

In order to expedite our development and testing of new modules for MINET, we will isolate it from the export cycle of SSC. A set of updates, to be used against the SSC code library, will be developed so as to suppress all portions of SSC unnecessary to MINET operations. In this way, all modifications to MINET will concurrently impact on both the stand-alone version and the version run in tandem with SSC.

3.2 MINET Improvement (G. J. Van Tuyle, T. C. Nepsee)

The treatment of the heat transfer term in the coolant energy equations was altered from fully explicit to implicit with respect to fluid enthalpy and mass flow rate. Corresponding limits on the timestep were removed.

When the implicit treatment of the heat flux term was introduced into on-going application runs, surprising improvements in computation speed were noted throughout the code. Further investigation led to the discovery that when the steam generator took smaller steps than the master clock, the pressure drops in the part of the intermediate loop treated in the steam generator were sufficiently irregular so as to restrain the allowable master clock timestep. The source of the difficulty proved to be the way in which the advanced time intermediate loop mass flow rate was introduced into the steam generator, i.e., as a step instead of a ramp.

An update set that facilitates the representation of co-current (in addition to counter-current) heat exchangers was incorporated into the code. As a test, we altered the flow direction in a helical coil heat exchanger representation and found that a much higher hot-side temperature was needed to

transfer the same amount of heat. Of course, this is consistent with the reduced efficiency of co-current units.

As part of the nodal calculations in the momentum integral network method, it is necessary to provide constraints for junction enthalpies on both ends of a node with diverging flow, i.e., flow exiting both ends originally. These constraints were provided using two half-node energy equations, donor-cell differenced outward from the node center. When the treatment of the heat transfer term was changed to implicit, the resulting complexities in these half-node energy equations induced us to convert to simpler constraints. We now assume the enthalpy changes uniformly throughout such a node during a timestep.

During recent applications, it was determined that improvements could be made in the steady state calculational procedure. Because convergence on the heat exchanger area correction factor becomes increasingly difficult at lower power levels (e.g., higher secondary to primary flow rates), a highly reliable bisection scheme was substituted for the faster scheme that was in use. A counter was installed in the printout to tell the user how the calculations were proceeding, in case the code fails to complete the steady state calculation. Finally, the logic was altered so that the user could request a full printout of current iteration system values simply by changing one input value.

The introduction of cold (70°F) auxiliary feedwater into the steam generator system (MINET) exposed a shortcoming in the steam table functional fit package. Because the density function was applicable only for considerably higher temperatures, the density and density derivatives at 75°F were non-physical. To correct this shortcoming, the liquid density function from a 1967 report by Jordan (KAPL-M-6734) was taken and incorporated into the steam tables. The results have been quite satisfactory.

With the immediate problem corrected, the steam tables were then tested over a wide range. Pressures were varied from 0.5 to 14.0 MPa, and temperatures were varied from 300 to 1000°K. The calculated properties, in the subcooled, saturation, and superheated regimes were compared against a tabular version of the 1967 ASME steam tables. In general, the errors in the fuctions are quite small, never greater than 1%. Functional derivatives were verified via perturbation techniques, and also checked out quite well.

3.3 MINET Improvements in Process (G. J. Van Tuyle, T. C. Nepsee)

Modifications have been developed to allow representation of a check valve as a valve with a minimum allowable mass flow rate. It will be factored into the code library as soon as the code is resequenced for export.

When the two steady state network solvers were developed, little effort was made to minimize the use of temporary data storage space. As the CRBRP system representation has grown larger,this inefficiency has become a problem. Therefore, the larger network solver (pressure and flow) has been modified to reduce its storage requirements by 70%. Again, these modifications will not be implemented until the SSC code library has been resequenced for export.

A somewhat larger set of modifications was developed to allow representation of volumes principally for the CRBRP steam drum using a three region non-equilibrium model.

Work is underway on an air-cooled condenser model. Current plans are for a relatively simple model initially that will have minimal impact on the current calculational process.

3.4 Balance of Plant Models (G. J. Van Tuyle)

An extensive computer search for published models of feedwater heaters and turbines was performed. With the majority of the abstracts now reviewed, there have been no existing generic balance of plant models identified. However, there appear to be many interesting papers, including some making reference to existing LWR data for plant transients involving BOP components.

3.5 MINET Input Deck C-1 (G. J. Van Tuyle, T. C. Nepsee)

The input deck used in the CRBRP Part Load Study and the analysis of a station blackout event without auxiliary feedwater has been designated MINET Deck C-1, and documented accordingly. This representation (Figure 3.1) includes the evaporator and superheater, the recirculation pump, the safety/relief valves, the steam generator auxiliary heat removal system vent valves, the steam drum drain line, a protected air-cooled condenser (PACC) related heat sink term, and the main steam isolation (superheater outlet), turbine throttle, and turbine bypass valves. It does not include check valves at the outlets of the heat exchangers.

3.6 CRBRP Part Load Study (G. J. Van Tuyle)

The latest available information from the CRBRP PSAR was used to obtain the anticipated system temperatures and mass flow rates at operating conditions between 40% and 100% of full power. Using SSC/MINET, the plausibility of these projected conditions was assessed. Seven cases were run using MINET Deck C-1 to determine how much of the available heat transfer area was needed, according to the SSC/MINET heat transfer correlations. The calculated fractions of available heat transfer area used for the IHX, evaporator, and superheater are shown in Table 3.1. According to the PSAR, the project's analysis was performed with the heat transfer fouled by 10%. Thus, the SSC numbers for the IHX and superheater tend to support their analysis. Variation in the fractions for the IHX and superheater is not very significant because these units are highly responsive to temperature. However, a problem area may be in the evaporator, according to our analysis. At this time, questions for the CRBR project regarding the source of their estimates for the heat transfer across the evaporator are being prepared.

Table 3.1 Fraction of Available Heat Transfer Area Utilized

Power Frac	40%	50%	60%	70%	80%	90%	100%
f^{IHX}_{Tubes}	.807	.860	.877	.877	.868	.842	.863
f^{Evap}_{Tubes}	.647	.666	.666	.700	.707	.726	.730
f^{Suph}_{Tubes}	.951	.844	.836	.848	.814	.812	.782

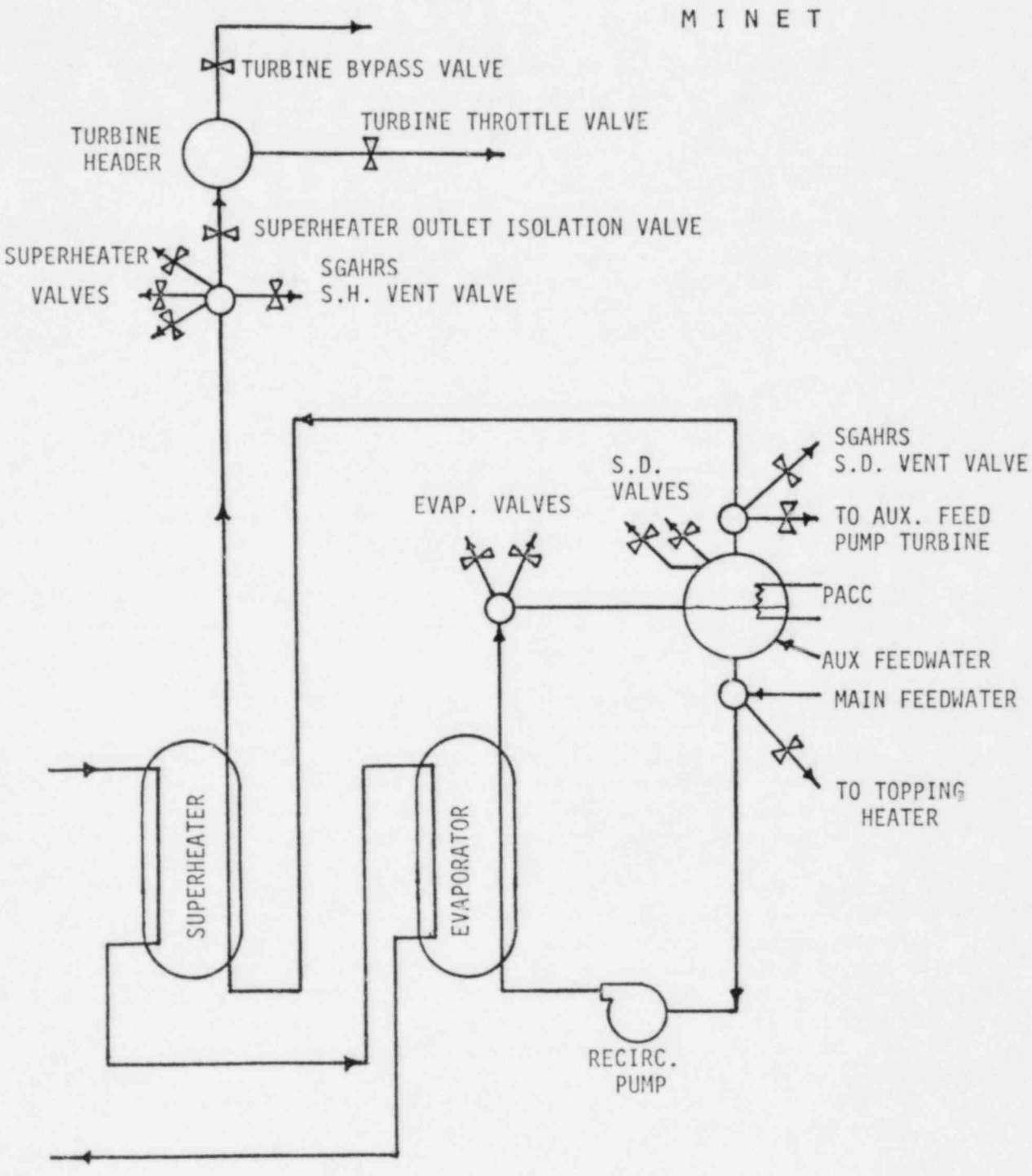

Figure 3.1 MINET Deck C-1 Representation of CRBRP Steam Generator System

3.7 MINET Applications to CRBRP Station Blackout (G. J. Van Tuyle)

Analysis of a CRBRP Station Blackout event with pony motors and auxiliary feedwater unavailable, performed using MINET Deck C-1, is reported in a paper to be presented at the 2nd Joint ANS/ASME Nuclear Engineering Conference, to be held in Portland, July 25-28. In this analysis, the steam drums dried out eight minutes after the loss of power. A check of the net outflow of water/steam during these eight minutes (22 metric tons) against the initial liquid inventory in the three drums (23 metric tons) tends to support the code results.

The analysis of the same station blackout event is more difficult when auxiliary feedwater is available. This is because we have to rely on the CRBRP project office for control system setpoints that have not yet been incorporated into the PSAR. In particular, the control of the auxiliary feedwater system is critical to the progression of this transient. In the analysis performed thus far, we observe a significant reduction in the steam generator system pressure while the cold auxiliary feedwater is being sprayed into the steam drum, causing the SGAHRS vent valves to close, and flow to reverse from the superheater line. At this point, the check valve at the superheater outlet becomes important, and we have to incorporate it into the representation.

The CRBRP project office has recently released a report (WARD, 1982), presenting the DEMO (WARD, 1976) analysis of a station blackout event without pony motors, also known as a "natural circulation event". Because a critical parameter, the steam drum level, was inexplicably omitted from this report, we cannot ascertain whether the DEMO analysis was performed with the same control system setpoints that we are using. There is significant disagreement between DEMO and MINET on the behavior in the steam generator system during this event.

REFERENCES

AGRAWAL, A. K., et al., (1978), "An Advanced Thermohydraulic Simulation Code for Transients in LMFBRs (SSC-L Code)", BNL-NUREG-50773, (1978).

GUPPY, J. G., et al., (1981), "Generic BOP Modeling", in Reactor Safety Research Programs Quarterly Progress Report, October 1 - December 31, 1981, Brookhaven National Laboratory, (to be published), 1982.

WARD (1976), "LMFBR Plant Simulation Model (DEMO)", WARD-D-0005, Rev. 4, (1976).

WARD (1982), "Summary Report on the Current Assessment of the Natural Circulation Capability with the Heterogeneous Core", WARD-D-0308 (1982)

PUBLICATIONS

VAN TUYLE, G. J., "Analysis of CRBRP Loss of Electric Power Using the New SSC Steam Generator", (to be published), (1982).

4. Thermal-Hydraulic LWR and LMFBR Safety Experiments

4.1 Core-Concrete Heat Transfer Studies (G. A. Greene and J. C. Chen (Lehigh University))

The purpose of this task is to study and characterize the various heat transfer phenomenologies involved in the analysis of the ex-vessel attack of molten core-steel mixtures upon concrete in a reactor cavity. These studies are principally in support of the CORCON development program at Sandia National Laboratory.

4.1.1 Heat Transfer Between Immiscible Liquid Layers with Gas Bubbling

In previous quarterly reports, it was mentioned that the heat transfer between two overlying immiscible liquid layers agitated by a vertical gas flux would depend predominantly on whether or not there was mass transfer or entrainment across the interface driven by the gas flux. In the case of no entrainment, the magnitude of the heat transfer could be calculated by the surface renewal model within a factor of two, based on comparison of the model to available experimental data. The principal role played by the gas flux would be to disturb the temperature gradients at the interface between the liquid layers. In this manner, heat transfer augmentation would be due to transient conduction. Recent data have shown the Szekeley model to represent a lower bound to the non-entrainment heat transfer data. Since the Szekeley formulation does not model surface disturbances (waves) or heat transfer enhancement beyond the impact area of the bubble cross-section, accounting for these effects should improve the agreement between the model and the data.

For the case of fluids which will exhibit mass transfer or entrainment when subjected to a transverse gas flux, the heat transfer rate is not well characterized by the Szekeley surface renewal model and, under these conditions, it and similar models should not be employed. As shown in previous quarterly reports, for the same gas velocity as non-entraining fluids, heat transfer with entrainment was found to be greater in magnitude by as much as two orders of magnitude or more. This effect certainly cannot be explained by modification to the surface renewal theory nor can it be ignored.

4.1.2 Entrainment Heat Transfer Modeling

It was reported that the entrainment cases fell into two categories, a droplet entrainment regime and a "gross" entrainment regime. Current modeling of liquid-liquid entrainment due to gas bubbling is crude at best. Although we have been able to develop a model, based upon a static force balance, which appears to describe the conditions for the onset of entrainment, calculated entrainment rates have been greater than measured rates in single bubble entrainment tests by approximately a factor of ten. For the purposes of this discussion, therefore, the entrainment will be treated in a parametric fashion, subject to future refinement in the entrainment rate model.

For the entrainment heat transfer model, it is assumed that the heat transfer is composed of a component due to the interfacial agitation (surface

renewal) and a component due to the mass entrainment itself. The Szekeley heat transfer coefficient is

$$h_{SZE} = 1.69\ k(j_g/\kappa r_b)^{1/2} \tag{4.1}$$

where k is the fluid thermal conductivity, j_g is the gas superficial velocity, κ is the fluid thermal diffusivity, and r_b is the bubble radius. The interfacial disturbance heat transfer rate (surface renewal), subject to the reservations outlined in Section 4.1.1, is then

$$q_{interface} = h_{SZE}\ A\ \Delta T_{12} \tag{4.2}$$

where A is the interfacial cross-sectional area and ΔT_{12} is the temperature difference between the upper (1) and lower (2) layers.

The component of the heat transfer due to entrainment can be expressed as the product of the mass rate of entrainment times the excess enthalpy of the entrained phase (2) transferred to the continuous phase (1), that is

$q_{entrain}$ = (mass entrainment rate) (excess enthalpy transferred/unit mass)

or

$$q_{entrain} = (j_2\ A\ \rho_2)\ \ (C_1\ C_{p2}\ \Delta T_{12}) \tag{4.3}$$

where j_2 is the superficial velocity of the entraining fluid, ρ_2 is the density, C_{p2} is the specific heat, and C_1 is the fraction of the excess enthalpy of fluid 2 that is transferred to fluid 1. It can be easily shown by analysis of transient convective heat transfer around a sphere, under conditions of the entrainment heat transfer data, that $C_1 \sim 1$.

Combining Equations (4.2) and (4.3), we have

$$q_{total} = h_{SZE}\ A\ \Delta T_{12} + j_2 A\ \rho_2\ C_{p2}\ \Delta T_{12} \tag{4.4}$$

If the effective heat transfer coefficient is defined as $h_{eff} = q_{total}/\ AT_{12}$, then this reduces to

$$h_{eff} = h_{SZE}\ + j_2\ \rho_2\ C_{p2} \tag{4.5}$$

Let $j_2 = C_2 j_g$, where C_2 is the ratio of the volumetric entrainment rate of fluid 2 to the volumetric gas flux. Then Equation (4.5) becomes

$$h_{eff} = h_{SZE} + C_2 j_g \rho_2 C_{p2} \tag{4.6}$$

In the oil-water experiments, the component of the interfacial heat transfer resistance on the water side of the interface can be shown to be negligible with respect to that on the oil side of the interface. As a result the overall interface heat transfer coefficient from the Szekeley model is simply that calculated for the oil. In the general case, where both sides of the interface must be considered, the overall interfacial heat transfer coefficient due to interfacial disturbances (not entrainment) would be

$$\frac{1}{h_{overall}} = \frac{1}{h_{SZE1}} + \frac{1}{h_{SZE2}} \qquad (4.7)$$

At present, the major uncertainty in applying Equation (4.6) to the case of heat transfer with entrainment is the determination of the coefficient C_2. Comparison of Equation (4.6) to the available BNL and KFK entrainment heat transfer data suggests that the data are bracketed by the choice of C_2 in the range (0.3, 1.0). Further work is underway to improve this aspect of the heat transfer model.

4.2 Core Debris Thermal Hydraulic Phenomenology (Steam Spike Phenomenology)
(T. Ginsberg, J. Klages, J. Klein, C. E. Schwarz; J. C. Chen, Lehigh University)

This task is directed towards development and experimental evaluation of analytical models for prediction of the rate of steam generation during quenching of core debris under postulated LWR core meltdown accident conditions. This program is designed to support development of LWR containment codes.

4.2.1 Experimental Results and Interpretation

Prior experiments (Ginsberg, 1981) with the first particle quench test apparatus indicated that the vessel wall temperature significantly affected the mode of packed bed quenching. This observation led to redesign of the test apparatus to allow preheating of the vessel wall to the same temperature as the spherical particles. Experiments were subsequently carried out with the new test apparatus with both cold and hot walls, in order to demonstrate the effect and to verify previous observations. These tests and their interpretation are presented below.

Table 4.1 presents the experimental parameters for two runs conducted under nominally identical conditions, except for the test vessel wall temperature. Run No. 114 was carried out with the wall initially at room temperature, while for Run No. 116 the wall was preheated to the same temperatures as the spheres.

TABLE 4.1 - TEST RUN CONDITIONS

Run Number	Sphere Temperature (K)	Water Temperature (K)	Wall Temperature (K)	Bed Height (mm)	Mass Water (kg)
114	821.8	364.	294.	327	8
116	818.0	361.	800.	327	8

The experimental results are presented in Figures 4.1 and 4.2. The temperature traces presented were obtained from the bed thermocouples, where thermocouple number 8 (TC8) is located at the top of the packed bed. The remaining thermocouples are located beneath TC8 in sequential order, TC2 is located at the bottom of the particle bed. The temperature traces for Run No. 116 [shown in Figure 4.1(a)] in which the vessel wall was preheated, suggest that a cooling front propagates down the column and cools the thermocouples to the water saturation temperature in a sequential pattern. The times of arrival of this front at the thermocouple locations are shown in Figure 4.1 (b) as the "+" data points. The downward-directed front reached the bottom of the vessel at approximately 150 seconds following liquid contact with the bed. Figure 4.1 (a) further indicates that the temperatures of TC Nos. 4, 6, 7 and 8 increase at times following passage of the first cooling front. These temperature recoveries indicate that only a fraction of the initial sphere internal energy is removed upon passage of the downward-progressing cooling front. The thermocouples dry out subsequent to passage of the front and are reheated by the neighboring spheres. The final quench of the particle bed occurred during passage of an upward cooling front as indicated by the frontal propagation results shown in Figure 4.1 (b). The wall quench pattern closely coincides with the quench of the particle bed.

Figure 4.2 presents the results of the experiment characterized by an initially cold wall. Figure 4.2 (a) indicates that the uppermost thermocouple in the bed, TC8, was first contacted by water. Subsequently however, TC8 reheated and returned to its initial temperature reading. The bed proceeded to quench from the bottom upward. TC2 was the first thermocouple to be quenched, followed sequentially by TC3, TC4, etc. This upward-progressing frontal pattern which is shown in Figure 4.2(b), began at approximately 50 seconds following water contact with the bed, at which time water had penetrated to the base of the particle bed. No downward-frontal progression is observed in the experiments with an initially cold vessel wall.

The results of the cold wall experiments suggest that cooling water flowed to the base of the test vessel and bypassed the central packed bed thermocouples. It is hypothesized that the water flowed down along the test vessel wall to the bottom of the bed. Since the wall was cold the vaporization rate in the vicinity of the wall was low. The liquid which flowed downward along the wall was, therefore, relatively unimpeded by vapor upflow in the region. Thus, the wall region was a low impedance path for liquid flow to the bottom of the bed. Once a liquid path to the bottom of the vessel was developed the liquid began to quench the spheres in a frontal cooling pattern proceeding from the bottom to the top of the bed. Liquid downflow within the bed itself probably did not occur. The upward-directed frontal cooling pattern is clearly observed in Figure 4.2 (b). The sequence of events postulated here is supported by photographic observation of packed bed quench characteristics which were made in earlier experiments which made use of a glass test vessel (Ginsberg, 1981).

In the experiments with a preheated vessel wall the bottom of the bed remained dry until the downward-directed front advanced to that region. A distinct difference was observed in the experiments with a cold wall. In this

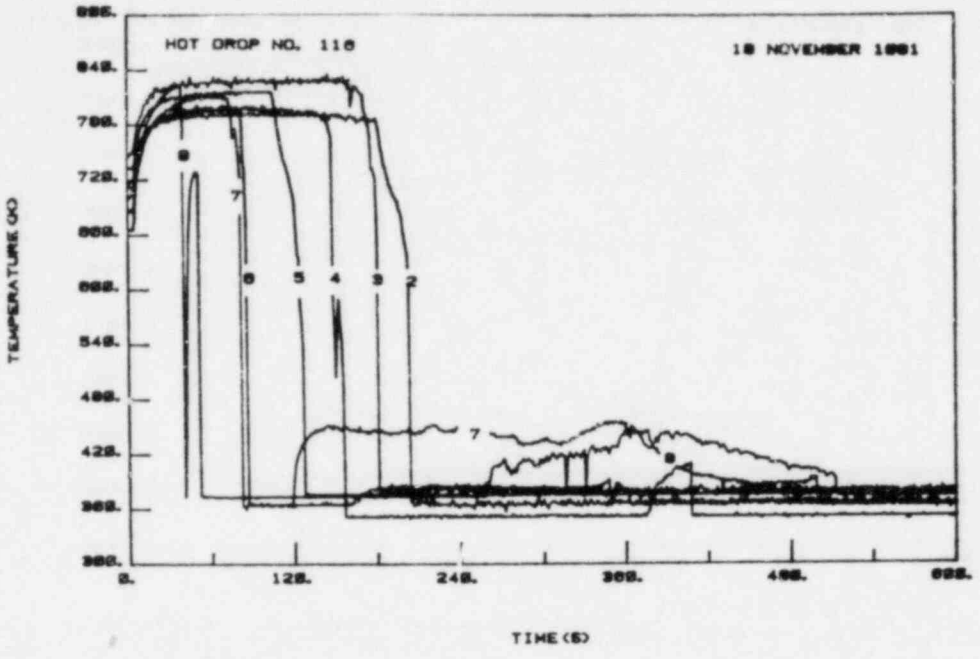

(a)

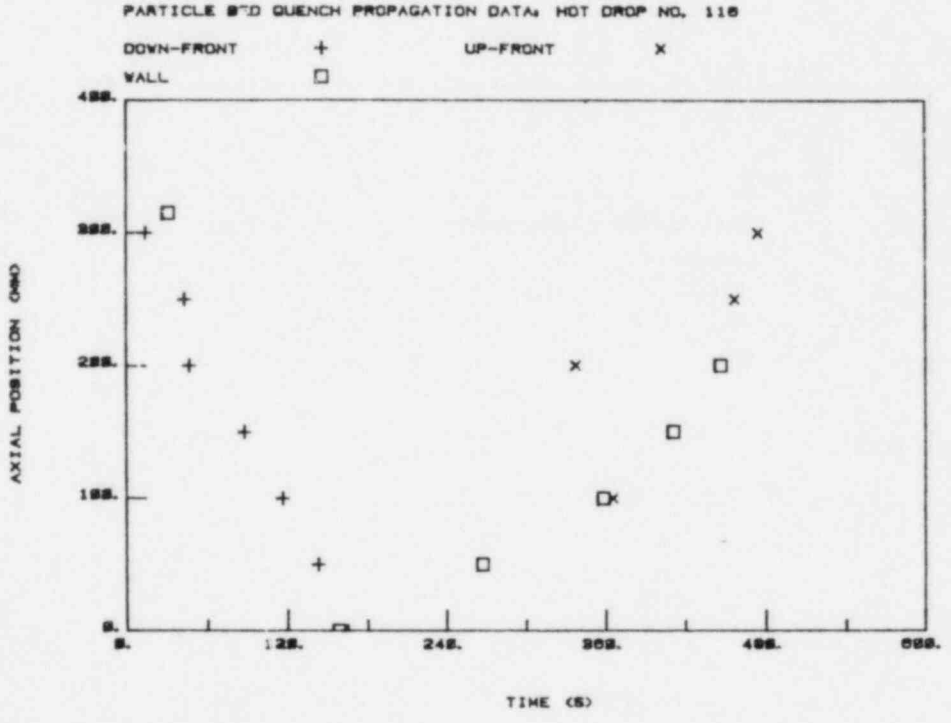

(b)

Figure 4.1 Results of Run No. 116: (a) Temperature Traces, (b) Frontal Propagation Data

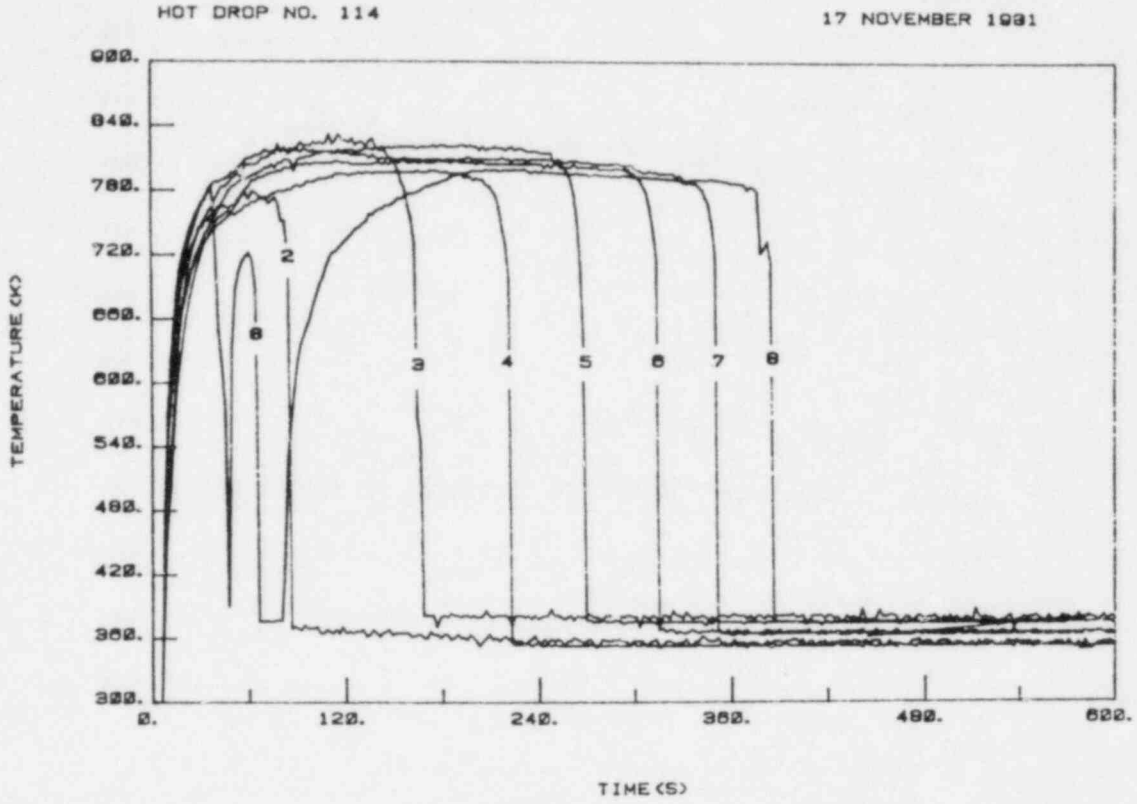

(a)

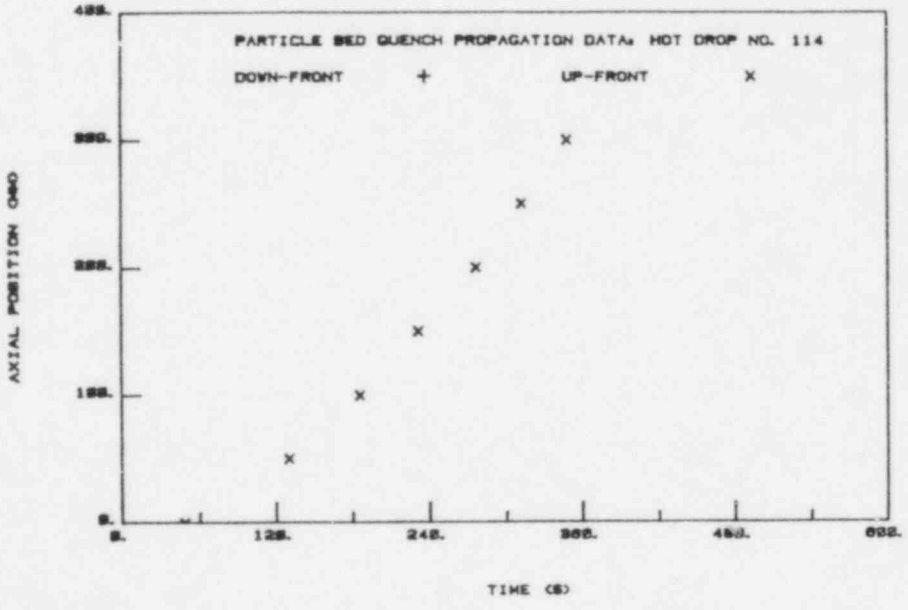

(b)

Figure 4.2 Results of Run No. 114: (a) Temperature Traces, (b) Frontal Propagation Data

case water reached the base of the bed relatively rapidly (50 seconds in Run 114 compared with 150 seconds in Run 116) and the uppermost region of the bed remained dry until the upward-directed front advanced to that region.

4.2.2 Implications with Respect to Reactor Safety

The following is a qualitative discussion of the implications of the experimental observations as applied to degraded core accident conditions. Quantitative models are being developed and will be discussed and presented in future reports.

The packed bed experiments with the pre-heated vessel wall are designed to simulate a debris bed which is of uniform height and is large enough in lateral dimensions such that boundary effects are negligible. The heated wall itself, in this case, simulates a layer of heated debris. Consider a superheated particulate bed of core debris which is spread across the floor of the reactor cavity and which is cooled by an overlying pool of water. If the bed is spread uniformly across the cavity floor then the results of the pre-heated wall experiments imply that the debris which is at the bottom of the bed and is in contact with the concrete basemat would be devoid of water until a downward-directed cooling front reached the bottom. Until this front reached that location the hot debris would transfer heat to the concrete and, at the same time, would continue to increase in temperature due to decay heating. The heat transfer to the concrete would lead to gas evolution from the concrete which would further inhibit water supply to the bed as a result of countercurrent flow limitations. The coolability of superheated debris beds with gas evolution from concrete has not been addressed in prior analyses.

References

GINSBERG, T., et al., "Safety Research Programs Sponsored by Office of Nuclear Regulatory Research Quarterly Progress Report, July 1 - September 30, 1981," BNL-NUREG-51454, NUREG/CR-2331, Vol. 1 (November 1981).

5. RAMONA-3B Code Modification and Evaluation

(P. Saha, H. R. Connell, D. I. Garber, J. H. Jo, and L. Neymotin)

This project includes the modifications, improvements and preliminary (or developmental) assessment of the BWR transient analysis code called RAMONA-3B prior to its release for application purposes.

During this reporting period of January to March 1982, the later stage of the partial-ATWS calculation reported in the previous quarterly report (Garber, 1982), was recomputed with a high boron injection rate to demonstrate the effect of boron concentration on the predicted core power. In addition, work on code improvements in many areas such as low and reverse flows, level tracking in the downcomer and steam separator model has begun. The block diagrams and control equations for the feedwater and recirculation flow controls have also been formulated.

The details of the progress achieved during this reporting period are described below.

5.1 Partial-ATWS Calculation (D. I. Garber and H. R. Connell)

The RAMONA-3B calculation for a hypothetical partial-ATWS event was described in the previous quarterly progress report (Garber, 1982). In that calculation boron was injected in the lower downcomer (or, the jet pump location) at 300 seconds. Boron started to enter the core approximately 20 seconds later and increased to a concentration of approximately 20 ppm by the time the calculation was terminated at 400 seconds. This was insufficient to shut down the reactor. It is expected that a boron concentration of approximately 400 ppm is needed before the fission rate is reduced to a negligible level and this could take as long as 2000 seconds.

Since it was not practical to calculate this test run for such a long time, an artificial problem was set up to demonstrate the effect of boron. The later part of the calculation was rerun with a boron injection rate ten times the (correct) rate used originally. The resulting boron concentration in the lower downcomer region and in the bottom third of the core is shown in Figure 5.1. The boron concentration increases in steps determined by the transit time of the recirculating water which is approximately 100 seconds for the conditions experienced in this transient. Figure 5.1 shows the first step of boron concentration for both the downcomer and core regions.

The relative power during this time interval is shown in Figure 5.2. Although the power is a function of several parameters that are changing in the reactor (e.g., flow rate and inlet subcooling) the clear trend toward lower peaks in the power oscillation is due to the increasing boron concentration in the core. This demonstrates that the effect of boron is being correctly accounted for in RAMONA-3B and if the calculation were continued the code would have predicted the reactor shutdown.

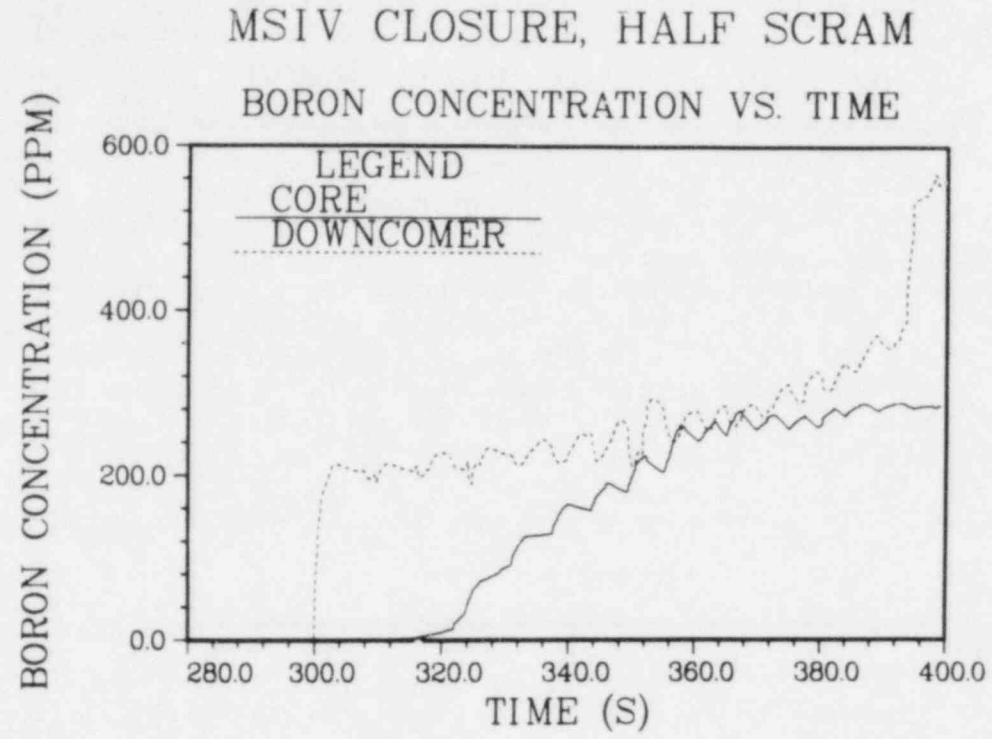

Figure 5.1 Calculated Boron Concentration in the Lower Downcomer and Core vs. Time (BNL Neg. No. 5-240-82).

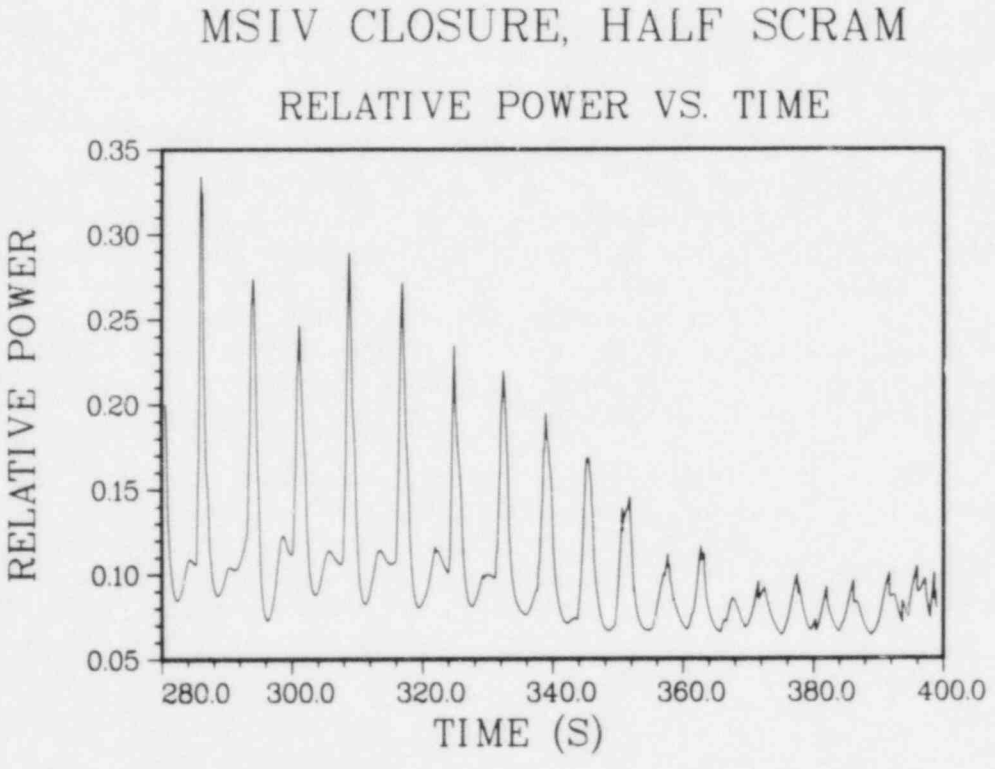

Figure 5.2 Calculated Core Relative Power vs. Time (BNL Neg. No. 5-241-82).

5.2 Programming Consideration (H. R. Connell)

In this reporting period the work on RAMONA-3B was directed toward preparing a program file that combines all the models and programming improvements generated to date. In addition, other programming was included to provide an expanded plotting capability and initialization and editing improvements.

The present version of the code is designated as MOD104. Check out and verification of this version is being done by rerunning the partial-ATWS calculation on a stand-by basis. A Control Rod Drop Accident (CRDA) is also being simulated with this version under the NRR sponsorship.

5.3 Code Improvements

5.3.1 Low and Reverse Flow (L. Neymotin)

A number of corrections and modifications in the area of low and reverse flows have been made during this reporting quarter. They are as follows:

a) A part of the inertia or convective term in the mixture momentum equation was erroneously written as $w|w|$ (see footnote to Equation 4.4.6 in Wulff, 1981). This has been corrected to w^2.

b) In order to address anticipated low flow situations in different reactor components (for instance, after the reactor is scrammed and the recirculation pump is tripped) the single phase friction factor correlation for the laminar flow regime has been added to the code's constitutive relations package. Note that the low and zero flow situations will also take place if the flow changes direction.

c) Some of the code's constitutive relationships or correlations are expressed in terms of local flow qualities (see, for example, Eqs. 4.4.40, 4.4.41, 4.4.47 in Wulff, 1981). These pose a problem during the counter-current flow situations where the flow quality is meaningless. Therefore, until a more mechanistic approach of treating the counter-current flow can be developed, the static quality will be used instead of the flow quality in all correlations.

d) Work has begun on modifying the code in order to account for reverse flow situations. To complete this task, certain revisions and reprogramming are needed for the junctions coupling the single channel components such as Lower Plenum 2 and Riser with the multichannel component, i.e, the Core.

5.3.2 Level Tracking (D. Garber)

Work has begun to restructure the water (mixture) level logic in the code. At present, twelve (12) FORTRAN variables and indices are used in RAMONA-3B to specify the water level location leading to a complex programming logic.

5.3.3 Steam Separator (P. Saha)

A brief literature survey (Wolf, 1973 and Rouhani, 1978) showed that the carryunder for typical BWR steam separators depends on both the flow quality at the separator inlet and the water level. Therefore, the present RAMONA-3B model of a constant value for carryunder should be changed.

5.3.4 Feedwater and Recirculation Flow Control (J. H. Jo)

The formulation of the feedwater and recirculation flow control has been completed. The control scheme was mainly based on information from the FSAR's of various BWR plants including Quad Cities (BWR/3), Browns Ferry (BWR/4) and Grand Gulf (BWR/6). Several other documents (Linford, 1973 and Forkner, 1978) were also consulted.

Figures 5.3 and 5.4 show the block diagrams for the feedwater control and the recirculation flow control, respectively. The control equations corresponding to these block diagrams have been written, but no programming has begun.

5.4 Code Documentation

A draft report (Wulff, 1981) on the description and assessment of RAMONA-3B code has been completed and transmitted to USNRC. Another report on the code structure, programming information and users guide is under preparation.

REFERENCES

FORKNER, S. L., (1978), "Calculation of Generator Load Rejection Transient for 3293 MW BWR With RETRAN-01-RET12B," TVA Report, July 1, 1978.

GARBER, D. I., and CONNELL, H. R., (1982), "Partial-ATWS Calculation," in Safety Research Programs Sponsored by Office of Nuclear Regulatory Research, Quarterly Progress Report for October 1 - December 31, 1981, NUREG/CR-2331, BNL-NUREG-51454, Vol. 1, No. 4, Section 5.1, February 1982.

LINFORD, R. B. (1973), "Analytical Methods of Plant Transient Evaluation for the General Electric Boiling Water Reactor," NEDO-10802, February 1973.

ROUHANI, Z., (1978), "Steam-Water Separation," in Two-Phase Flows and Heat Transfer with Application to Nuclear Reactor Design Problems, J.J. Ginoux, ed., Hemisphere Publishing Corporation, Chapter 13, pp. 275-300, 1978.

WOLF, S., and MOEN, R. H., (1973), "Advances in Steam-Water Separators for Boiling Water Reactors," ASME Paper No. 73-WA/Pwr-4, 1973.

WULFF, W., et al., (1981), "A Description and Assessment of RAMONA-3B: A Computer Code with Three-Dimensional Neutron Kinetics for BWR System Transients," Draft BNL Report for NRC Use only, October 1981.

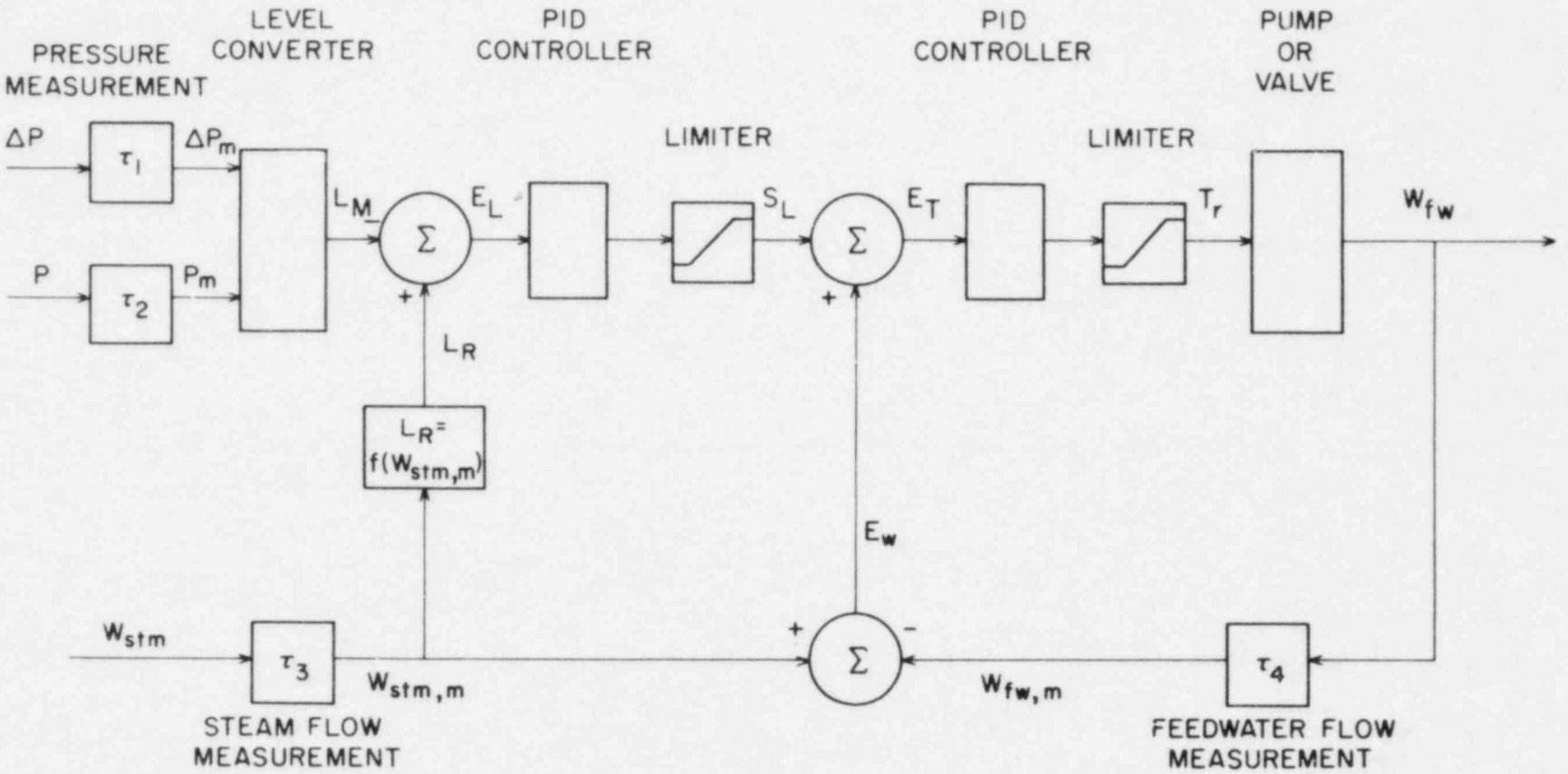

FEED WATER CONTROL

Figure 5.3 Block Diagram for the Feedwater Control for a Typical BWR System (BNL Neg. No. 5-591-82).

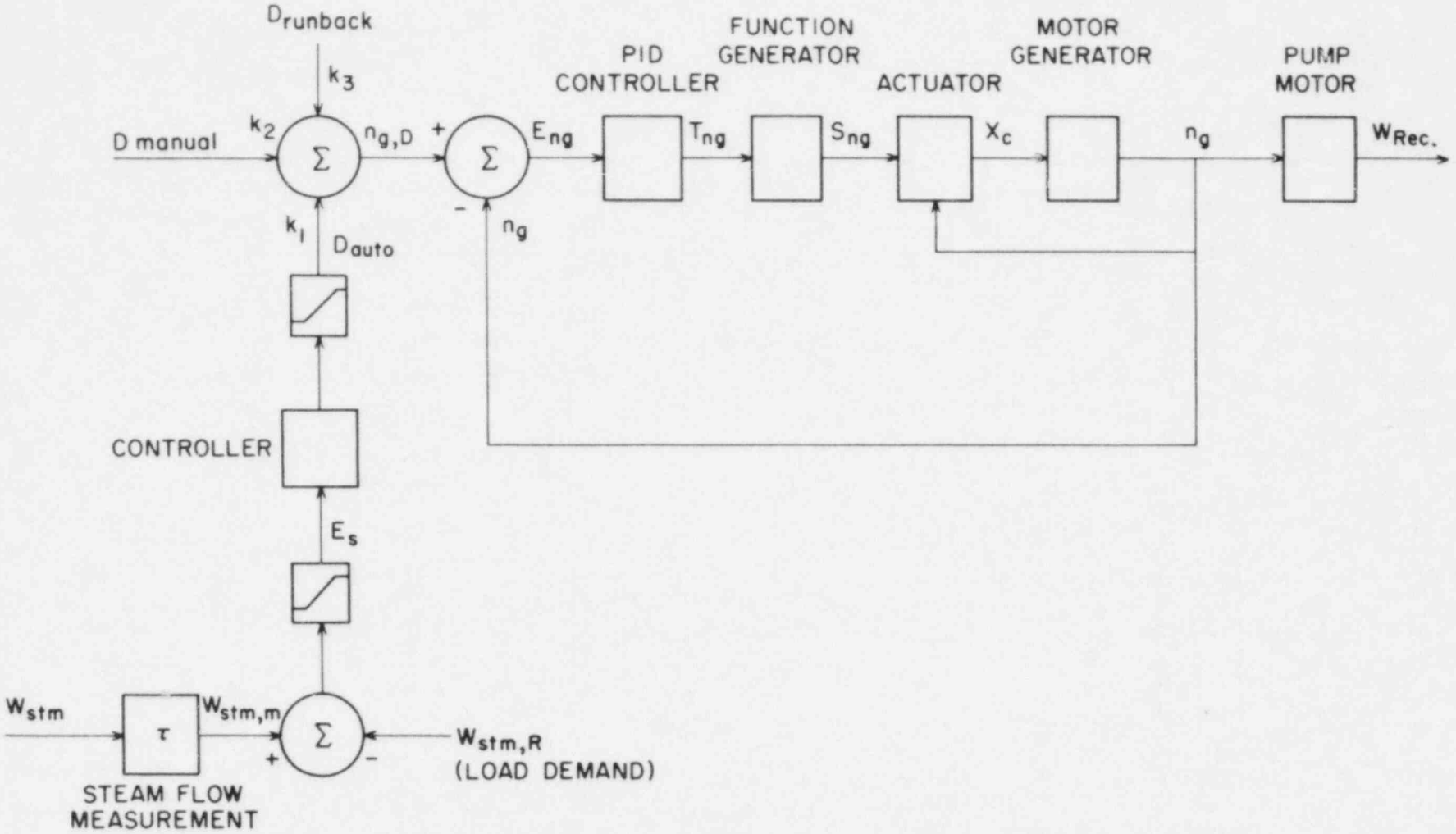

RECIRCULATION FLOW CONTROL

Figure 5.4 Block Diagram for the Recirculation Flow Control for a Typical BWR System (BNL Neg. No. 5-592-82).

6. LWR PLANT ANALYZER DEVELOPMENT
(W. Wulff)

6.1 Introduction

This program is being conducted to establish the feasibility of developing an engineering plant analyzer, capable of performing accurate, real-time and faster than real-time simulations of plant transients and Small-Break Loss of Coolant Accidents (SBLOCA) in LWR power plants. An engineering plant analyzer is being developed by utilizing a modern, interactive, high-speed special-purpose peripheral processor, which is designed for time-critical systems simulations. The engineering plant analyzer supports safety analyses and serves as the technology development for nuclear power plant monitoring, for accident diagnosis and mitigation, and for upgrading operator training programs and existing training simulators.

There were three activities started in the LWR Plant Analyzer Development Program; namely, (1) the assessment of the capabilities and limitations in existing simulators for nuclear power plants, (2) the acquisition of a special-purpose, high-speed peripheral processor, suitable for real-time and faster than real-time simulation of power plant transients and (3) the development of the software for this peripheral processor.

(1) One each of operating PWR and BWR power plants and their simulators had been selected to establish the status of current real-time simulations with respect to modeling fidelity for the thermohydraulics in the Nuclear Steam Supply System (NSSS). The assessment consisted of establishing the modeling assumptions in the process descriptions for the NSSS, and of comparing NSSS-related simulator results with results from RETRAN calculations. The evaluation was performed to determine the current simulator capabilities and limitations of providing engineering predictions for operational transients and for transients caused by loss of coolant injection, by a loss of feedwater or feedwater heaters, by a loss of heat sink (steam generator failure), or by a mismatch between fission power and cooling rate.

(2) The AD10 of Applied Dynamics International (ADI) in Ann Arbor, Michigan, had been selected as the special-purpose, high-speed peripheral processor on the basis of its capacity to execute faster and more efficiently the operations which are currently being performed in training simulators by general-purpose computers. Specifically, the special-purpose processor was selected for efficient, high-speed integration of ordinary differential equations and for direct, on-line interactions with the user, with instrumentation, with both digital and analog signals from other computers and with graphic devices for continuous, on-line display of a large number of computed parameters.

(3) The software development for the new peripheral processor is carried out in two phases. One phase is the implementation of an existing BWR system code for operational transients on the new processor. This phase serves to compare the computing speed and accuracy of the AD10 processor with those of

the CDC-7600 main-frame computer, and thereby to demonstrate in principle the feasibility of computing realistic transients at faster than real-time computing speeds. The second phase is the formulation and implementation of a thermohydraulic model for the faster-than-real-time analysis of operational and SBLOCA transients in PWR power plants.

6.2 Assessment of Existing Simulators (W. Wulff and H. Cheng)

The assessment of current simulator capabilities consisted of evaluating qualitatively the thermohydraulic modeling assumptions in the simulator and of comparing quantitatively the predictions from the simulator with results from the detailed systems code RETRAN.

The results of the assessment have been published earlier in three reports (Wulff 1980, Wulff 1981a and Cheng and Wulff 1981). It has been found that existing training simulators are limited to the simulation of steady-state conditions and quasi-steady transients within the parameter range of normal operations. Current PWR simulators cannot simulate two-phase flow conditions in the primary reactor coolant loops, nor the motion of the two-phase mixture level beyond the narrow controls range in the steam generator secondary side. Current BWR simulators cannot simulate two-phase flow conditions in the recirculation loops or in the downcomer and lower plenum, nor can they simulate coolant level motions in the steam dome, the lower regions of the downcomer (below the separators), or in the riser and core regions. These limitations arise from the lack of thermohydraulic models for phase separation and mixture level tracking (Wulff 1980, 1981a).

The comparison between PWR simulator and corresponding RETRAN results, carried out for a reactor scram from full power, showed significant discrepancies for primary and secondary system pressures and for mean coolant temperatures of the primary side. The discrepancies were found even after the elimination of differences in fission power, feedwater flow and rate of vapor discharge from the steam dome. Good agreement was obtained between simulator and RETRAN calculations for only the early part (narrow control range) of the water level motion in the steam generator. The differences between simulator and RETRAN calculations have been explained in terms of modeling differences (Cheng and Wulff 1981).

6.3 Acquisition of Special-Purpose Peripheral Processor (A.N. Mallen and R.J. Cerbone)

The AD10 had been selected earlier as the special-purpose peripheral processor for high-speed, interactive systems simulation. A brief description of the processor has been published in a previous Quarterly Progress Report (Wulff, 1981b). A PDP-11/34 DEC computer serves as the host computer.

The PDP-11/34 host computer with console, 67 megabyte disc drive and a 800/1600 byte per inch tape drive, have been purchased and installed in the Applied Mathematics Department (AMD) at BNL. The host computer system has been operating since March 1, 1982.

The AD10 peripheral processor had been leased originally, with an option to buy, from Applied Dynamics International. Following its delivery in January of 1982, the AD10 processor has been installed also in the AMD building, and interfaced with the host computer. The AD10 has been operating since March 15, 1982, except for a minor disturbance problem with one PDP-AD10 interface component from Applied Dynamics International. This interface component causes spurious execution halts in the AD10. A substitute component has been ordered. Acceptance testing of the AD10 system will be carried out after the successful installation of this interface component.

Following DOE's approval on March 17, 1982 for purchasing the AD10 system, BNL has prepared the purchase contracts for execution immediately after the completion of the AD10 acceptance tests.

The PDP/AD10 system is being accessed remotely via four ADDS CRT terminals (1200 baud rate) and one DEC Writer (300 baud rate) from the DNE building with the staff offices. Interactive operation is achieved with a DEC Writer terminal and a Tektronix oscilloscope (on temporary loan pending delivery of a new oscilloscope) from an office in the AMD building which houses also the high-speed line printer. A third DEC Writer terminal serves as a (slow) line printer in the DNE building.

6.4 Software Implementation on AD10 Processor

The thermohydraulic models of an existing BWR systems code have been adapted for the AD10 processor to simulate the Peach Bottom-2 power plant. The resulting High-Speed Interactive Plant Analyzer code (HIPA-PB2) is being programmed in the high-level language MPS10 (Modular Programming System) of the AD10. After implementing the thermohydraulics of HIPA-PB2 on the AD10, we will compare the computed results and the computing speed of the AD10 with the results and the computing speed of the CDC main-frame computer. Following this comparison, the program will be expanded to include the models for neutron kinetics and thermal conduction in the fuel elements.

6.4.1 MOS10 Program Development (H.S. Cheng, S.V. Lekach, A.N. Mallen and W. Wulff)

An existing four-equation model (one vapor mass and three mixture balance equations of mass, energy and momentum) for nonhomogeneous, nonequilibrium two-phase flow is being programmed in the high-level AD10 language MPS10. The resulting High-Speed Interactive Plant Analyzer program (HIPA) is specifically programmed ("hard-wired") for the Peach Bottom-2 BWR power plant and therefore designated "HIPA-PB2". HIPA-PB2 is being developed for the purpose of comparing the computing speed and accuracy with those of the large main-frame computer CDC-7600. This comparison should demonstrate the feasibility of computing realistic two-phase flow transients at faster-than-real-time speed. After this demonstration, HIPA PB2 will be expanded for a wide variety of BWR systems simulations.

It has been discovered early in this reporting period that only 7.6% of the total data memory purchased with the AD10 system is available for instructional memory, the remainder being reserved for the storage of variables and function tables. The previously coded HIPA-PB2 program for the BWR system hydraulics required approximately 5,100 words of instructional memory and would have necessitated the use of memory allocated for neutron kinetics and plant control simulations, as well as the use of the bus-to-bus data transfer during hydraulics calculation.

Therefore, the MPS10 coding of HIPA-PB2 has been reorganized into six segments and compacted within each segment. The program has been rescaled and simplified by eliminating unimportant intermediate results, by combining products and sums of function, where possible, into a single function for table interpolation, and by utilizing a newly available MPS10 module for fixed-point arithmetic operations which had been previously executed by floating-point modules requiring much more computing time and instructional memory. The newly available, fixed-point arithmetic modules have the features of FORTRAN subroutines and can be repeatedly used without the need for additional instructional program memory.

The compacted HIPA-PB2 code requires only 2,792 words of program memory, i.e. 73% of the 3,823 words available in one AD10 unit, or 36% of the total available program memory space.

It has been estimated that the computing cycle time (frame time), for the advancement by one integration step is approximately 5.38 milliseconds, or 98 microseconds per computational cell. This may be compared with approximately two milliseconds per computational cell currently required by large systems code executions (TRAC) on main-frame computers. The computing speed of the AD10 will be controlled, however, by computational stability. The integration step size for stable integration is expected to range between 50 and 100 milliseconds. This implies ten to twenty times real-time computing speed.

Debugging of the HIPA-PB2 is in progress and expected to be completed during the next reporting period.

6.4.2 Modeling for HIPA-PB2

HIPA-PB2 will be completed by implementing models for neutron kinetics (point kinetics at first and one-dimensional kinetics later), for conduction in the fuel elements and in structural components, and for the recirculation loop. During the previous reporting period, we have decided to employ for the fuel conduction a lumped-parameter model with a single, ordinary differential equation for every axial segment (computational cell) of a hydraulic core channel. This model has been described in the previous Quarterly Progress Report (Wulff, 1982). Work has started to verify the model. No work has been performed on the modeling of the recirculation loop.

Point Kinetics Model (K. Fujiki)

The point kinetics model (Cheng 1976) has been formulated and scaled for MPS10 coding. Two approaches are being followed to accommodate the large range of time constants in the model (five orders of magnitude) and the associated stiffness of the state equation system. One consists of an algebraic algorithm for integrating the prompt neutron equation implicitly as in the BNL-TWIGL code (Cheng 1976) and the delayed-neutron equations by the explicit algorithms of the Numerical Integration Processor (NIP) in the AD10. The other approach consists of the direct integration by NIP and involves the synchronization of two NIP processors. We plan to select the more efficient method.

The neutron kinetics model in either formulation accounts for one prompt neutron energy group and for six precursor groups.

6.4.3 CDC-7600 Reference Calculations for Assessing HIPA-P32/AD10 Computing Speed and Accuracy (H.S. Cheng)

As described in the previous Quarterly Progress Report (Wulff, 1982), the Design Basis Transient was selected for assessing the computational speed and accuracy of the AD10. This transient constitutes a turbine trip at full power, with the steam bypass shut off and the recirculation pump trips disabled. The reactor scram is initiated 2.7 seconds after turbine trip and completed 4 seconds after turbine trip.

The transient has been recomputed with output edits for additional parameters, and to accommodate a new, slightly modified nodalization scheme. The new computation provided also the time-dependent tabulations for the six boundary conditions, namely

feedwater mass flow rate,
steam mass flow rate at steam line entrance,
feedwater energy flow rate,
steam line energy flow rate,
jet pump pressure head,
rate of heat addition to coolant in core channel,

with 1025 equally spaced data pairs instead of the normally obtained 349 unequally spaced data pairs. Table interpolation from equally spaced data pairs is faster and simpler. The tabulations are being translated from CDC storage tapes to the AD10 memory.

REFERENCES

CHENG, H.S. and WULFF, W. (1981) "A PWR Training Simulator Comparison with RETRAN for a Reactor Trip from Full Power," Informal Report, BNL-NUREG-30602 (Sept. 1981).

WULFF, W. (1980) "PWR Training Simulator, An Evaluation of the Thermohydraulic Models for its Main Steam Supply System," Informal Report, BNL-NUREG-28955 (Sept. 1980).

WULFF, W. (1981a) "BWR Training Simulator, An Evaluation of the Thermohydraulic Models for its Main Steam Supply System," Informal Report, BNL-NUREG-29815 (July 1981).

WULFF, W. (1981b) "LWR Plant Analyzer Development Program," Ch. 6 in Safety Research Programs, Sponsored by Office of Nuclear Regulatory Research, Quarterly Progress Report, April 1 - June 30, 1981; A.J. Romano, editor, NUREG/CR-2231, BNL-NUREG-51454, Vol. 1, No. 1-2.

CHENG, H.S. (1976) "PTKINS - A Point Kinetics Program," Memorandum to D.J. Diamond, BNL, April 1976.

7. LWR Code Assessment and Application

(P. Saha, J. H. Jo, U. S. Rohatgi, G. Slovik and N. Popov)

This program includes independent assessment of the latest released versions of TRAC and RELAP5 codes, and application of such codes to the simulation of plant accidents and/or transients. At present the assessment of TRAC-PD2/MOD1 code (Version 27.0) with the BCL downcomer tests has been completed and that of TRAC-PF1 (Version 7.0) and RELAP5/MOD1 (Cycle 14) is in progress with various separate-effects tests. The progress achieved during the reporting period of January to March 1982 is described below.

7.1 TRAC-PD2/MOD1 Assessment

7.1.1 BCL Downcomer Tests (G. Slovik)

To complete the BCL Downcomer analysis with TRAC-PD2/MOD1 as reported in the last quarterly (Slovik, 1982), some additional work was performed during this reporting quarter. As shown in Figure 7.1, Test ID=26505 was experimentally determined to be a complete bypass event, but TRAC-PD2/MOD1 predicted a near complete delivery point. To study the sensitivity of the code prediction to reverse core steam flow rate, the steam mass flow rate was increased from that for ID=26505 in steps of 2% until the code predicted a complete bypass situation. The break pressure boundary condition was kept constant at the experimental value for Test ID=26505. It was surprising that with only a 4% increase in the steam mass flow rate, the code predicted a complete bypass event. This demonstrates that for high ECC water subcooling ($\sim$100°C), TRAC-PD2/MOD1 may switch from an almost complete ECC-delivery to a complete ECC-bypass situation with very little increase in the reverse core steam flow. In other words, the code may predict a on-and-off type behavior regarding ECC water delivery into the lower plenum.

An attempt has been made to check whether the code (TRAC-PD2/MOD1) can predict the details of the flow pattern in the downcomer during ECC water penetration or bypass. The raw data for void fraction measurement (by using 3-prong sensors) at 96 different locations were obtained from BCL for Test ID=26502 and ID=26505. Measurement of Test ID=26502 was chosen for comparison because the code predicted this complete delivery test quite well (see Figure 7.1). Location of the 96 void distribution measurement (VDM) probes with respect to the TRAC-PD2/MOD1 nodalization is shown in Figure 7.2. For the sake of easier understanding, the downcomer annulus is shown as unwrapped in Figure 7.2. In Figures 7.3 through 7.8 the data from the void measurement probes have been plotted along with the predicted void fractions at six different locations. With the exception of Cell 5 of Level 9 (see Figure 7.3) where the code predicted a much lower void fraction, TRAC-PD2/MOD1 showed a tendency of predicting a higher void fraction than the experimental value. Therefore, although the code may predict the total water penetration rate correctly, it may not predict the correct flow pattern and void fraction at all locations. However, the above comparisons should be looked at from the qualitative rather than the quantitative viewpoint since the void measurement technique is not accurate for all flow regimes, particularly for the film flow regime.

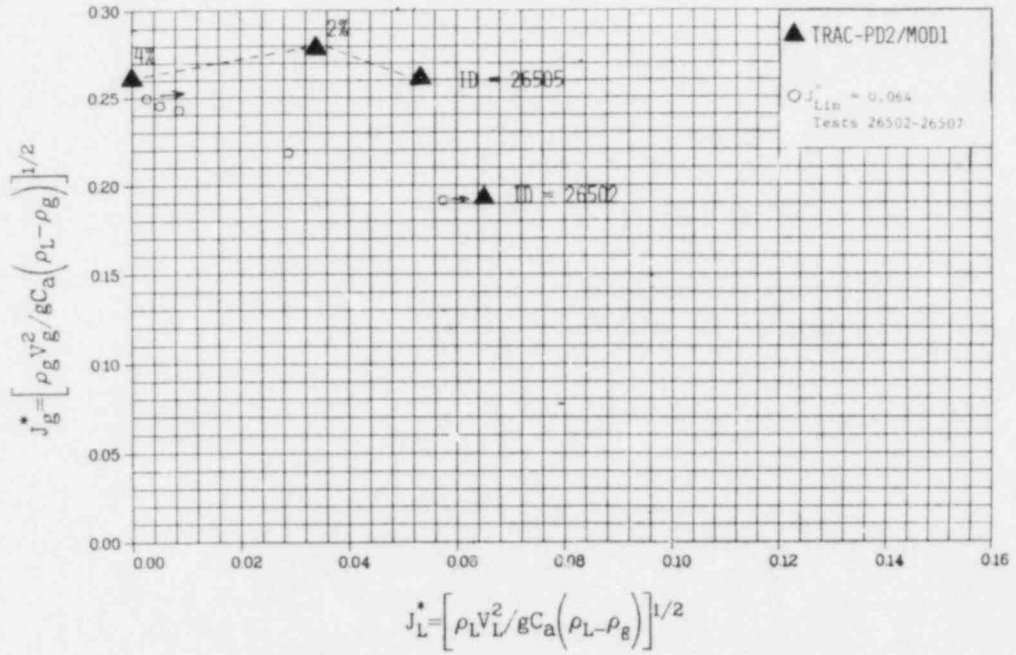

Figure 7.1 Comparison Between the Measured and Predicted Non-Dimensional Liquid Penetration Rates for Tests 26502 and 26505 (BNL Neg. No. 5-12-28).

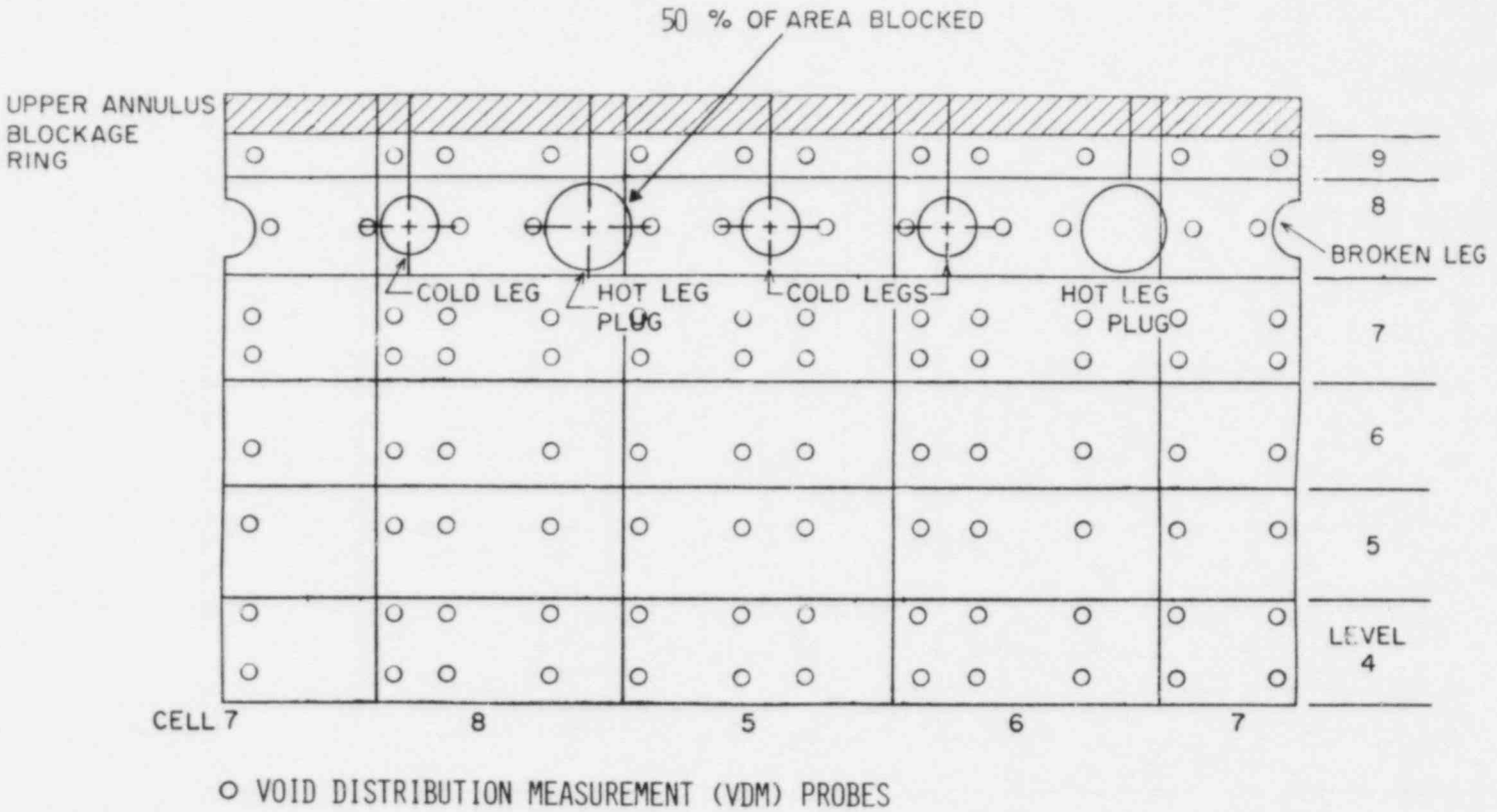

Figure 7.2 Location of the Void Measurement Probes With Respect to TRAC Nodalization (BNL Neg. No. 5-4-82).

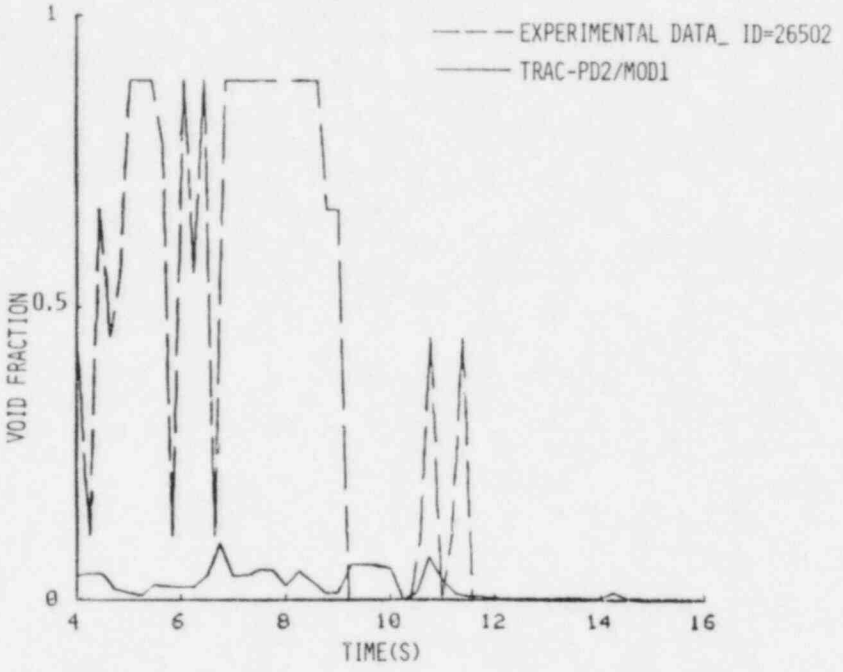

Figure 7.3 Comparison Between the Measured and Predicted Void Fraction at Cell 5 of Level 9 (BNL Neg. No. 5-7-82).

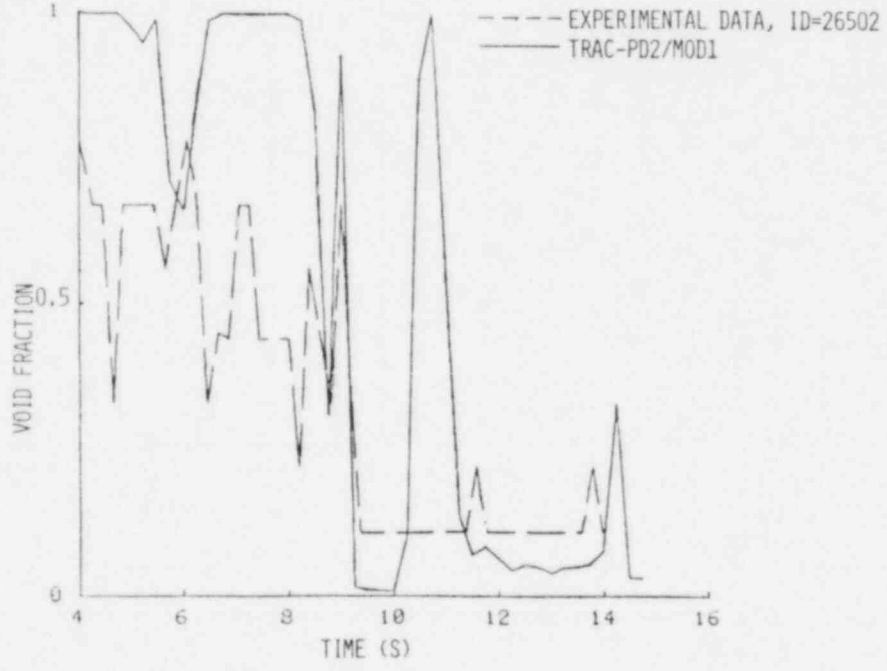

Figure 7.4 Comparison Between the Measured and Predicted Void Fraction at Cell 7 of Level 9 (BNL Neg. No. 5-6-82).

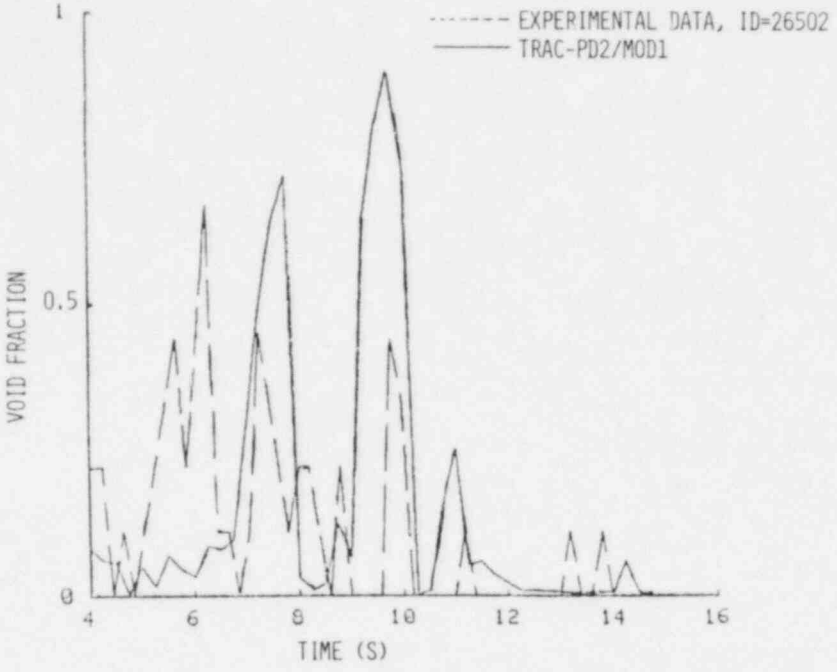

Figure 7.5 Comparison Between the Measured and Predicted Void Fraction at Cell 5 of Level 8 (BNL Neg. No. 5-8-82).

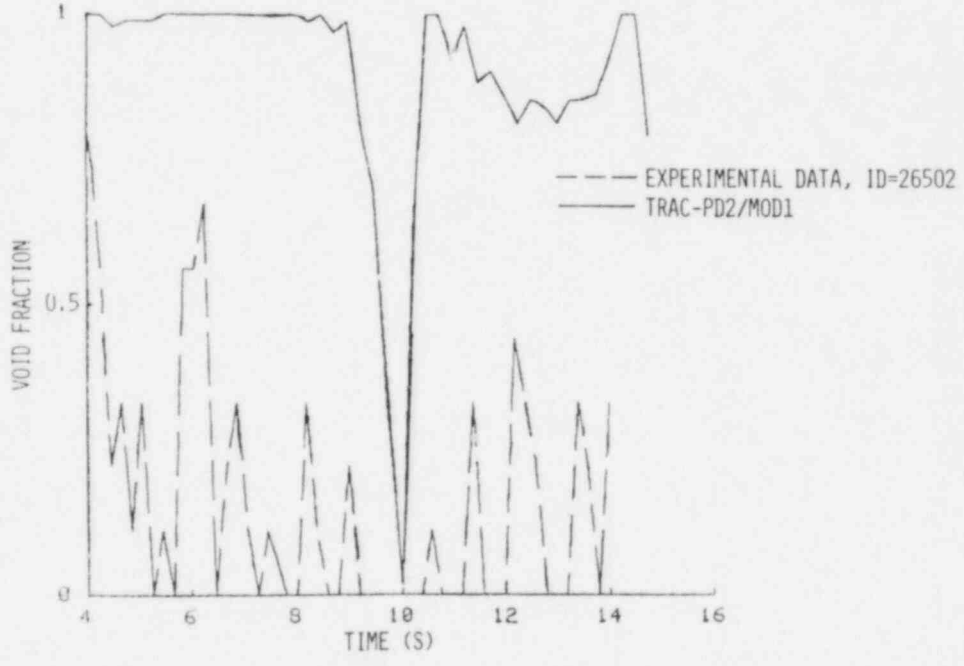

Figure 7.6 Comparison Between the Measured and Predicted Void Fraction at Cell 7 of Level 8 (BNL Neg. No. 5-5-82).

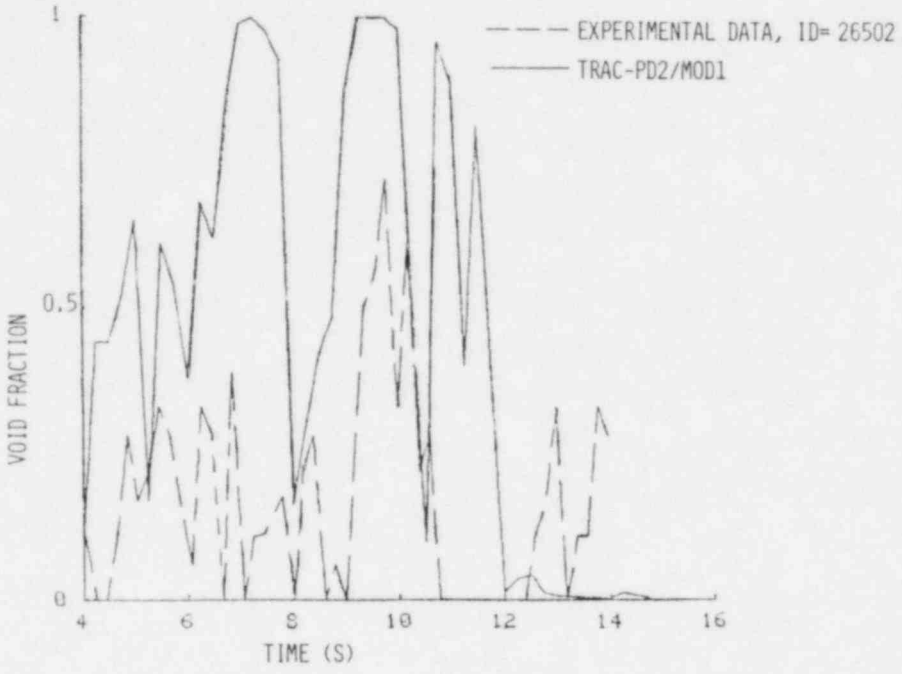

Figure 7.7 Comparison Between the Measured and Predicted Void Fraction at Cell 5 of Level 7 (BNL Neg. No. 5-9-82).

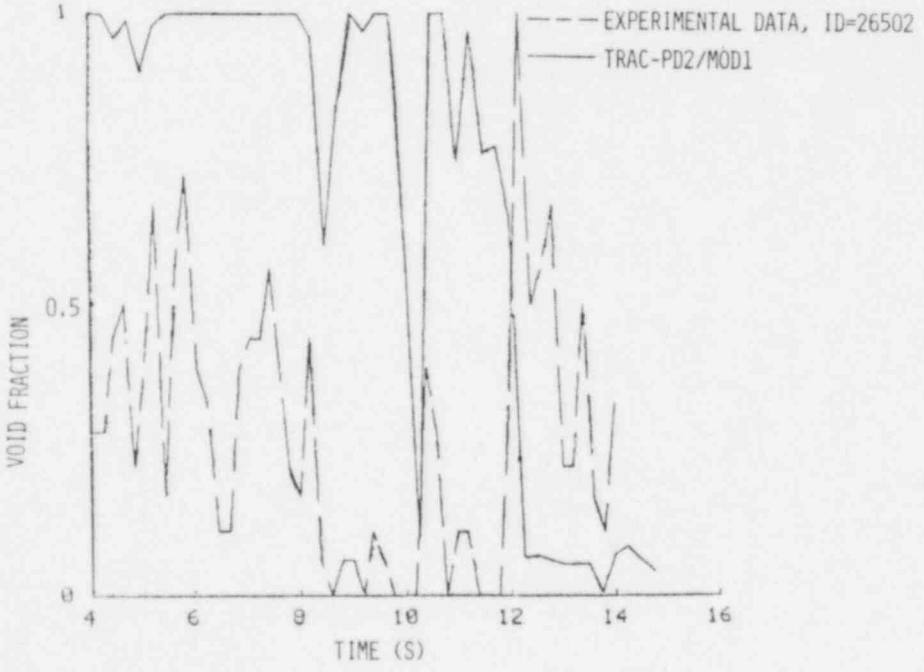

Figure 7.8 Comparison Between the Measured and Predicted Void Fraction at Cell 7 of Level 7 (BNL Neg. No. 5-10-82).

The final analysis consisted of predicting two extreme points in the 26700 series (i.e., ID=26716 and ID=26719). In this series the ECC water subcooling was approximately 27.8°C as compared to 94.5°C in the 26500 series. Even though a subcooling of 28°C may cause significant interfacial condensation, there were the only data with low subcooling so that the effect of subcooling on the ECC water penetration could be studied. Figure 7.9 shows the predicted values of J_g^* for the two extreme data points. It is seen that the predicted values for this series are in better agreement with the data than that for high ECC water subcooling as shown in Figure 7.1. This reinforces the earlier conclusion that the high interfacial condensation was the cause for discrepancy in the 26500 series, i.e., the high subcooling tests.

7.2 TRAC-PF1 (Version 7.0) Assessment

7.2.1 Marviken Critical Flow Test 24 (U. S. Rohatgi)

It was stated in the previous quarterly report (Rohatgi, 1982a) that a TRAC-PF1 input deck for Marviken Test 24 was sent to LANL because of some difficulties during the preliminary runs. The LANL staff suggested that the choking option should be used through NAMELIST. So in this reporting quarter, the input deck with the 40-cell nozzle was modified and another deck with a two-cell nozzle was prepared. In the first case, i.e., with the 40-cell nozzle, the code was allowed to have self or natural choking. In the second case where the nozzle was represented with only two cells, the choking option available in the code was used.

Figure 7.10 shows a comparison of computed break mass flow rate with the data. TRAC-PF1 underpredicted the break mass flow rate for both cases. However, the first case with the 40-cell nozzle was slightly better than the second case with the two-cell nozzle. Figure 7.11 shows a comparison of computed vessel top pressure with the data. Here again, the code underpredicted the pressure during the subcooled blowdown stage, and overpredicted the same during the saturated blowdown stage. However, both calculations are self consistent, i.e., the case with the lower mass flow rate prediction computed the higher pressure. On the other hand, there is an anomaly between the computed break mass flow rate and the vessel top pressure; both are underpredicted during the subcooled blowdown period. This discrepancy is being studied by simulating the nozzle and the vessel part separately.

7.2.2 B&W Steam Generator Tests (J. H. Jo)

The TRAC-PF1 calculation of the B&W steam generator test series 28-29 (OTSG) has been completed. The test was a simulation of a loss-of-feedwater transient in a 19-tube model of a once-through steam generator including an aspirator and a downcomer. Using ten (10) nodes in each side of the steam generator we did not observe any significant oscillation in either the steady-state or the transient calculation. However, at steady-state, a substantial portion of the recirculated steam into the downcomer through the aspirator (steam-mixer valve in the test) remained as vapor even at the bottom of the downcomer. Therefore, the fluid entering the tube region still contained a significant amount of voids even though the liquid was substantially

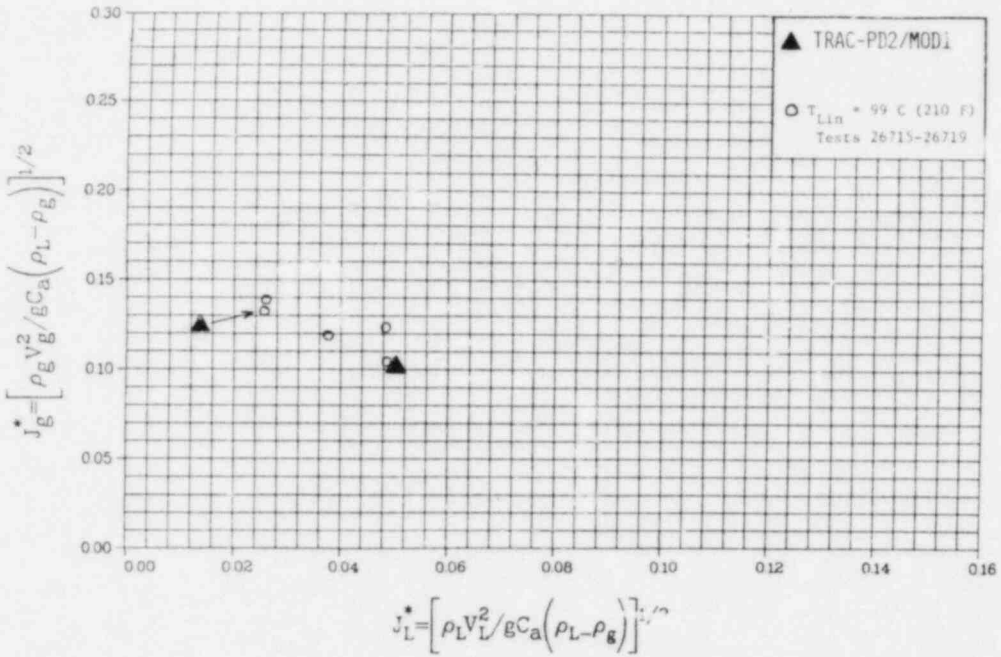

Figure 7.9 Comparison Between the Measured and Predicted Non-Dimensional Liquid Penetration Rates for Tests 26716 and 26719 (BNL Neg. No. 5-11-82).

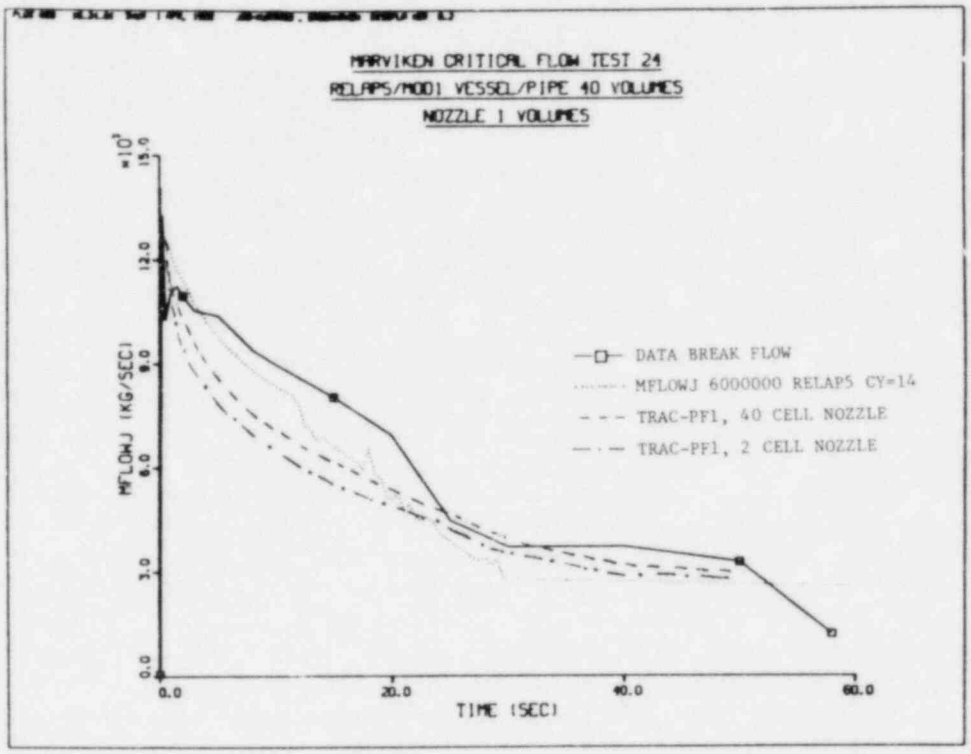

Figure 7.10 Comparison Between the Measured and Predicted Break Mass Flow Rate for Marviken Test 24 (BNL Neg. No. 4-799-82).

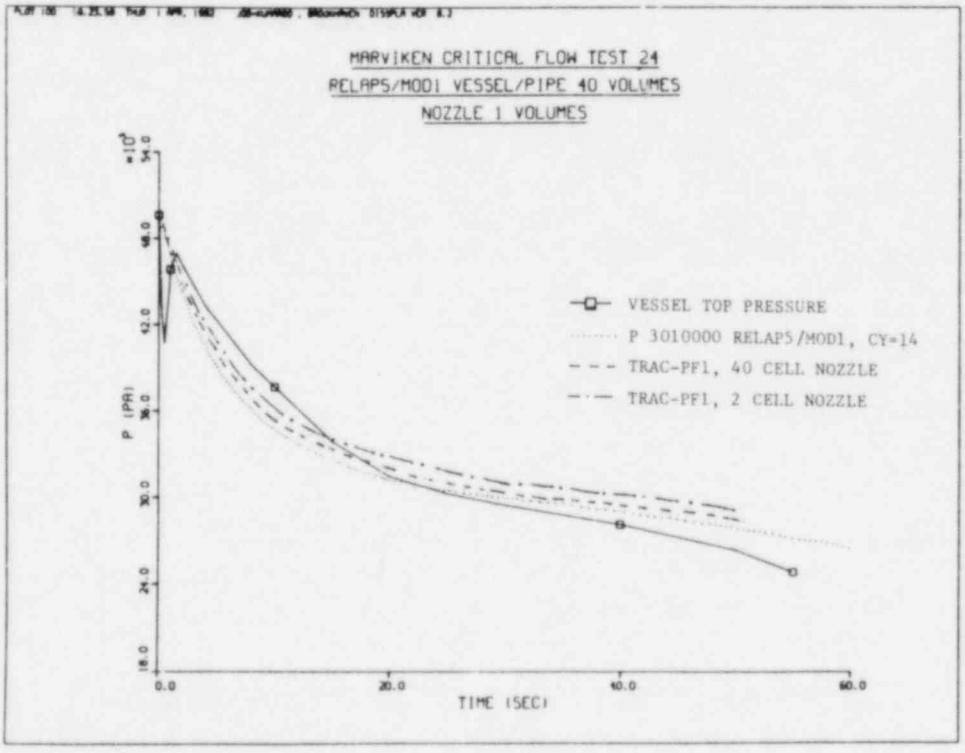

Figure 7.11 Comparison Between the Measured and Predicted Vessel Top Pressure for Marviken Test 24 (BNL Neg. No. 4-798-82).

subcooled. This was contrary to the expectation. As a result, the initial water inventory in the downcomer was significantly less than that in the test and, consequently, the computed exit steam flow rate decreased faster than the test flow rate during the transient. This effect of condensation (or, lack of sufficient condensation) was confirmed when the calculation was repeated with the interfacial condensation rate increased by a factor of 10^4 to insure complete condensation. The calculated results were now very close to the experimental data. (No comparison between the data and the calculations is shown here because the data are B&W proprietary.)

To study the effect of nodalization, the calculations were repeated with 40 nodes in each side of the steam generator. The results were not very different from the 10-node calculation.

The same OTSG can be simulated using two STGEN modules in case both the aspirator and the auxiliary feedwater connection are needed (e.g., to simulate the Rancho Seco overcooling transient). Therefore, the above calculation was repeated using the two STGEN configuration (see Figure 7.12). The results as shown in Figure 7.13, were not very different from the case where only one STGEN module was used, and the computing times were close. This indicates that, if needed, one may use the configuration with two STGEN modules without incurring any significant penalty in either computer time or accuracy.

7.2.3 FLECHT-SEASET Steam Generator Tests (G. Slovik)

During this reporting quarter, two tests from the FLECHT-SEASET steam generator experiments (Howard, 1980), namely test ID = 22010 and ID = 21806 have been simulated. The test conditions are given in Table 7.1. Both tests were run with the basic noding described in the previous quarterly (Rohatgi, 1982b) except that the number of nodes in the secondary side of the steam generator was increased from 8 to 12 cells. Accordingly, the number of active nodes in the primary side was increased from 14 to 22 cells. Also, the bottom half of the steam generator's inlet plenum was added to the TEE component. Most of these changes were done to position the cell-centers at the thermocouple locations and to have more evenly sized cells in the steam generator.

Although these two test runs have been simulated with TRAC-PF1, a comprehensive analysis of the results has not yet been completed. A detailed analysis of the results and their comparison with the data will be presented in the next quarterly report.

7.2.4 GE Large Vessel Blowdown Test (J. H. Jo)

The GE large vessel blowdown Test No. 5801-15 (Findlay, 1981) was simulated with the TRAC-PF1 (Version 7.0) code. The test apparatus is shown in Figure 7.14. The purpose of this experiment was to study the level swell phenomenon during blowdown from a partially water filled vessel.

The vessel was represented with seven volumes whereas three volumes were used for the discharge nozzle. The code pressure calculation agreed closely

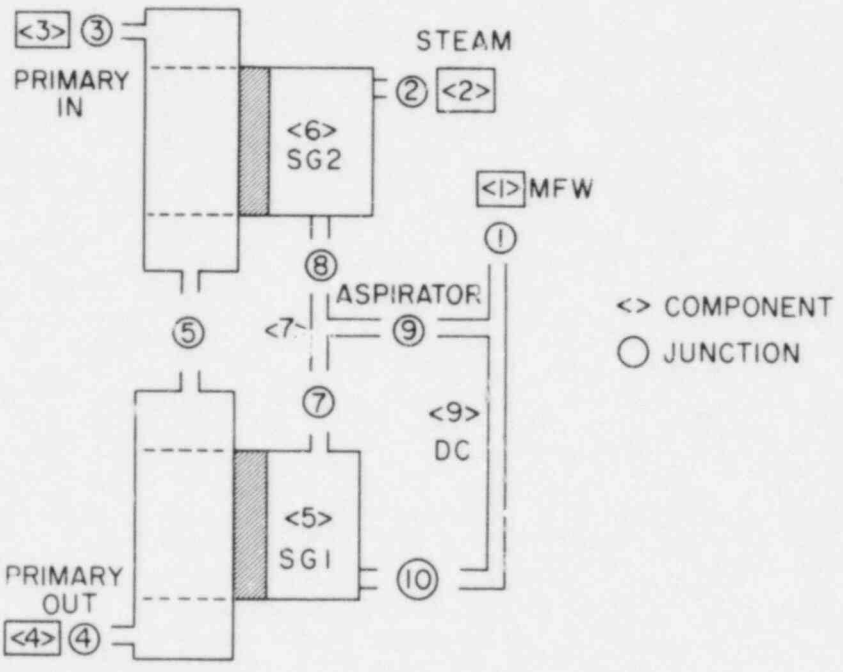

Figure 7.12 Representation of a Once-Through Steam Generator With Two STGEN Modules (BNL Neg. No. 10-669-81).

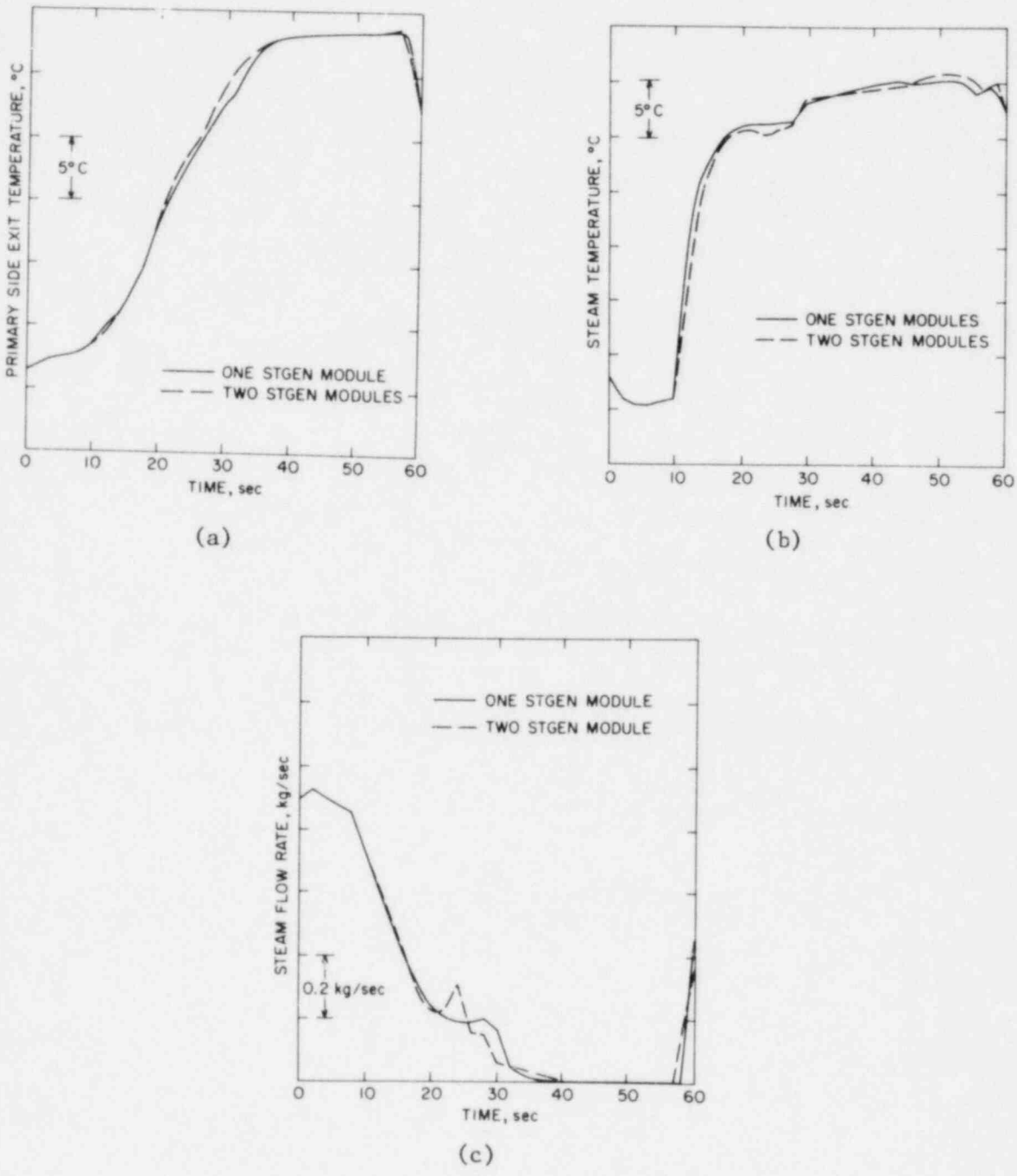

Figure 7.13 Comparison Between Two TRAC-PF1 Calculations With One and Two STGEN Modules (BNL Neg. Nos. 4-732-82, 4-735-82 and 4-738-82).

Table 7.1 Operating Conditions for the Simulated

FLECHT-SEASET Steam Generator Tests

TEST ID	Time Averaged Boundary Conditions					Secondary Side Initial Conditions	
	Steam Flow kg/s	Steam Temp. °K	Water Flow kg/s	Water Temp. °K	Flow Quality	Average Temp. °K (above 0.3m)	Pressure MPa (top most level)
21806	0.045	421.2	0.181	401.2	0.20	544.2	5.69
22010	0.182	427.2	0.045	398.2	0.80	546.7	5.75

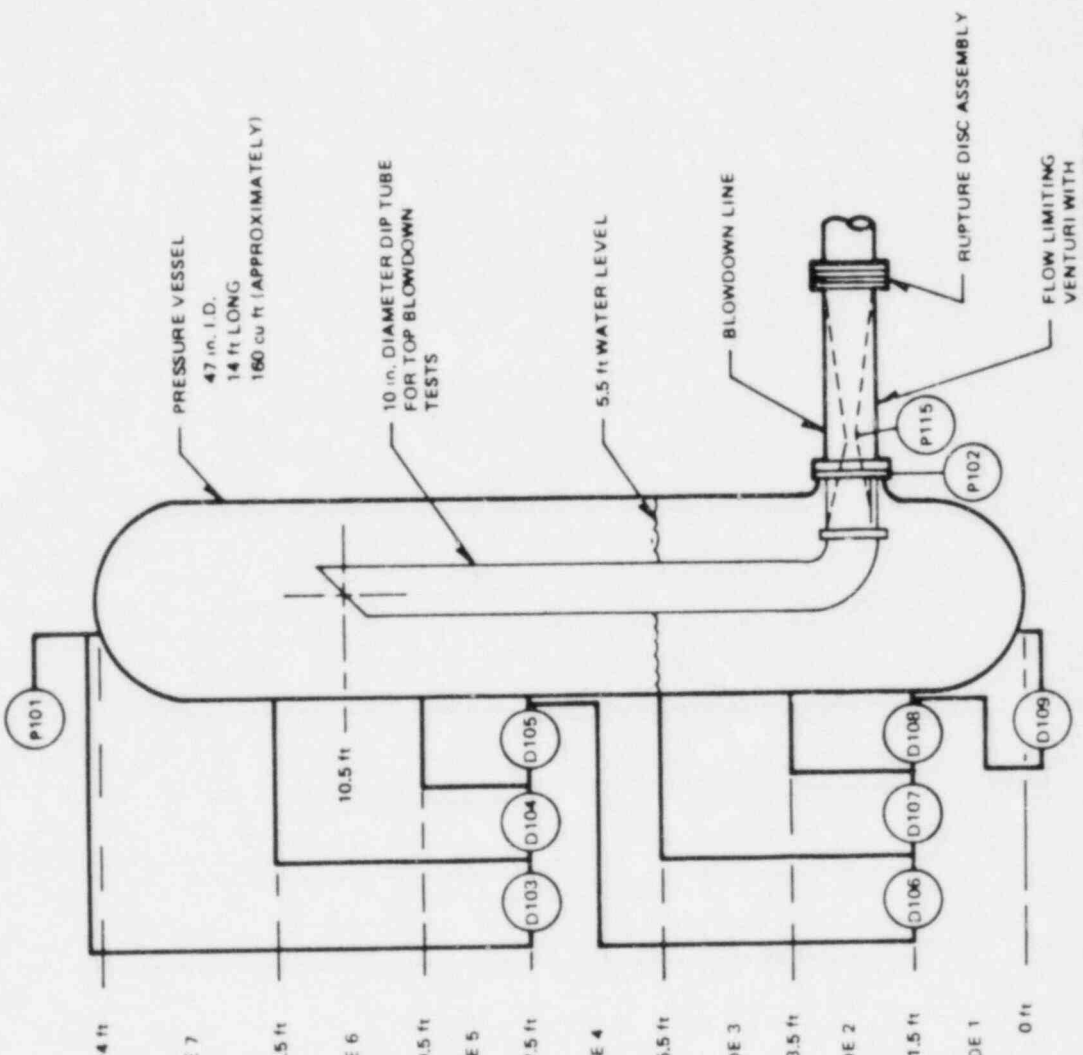

Figure 7.14 Schematic of the GE Large Vessel (BNL Neg. No. 5-685-82).

with the data except for the initial two seconds (see Figure 7.15). The data showed a slight dip in pressure before a steady decline occurred; the TRAC calculation, however, did not show this dip. This is to be expected since TRAC does not have a flashing delay model. Also, the TRAC calculation for void fraction was generally higher and the calculated level swell rate was faster than the data (see Figure 7.16). This is similar to the results obtained for the Battelle-Frankfurt top blowdown test with the TRAC-PD2 code (Saha, 1982). A high interfacial shear is believed to be the reason for this discrepancy.

Even though the calculation was repeated with different nodalizations (21-volume vessel with 3-volume nozzle, 7-volume vessel with 2-volume nozzle, and 7-volume vessel with 6-volume nozzle), the results remained very close to the base calculation with 7-volume vessel and 3-volume nozzle.

7.2.5 University of Houston Counter-Current Flow Tests (U. S. Rohatgi and N. Popov)

In the current reporting quarter some of the University of Houston counter-current flow tests were simulated with TRAC-PF1. The nodalization for the test section was retained from the previous simulation with TRAC-PD2 and was described elsewhere (Saha, 1982). Initially this test was modeled with the one-dimensional VESSEL component, but the computer run time was excessive. In the subsequent runs, the test section was modeled by using two TEE components. This is now possible as all the components in TRAC-PF1 are based on a two-fluid formulation. In the current representation the bottom TEE has 8 cells in the primary pipe and the side pipe which brings the air, is connected at the 6th cell. The top TEE which includes most of the test section, has 23 cells in the primary pipe and water is injected through a side pipe at the 12th cell. The top of this TEE is connected to a BREAK component where the system pressure is imposed as boundary condition. In the current quarter the tests with water injection rate of 100 lb/hr (0.0126 kg/s) and 1000 lb/hr (0.126 kg/s) were simulated.

During the change from the VESSEL component to TEE component, it was found that the code predicted different flow situations for the same test conditions. Figure 7.17 shows a comparison of liquid velocity and void fraction distribution along the length of the test section above the liquid entrance station. In this case all the liquid was predicted to go up and the flow was co-current. The VESSEL option predicted higher liquid velocity and correspondingly higher void fraction. Furthermore, there was a jump in these variables at the junction between the VESSEL and the PIPE components. The calculation with the TEE components, on the other hand, was smooth and did not show any jump at component junctions. This difference between two approaches will be investigated further.

Figures 7.18 and 7.19 show the liquid film downflow for two liquid injection rates. These calculations were performed with the two TEE components. Figure 7.18 is for the liquid injection rate of 100 lb/hr and shows that the code predicted inception and completion of co-current flow at lower gas flow rate than the data. Furthermore, the TRAC-PF1 prediction was in poorer agreement with the data than that of TRAC-PD2. Both versions of TRAC use the same entrainment model but different interfacial shear correlation for the annular flow regime. TRAC-PF1 uses a correlation for interfacial shear

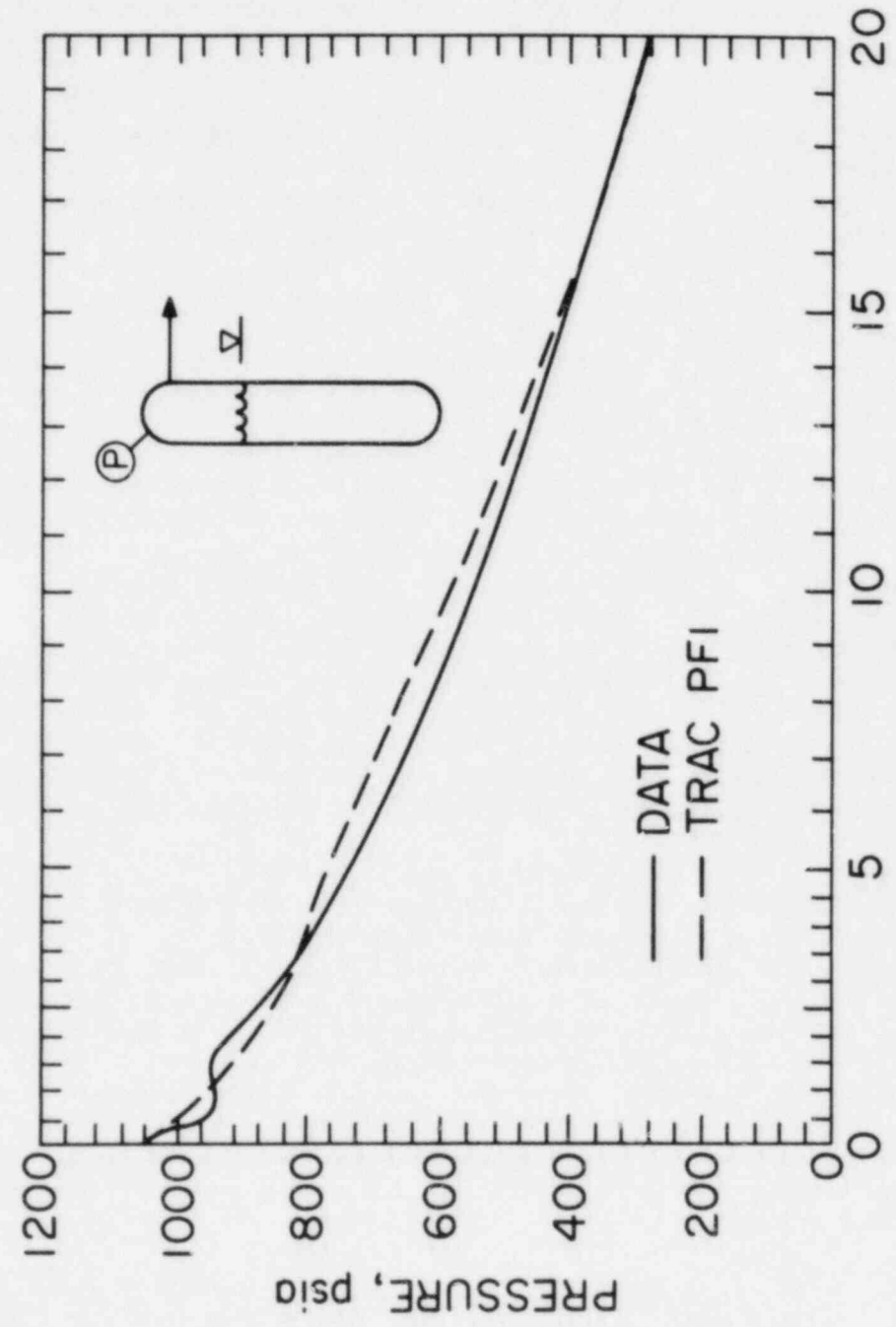

Figure 7.15 Comparison Between the Measured and Predicted Vessel Pressure (BNL Neg. No. 4-730-82).

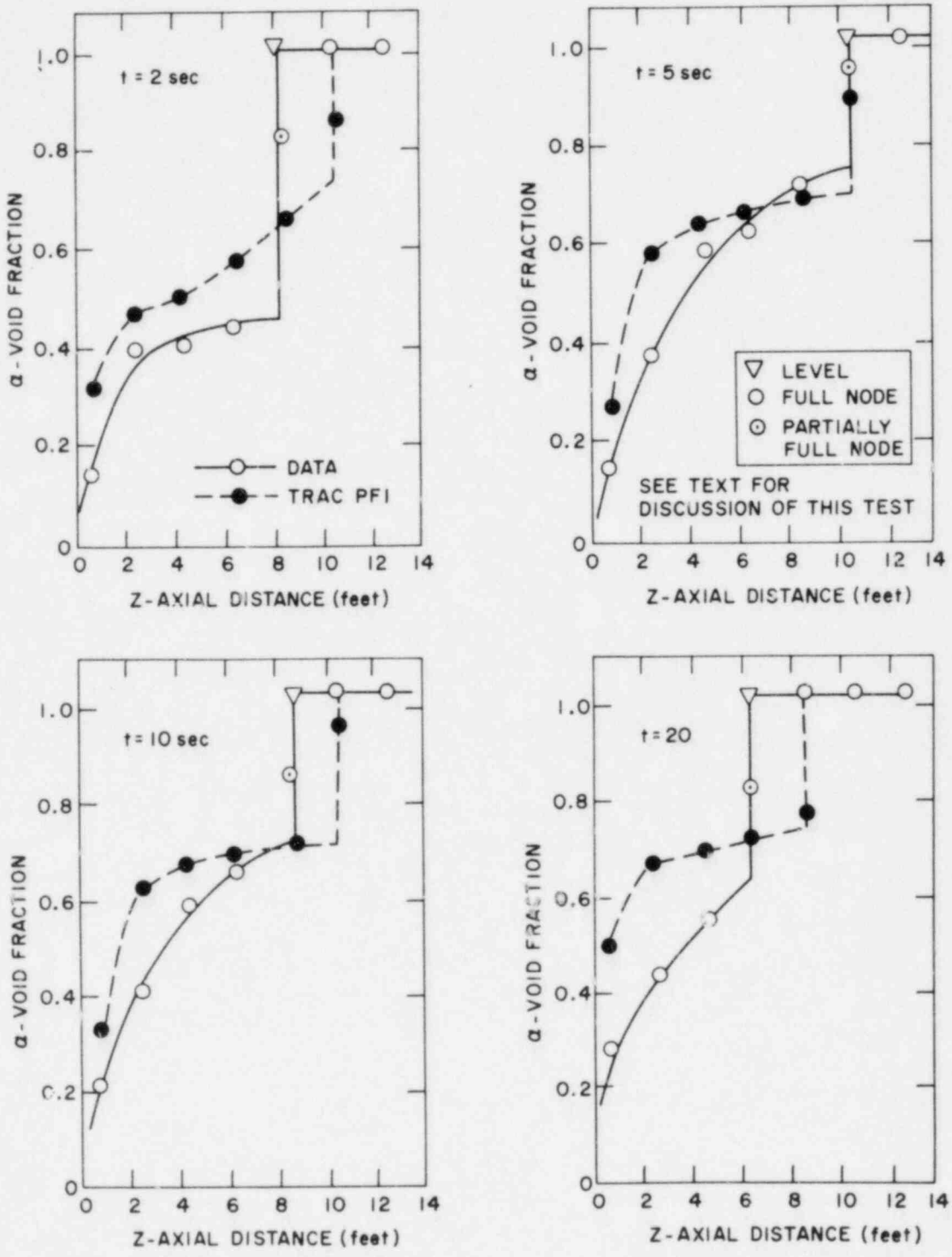

Figure 7.16 Comparison Between the Measured and Predicted Axial Void Distribution at Various Times (BNL Neg. No. 4-727-82).

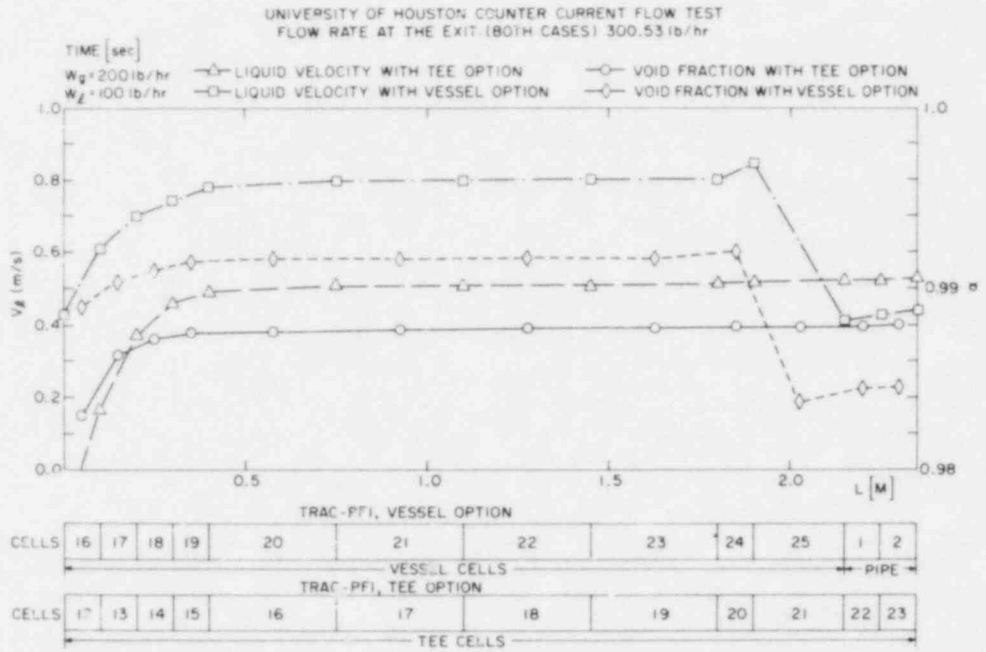

Figure 7.17 Comparison Between Two TRAC-PF1 Calculations for Water Feed Rate of 100 lb/hr and Air Injection Rate of 200 lb/hr (BNL Neg. No. 4-795-82).

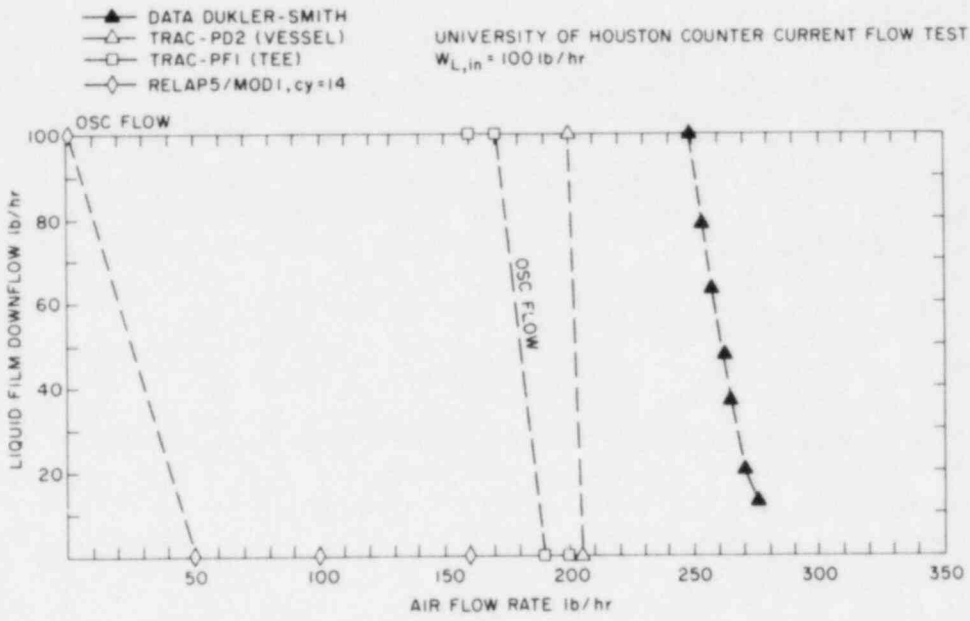

Figure 7.18 Comparison Between the Measured and Predicted Water Downflow Rate vs. Air Flow Rate for Water Feed Rate of 100 lb/hr (BNL Neg. No. 4-796-82).

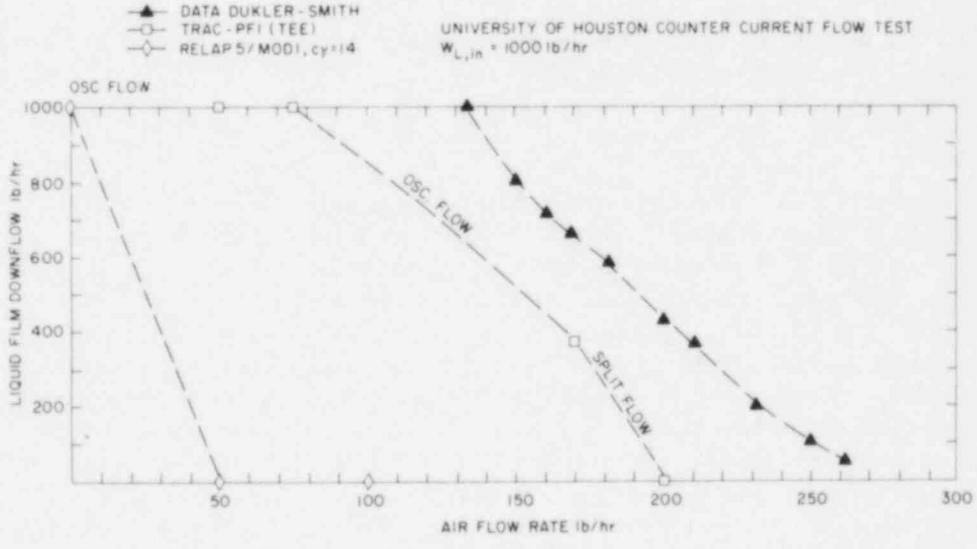

Figure 7.19 Comparison Between the Measured and Predicted Water Downflow Rate vs. Air Flow Rate for Water Feed Rate of 1000 lb/hr (BNL Neg. No. 4-797-82).

based on Dukler's data which predicts a higher interfacial shear coefficient than the Wallis correlation used in TRAC-PD2. This explains the relatively early inception of co-current flow for TRAC-PF1. Furthermore, the code did not predict split flow for liquid between the inception and completion of co-current flow. Instead, it predicted oscillations in liquid film downflow. Figure 7.19 shows similar behavior for liquid injection rate of 1000 lb/hr. However, in this case, the code predicted some stable split flow where some liquid flowed down and the remaining liquid went up with the air.

In summary, TRAC-PF1 did compute flow reversal from counter-current to co-current flow as the air flow rate was increased. However, the results were no improvement over TRAC-PD2.

7.3 RELAP5/MOD1 (Cycle 14) Assessment

7.3.1 Marviken Critical Flow Test 24 (U. S. Rohatgi)

During this reporting quarter, Test 24 has been simulated with the RELAP5-/MOD1 (Cycle 14) code. The nodalization in the vessel and the discharge pipe was maintained exactly like the TRAC-PF1 calculation as described in Section 7.2.1. However, the nozzle was modeled with a single volume and the RELAP5 choking model was applied.

Figure 7.10 shows a comparison between the computed break flow rate and the data for both the RELAP5 and TRAC-PF1 calculations. Although RELAP5 underpredicted the mass flow rate, its prediction is somewhat better than that of TRAC-PF1. Figure 7.11 shows a comparison of the computed vessel top pressure with the data. Here, RELAP5 underpredicted the pressure and the comparison is worse than TRAC-PF1. This problem will be studied further by simulating only the nozzle and part of the discharge pipe where boundary conditions can be imposed from the experimental measurements.

7.3.2 B&W Steam Generator Tests (J. H. Jo)

The calculation of the B&W steam generator test series 28-29 (OTSG) has been attempted with the RELAP5/MOD1 (Cycle 14) code. The results indicate significant oscillations, and no acceptable steady-state has been achieved even with very fine nodalization and adjustments in the initial conditions.

It was suspected that this difficulty might be due to oscillation or fluctuation in the heat transfer regime and the heat transfer coefficient in the secondary side of the steam generator. A calculation was, therefore, performed by isolating the primary side and imposing a constant power (or heat) into the wall. A very stable steady-state for the secondary side was now achieved. This indicates that further investigation of the effect of secondary side heat transfer coefficient on the coupling between the primary and secondary sides of a steam generator in RELAP5 is needed. The RELAP5 input decks for the B&W Test Series 28-29 (OTSG) and 68-69-70 (IEOTSG) have been sent to the INEL staff for their examination and comments.

7.3.3 FLECHT-SEASET Steam Generator Tests (G. Slovik)

During this reporting quarter the FLECHT-SEASET steam generator tests ID=21806 and ID=22010 have been simulated with the RELAP5/MOD1 code. The operating conditions for these tests are presented in Table 7.1.

The noding was modified to match the TRAC-PF1 alterations, as indicated in Section 7.2.3. This was done by increasing the number of volumes in the steam generator, removing the inlet plenum modeling with a SINGLE VOLUME (Rohatgi, 1982b) and extending the hot leg PIPE to absorb the steam generator inlet plenum. Also, the exit SINGLE VOLUME was removed.

Although these tests have been simulated with the RELAP5/MOD1 code, a comprehensive analysis of the results has not yet been completed. Therefore, a detailed analysis of the results and their comparison with the data will be presented in the next quarterly report.

7.3.4 GE Large Vessel Blowdown Test (J. H. Jo)

The GE large vessel blowdown Test No. 5801-15, which is described in Section 7.2.4, was also simulated with the RELAP5/MOD1 (cycle 14) code. The vessel was represented with 7 volumes, whereas the discharge nozzle was modeled using different number of volumes (6, 3,and 2). The results for each case were quite close. Since the computing time was decreased substantially with decreasing number of nozzle volumes, it is recommended to use the minimum number of nozzle volumes which can describe the correct geometry of the nozzle (in this case, it was two volumes).

The agreement between the computed (with RELAP5/MOD1) and the measured vessel pressure (see Figure 7.20) was not as good as that obtained with TRAC-PF1. The calculation for the void fraction (see Figure 7.21), while relatively close to the data, shows an irregular axial distribution. It is suspected that improper interfacial shear might be responsible for this discrepancy. Another calculation with a large number of volumes in the vessel is underway.

7.3.5 University of Houston Counter-Current Flow Tests (U. S. Rohatgi and N. Popov)

In the current quarter, two of these tests were also simulated with the RELAP5/MOD1 (Cycle 14) code. The nodalization was kept similar to that used in the TRAC-PF1 calculation with two TEE components (see Section 7.2.5). The representation consisted of two BRANCH components for water and air injection, and three PIPE components for the bottom collection, the intermediate test section and the upper exit section. A total of 29 volumes was used which were of the same size as used for the TRAC-PF1 calculation.

Figures 7.18 and 7.19 show the computed liquid film downflow for various amounts of air flow rates. The tests were simulated for air flow rates ranging from 50 to 150 lb/hr. In all cases the RELAP5 code predicted no downflow.

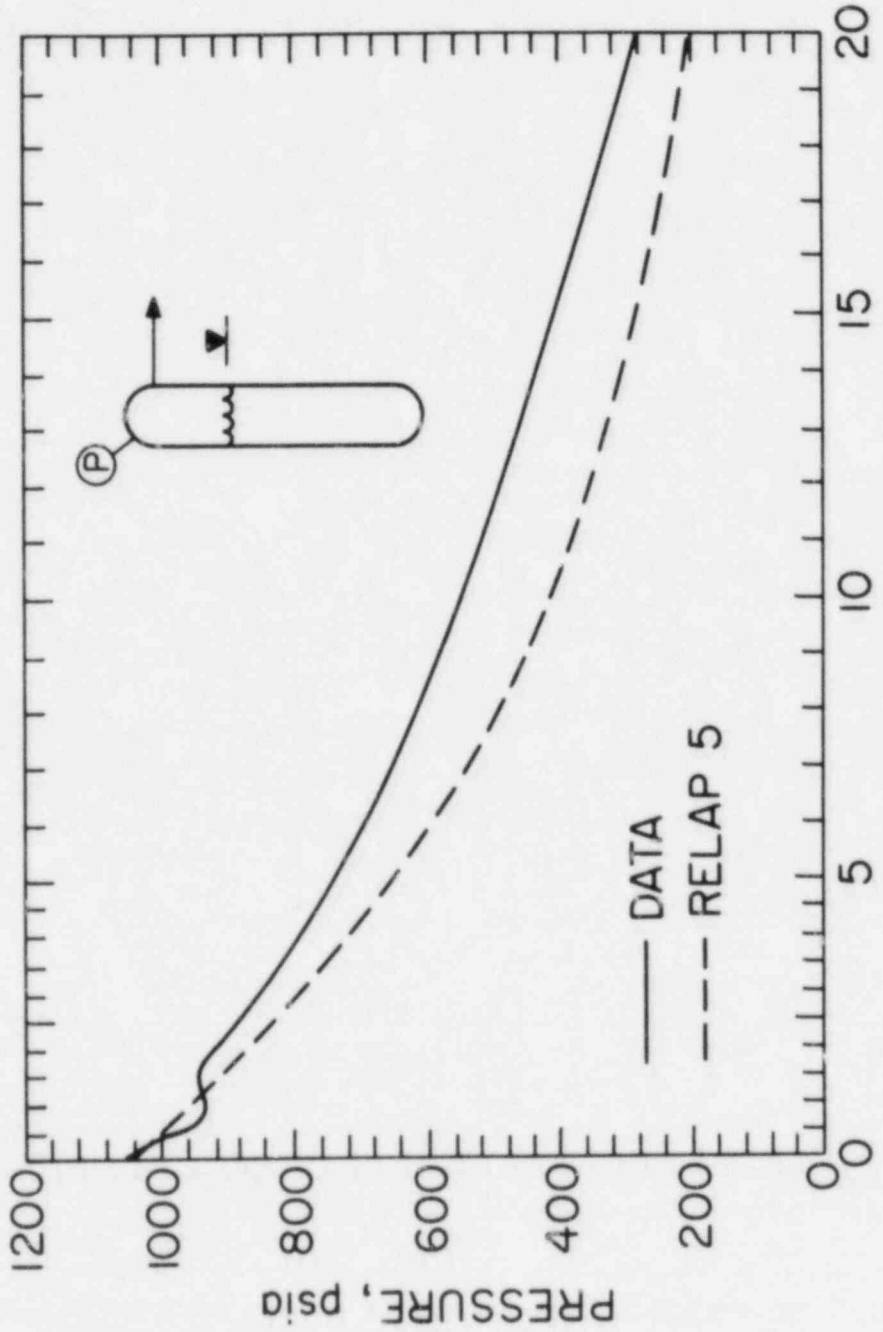

Figure 7.20 Comparison Between the Measured and Predicted Vessel Pressure (BNL Neg. No. 4-729-82).

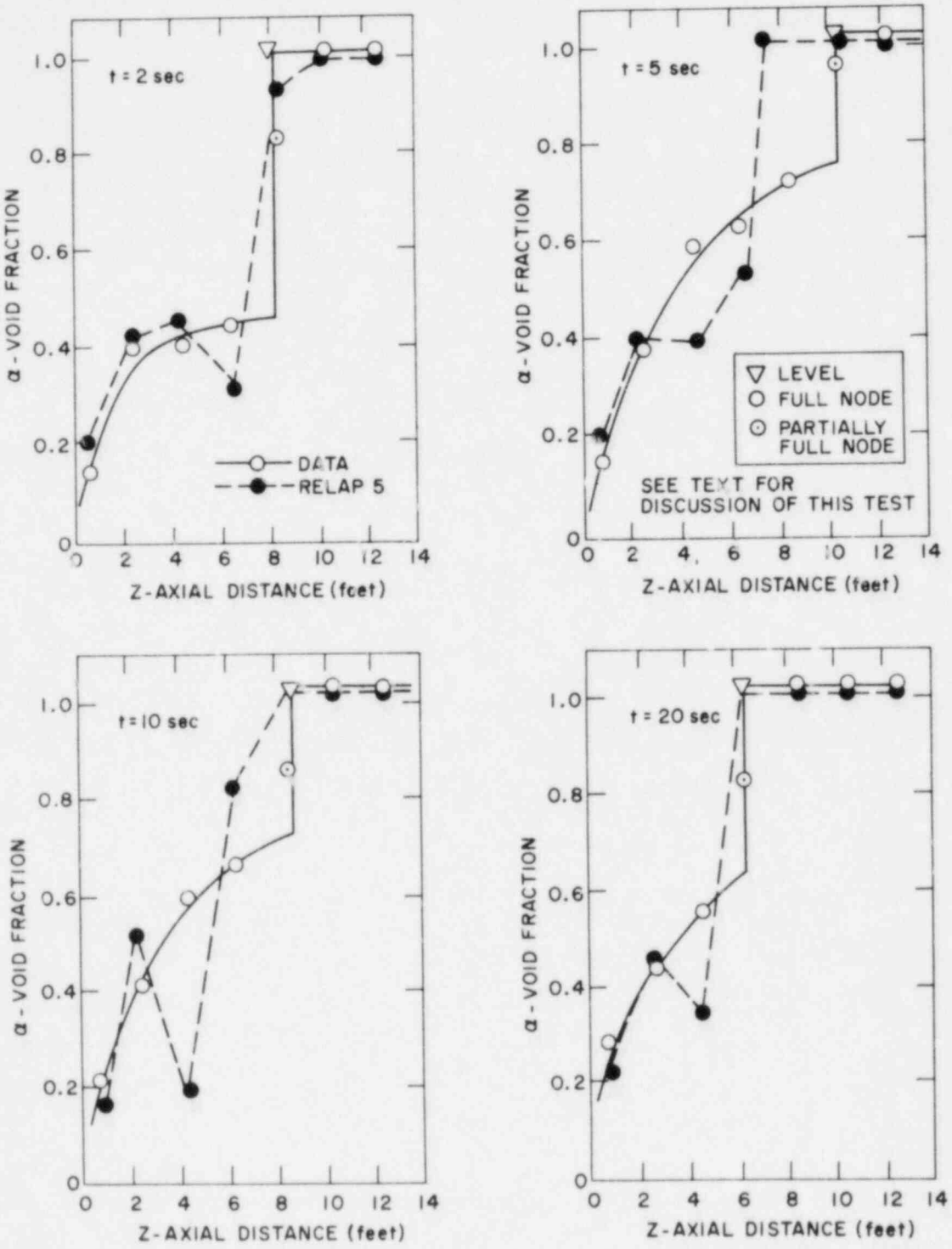

Figure 7.21 Comparison Between the Measured and Predicted Axial Void Distribution at Various Times (BNL Neg. No. 4-726-82).

This discrepancy in the code prediction is due to the flow regime map as used in RELAP5. The void fraction in these tests was generally greater than 0.95, even for the liquid injection rate of 1000 lb/hr. For void fractions greater than 0.95, RELAP5 assumes a dispersed droplet flow regime with no liquid film on the wall and so all the droplets are carried over with the air due to high interfacial momentum transfer.

Even for no air flow rate all the liquid did not flow down. Instead, the liquid spread above and below the volume of liquid injection and finally the computation ceased as pressure became negative in some volumes. This case was run earlier, where the bottom collecting pipe and the top exit pipe were slightly smaller in size and the code had no difficulty in computing. In that simulation most of the liquid flowed down but some liquid was also above the liquid injection volume. These discrepancies will be investigated further.

REFERENCES

FINDLAY, J. A., (1981), "BWR Refill-Reflood Program Task 4.8 - Model Qualification Task Plan," NUREG/CR-1899, EPRI NP-1527, GEAP-24898, August 1981.

HOWARD, R. C., McGUIRE, M. F., and HOCHREITER, L. E., (1980), "PWR FLECHT-SEASET Steam Generator Separate Effects Task Data Report," NUREG/CR-1366, January 1980.

ROHATGI, U. S., (1982a), "Marviken Critical Flow Test 24," in Safety Research Programs Sponsored by Office of Nuclear Regulatory Research, Quarterly Progress Report October 1 - December 31, 1981, NUREG/CR-2331, BNL-NUREG-51454, Vol. 1, No. 4, Section 7.3.3, February 1982.

ROHATGI, U. S., (1982b), "FLECHT-SEASET Steam Generator Tests," Ibid, Sections 7.3.2 and 7.4.2, February 1982.

SAHA, P., JO, J. H., NEYMOTIN, L., ROHATGI, U.S., and SLOVIK, G., (1982), "Independent Assessment of TRAC-PD2 and RELAP5/MOD1 Codes at BNL in FY 1981," BNL-NUREG Draft Report, March 1982.

SLOVIK, G., (1982), "BCL Downcomer Tests," in Safety Research Programs Sponsored by Office of Nuclear Regulatory Research, Quarterly Progress Report October 1 - December 31, 1981, NUREG/CR-2331, BNL-NUREG-51454, Vol. 1, No. 4, Section 7.1.1, February 1982.

II. DIVISION OF ENGINEERING TECHNOLOGY

SUMMARY

Stress Corrosion Cracking of PWR Steam Generator Tubing

U-bend samples of Inconel 600 continue in exposures at 290°C and 315°C in pure water without oxygen. Cracks in these U-bends are anticipated to start in about six months to a year. Constant extension rate (CER) tests with 0.01% carbon material are practically complete in pure water. Similar tests are continuing with the 0.03% carbon material, but strain rates for best results appear to be somewhat lower than for the 0.01% C heats. So far, the Arrhenius plots for crack velocity show a consistent activation energy over the range of temperature tested. Our data are in general agreement with results from other laboratories in dilute deaerated sodium hydroxide. From these data tentative predictive numbers for times to failure fall well within experience at some plants where leaks have occurred as a result of tube deformation. Tests at constant load are consistent with a log-log relationship between the applied stress and time to fracture. Data have been obtained at both 365°C and to a lesser extent at 345°C, with a cracking dependence on the fourth power of applied stress.

Standards for Materials Integrity in LWRs

Participation in ASTM activities associated with evaluating the Nuclear Regulatory Commission (NRC)-developed electrochemical potential kinetic reactivation tests for sensitization of stainless steels is continuing, with a possible standard practice due this year. Extensive discussions of the EPRI industry programs on the roll of ferrites in the susceptibility of stainless steels to intergranular stress corrosion cracking and on the technique for controlling oxygen in BWRs were held during the period, and formal reports will be submitted to NRC during the next quarter.

Probability Based Load Combinations for Structural Design

The analytical and numerical procedures established in the last quarter for the frequency domain finite element analysis of Category I nuclear structures were applied to a reinforced containment concrete structure subjected to horizontal earthquake ground acceleration with a Kanai-Tajimi spectral density.

The task of developing a FEM-based frequency domain reliability analysis method for dynamic loads is in its final stage. However, a substantial amount of work is still required for cleanup and documentation.

The reliability analysis method for dynamic loads was combined with the existing standard reliability analysis procedure for static and quasi-static

loads for the purpose of developing a load combination methodology. Preliminary computations were performed to evaluate the limit state probabilities under each load combination separately and also under all the possible load combinations, involving dead load, accidental internal pressure and earthquake acceleration.

From the response and comments on the first-round questionnaire and from the advice of the study committee, the consensus estimation form has been revised.

Mechanical Piping Benchmark Problems

Analytical estimates of the absolute response of the HDR URL loop piping were developed for both uniform and independent support excitation. The absolute results correspond as well to the measured results as the relative results presented last period.

A number of permanent changes designed to enhance the capabilities of the PSAFE1 and PSAFE2 computer codes were completed. This included the introduction of new algorithms which permit the prediction of absolute acceleration response for systems subjected to uniform and independent support excitations.

The informal agreement with EPRI was formalized and should provide BNL access to data pertinent to the development of physical piping benchmarks. The current testing being conducted by the EPRI contractor, ANCO, is to be included in this agreement.

1. Stress Corrosion Cracking of PWR Steam Generator Tubing

(D. van Rooyen)

The objective of this program is to establish quantitative relationships between factors influencing stress corrosion cracking (SCC) of Inconel 600, and to use these data to set up a model for determining the useful life of Alloy 600 tubing in service. For this purpose, tests are being run with production tubing of Inconel 600 at different carbon levels to determine crack initiation times and propagation rates. During the previous quarter, tests have continued with U-bend samples, in the CER test apparatus and under constant load. The basic equations based on the effects of temperature, stress and CER test are:

For Crack Initiation:

$$T_f^{-1} = K \cdot \sigma^B \cdot \text{Exp.} - \frac{Q}{RT} \quad \text{----------1)*}$$

1) Is composed of two equations:

$$\text{Log } T_f^{-1} = K_1 \text{ Log} \sigma^B \quad \text{----------2)**}$$

$$\text{and} \quad T_f^{-1} = K_2 \cdot \text{Exp} - \frac{Q}{RT} \quad \text{----------3)***}$$

where constants in 2) & 3) are determined experimentally

* Velocity = Inverse of failure time.
** Eq. 2 is for constant load tests.
*** Eq. 3 applies to Arrhenius plots of U-bend and constant load data.

For Crack Propagation:

$$\text{Growth Rate} = T_f^{-1} = K_3 \cdot \text{Exp} - \frac{Q}{RT} \quad \text{-------4)}$$

Constants Q and K_3 are determined in CER tests

Most of the U-bend testing is now being done at lower temperatures, near those found in operating reactors. As a result, we do not expect cracks to develop in U-bends for several months yet, and therefore, there are no new results in this particular area. Work also continued with specimens heat treated after cold working in order to replenish our supply of susceptible tubing at 0.03% carbon, and it appears that our procedure is producing the required samples for the purposes of the program.

CER tests with .01% carbon material are practically complete in pure water. At this time, testing with 0.03% carbon tubing is underway. For the low carbon alloy, results to date indicate that as-received alloys crack with somewhat greater difficulty, (i.e. initiation is apparently somewhat slower, and crack propagation velocities are lower) than cold worked material, as shown in Figure 1. Our data agree very well with results in dilute deaerated sodium hydroxide which were obtained in other laboratories. Examples of calculations for expected times to initiate and propagate stress corrosion cracks into Inconel 600 in a plant which is undergoing active denting have been prepared for the mid-year review in April, and these are based on a computer program prepared for this purpose. Somewhat more accurate calculations will be possible within the next few months when data are better refined; at the moment, however, it is already evident that best predictive numbers fall well within what has been experienced in some plants where leaks occurred as a result of tube deformation. Some of the CER tests have been run at a somewhat lower strain rate than we used to estimate the duration of this program, according to the matrix that was set up a few months ago. It is now anticipated that the CER test will take somewhat longer to complete, but an additional test apparatus has been procured to speed up the data gathering.

The constant load tests with 0.01% carbon alloys in the as-received condition have indicated a log-log relationship between the fraction of the yield stress (applied) and the time to fracture. Most of the testing has been done at 365°C, although some results at higher stress levels are also available at 345°C; these were all done in pure water, deaerated. Use is made of an equation of the form

$$T_f^{-1} = k\sigma^B$$

in which T_f is the failure time, σ = stress, and k the proportional constant. From the plot of log T_f vs. log σ, as shown in Fig. 2, B = 4, while k increases with temperature and cold work. A comparison of our data with results from B&W, which they obtained in caustic solutions, showed the same trends, and predicted cracking at stresses below the yield stress. In fact, we have recently had the first failures at applied stress just <u>below</u> the 365°C yield point of the low carbon alloy, and these points are included in Fig. 2. One more set of specimens is in test at even smaller applied load, and these results should be available in the next quarter for 0.01% carbon in pure water at 365°C.

The calculation of activation energy in the constant load tests at 365°C and 345°C gives a value between 30 and 35 Kcal/mole, which is higher than projected by U-bend data. We feel that the constant load value is more reliable, since the stresses were controlled precisely.

The effect of testing in the presence of hydrogen is dramatically evident in results shown below where the presence of H_2 at levels equal to those in primary water caused a large increase in SCC in 12 weeks tests at 365°C:

Effect of H_2:

(9 Heats 365°C.)

Results of 12 Week Tests

H_2O	$H_2O + H_2$
1/45	15/18

(# Failed/#Tested)

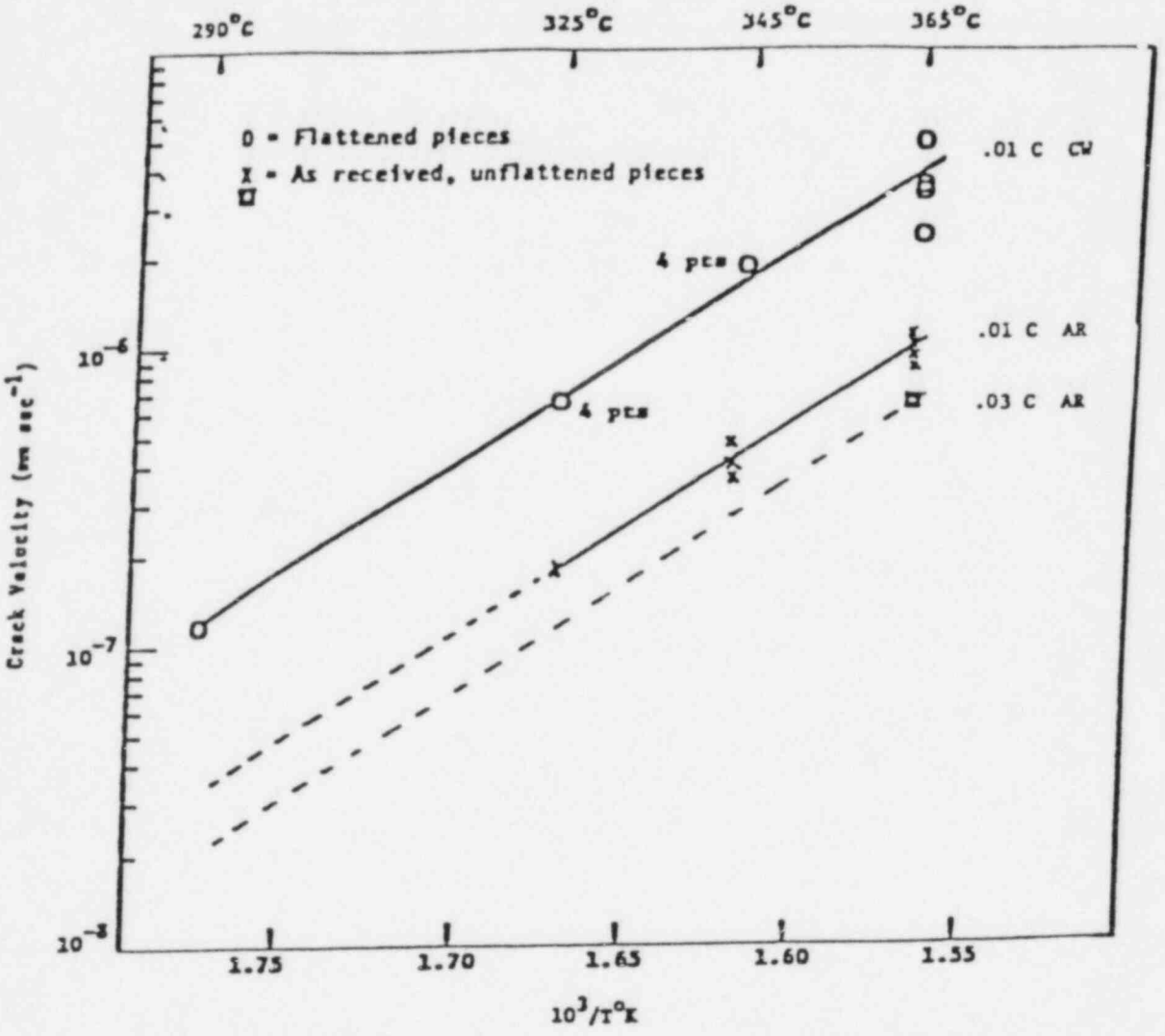

Comparison of CERT Data Between As Received (x) and Flattened Tube Tensile Pieces (o). Inconel 600, 365°C, Pure H_2O Deaerated

FIGURE 1

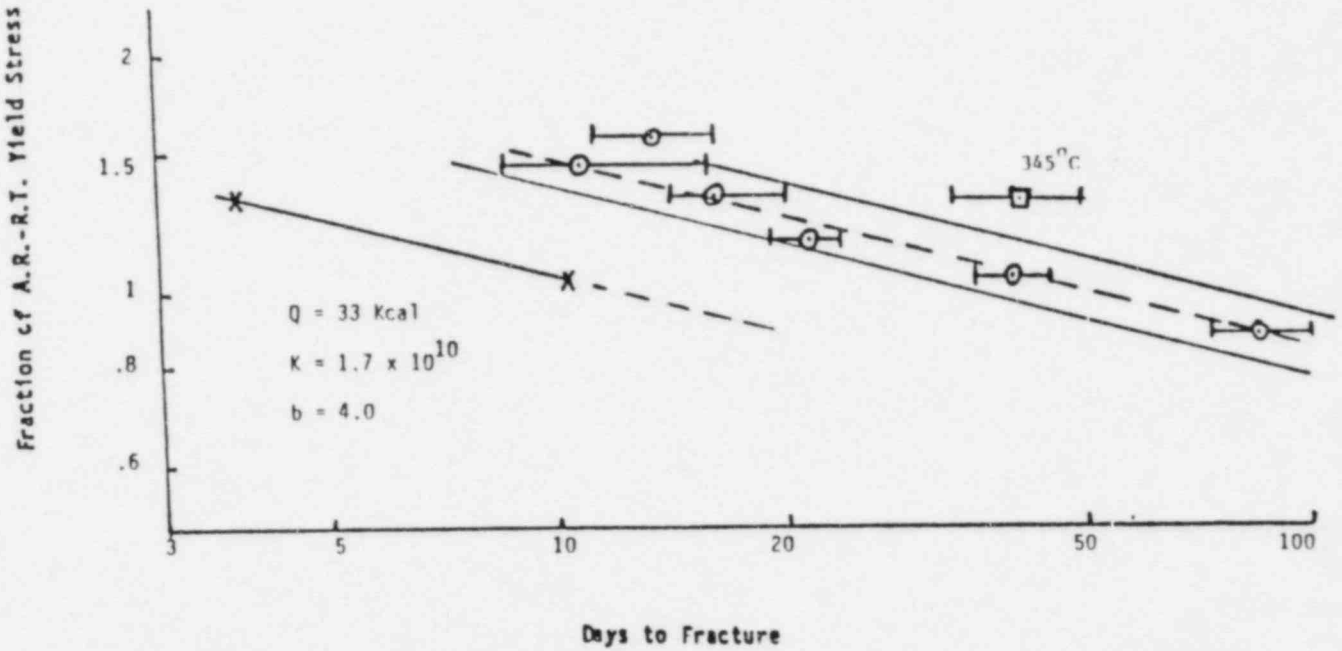

On Failure Time. Inconel 600, 0.01%C, Pure H_2O, Deaerated

NOTE: X = Cold Worked (Flattened Tube) θ = As Received, 365°C ⊡ = As received, 345°C

Points (X) Are From Earlier Tests using Flattened Tensile Pieces made from the Same Tubing.

FIGURE 2

2. Standards for Materials Integrity in LWR's

(J. R. Weeks)

Introduction

Brookhaven National Laboratory (BNL) is providing technical assistance to the Materials Branch, Office of Research, in the area of standards for materials compatibility, corrosion, stress corrosion, water chemistry, and eddy current inspection of steam generator tubing in light water reactors.

Results

Work during the second quarter of fiscal year 1982 has been concerned with areas in the statement of work as follows:

Review EPRI and industry programs on oxygen control in BWR's and prepare input for revisions to Regulatory Guide 1.56 maintenance of water purity in BWR's. Extensive discussions were held in this area at EPRI and at the General Electric Company in February. The formal report containing our evaluation of these programs and a recommended revisions to Regulatory Guide 1.56 will be submitted to NRC during the third quarter.

Evaluate the results of the ASTM Round Robin Test of EPR. A status report summarizing the present situation regarding the use of the EPR tests was submitted to the USNRC on April 6, 1982. Round Robin Tests will still be continued since one or two more laboratories have expressed an interest in participating. We believe a standard will be adopted by the ASTM later this year.

Review recent data on the role of ferrites in the susceptibility of stainless steel intergranular stress corrosion cracking. For inputs to revision of Regulatory Guide 1.44 detailed discussions in this area were held at EPRI and at General Electric during February and a formal report containing our recommendations for revisions to the subject guide will be provided NRC during the third quarter of the fiscal year.

Anticipated Results During the Next Period

Work will continue on the ASTM activities and formal reports on the discussions with EPRI and industry personnel will be submitted to the NRC. Draft recommendations for revision to Regulatory Guide 1.121 based on the predictive models on stress corrosion cracking service life of Inconel 600 tubing will be submitted to NRC late in the quarter.

3. Probability Based Load Combinations for Structural Design

H. Hwang, M. Reich, P. Brown,
M. Shinozuka, B. Ellingwood, P. C. Wang and S. Kao

Accomplishment

The major accomplishments during the report period are as follows:

3.1 Structural Analysis and Limit State Identification

The analytical and numerical procedure established in the last quarter for the frequency domain finite element analysis of category I nuclear structures was applied to a reinforced containment concrete structure (see Figure 1 and 2) subjected to horizontal earthquake ground acceleration with a Kanai-Tajimi spectral density. A method that makes it possible to integrate in closed form the cross-spectral density matrices of response quantities was utilized for the evaluation of the corresponding auto- and cross-correlations. Limit states for concrete structures were defined either by concrete crushing at the extreme fibers or by yielding of reinforcing bars. The limit states so defined are to be considered in two directions, one in the meridional direction and the other in the circumferential direction for each of the finite elements of the model.

3.2 Reliability Analysis Methods

The task of developing a FEM-based, frequency domain reliability analysis method for dynamic loads is in its final stage. A substantial amount of work, however, is still required for clean-up and documentation. In general, the method can evaluate the structural response to dynamic loads characterized as stationary vector processes with specified cross-spectral density matrices. The response is obtained in the form of a cross-spectral density matrix, which, upon integration, produces a response second moment (cross-correlation) matrix. Under the assumption that the loads are Gaussian and therefore that the response is also Gaussian, techniques for estimating the rate at which the response vector outcrosses the limit state surface, were developed and implemented into the computer program. This outcrossing rate can, in turn, be used to evaluate the limit state probabilities of the structure subjected to these loads. Indeed, such limit state probabilities were estimated for a RC containment structure subjected to horizontal earthquake acceleration with a Kanai-Tajimi spectral density.

3.3 Load Combination Methodology

The reliability analysis method for dynamic loads was combined with the existing standard reliability analysis procedure for static and quasi-static loads for the purpose of developing a load combination methodology. The significant parameters that enter into the methodology are: the occurrence rate, duration and intensity of each load (e.g., dead load, accidental internal pressure, earthquake, etc.) All these parameters are basically random variables for most of the loads to be considered. For dynamic loads,

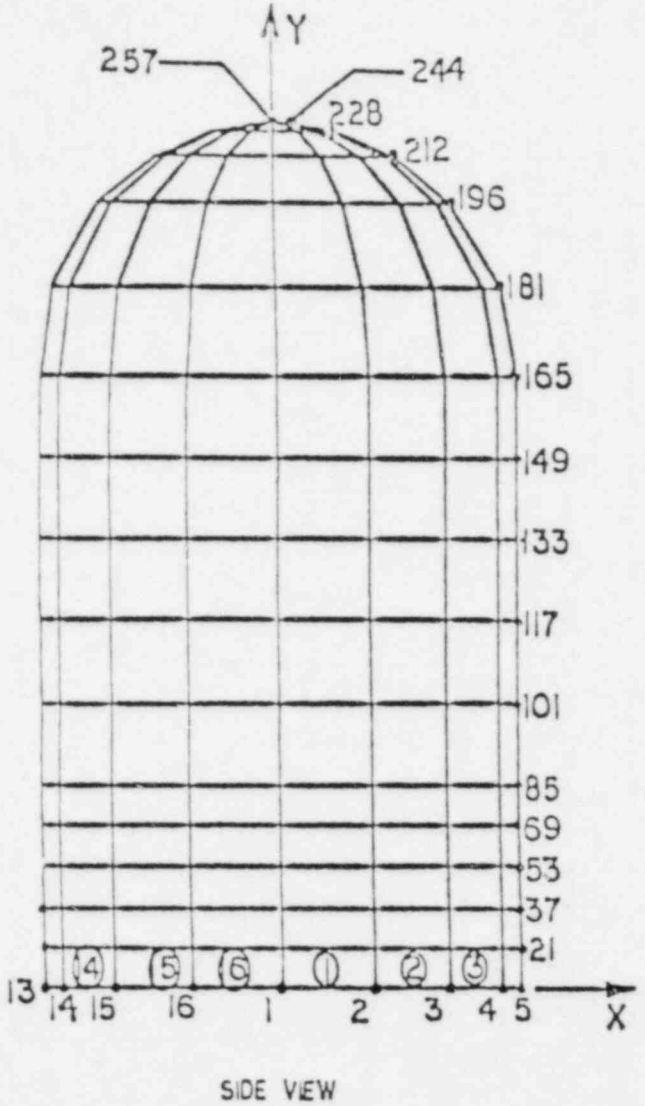

SIDE VIEW

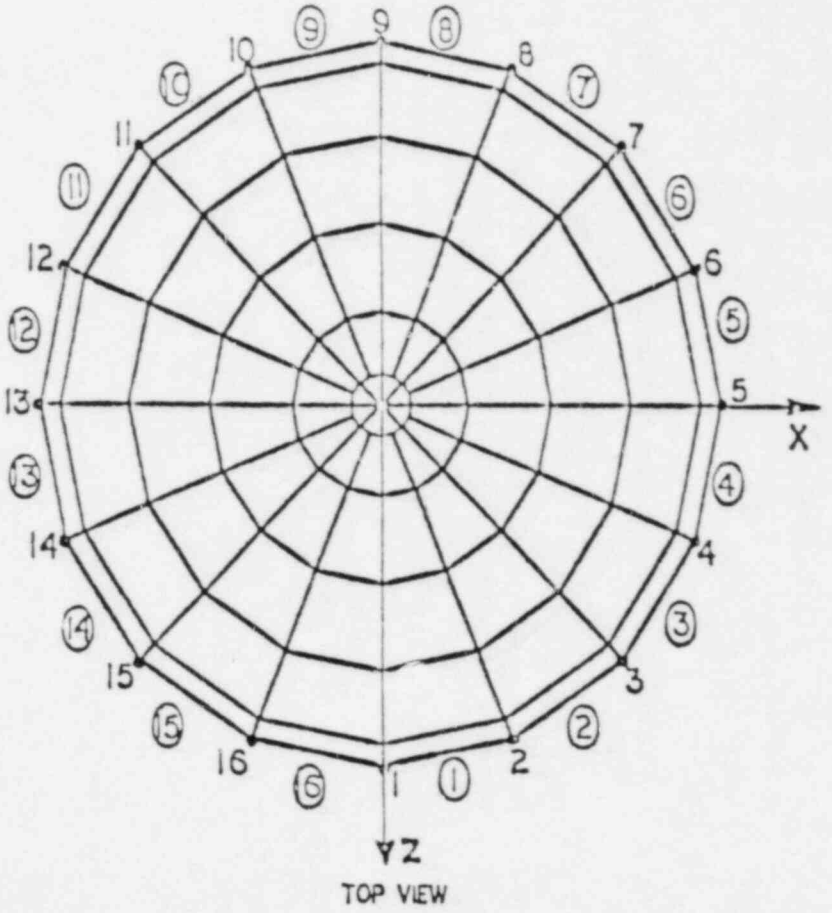

TOP VIEW

① DENOTES ELEMENT
1 DENOTES NODE

FIG. 1: SIDE VIEW AND TOP VIEW OF CONTAINMENT

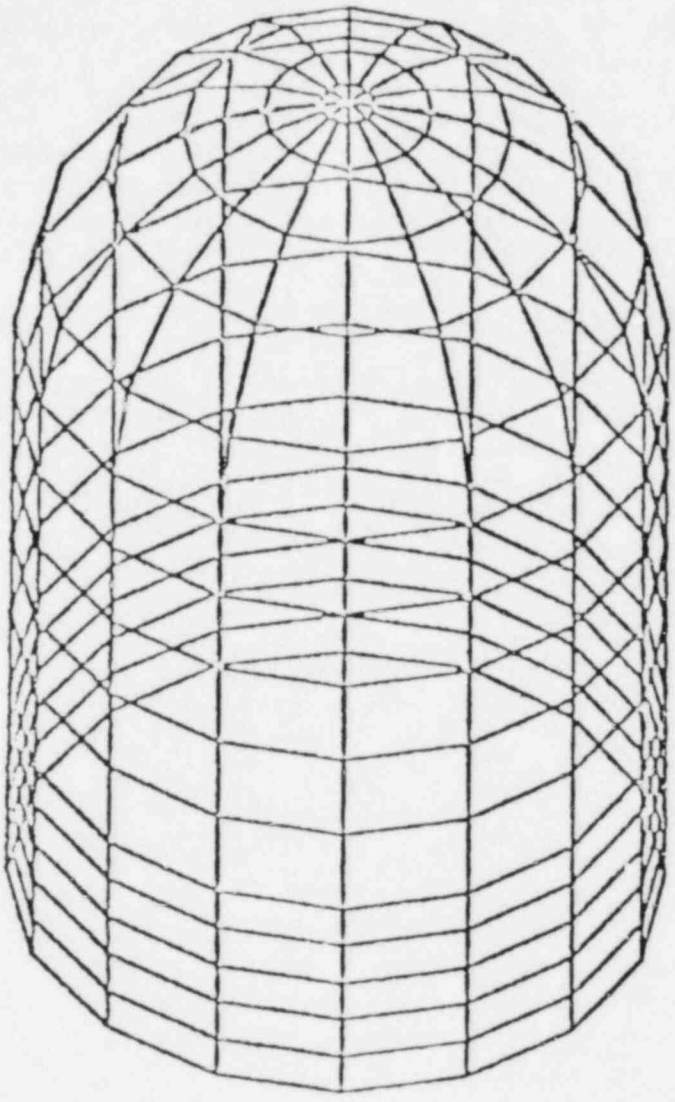

FIG. 2: 3D VIEW OF CONTAINMENT

the overall intensity is usually characterized not only by their dynamic components but also by their static components. Preliminary computations were performed to evaluate the limit state probabilities under each load combination separately and also under all the possible load combinations, involving dead load, accidental internal pressure and earthquake acceleration. These preliminary results for three different cases are shown in Figure 3-5. A complete description of this work will be issued in a forthcoming report. It was generally observed that, depending on the limit state condition to be specified, one of the load combinations tends to have a dominant contribution to the overall limit state probability. It was further observed that some of the load combinations contribute very little to the overall limit state probability under all practical limit state conditions. These observations provide insight into the complex problem of which load combinations must be considered for design, for which limit states and at what level of limit state probabilities. Of course these are only preliminary investigations, and as noted in our work plan more in-depth studies in this area will be undertaken.

3.4 Consensus Estimation of Loads

From the responses and comments of the first round questionaire and also the advice from the study committee, the consensus estimation form has been revised. A typical table of this form is on the following page. The revised questionnaire has been sent out to the original participants and to other experts from utility companies as well. It is expected that a useful response from this questionnaire will be forthcoming.

Publication

Progress Report on Data Base for Operational and Accidental Loads for Seismic Category I Structures will soon be published.

PWR - Abnormal Loads

Load Type		Design Value	Actual Peak Value		Duration	Occurrence Rate	Comments
			Mean / Design Value	Variation (%)			
LOCA Pressure (psig)	Containment						
	Primary Shield Wall						
	Refueling Cavity						
	Steam Generator Encl.						
	Pressurizer Enclosure						
LOCA Temperature	Gross (^{O}F)						
	Gradient (^{O}F/ft)						
Post-LOCA Flooding Head (ft)							

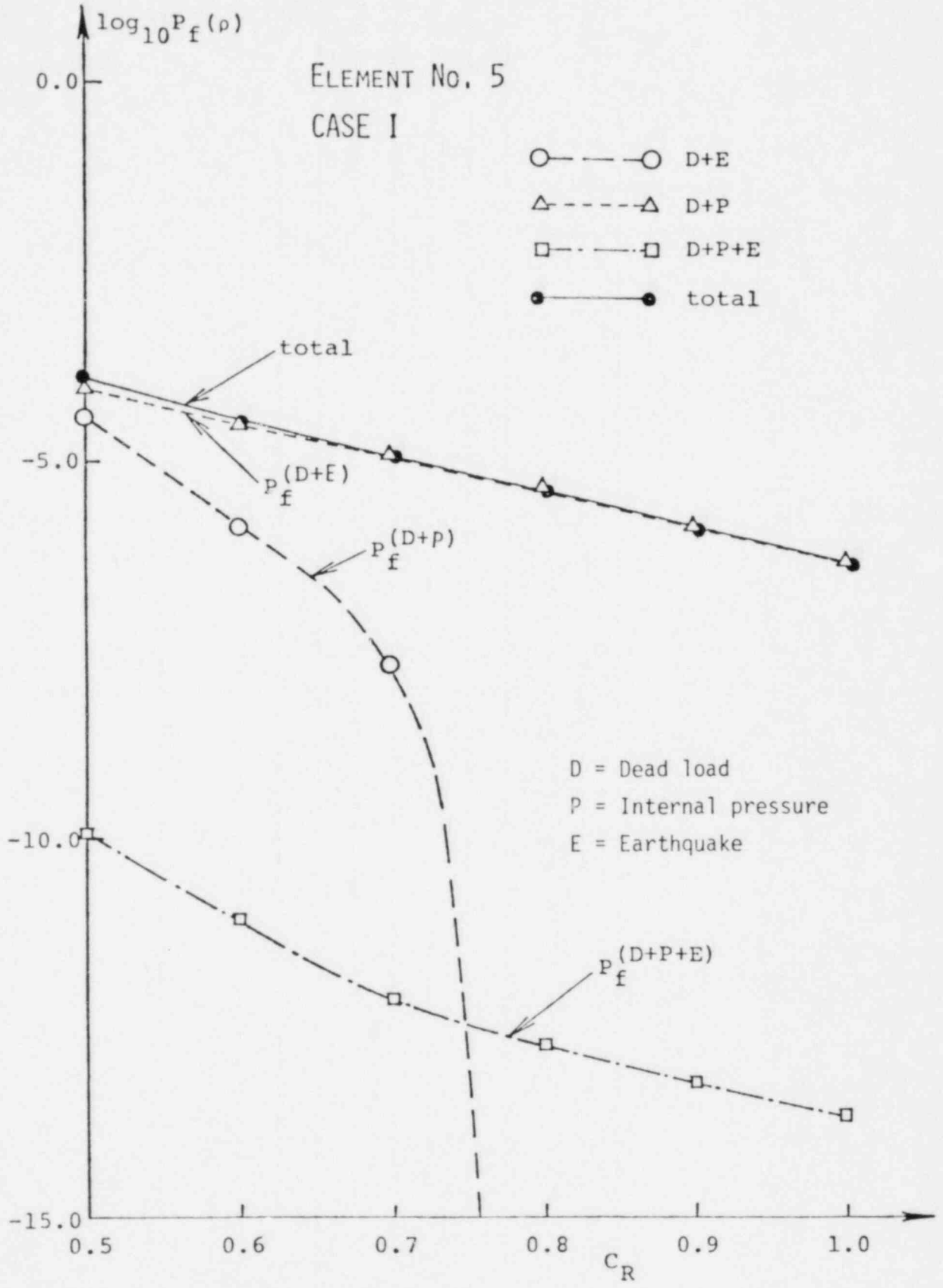

FIG. 3: LIMIT STATE PROBABILITIES UNDER LOAD COMBINATIONS

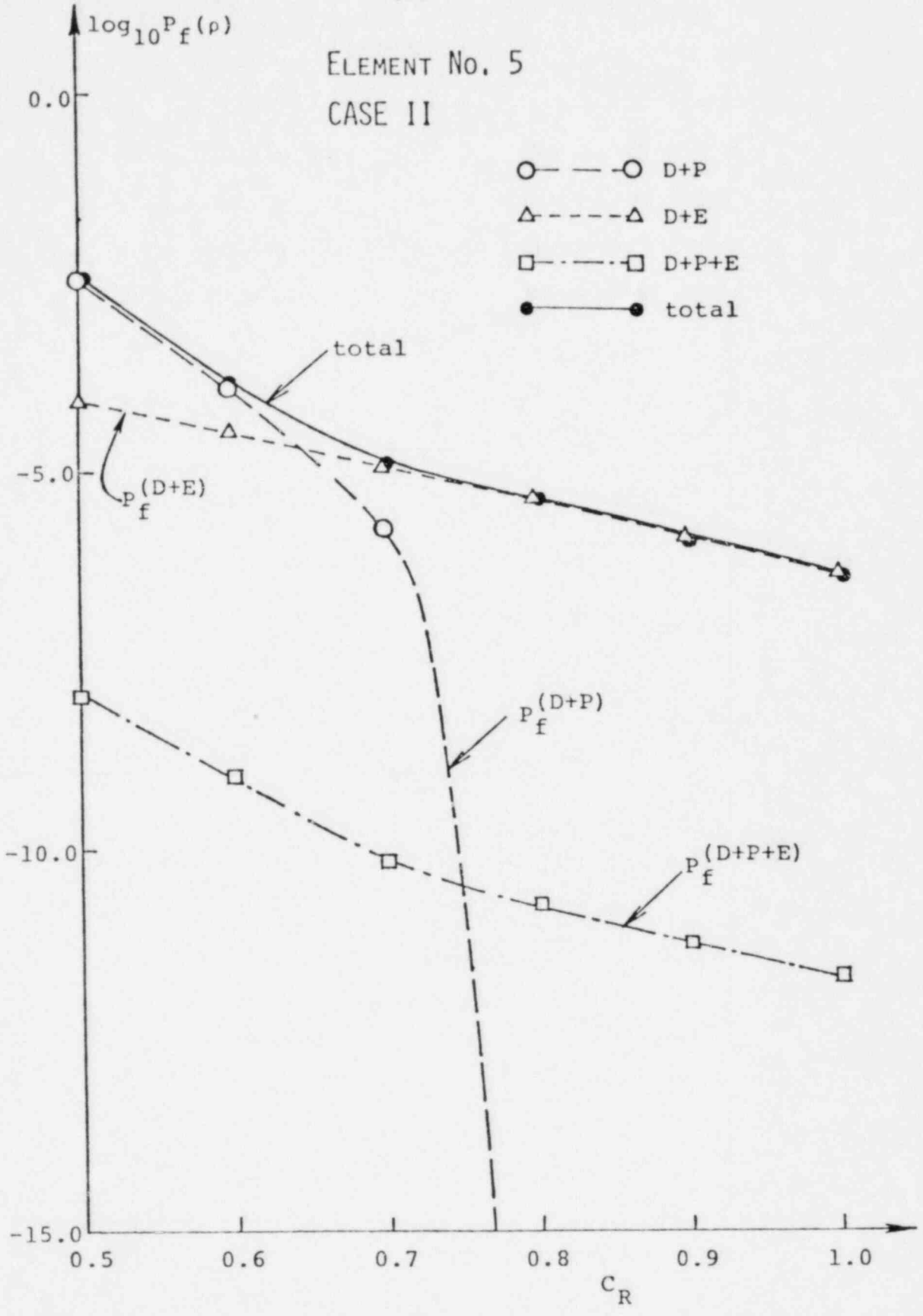

FIG. 4: LIMIT STATE PROBABILITIES UNDER LOAD COMBINATIONS

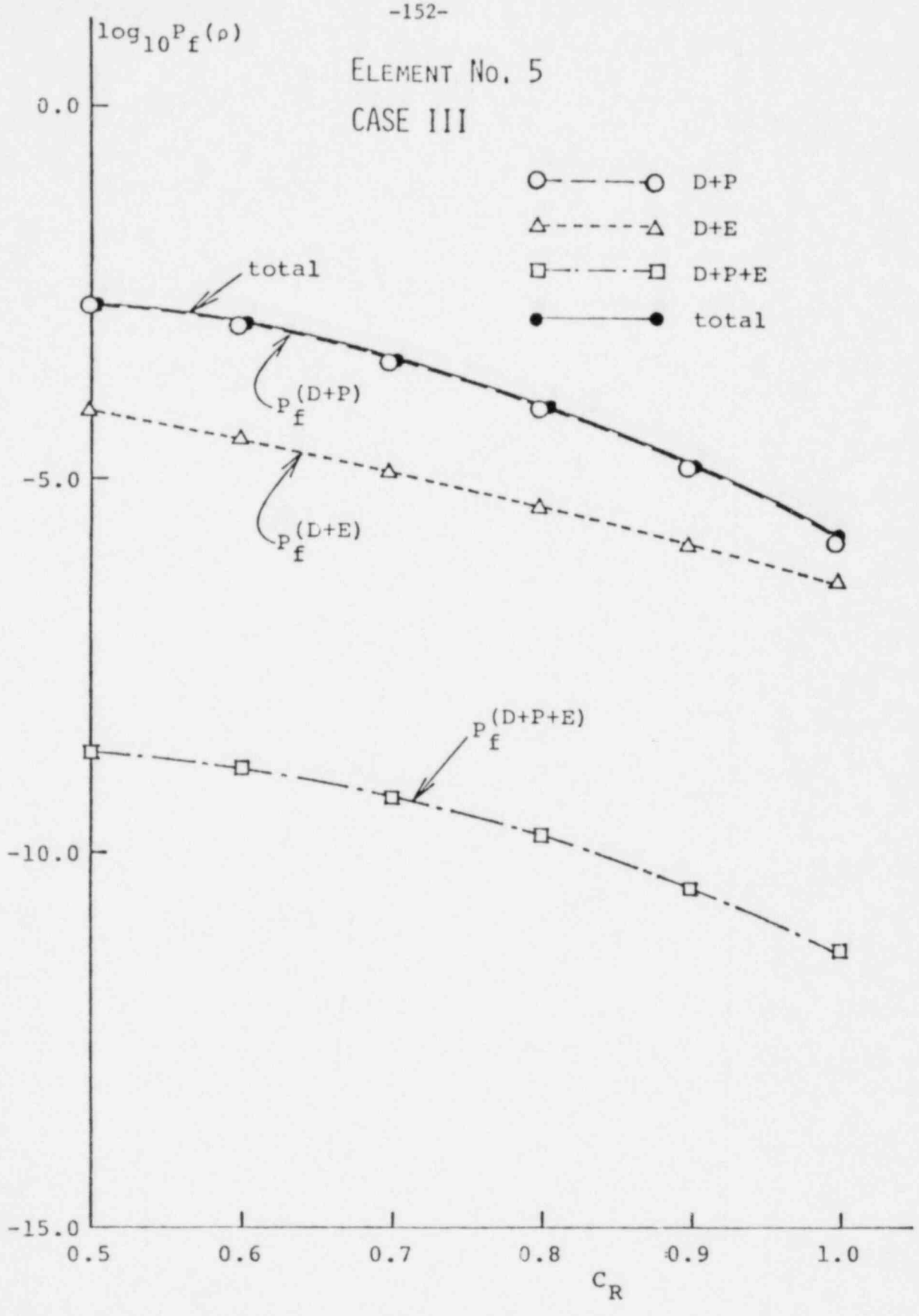

FIG. 5: LIMIT STATE PROBABILITIES UNDER LOAD COMBINATIONS

4. Mechanical Piping Benchmark Problems

P. Bezler, M. Subudhi, Y. K. Wang and S. Shteyngart

Efforts this period were directed towards completing the HDR URL loop piping study and extending the other ongoing experimental benchmark studies to the extent which data were available. In addition a number of changes to the PSAFE1 and PSAFE2 computer codes were completed including the development of new algorithms designed to predict the absolute acceleration response of systems subjected to uniform and multiple independent support excitations. Lastly a new work task was added to the program involving the investigation of piping systems subjected to multiple independent support excitations and efforts were expended preparing a work plan and initiating this effort.

4.1 Elastic Benchmark Development

Draft copies of Volume 2 of the Benchmark Report Series "Dynamic Analysis, Independent Support Motion, Response Spectrum Method" have been forwarded to four organizations designated by the NRC technical monitor for applicant evaluations. These evaluations will serve as a test run of the new benchmark problem set uncovering any errors, ambiguities or inconsistencies inherent in them. Additionally when trial applicant solutions are completed they should corroborate the benchmark solutions validating their correctness.

It is anticipated that the applicant solution effort will encounter certain difficulties. In particular, when response spectrum methods are used to evaluate systems undergoing independent support motion excitation, support group combinations must be made for which there is as yet no formal guidance. The combination between support groups can be made via the absolute sum rule or SRSS. This combination can be performed before the combination of modal and excitation components or after. It is reasonable to assume that each organization having the independent support motion calculational option will have coded this option in a different way. In the benchmark report the methods used to perform group combinations are clearly delineated.

The evaluation of several large class 1 and class 2/3 problems for potential use in Volume 3 of the benchmark report series continues. In addition class 2/3 evaluations are presently being performed for two new problems under the confirmatory analysis program and their use as benchmarks is also being evaluated.

4.2 PSAFE1/PSAFE2 Code Modifications

The following modifications were made permanent updates to the PSAFE1 and PSAFE2 computer codes.

1) The transfer of moment data for individual load cases from PSAFE2 (where data is developed) to PSAFE1 (where data is used for class 1 evaluations) has been automated.

2) The input coding for boundary elements has been revised. The new format requires as input direction cosines for the line of action of a boundary element, the node to which it is attached and the element spring constant.

3) The independent support motion time history analysis option has been modified such that group load vectors are summed algebraically before integration in the modal superposition analysis mode. This modification eliminates the group by group calculations and outputs, resulting in significant running time reductions.

4) The format of the moment data files in PSAFE2 have been revised to be consistent with those required for class 1 and class 2/3 evaluations.

5) PSAFE2 has been revised to accept as input for a class 2/3 evaluation the results from earlier analyses. In the unmodified version of the code only the results for those analyses being done concurrently with the class 2/3 evaluation were considered (i.e., all analyses and the evaluations had to be processed in one computer run).

6) The SAM option has been updated to allow the use of separate SAM moment files for OBE & SSE analyses. In the unmodified code, one set of SAM moment data was used for both the OBE and SSE analyses.

Each of these updates was completed and debugged during the period. Further efforts are being made to optimize the output format and the check run option.

In the course of the evaluation of the HDR URL loop piping it became evident that there was an omission in the PSAFE2 independent support motion time history code option. The capacity to predict the absolute motion of piping systems subjected to independent support excitations did not exist. The lack of this capacity was of no consequence when the relative displacement dependent, pipe stresses were computed but was of major importance when a comparison to measured absolute acceleration data was to be made. Needless to say the HDR studies required just such a code option.

New algorithms were prepared which allow the prediction of absolute acceleration records by either response spectrum or time history methods for both uniform and independent support motion cases. The algorithms were programmed into PSAFE2 and debugged. To the extent possible, computer check runs against previously developed data were performed and found to yield good results.

4.3 HDR URL Loop Piping Evaluations

The evaluations of the HDR URL loop piping were completed during this period. A draft report of the findings will be prepared and issued during the next period.

In the previous quarterly, Figures 4.4 - 4.20 showed the comparison between the measured absolute acceleration of selected points and the predicted relative acceleration for those same points for both uniform and independent support excitation computations. Unfortunately it was not explicitly stated in that report that the predicted accelerations were relative quantities. Additionally the absissca scale for all those figures were mislabeled ACC(G) when they should have appeared as ACC(M/S^2). Thus one of the efforts this period was to compute the absolute accelerations for all the points in the system.

Following the completion of the coding efforts both the uniform and independent support excitation computations were repeated. The results of those computations, the predicted absolute accelerations, are shown in Figures 4.1 - 4.18. These figures are in the same sequence as those presented in the last quarterly and also show the corresponding measured accelerations.

A comparison of Figures 4.1 - 4.18 with Figures 4.4 - 4.20 of the last quarterly will show that the predicted absolute acceleration data show the same characteristics as the predicted relative acceleration data. In fact all the observations drawn on the basis of the relative acceleration data apply as well to the data presented herein. Specifically for all cases the response predicted for independent support excitation almost coincides with the response predicted for uniform support excitation. Where these two response curves differ the predicted response for the uniform support excitation case in general envelopes that predicted for independent support excitation. No consistent trend is apparent when the measured absolute acceleration time histories are compared to the predicted absolute acceleration time histories. For some points the agreement is good while for others it is poor.

Another comparison betwen the measured and predicted response data is presented in Figures 4.19 - 4.26. Each of these figures shows two curves each showing the results of a fourier decomposition of the response signal. One curve, labeled, shows the fourier content of the measured acceleration record for the point while the other curve shows the fourier content of the predicted acceleration record, either uniform or independent support excitation case, for that point. These curves are presented only for acceleration components 36X, 53X, 77Z and 101Y, Figures 4.19 - 4.22 corresponding to the uniform support motion predictions while Figures 4.23 - 4.26 correspond to the independent support motion predictions. A set of this data have been developed for all acceleration components for which measured response data are available.

Referring to Figures 4.19, 4.22, 4.23 and 4.26, the frequency content of the predicted and the measured responses for points 36X and 101Y are very similar with near identical peak values. This level of correspondence occurred for approximately 2/3 of the points considered even though the comparison of the actual response curves for these points did not show good correspondence. Relatively poor correspondence of frequency content between the predicted and measured responses was noted for the remaining 1/3 points, as typified in Figures 4.20, 4.21, 4.24 and 4.25 for points 53X and 77Z.

It was mentioned in the previous quarterly that a brief comparison was made between the BNL computerd response data and the computed response data for the HDR URL loop developed by an alternate NRC contractor. The agreement for the relative acceleration component, elastic code analysis, uniform excitation case, was excellent. When comparing the predicted absolute acceleration quantities for the same case a distinct difference was noted. On further investigation the difference seems to be related to the phasing of the relative acceleration component relative to the input acceleration component, absolute acceleration being the algebraic sum of the input and relative acceleration components. If the BNL predicted relative acceleration component is shifted 180° in phase, that is subtracted instead of added, the two results are identical. A number of facts tend to support the BNL solution:

1) The BNL predictions developed using uniform support excitation and independent support excitation yield similar results although the computational algorithms are completely independent.

2) The BNL elastic analysis results correspond well with those developed by the alternate contractor using a nonlinear analysis code.

3) A corroborative check of the BNL algorithms against a simple two mass problem for which a closed form solution was developed indicated that the BNL algorithms are correct.

At this point it is the opinion that the BNL solutions are correct however this aspect is still receiving consideration.

4.4 Physical Benchmark Development

Every effort has been made to further the cooperative program between BNL and EPRI in the development of physical benchmarks. As stated in the last quarterly the first phase of this program involves the evaluation of data measured during the in-situ testing of a pipe run in the shutdown Indian Point Nuclear Power Plant. Although it was anticipated that the Indian Point digitized data pertinent to the benchmarking effort would be transmitted during this report period, this was not forthcoming. The process of formalizing the cooperative program between EPRI, its contractor ANCO, and NRC, informally arranged during the last quarter, required the better part of this whole period. BNL representatives have just been notified that transmittal of the desired data is imminent.

Another sequence of tests being conducted for EPRI by its contractor ANCO hold promise to be of even more importance to the benchmarking effort than the Indian Point tests. The new tests involve simple pipe configurations excited by a number of independently acting single axis hydraulic actuator heads. The tests are being conducted under controlled conditions at the ANCO facility. The intended purpose of the test program is to measure the actual margins of safety inherent in piping systems designed to current standards by testing to failure. However every destructive test sequence is preceeded by a series of tests at elastic levels which could be

of use in benchmarking. Further, through discussions between representatives from EPRI, ANCO, BNL and NRC it has been tentatively agreed that the scope of the elastic test sequences be expanded within the confines of EPRI scheduling to more directly impact on the benchmarking program. Suggestions regarding test configuration shaker placements instrumentation and test sequences for future tests will be given serious consideration by the EPRI organization.

The first pipe run tested under this EPRI investigation was a planar configuration of 4" Sch 40 pipe consisting of three straight lengths and two elbows, Figure 4.27. The pipe was supported from and excited by three independently acting hydraulic actuators located as shown in the figure and driving the pipe in the Z or outplane line direction. The testing, involving initially in phase seismic excitation, was expanded to include both in phase and out phase, sinosoidal and seismic excitation of the three supports. BNL analytical estimates for the first 10 frequencies for this test configuration are shown in Table 4.1. Experimentally determined estimates for two of the frequencies are also presented in the table. As can be seen, the correspondence between the measured and predicted natural frequencies is good.

As mentioned above the transmittal of the Indian Point data is imminent. In fact the data being transmitted also includes the measured data for the planar configuration (BNL designated Z Bend Configuration) and in phase, seismic excitation. It is anticipated that the data for the other tests for this configuration will be transmitted to BNL at a later date.

4.5 Multiple-Supported Piping Systems

A new work area has been added to the Mechanical Piping Benchmark Program entitled "Development of Criteria for Multiple-Supported Piping Systems Subjected to Distinct Inputs". The inclusion of this new task was preceeded by several activities during the period. On March 2, 1982 members of the BNL staff delivered a presentation to the NRC staff at the Nicholson Lane Building on the general topic of Multiple-Supported Piping Systems describing the BNL analytical capabilities and delineating potential areas of study in this topic. Following a NRC statement of interest, a second meeting was held at BNL on March 18, 1982 attended by representatives of BNL, LLL and NRC. At this meeting the outline of a cooperative program between BNL and LLL , with BNL designated as lead laboratory and LLL providing supportive calculations on this topic was developed. Each laboratory was requested to prepare detailed work plans for NRC approval.

Table 4.1

Z Bend Configuration

Natural Frequencies

Mode No.	Analytical Estimate (Hz)	Experimental Estimate (Hz)
1	7.11	7.2
2	13.03	13.0
3	16.42	
4	60.	
5	60.4	
6	71.12	
7	84.93	
8	91.22	
9	124.3	
10	128.2	

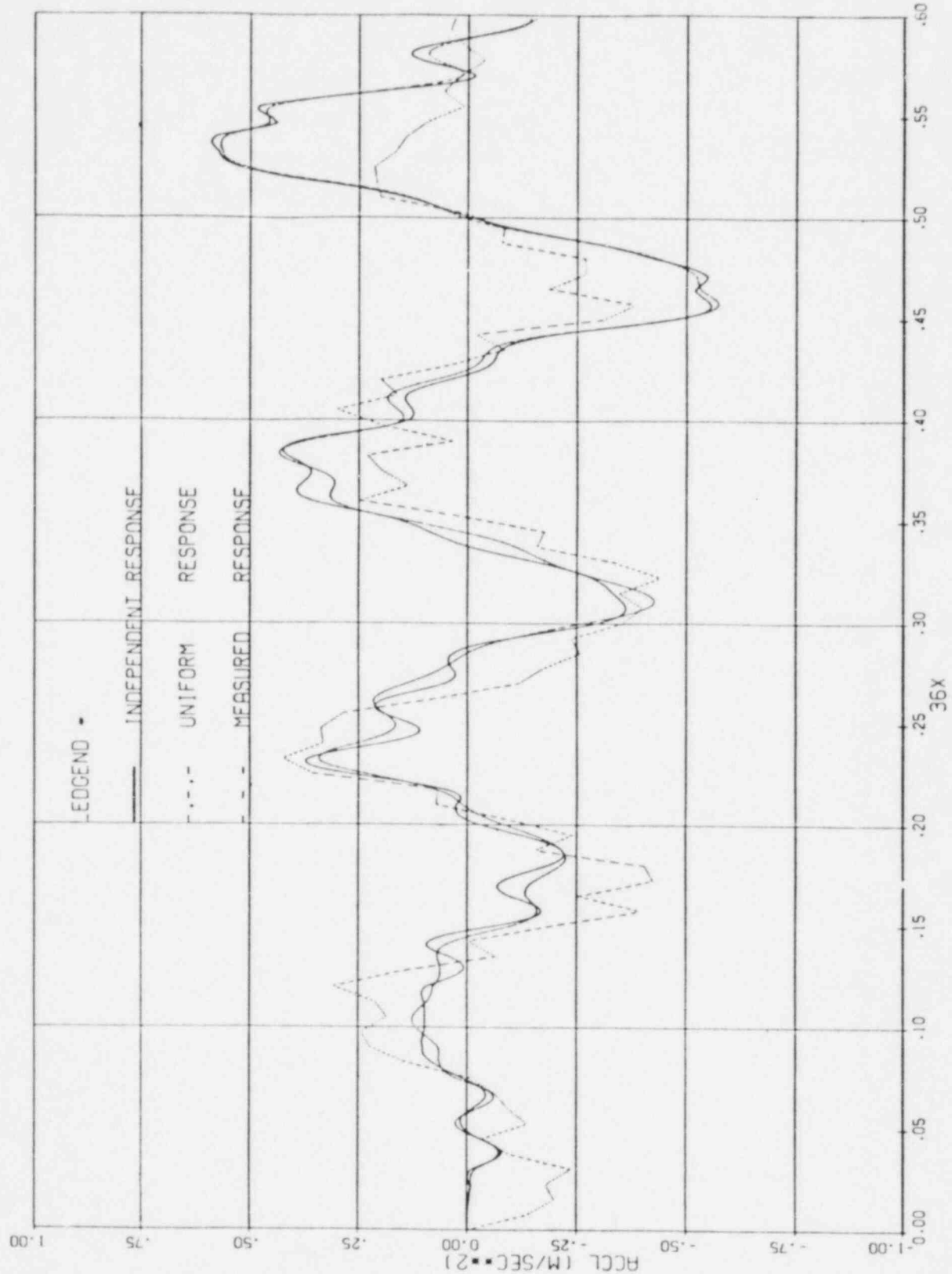
LEGEND -
INDEPENDENT RESPONSE
UNIFORM RESPONSE
MEASURED RESPONSE
ACCL (M/SEC**2)
1.00
.75
.50
.25
0.00
-.25
-.50
-.75
-1.00
0.00
.05
.10
.15
.20
.25
.30
.35
.40
.45
.50
.55
.60
36X

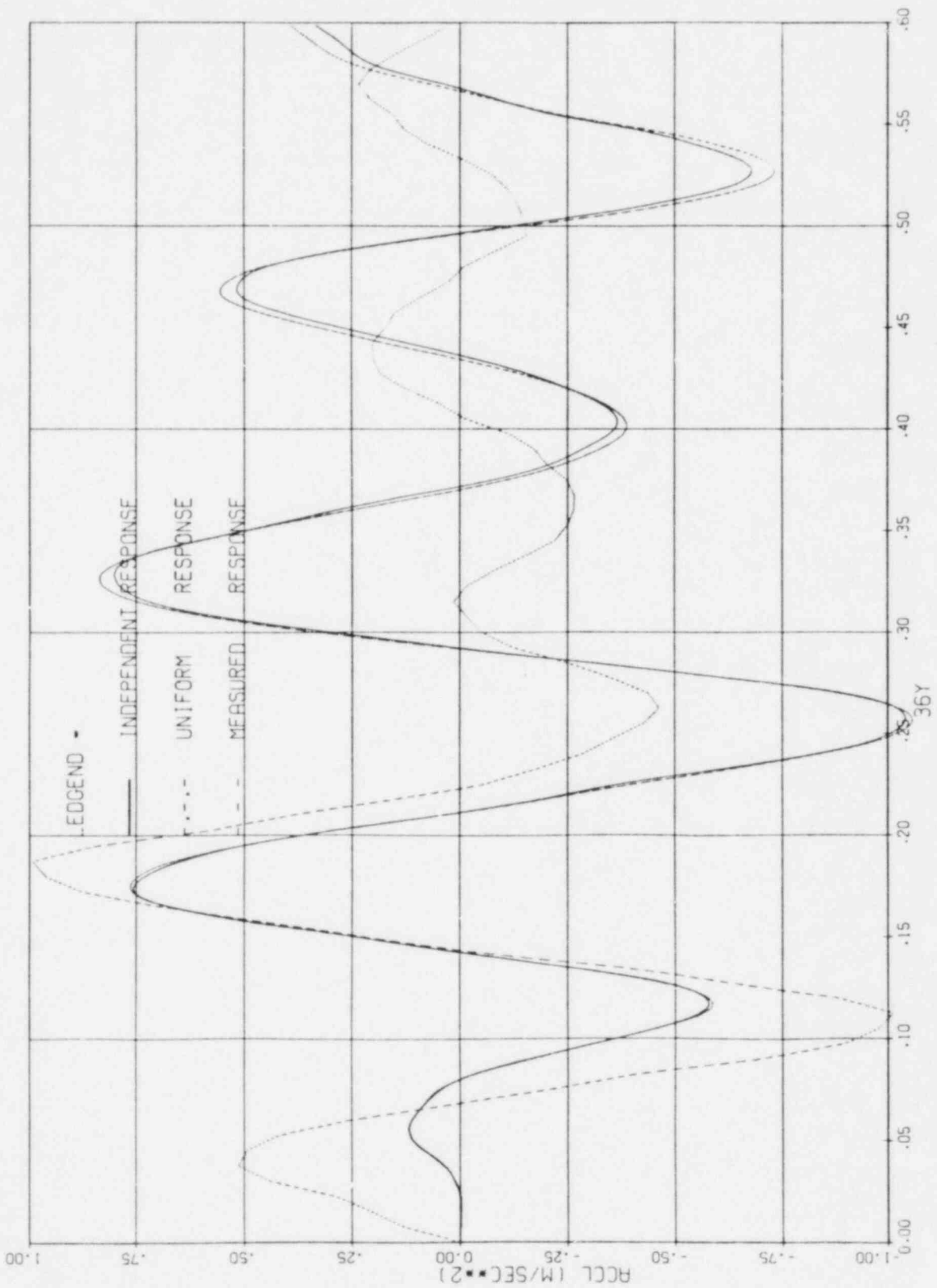

Figure 4.2 Absolute Acceleration Response

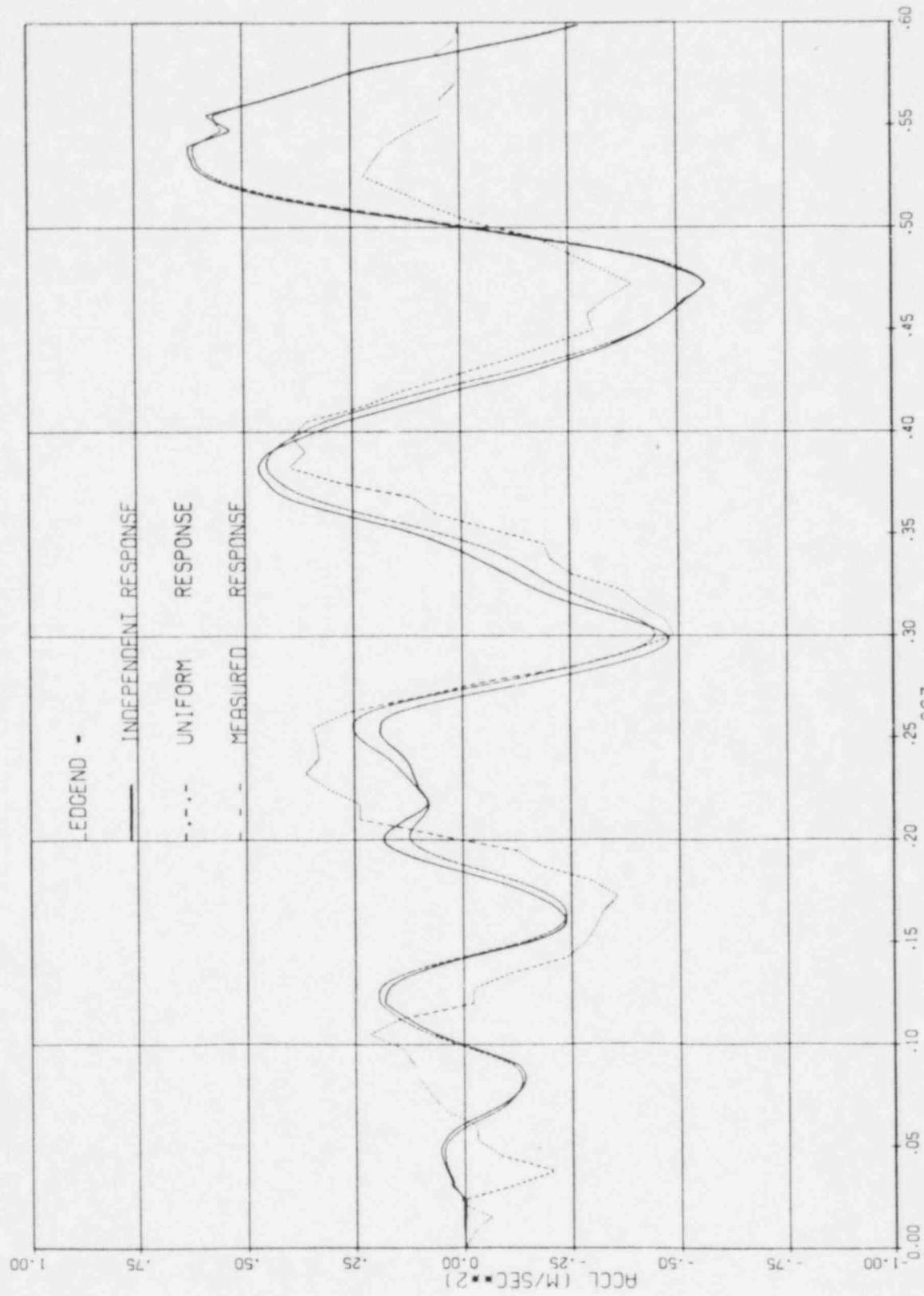

Figure 4.3 Absolute Acceleration Response

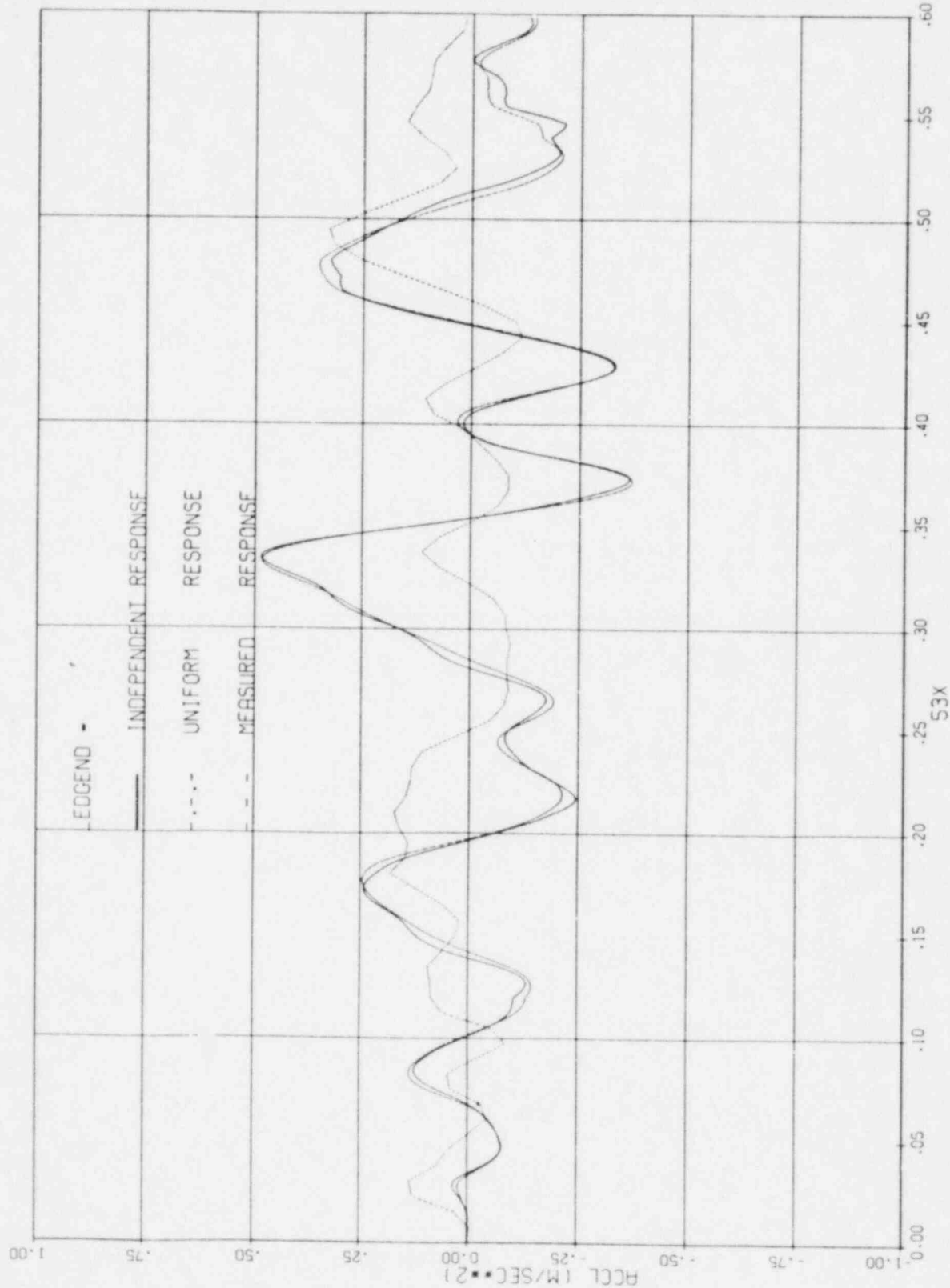

Figure 4.4 Absolute Acceleration Response

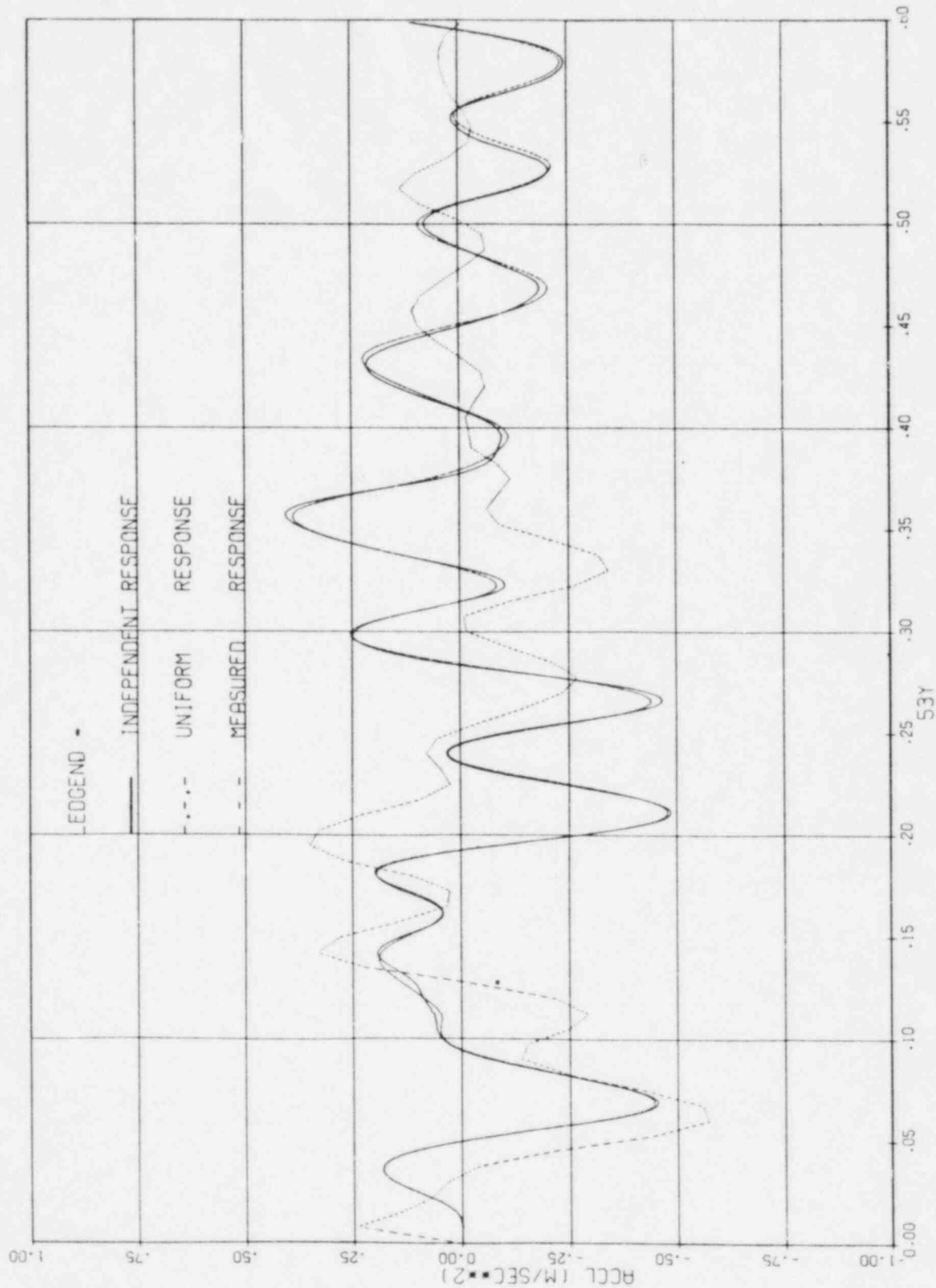

Figure 4.5 Absolute Acceleration Response

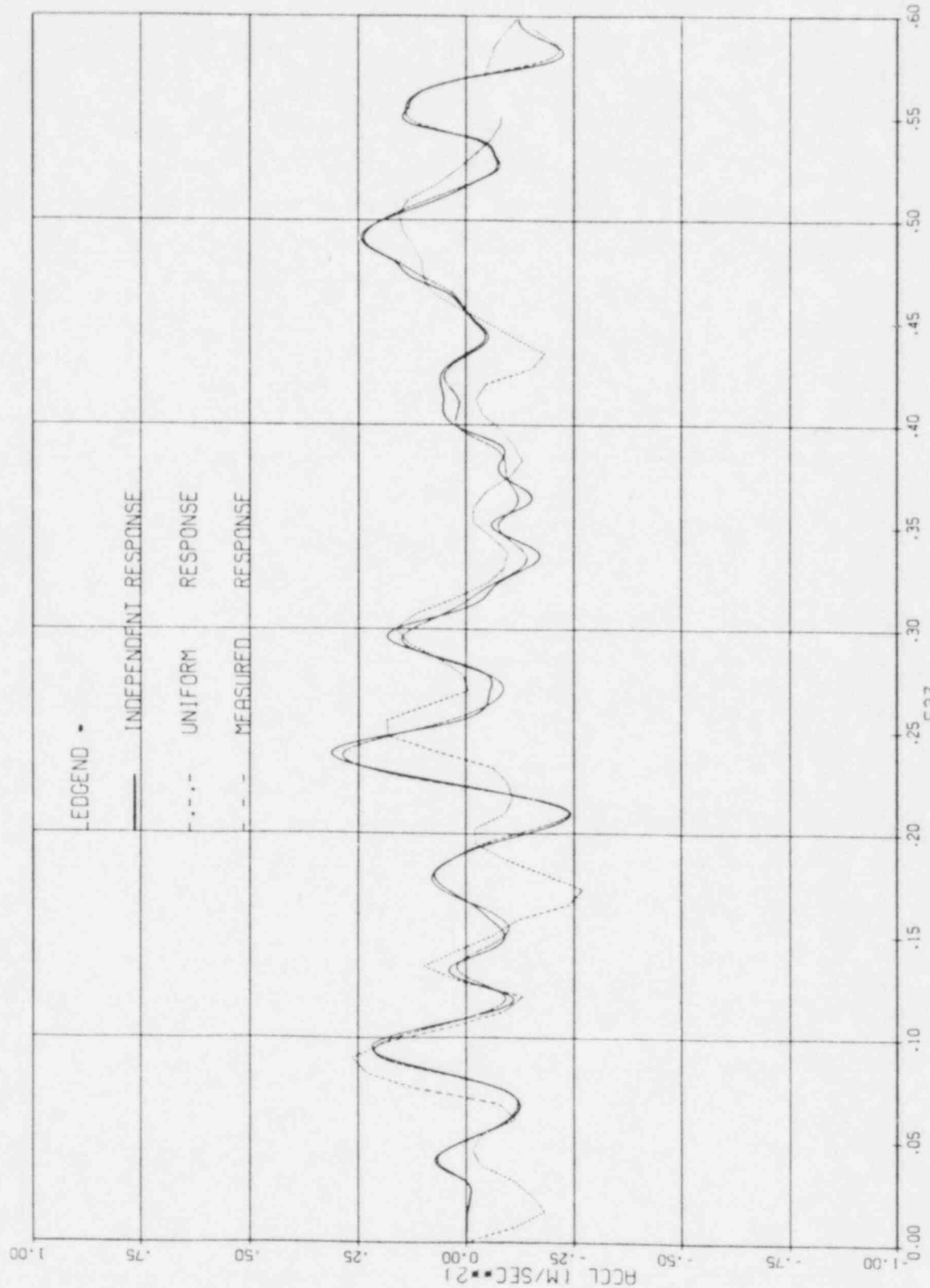

Figure 4.6 Absolute Acceleration Response

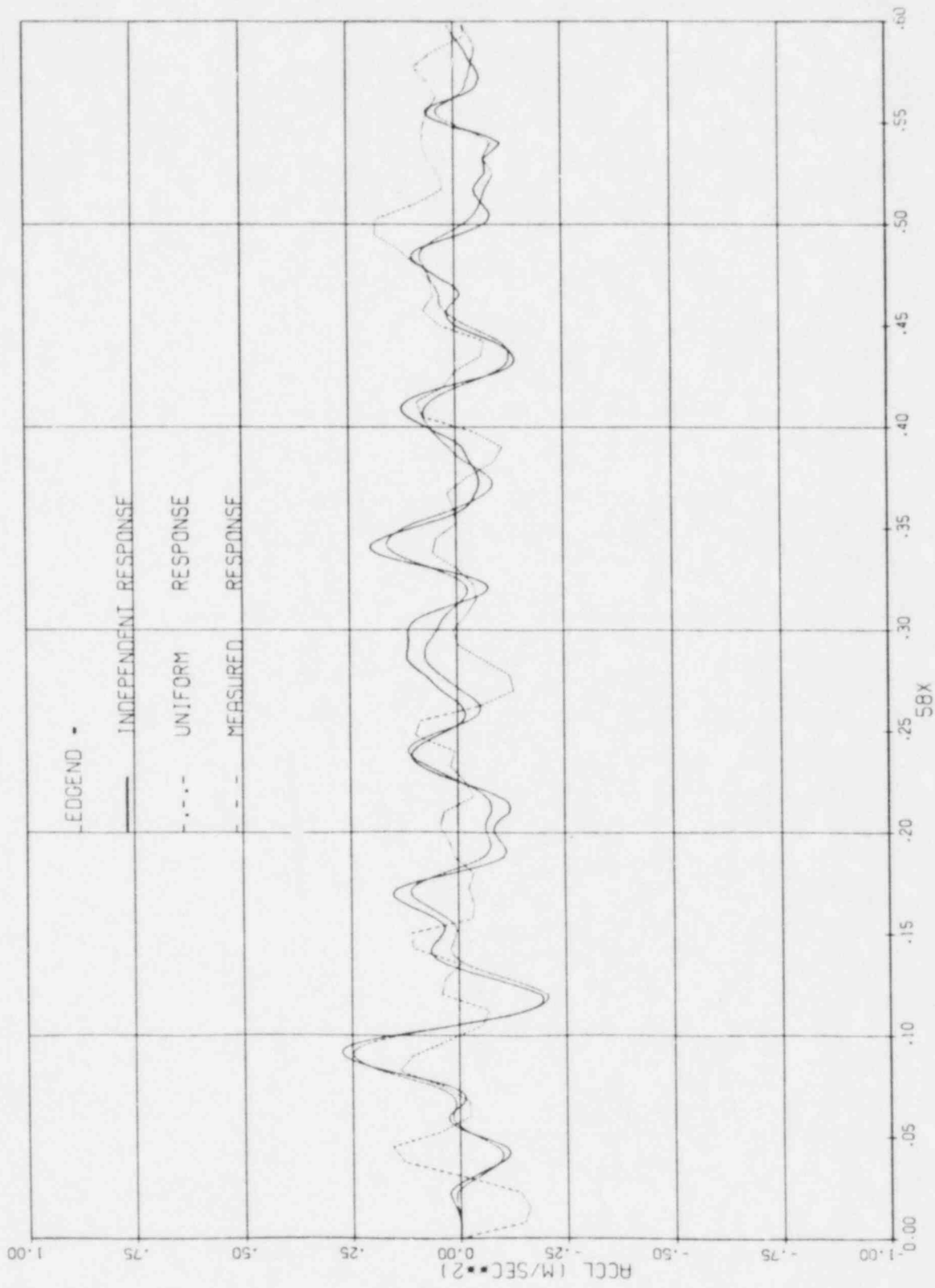

Figure 4.7 Absolute Acceleration Response

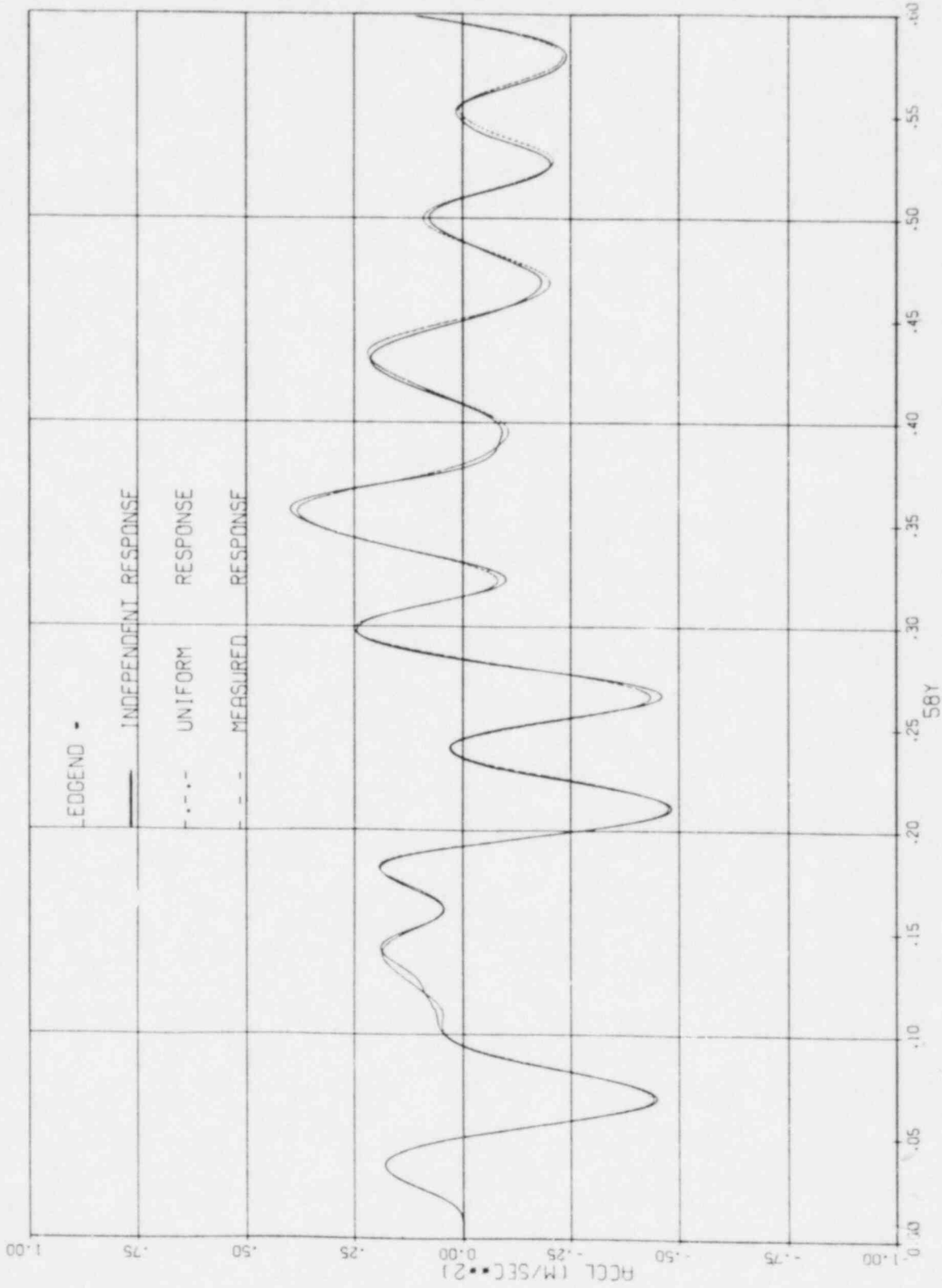

Figure 4.8 Absolute Acceleration Response

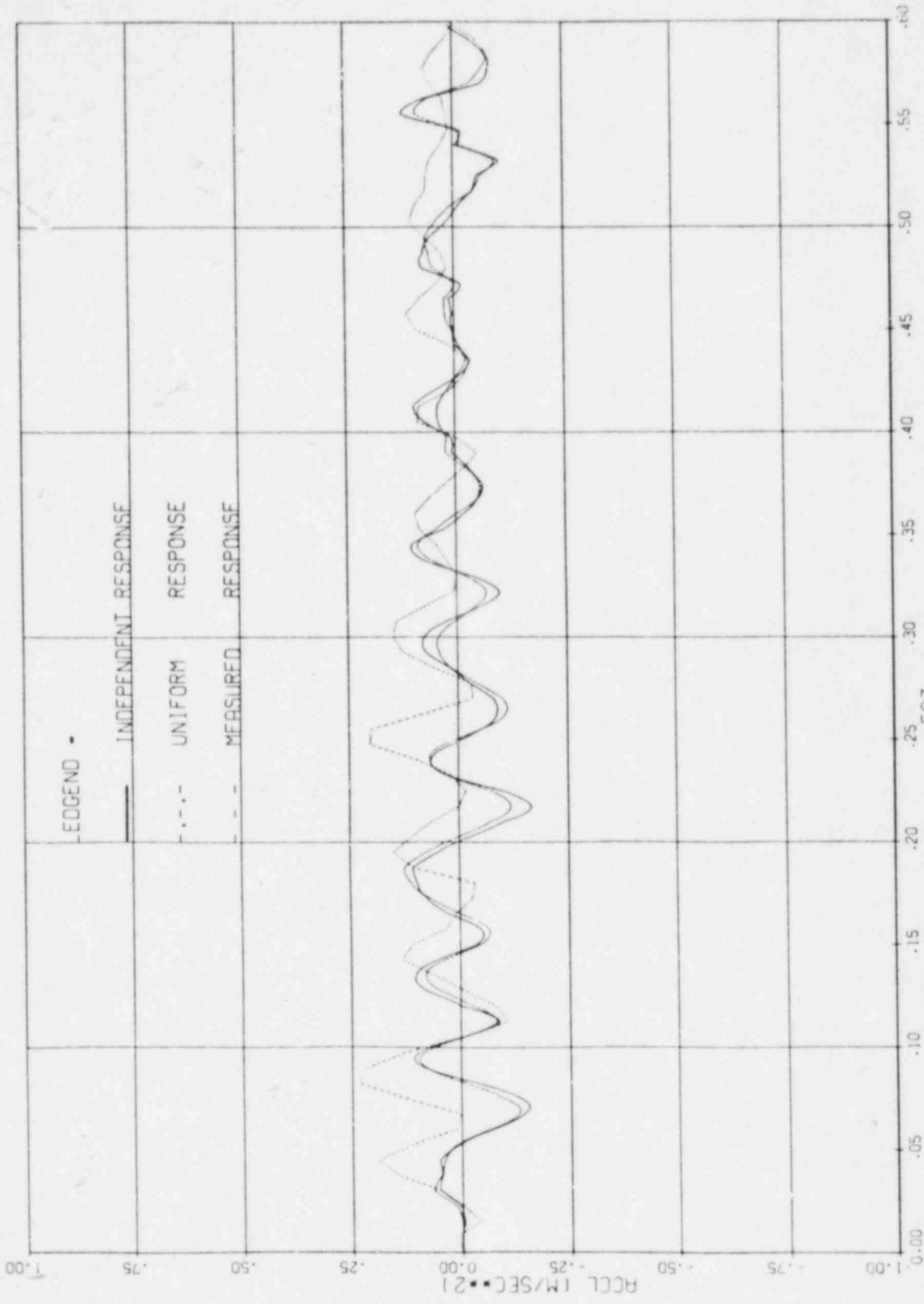

Figure 4.9 Absolute Acceleration Response

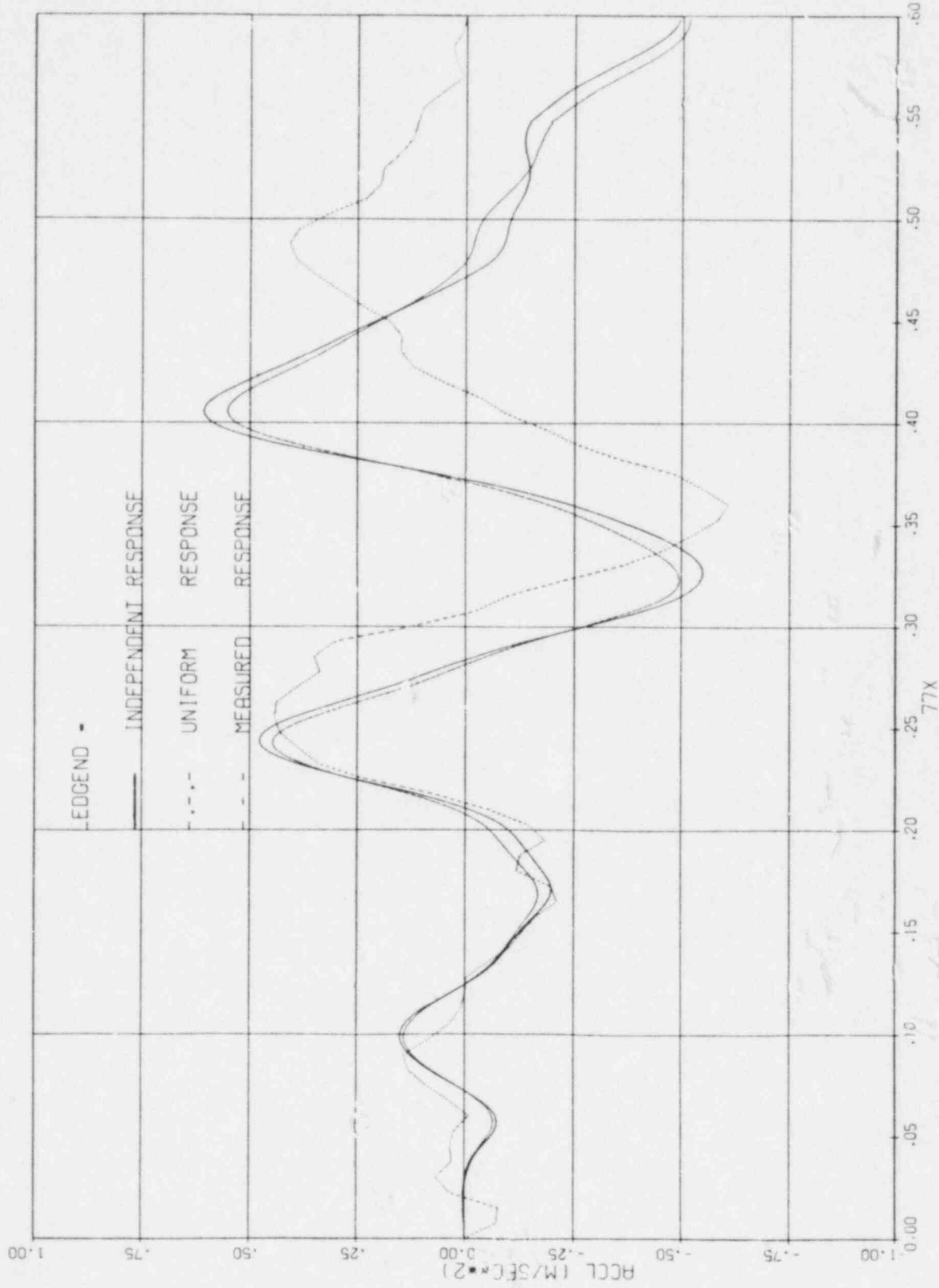

Figure 4.10 Absolute Acceleration Response

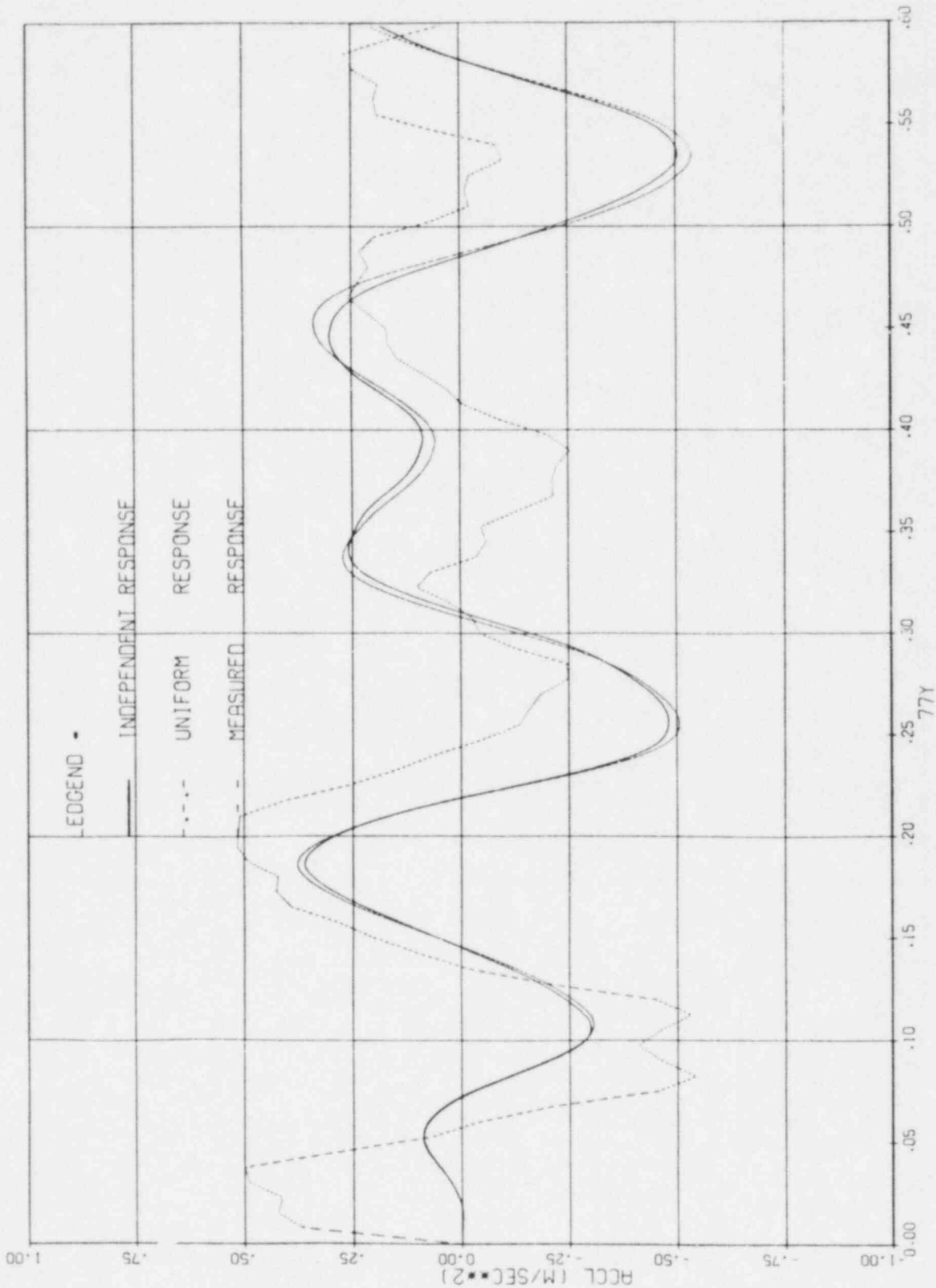

Figure 4.11 Absolute Acceleration Response

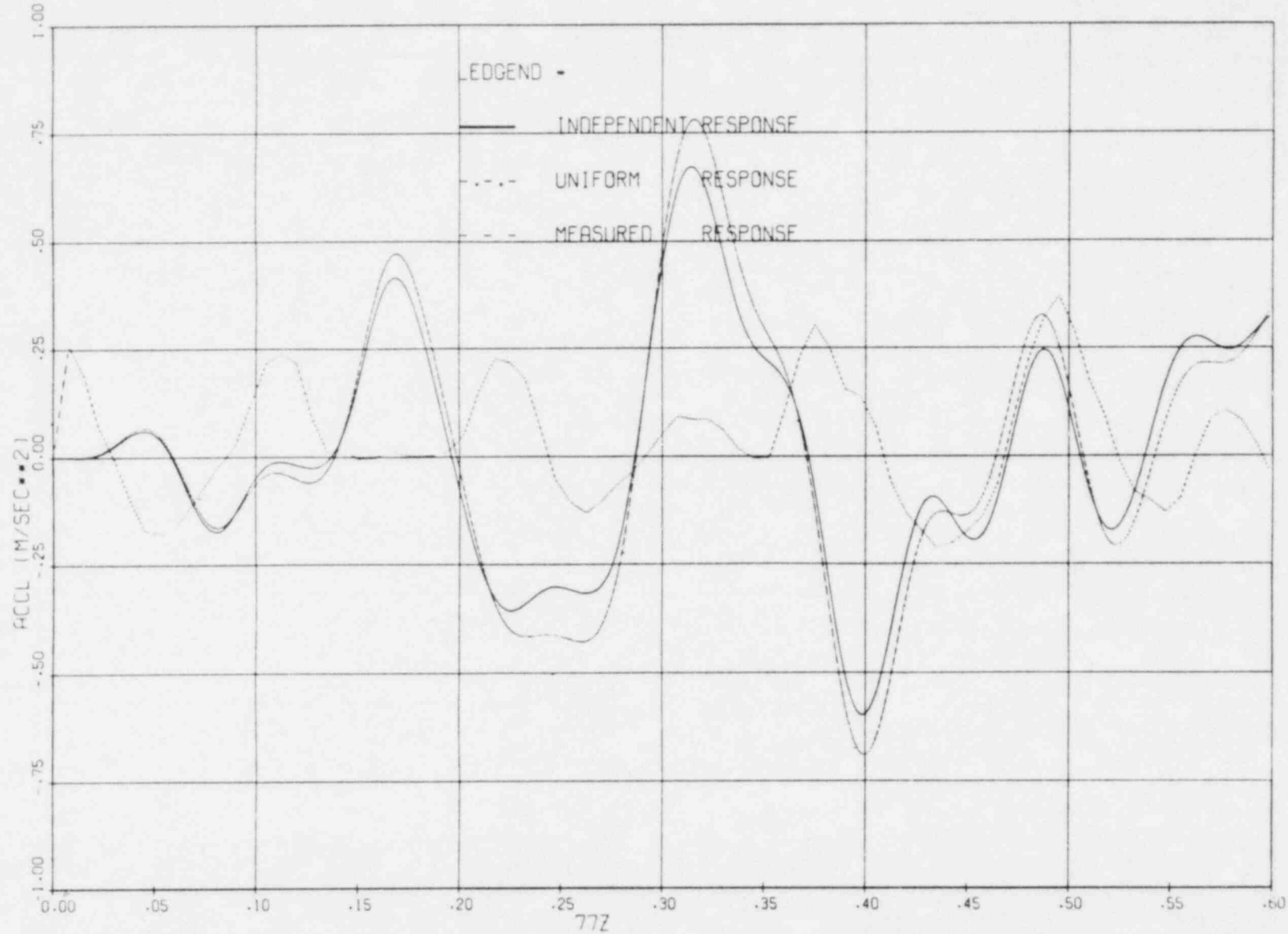

Figure 4.12 Absolute Acceleration Response

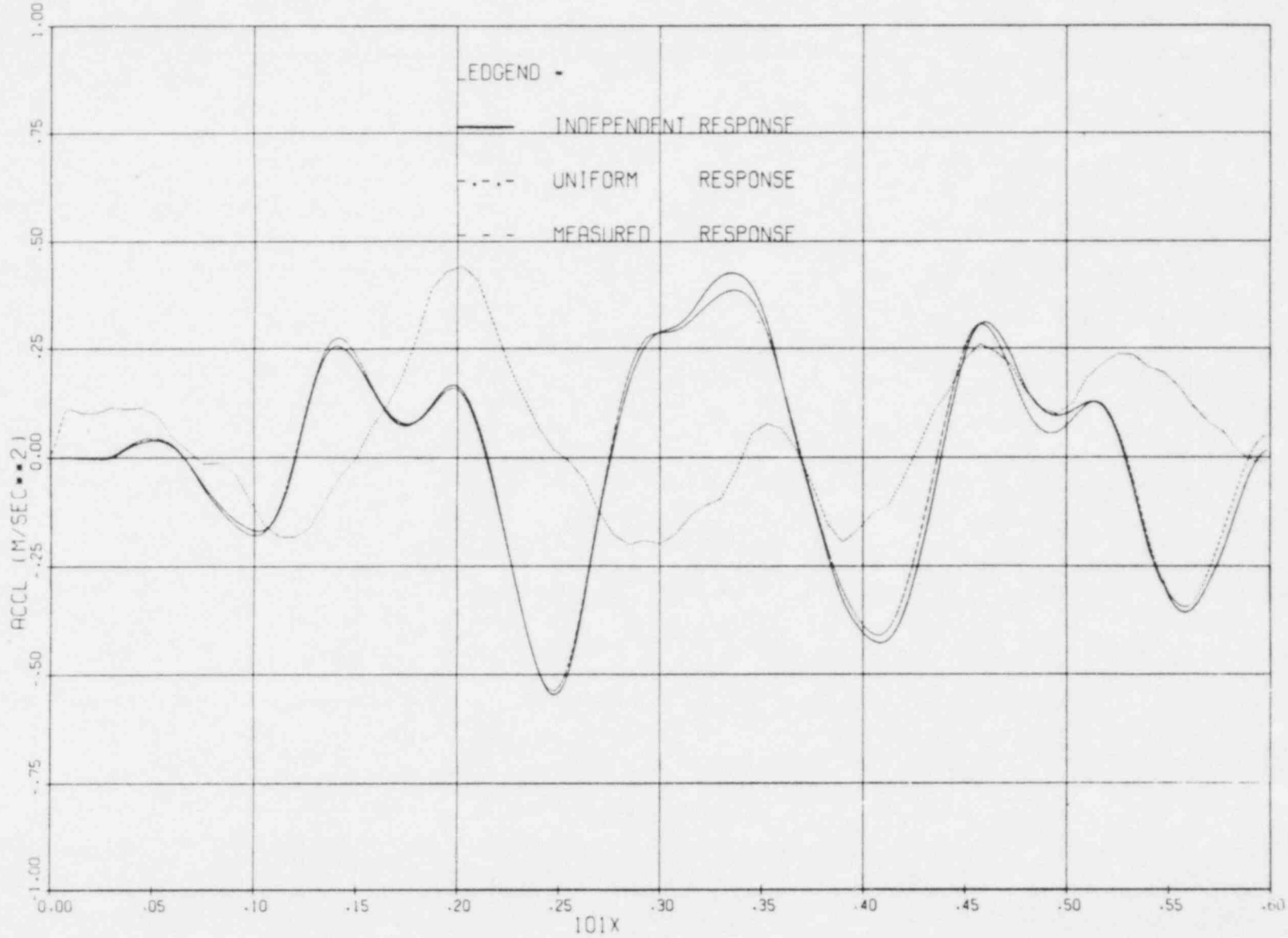

Figure 4.13 Absolute Acceleration Response

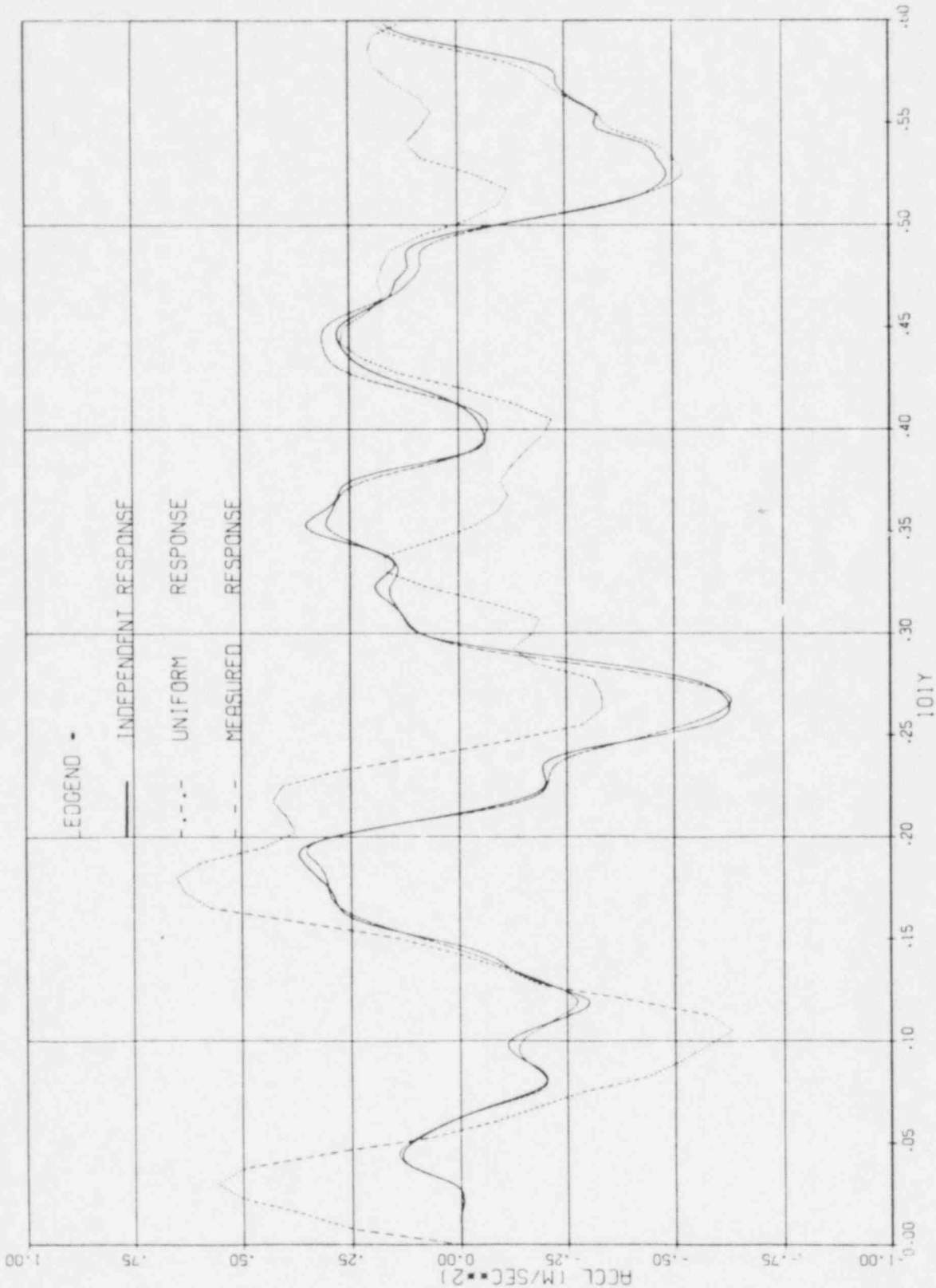

Figure 4.14 Absolute Acceleration Response

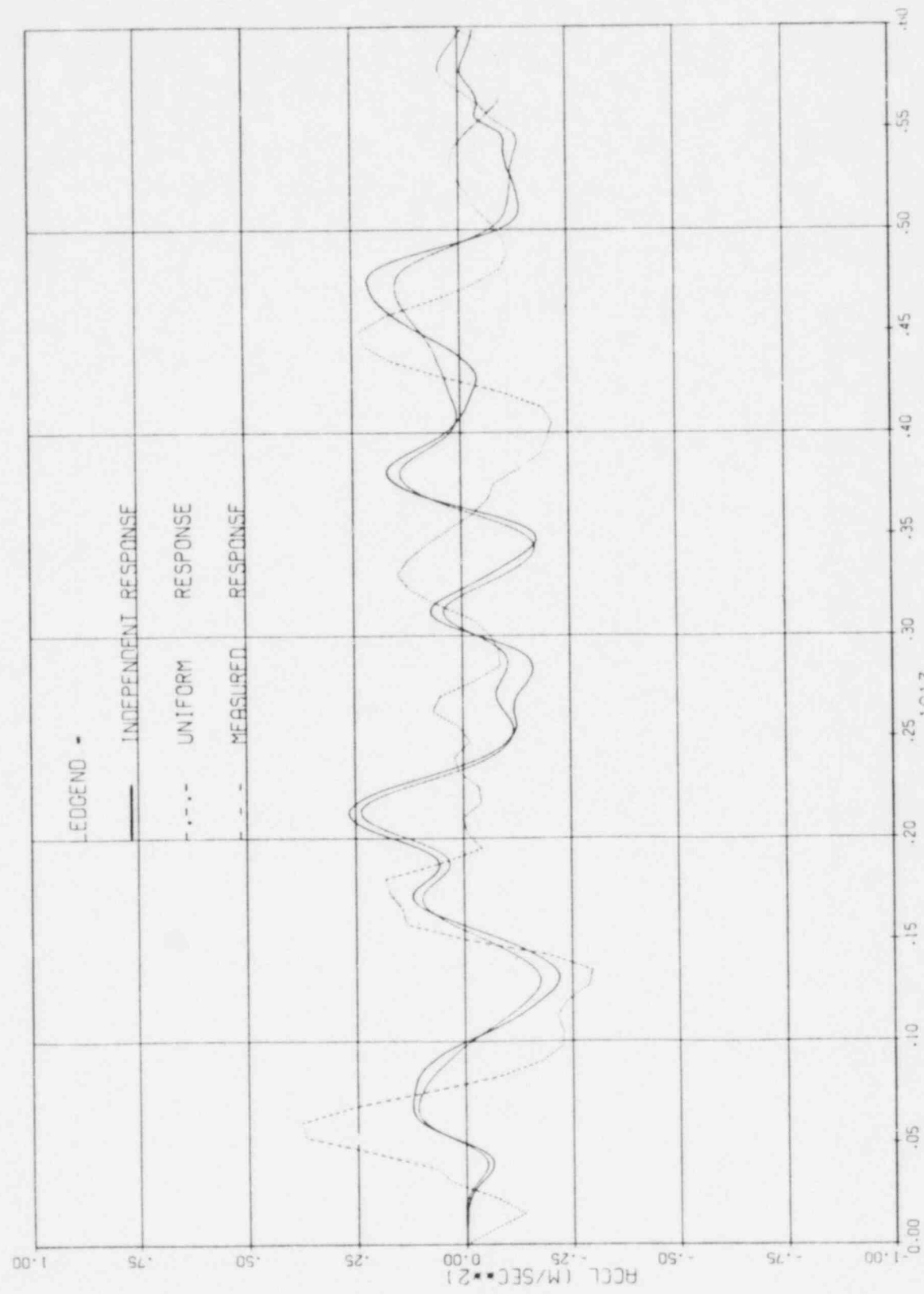

Figure 4.15 Absolute Acceleration Response

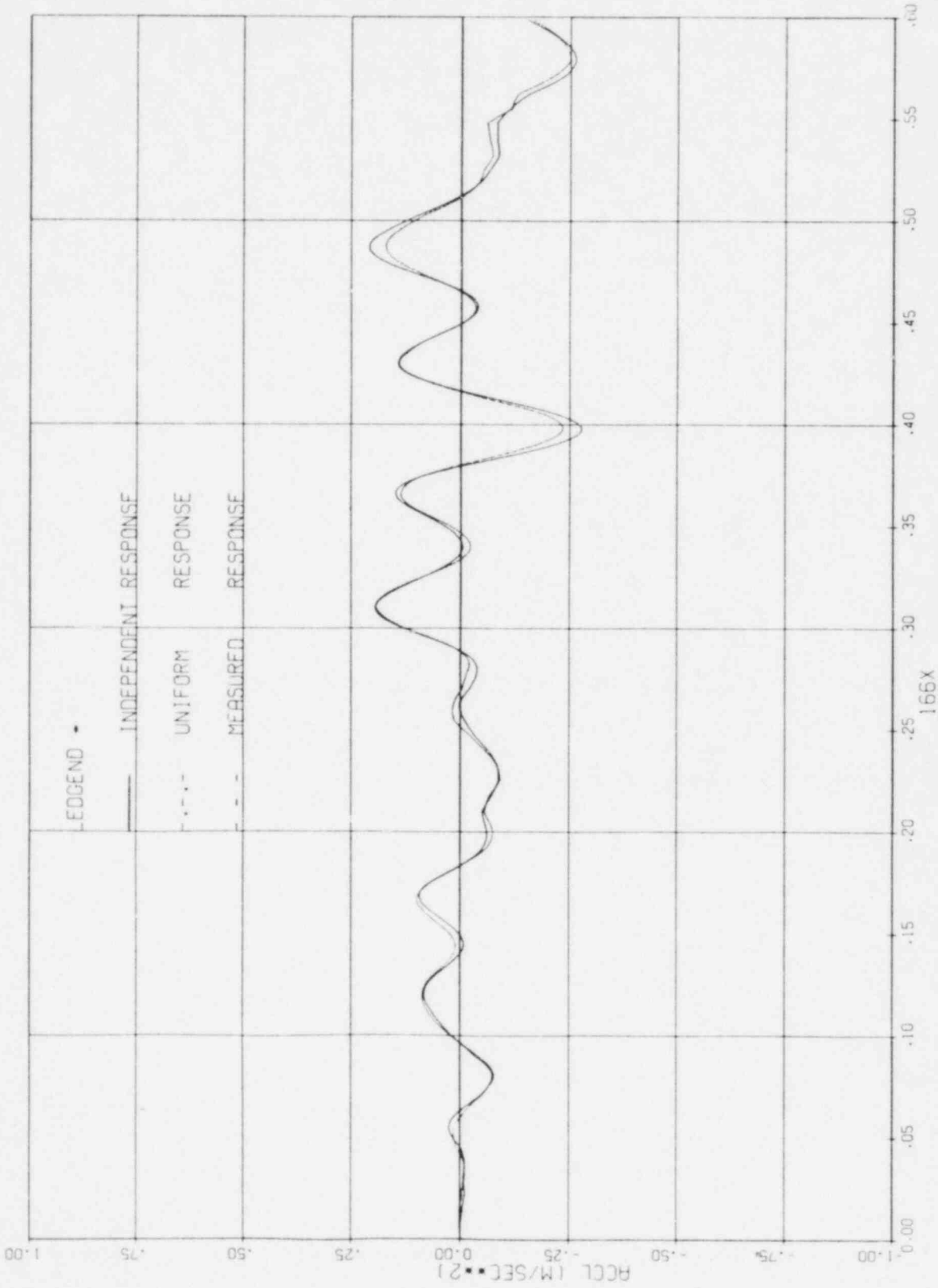

Figure 4.16 Absolute Acceleration Response

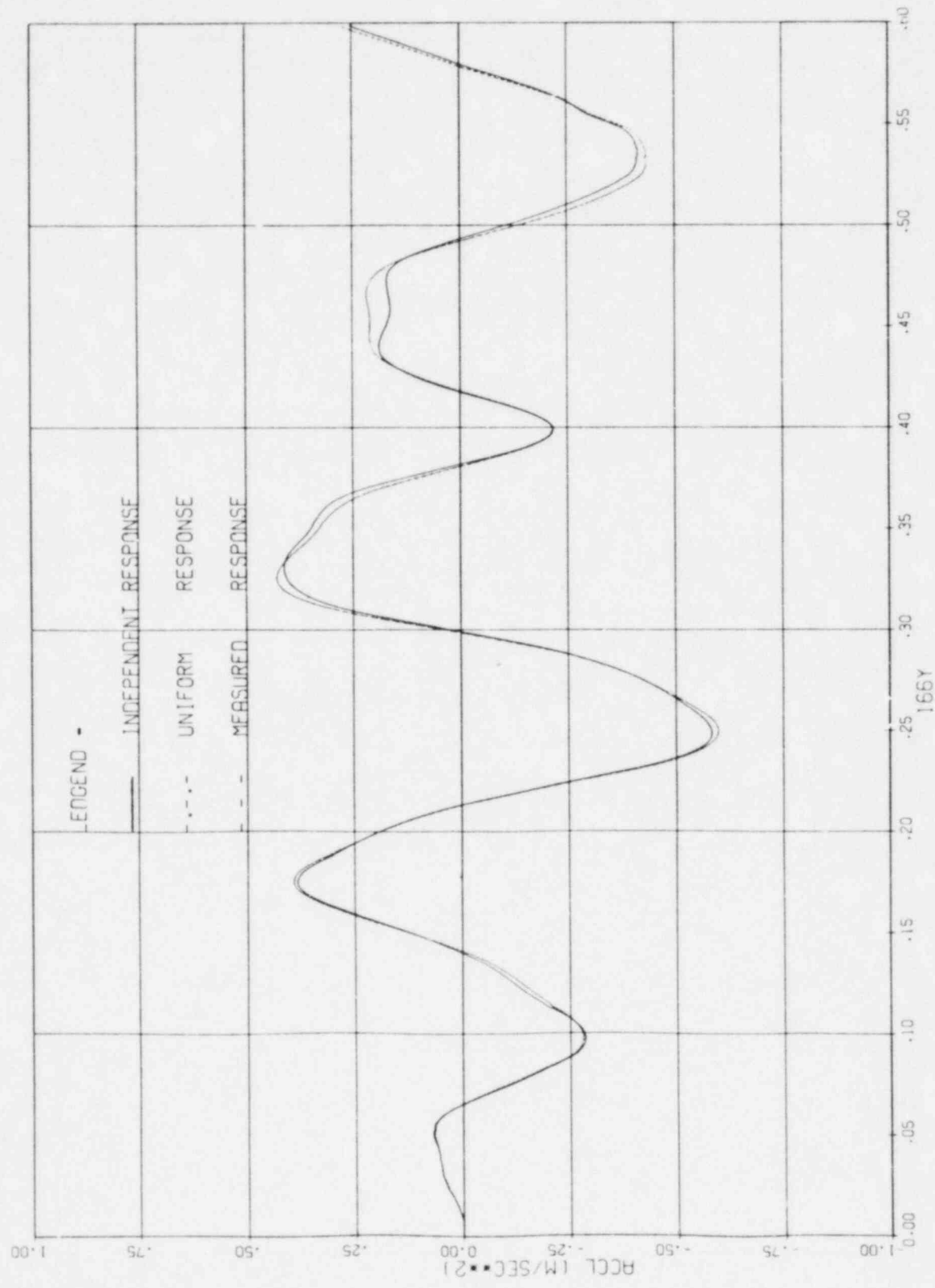

Figure 4.17 Absolute Acceleration Response

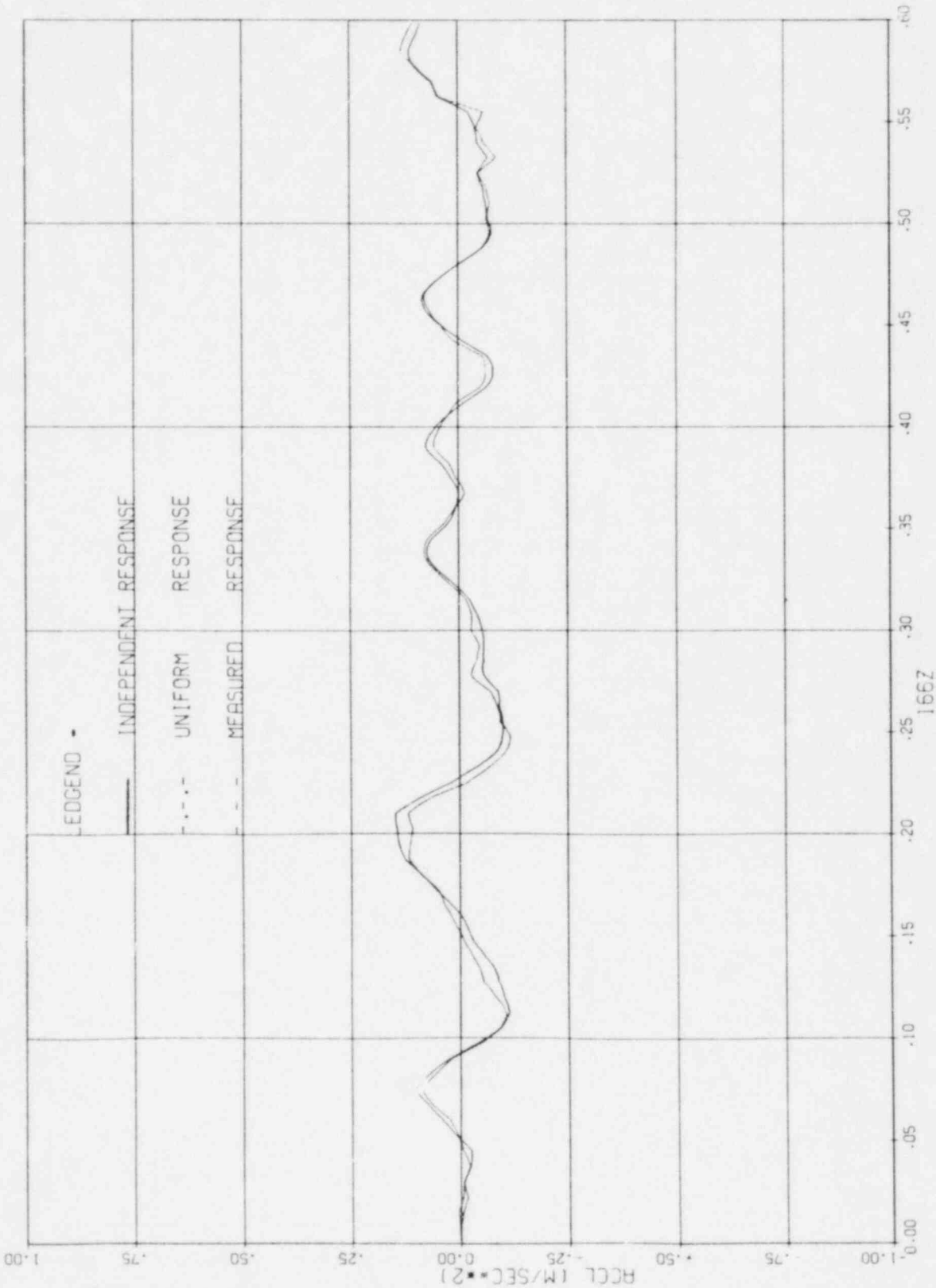

Figure 4.18 Absolute Acceleration Response

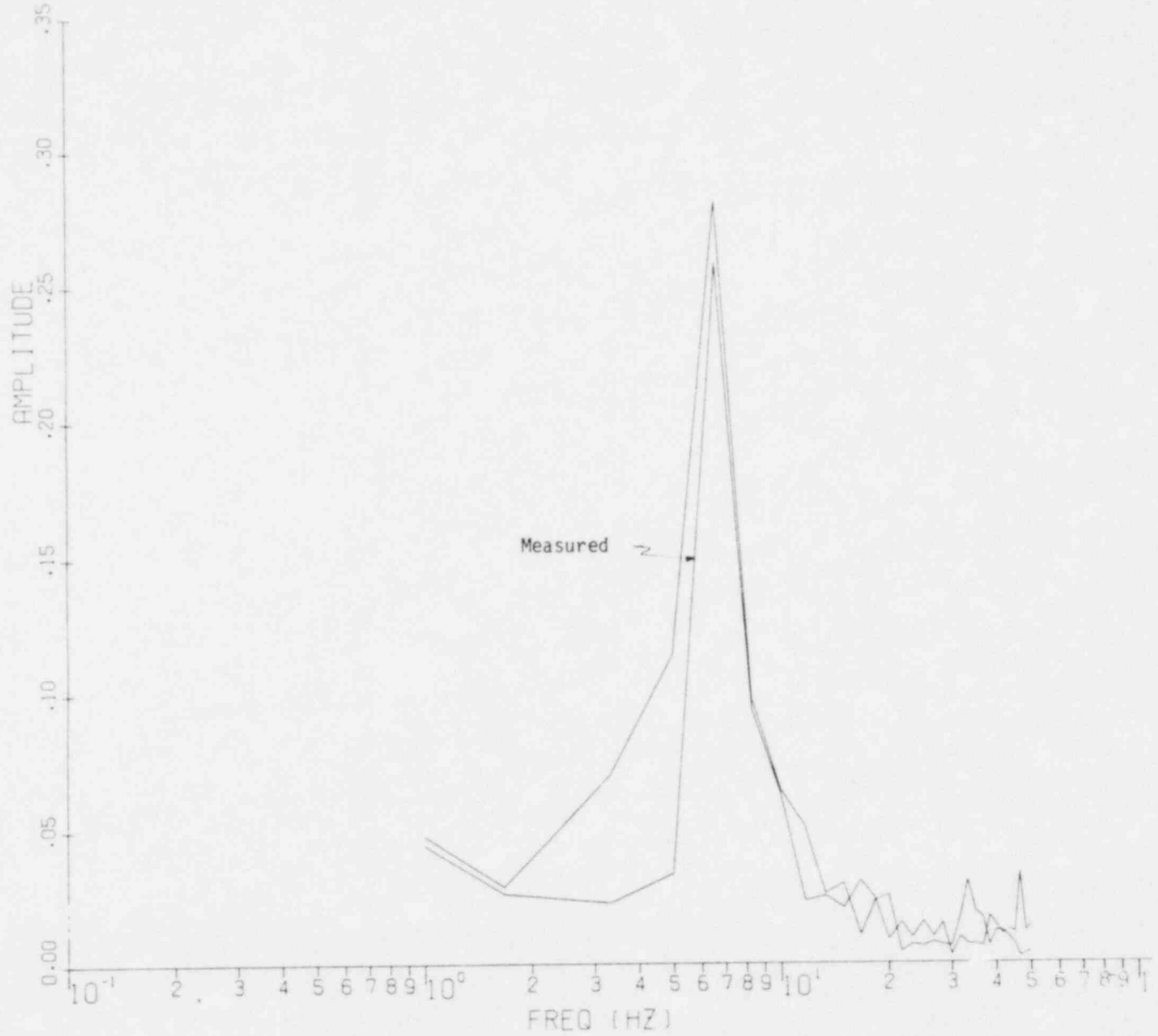

Figure 4.19 Fourier Spectra for 36X, Uniform Excitation

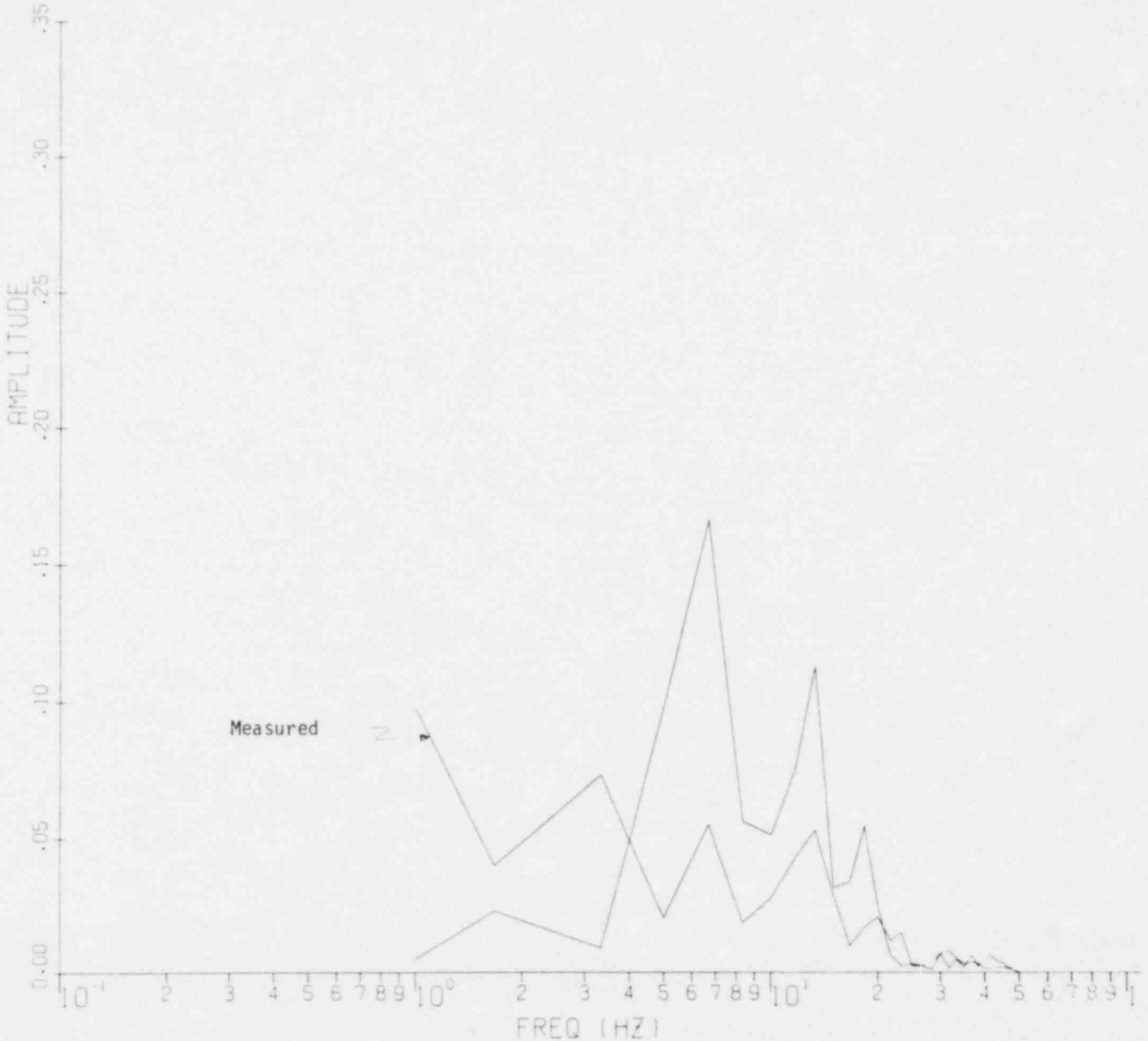

Figure 4.20 Fourier Spectra for 53X, Uniform Excitation

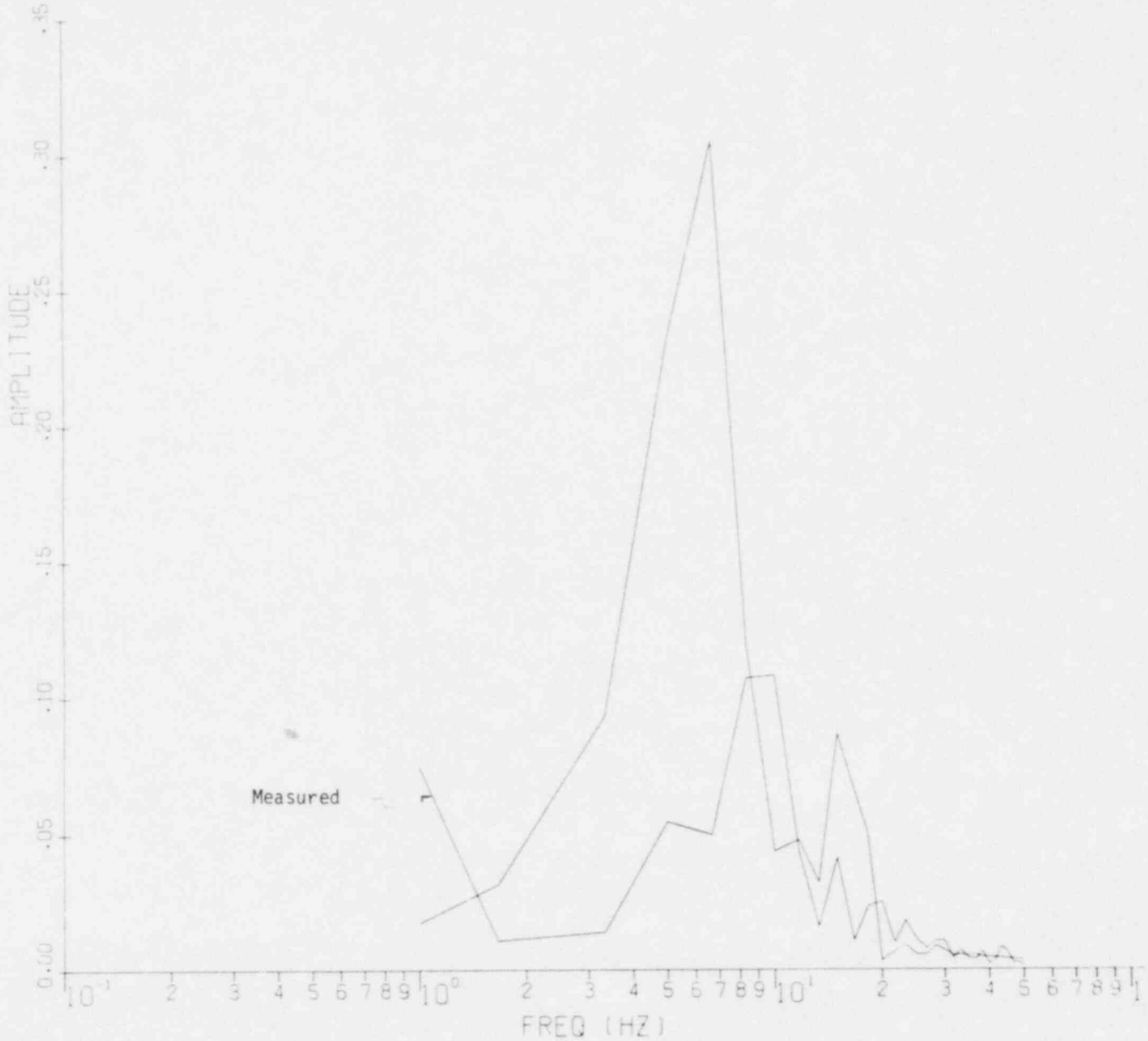

Figure 4.21 Fourier Spectra for 77Z, Uniform Excitation

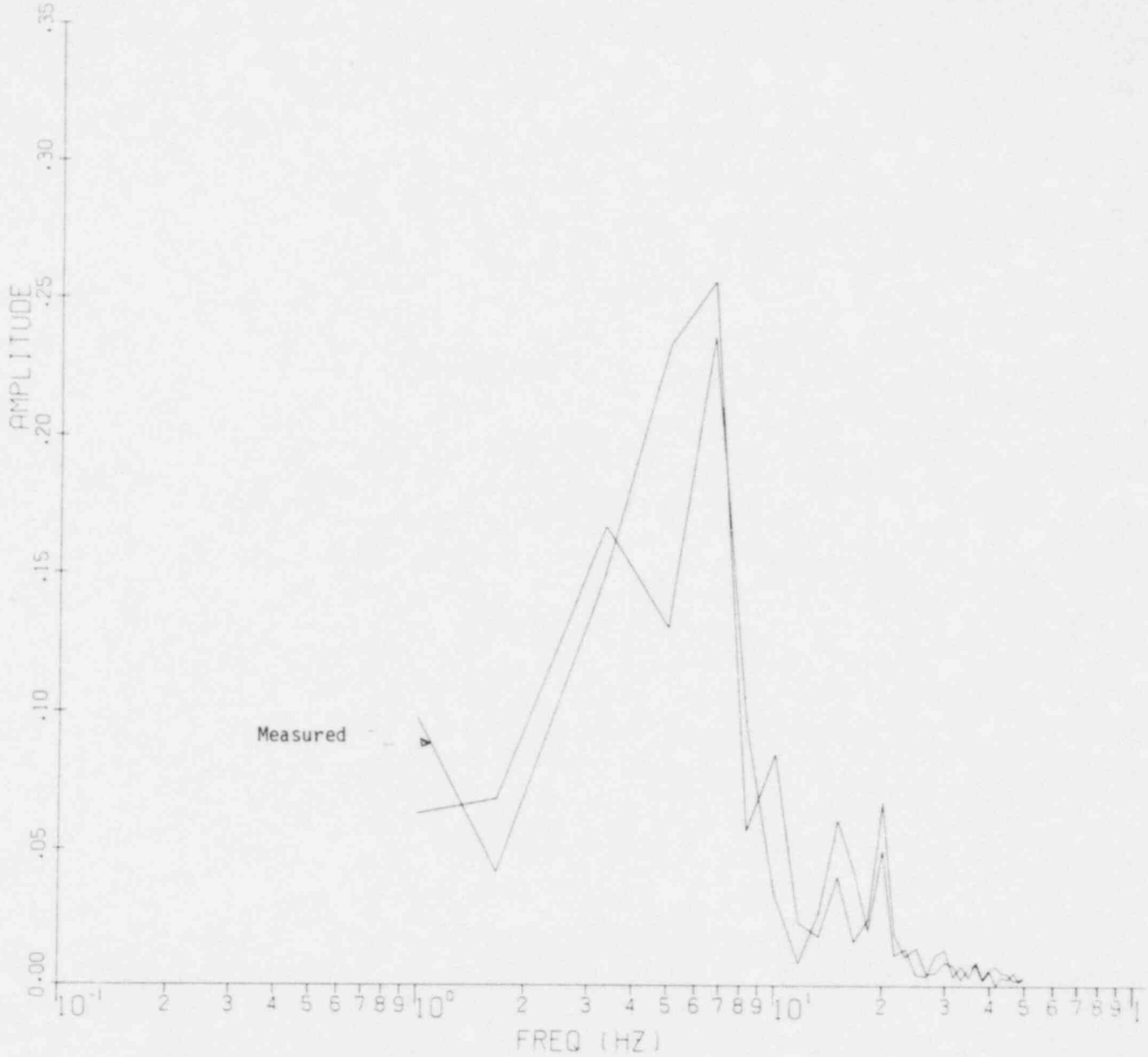

Figure 4.22 Fourier Spectra for 101Y, Uniform Excitation

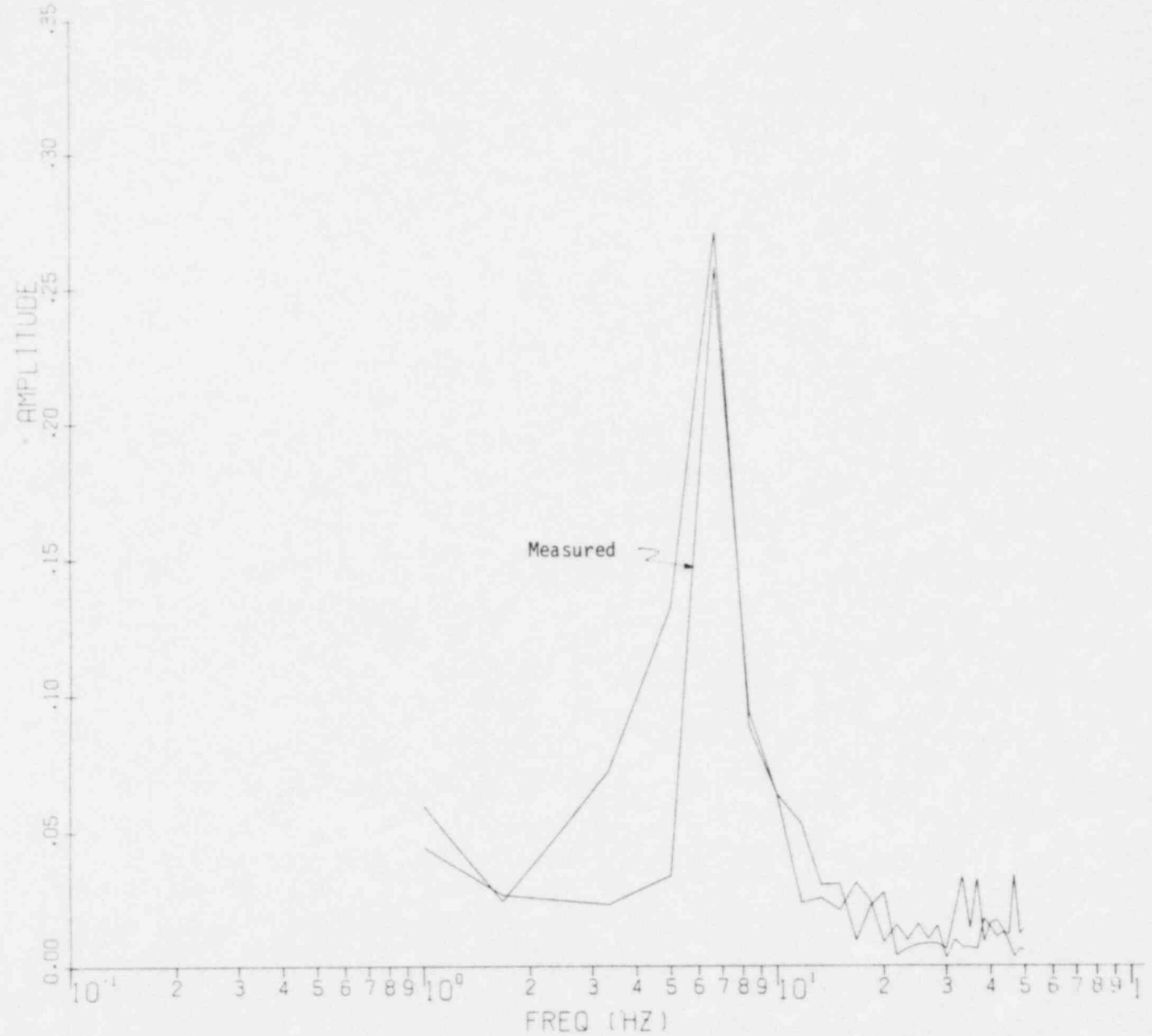

Figure 4.23 Fourier Spectra for 36X, Independent Excitation

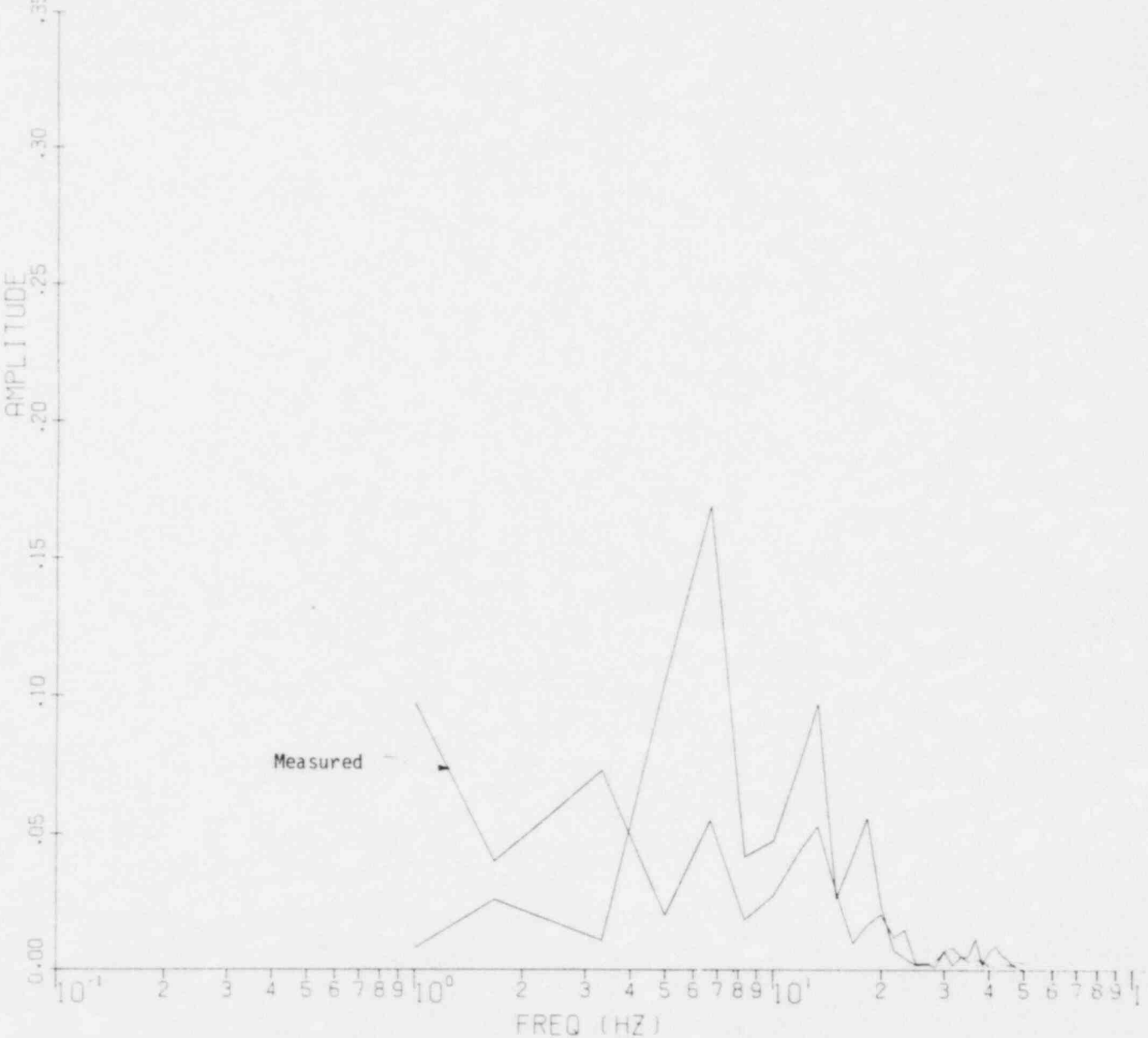

Figure 4.24 Fourier Spectra for 53X, Independent Excitation

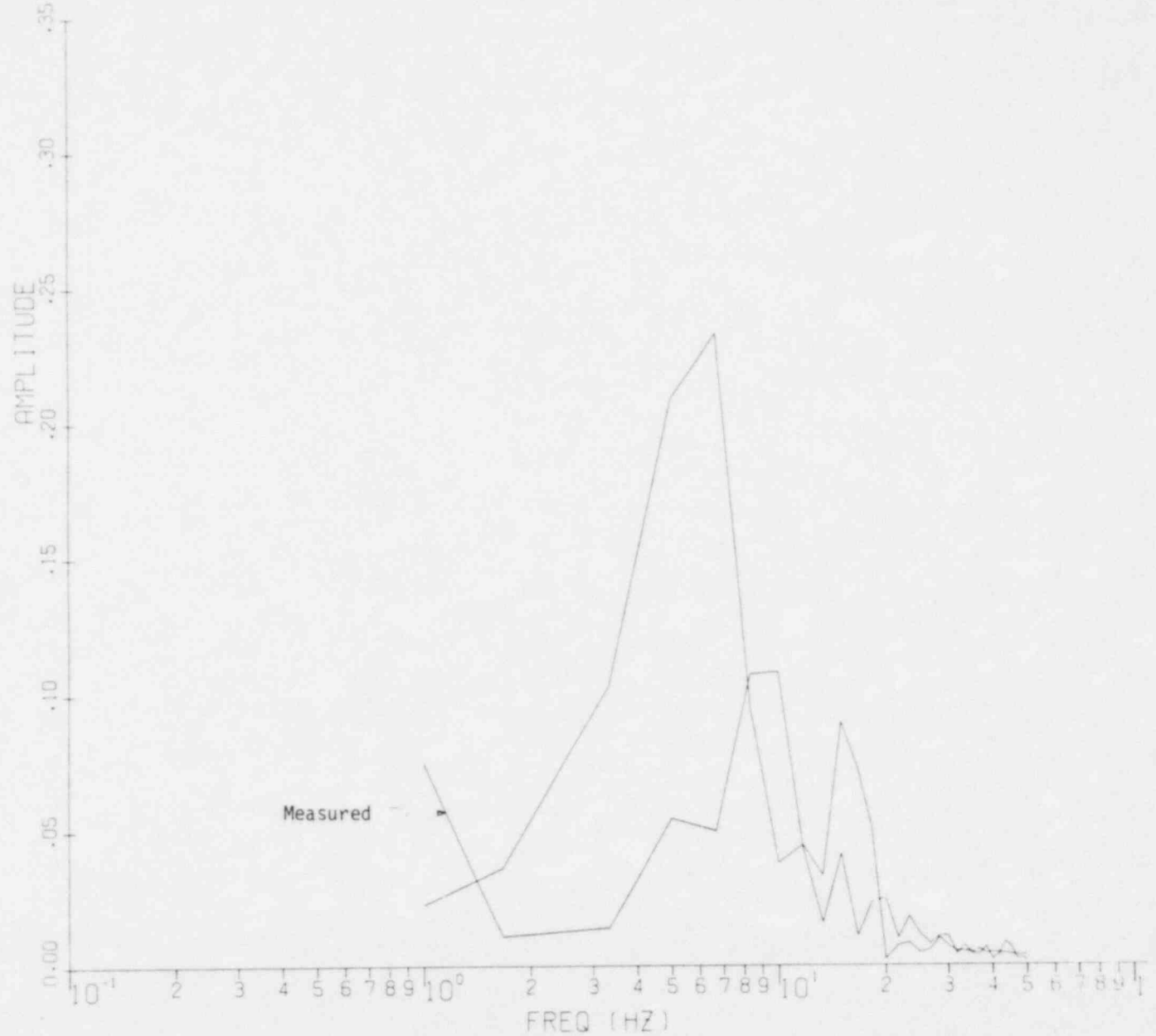

Figure 4.25 Fourier Spectra for 77Z, Independent Excitation

Figure 4.26 Fourier Spectra for 101Y, Independent Excitation

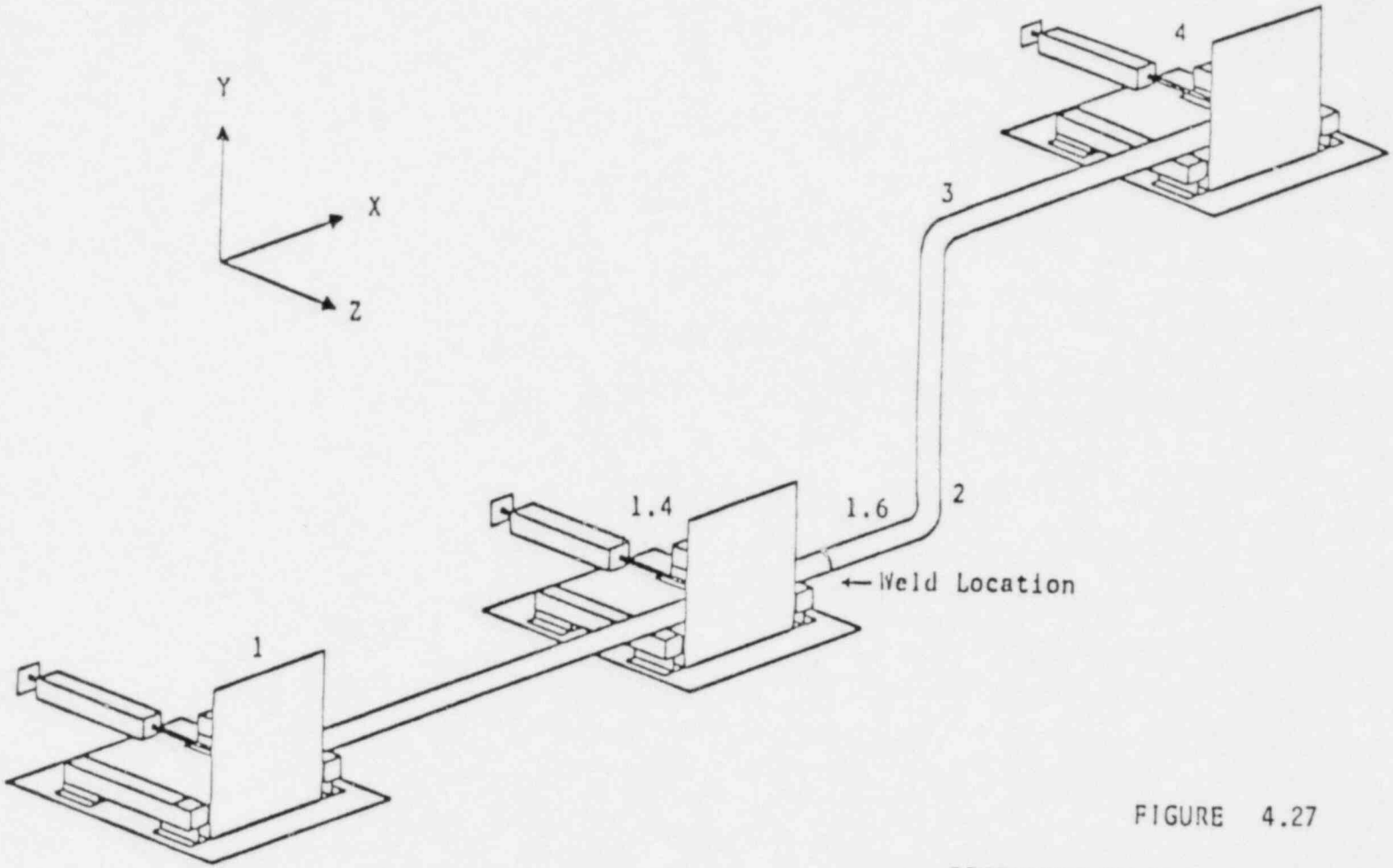

Z BEND CONFIGURATION

FIGURE 4.27

SCHEMATIC OF SLED AND PIPE SET-UP

- Pinned Supports at Pt's. 1 and 4
- Glide at Pt. 1.4
- Actuators at Pt's. 1, 1.4, and 4

5. Soil Structure Interaction
(S. Sharma)

5.1 Mark III Type Containment Ultimate Capacity Calculations

Further results were obtained for the containment vessel by superimposing self-weight gravity load on the internal pressure due to hydrogen burn. The results showed that the containment liner becomes plastic due to large axial stresses at the junction of the cylindrical wall and the foundation mat. The vertical reinforcement bars, however, do not show any plastic deformation. Superposition of the gravity load did not change hoop strains and stresses in the liner appreciably. A report describing these results in detail has been completed and will be issued shortly.

III. DIVISION OF FACILITY OPERATIONS

SUMMARY

Brookhaven National Laboratory (BNL) has been charted with the review and development of models and data for the statistical prediction of human performance. The work, to date, entails LER and similar data reductions through the use of the BNL developed task analysis. The human error probabilities so developed can then be utilized in both probabilistic risk assessment as well as design verifications to quantitatively include the human in the analysis. In addition, through the use of the sequential error model developed at BNL, an investigation into common human contributions to plant safety is continuing. The model is also being validated through the use of non-nuclear maintenance data. In this respect BNL is developing those areas of direct applicability of the model to licensing.

The Human Factors Program at BNL is also reviewing NUREGs 0700, 0801, and 0835 in order to evaluate the needed research to support licensing efforts as the NUREGs were to be utilized.

1. Human Error Rate Data Analysis

(R.E. Hall)

According to the agreed upon program scope for the model and collection of data on human performance, BNL is continuing to review the LERs along with source documents and has begun contacting Sandia and Oak Ridge National Laboratories for the data tapes of past training simulator runs. Both of these efforts are moving on schedule towards the expansion of performance data, specifically in the procedural behavior area. The second task in this program, which is nearing completion, has developed a set of criteria to identify the data needs for the quantification of human performance. Another task is reviewing existing data banks in order to develop the feasibility or including the criteria in them. In addition, BNL has reviewed and is presently documenting the needed data in this area. The final report will be published during the next reporting period, which addressed the human error availability and the applicability of each type of available data to the needs of the NRC.

BNL's sequential failure model for multiple human error is being validated through the use of the split pairs comparison techniques on military maintenance data. In this way a large volume of data can be utilized to first exercise the model and secondly compare results to actual performance. The results of this effort are expected to be submitted to the NRC by the latter part of the summer.

In addition to the data collection and analysis effort described above, BNL is beginning a program to incorporate and document the Operator Action Tree Approach with the Time Regime Reliability Data Curve. In this way an alternative method of quantifying human reliability for both procedural as well as cognitive performance can be made available for the NRC staff's review.

The last task in this program, the reviewing of the needs and proposed scope of a third workshop on the subject of human factors and nuclear safety, has started through open discussions with the IEEE Subcommittee 7 (Human Factors) under the Nuclear Engineering Program Committee (NPEC).

2. Criteria on Human Engineering Regulatory Guides

(W.J. Luckas, Jr.)

Work began on this new program to review NUREGs 0700, 0801, and 0835 for research. This effort has assembled human factors experts for independent review and comment on the present state-of-the-art in human factors and its capability of supporting the development of criteria for the above NUREGs in the licensing arena. In addition, the review will develop a prioritorized list of needed human factor research to better support licensing actions that are called for by the reports. During the quarter, this program was started and the first of several meetings of the peer group, including BNL representatives, has occurred with the NRC.

References

EMBREY, D.E., "The Use of Performance Shaping Factors and Quantified Expert Judgement in the Evaluation of Human Reliability: An Initial Appraisal," Draft, September 1981.

HALL, R.E., SAMANTA, P.K., and SWOBODA, A.L., "Sensitivity of Risk Parameters to Human Errors in Reactor Safety Study for a PWR," NUREG/CR-1879, BNL-NUREG-51322, January 1981.

IEEE, "Conference Record for 1979 IEEE Standards Workshop on Human Factors and Nuclear Safety," December 1979.

IEEE, "Conference Record for 1981 IEEE Standards Workshop on Human Factors and Nuclear Safety," Draft.

LUCKAS, W.J., Jr., and HALL, R.E., "Initial Quantification of Human Errors Associated with Reactor Safety System Components in Licensed Nuclear Power Plants, NUREG/CR-1880, BNL-NUREG-51323, January 1981.

LUCKAS, W.J., Jr., LETTIERI, V. and HALL, R.E., "Initial Quantifica tion of Human Error Associated with Specific Instrumentation and Control System Components in Licensed Nuclear Power Plants, NUREG/CR-2416, BNL-NUREG-51480, February 1982.

SAMANTA, P.K. and MITRA, S.P., "Modeling of Multiple Sequential Failures During Testing, Maintenance, and Calibration," NUREG/CR-2211, BNL-NUREG-51411, December 1981.

SPEAKER, D.M., THOMPSON, S.R., and LUCKAS, W.J., Jr., "Identification and Analysis of Human Errors Underlying Pump and Valve Related Events Reported by Nuclear Power Plant Licensees," NUREG/CR-2417, BNL-NUREG-51481, February 1982.